

THÈSE

Pour obtenir le grade de
Docteur

**Délivré par l'Ecole Nationale Supérieure de Chimie de
Montpellier**

Préparée au sein de l'école doctorale **Sciences Chimique
Balard ED 459**

Et de l'unité de recherche **Institut Européen des
Membranes (UMR 5635)**

Spécialité : **Chimie et Physicochimie des Matériaux**

Présentée par **Marleny CACERES NAJARRO**

« **Dépolymerization enzymatique d'Hydroxypropyl Methyl
Cellulose (HPMC) pour la conception des nouveaux
copolymères à blocs** »

“ **Enzymatic depolymerization of Hydroxy Propyl Methyl
Cellulose (HPMC) to design novel biobased block copolymers**”

Soutenue le 16/12/2015 devant le jury composé de

M. Philippe MIELE, Prof., IEM UMR 5635

Mme Florence DJEDAINI-PILARD, Prof., EA 4665

M. Luc PICTON, Prof., UMR 6270

Mme Corine GERARDIN, DR2, UMR 5253

Mme Catherine LADAVIERE, DR CNRS, UMR 5223

M. André DERATANI, DR, IEM UMR 5635

Examineur

Rapporteur

Rapporteur

Examineur

Examineur

Directeur de Thèse


enscm
CHIMIE Montpellier



Thesis Acknowledgements

Tout d'abord, je tiens à exprimer ma sincère gratitude au directeur de l'Institut Européen des Membranes, le Professeur Philippe Miele pour m'avoir accueilli au sein de son laboratoire et pour avoir présidé mon jury de Thèse. Je le remercie sincèrement pour le soutien moral et personnel qu'il m'a apporté.

Je souhaiterai également exprimer ma gratitude au directeur administratif de l'institut, M. Philippe Falque, pour m'avoir prodigué un profond réconfort tout le long de mon séjour à l'IEM.

A mon directeur de thèse, André Deratani, un grand merci pour sa patience, sa motivation, mais aussi pour toute la confiance dont il a fait preuve lors de la réalisation de ce projet de thèse. Son encadrement rigoureux et son apport scientifique a rendu ma recherche passionnante. Je ne peux que le remercier de m'avoir donné ma chance dans l'aventure scientifique.

Je tiens aussi à remercier Suming Li, qui m'a accompagné lors des moments délicats de mon travail en me faisant découvrir le monde de la synthèse de polymère. Je n'oublie pas toutes les fois où il a pris de mes nouvelles, aussi bien scientifiquement que moralement.

Je voudrais aussi remercier mon comité de thèse: Les professeurs Djedaini-Pilard et Luc Picton pour leurs commentaires perspicaces, une nouvelle fois le professeur Philippe Miele, mais aussi Corine Gerardin et Catherine Ladaviere pour leurs questions constructives.

*"Former les hommes, ce n'est pas remplir un vase, c'est allumer un feu".
Aristophane.*

Je tiens aussi à remercier les personnes qui ont collaboré à ce travail, en particulier Jean-Jacques Robin et Sophy Monge pour m'avoir ouvert les portes de leur Laboratoire (ICGM-IAM) et permit de fructueux échanges liés aux caractérisations LCST et DLS. Un grand merci aussi à Fabrice Azemar, Olinda Gimello, Donatien, Elena, Ania, Laetitia, Cécile, etc. pour votre disponibilité et soutiens.

Merci à Damien Quemener pour toutes les réponses précises à mes questions et ses conseils en synthèse de polymère, à Marc Rolland pour son soutien en chimie réactionnel,

à Celine Pochat pour ses encouragements, à Eddy Petit pour son expertise en RMN, à Yves-Marie Legrand sa disponibilité lors des analyses LCST, à Valérie Bonniol pour son aide lors des analyses au GPC, à Didier Cot lors des analyses de MEB. Je voudrais aussi élargir mes pensées à l'ensemble de l'équipes IP2 et GPM avec lesquelles j'ai beaucoup collaboré lors de mon travail expérimental.

Une sincère gratitude pour Anne Julbe qui a compté beaucoup pour moi durant mon séjour au laboratoire, à André Ayrat pour sa cordialité et son enthousiasme, à Sylvie Condom pour sa disponibilité, à Christophe Charmette qui me montre continuellement qu'il ne faut jamais sous-estimer un coureur, à Martin Drobek pour son amitié et à Christophe Innocent pour son aide précieuse dans mes démarches administratives. Sans vous, je n'aurais probablement pas pu finir le marathon de cette thèse.

Une pensée pour Arie Van Der Lee et Stéphanie Roualdes pour m'avoir motivé à inviter le Professeur William Moerner (prix Nobel en Chimie 2014) lors de l'organisation du congrès JMJC 2015. Cet évènement a été enrichissant et je suis heureuse d'y avoir collaboré. A ce sujet, une pensée va au bureau de la SCF-LR, Camille Oger, Claire Cuyamendous, Aurelien de la torre, Vincent Blanchard, Annabelle Biscans, Barbara Maret, Elena Dolci, etc. La liste est longue, merci à tous. Ce fut un bel travail en équipe.

Mes sincères remerciements vont également à tout le personnel administratif de l'IEM, et tout particulièrement à Jean-Pierre Ravier (d'une cordialité sans égale), Cathy, Christelle, Dominique, Florence, Carmela, Fabienne, Guylene, leur bonne humeur quotidienne communicative a égayé mes journées. Les filles du service de qualité Stelle Donadei et Inmaculada Dousoune, merci pour votre sympathie. Je remercie pareillement l'administration de l'école doctorale, en particulier le professeur Jean Jacques Vasseur, Marc Créatin et Karina Allenne pour s'être impliqué lorsque mon cas le nécessitait.

Bien évidemment, je n'oublie pas El Manssouri pour ses nombreux repas partagés ensemble. Nathalie Masqueles et Jean Paul Scotto. Aux personnel de l'atelier : Jean Pierre, Bruno, Bernard, Daniel et Patrice, merci pour leur collaboration. Les informaticiens, Jean-Michel Poulin et Henri Bourrasse.

« Certaines personnes nous font rire un peu plus fort, rendent nos sourires un peu plus vrais et rendent nos vies meilleures »

Tout mon remerciement à mes amis. Hervé Manzanarez pour tout le soutien pendant la rédaction. Hervé, Hervé, Hervé,Coffee. Et j'avais toujours un verre de café tout le matin.... Merci beaucoup, petit râleur. A mon chico « guapo...papi.. » le Dr. Antonin Azais merci pour m'avoir rendu la période de rédaction plus agréable. King Wo merci d'avoir surveillé mes manips, François Zaviska merci pour tes conseils, Florence Boch pour ton soutien. Adriana, Techer, Jojo des amis qui seront toujours dans mes pensées. Sana Gassara, Loic Dumazert, Marie Guerant, Anthony Grunenwald, Helene Gatelier, Prashant, Haitem, Guillem Bonniol, des rencontres qui resteront dans mes souvenirs. Alina, Romine, Florine, les filles de l'IEM..... la liste est longue, je m'excuse pour ne pas citer tout le monde mais vous êtes dans mes pensées. Les deux stagiaires qui m'ont beaucoup aidé Ayoub et Sonia. Merci à vous tous pour vos soutiens et pour tout le plaisir que nous avons eu tout au long de ces trois dernières années.

Pour la suite des remerciements, je suis amené à finir en espagnol :

Quisiera agradecer a mis padres, María y Andrés, por el apoyo incondicional y constante que me brindan en cada momento de mi vida. A mis hermanos porque siempre están al resguardo de mi bienestar. Ustedes son el soporte fundamental de mi vida, los Amo.

De igual manera quisiera agradecer a mis amigos que estuvieron en el gozo y en las adversidades de esta aventura llamada Tesis. A Sylvia Días y Mathieu Camier (los potis), Valentina Yauri y Maxime Le Mineur (los gatitos) gracias por estar siempre conmigo, los quiero mucho. A Amelia Ulloa por su benevolente ayuda. A Saliha y Menad mis primeros amigos en Montpellier, quienes no dudaron en abrirme su corazón. Asimismo, Jessica Orgeval, Charlotte Faucher, Nadege Perrine, Noemy Wirs, Mariene Vernar, las amigas que siempre cuidan de mi persona. A pesar de la distancia que nos separan, Ulrique Reichert, Berenice Bernal, Rosario Galindo, Aylin Kerstik, Alim Tello, Sacha....gracias por los alientos a seguir adelante.

Table of contents

ABBREVIATIONS

LIST OF FIGURES

LIST OF TABLES

GENERAL INTRODUCTION	1
CHAPTER I: BIBLIOGRAPHY	7
INTRODUCTION	8
I.1. BIOSOURCED POLYMERS	8
I.1.1. Polysaccharide and derivatives	9
I.1.1.1. Cellulose	10
I.1.1.2. Cellulose ethers	13
I.1.1.3. Hydroxypropylmethyl cellulose (HPMC)	15
I.1.2. Protein	16
I.1.2.1. Functional properties	18
I.1.2.2. Extraction process	18
I.1.2.3. Developments and uses	19
I.1.3. Polymers from lipids	20
I.1.3.1. Future trends/ Applications:	21
I.2. POLYSACCHARIDE BASED FILTRATION AND BIOMEDICAL MATERIALS	22
I.2.1. Polysaccharide based membrane materials	22
I.2.2. Method of membrane preparation	24
I.2.3. Polysaccharide based flat sheet membranes	24
I.2.4. Polysaccharide based hollow fiber	26
I.2.5. Polysaccharide based biomedical materials	27
I.3. POLYSACCHARIDE BASED BLOCK COPOLYMERS	29
I.3.1. Block copolymers	31
I.3.2. Synthesis	31
I.3.3. Structure of self-organization	32
I.3.4. Self-organization in solution	33
I.3.5. Lyotropic phases/bulk phase	34
I.3.6. Hierarchical self-assembly	35
I.3.7. Block copolymers based on polysaccharide	37
I.3.8. Synthesis	38
I.3.8.1. Block copolymers based on polysaccharides by coupling reaction	39
I.3.8.2. Block copolymer based on polysaccharide by Controlled radical Polymerization (CRP)	39
I.3.8.3. Block copolymer based on polysaccharides by Ring Opening Polymerization (ROP)	40
I.3.9. Self-assembly and properties	41
I.4. DEPOLYMERIZATION OF CELLULOSE AND DERIVATIVES	44

Table of contents

I.4.1. Methods for biopolymer degradation	45
I.4.2. Pretreatment processes	45
I.4.3. Depolymerisation methods	46
I.4.3.1. Depolymerisation by liquid acid	46
I.4.3.2. Depolymerisation by solid acids	47
I.4.3.3. Depolymerisation by Advanced Oxidation Process (AOPs)	48
I.4.4. Enzymatic depolymerisation	49
I.4.4.1. Enzyme	49
I.4.4.2. Mechanism of hydrolysis	51
CONCLUSION	53
REFERENCES	54
CHAPTER II: METHODS AND MATERIALS	66
INTRODUCTION	67
II.1. MATERIAL AND CHEMICAL PRODUCTS	67
II.1.1. HPMC	67
II.1.2. Enzymes	68
II.1.3. Citrate-phosphate buffer preparation:	68
II.1.4. Jeffamine® Polyetheramines:	69
II.2. METHODS OF SAMPLE PREPARATION	70
II.2.1. Short chains of hydroxypropyl methylcellulose (HPMC)	70
II.2.1.1. Hydrolysis process	70
II.2.1.2. Acetylation of free hydroxyl groups in HPMC	73
II.3. CHARACTERIZATION METHODS	74
II.3.1. Size-Exclusion Chromatography (SEC)	74
II.3.2. Dynamic Light Scattering (DLS)	75
II.3.3. Reducing end titration	76
II.3.4. Titration of thiol group using Ellman's reaction	78
II.3.5. Cloud Point (Cp)	79
II.3.5. Fourier transforms infrared spectroscopy (FT-IR)	80
II.3.7. Nuclear magnetic resonance (NMR) spectroscopy	80
II.3.8. Synthesis of block copolymer	82
II.3.9. Synthesis of HPMC- <i>b</i> -PLA, via UV- initiated thiol-ene click reaction	85
REFERENCES	86
CHAPTER III: DEPOLYMERISATION OF HYDROXYPROPYL METHYL CELLULOSE	87
INTRODUCTION	88
RESULTS AND DISCUSSION	89
III.1. ENZYMATIC HPMC DEPOLYMERISATION	89
III.1.1. Procedure	89

Table of contents

III.1.2. Effect of reaction time on the depolymerisation efficiency _____	91
III.1.3. Effect of the enzyme concentration on the depolymerisation efficiency _____	97
III.1.4. Influence of the HPMC source and chain length on the depolymerisation efficiency _____	102
III.1.4.1. Influence of the methylation degree _____	103
III.1.4.2. Influence of the chain length _____	105
CONCLUSION _____	106
III.2. ACIDIC HPMC DEPOLYMERISATION _____	106
III.3. SUMMARY OF HPMC DEPOLYMERISATION _____	108
CONCLUSION _____	110
REFERENCES _____	111
CHAPTER IV: PHYSICO-CHEMICAL CHARACTERIZATION OF SHORT CHAINED HPMCS _____	113
INTRODUCTION _____	114
RESULTS AND DISCUSSION _____	115
IV.1. MACROMOLECULAR FEATURES _____	115
IV.1.1. Starting HPMCS _____	115
IV.1.2. Short chained HPMCS _____	117
IV.2. CHEMICAL COMPOSITION OF THE DIFFERENT POLYMER FRACTIONS _____	123
IV.3. REDUCING END REACTIVITY _____	127
IV.4. THERMALLY INDUCED PHASE SEPARATION - CLOUD POINT _____	128
IV.4.1. Influence of M_w _____	130
IV.4.2. Influence of the chemical composition _____	133
IV.4.3. Influence of the depolymerisation procedure _____	134
CONCLUSION _____	135
REFERENCES _____	136
CHAPTER V: NEW POLYSACCHARIDE FRAGMENTS TO AMPHIPHILIC BLOCK COPOLYMER	
SYNTHESIS _____	138
INTRODUCTION _____	139
RESULTS AND DISCUSSION _____	140
V.1. HPMC-<i>b</i>-PO₂₉-EO₆ 140	
V.1.1. Synthesis _____	140
V.1.2. Average molar mass of the block copolymer _____	141
V.1.3. FTIR analysis _____	142
V.1.4. DOSY NMR analysis _____	142
V.1.5. Self-assembly of HPMC- <i>b</i> -PO ₂₉ -EO ₆ in H ₂ O _____	144
V.1.6. Thermoresponsive behavior of HPMC- <i>b</i> -PO ₂₉ -EO ₆ _____	147
V.2. Mikroarm block copolymer (HPMC)₃-<i>b</i>-PO₈₅ _____	148
V.2.1. Synthesis _____	148
V.2.2. Average molar mass of (HPMC) ₃ - <i>b</i> -PO ₈₅ block copolymer _____	149
V.2.3. FTIR of (HPMC) ₃ - <i>b</i> -PO ₈₅ block copolymer _____	150

Table of contents

V.2.4. DOSY NMR of (HPMC) ₃ - <i>b</i> -PO ₈₅ block copolymer	151
V.2.5. Self-assembly of (HPMC) ₃ - <i>b</i> -PO ₈₅ in H ₂ O	152
V.3. HPMC-<i>b</i>-PLLA by using the thiol-ene click reaction	154
V.3.1. HPMC-thiolation	154
V.3.2. PLLA synthesis	155
V.3.3. HPMC- <i>b</i> -PLA allyl by coupling using the thiol-ene click reaction	156
V.3.4. FTIR of PLA allyl- <i>b</i> -HPMC	157
V.3.5. DOSY NMR analysis for PLLA- <i>b</i> -HPMC	158
V.3.6. Self-assembly of PLA- <i>b</i> -HPMC in H ₂ O	158
V.3.7. Morphology of PLA- <i>b</i> -HPMC	159
CONCLUSION	161
REFERENCE	162
CHAPTER VI: CONCLUSION AND PERSPECTIVES	164

Abbreviations

ABBREVIATIONS

AAs	Auxiliary Activities
AGU	AnhydroGlucopyranose Unit
AOPs	Advanced Oxidation Processes
ATRP	Atom Transfer Radical Polymerization
BCA	Bicinchonic acid
CAC	Critical aggregate concentration
CDH	Cellobiose dehydrogenase
CEs	Carbohydrate Esterases
CuAAC	Copper(I)-Catalyzed Azide-Alkyne cycloaddition
CMC	Critical micelle concentration
CNT	Carbon nanotubes
CPB	Citrate phosphate buffer
Cp	Clouding point
CRP	Controlled radical polymerization
D	Distribution of diffusion coefficients
D_o	Translation diffusion coefficient
DIPS	Diffusion of non-solvent induced phase separation
DLS	Dynamic light scattering
DOX	Doxorubicin
DP	Degree of polymerization
DTNB	5,5'-dithio-bis-[2-nitrobenzoic acid]
DTT	Dithiothreitol
DS	Degree of substitution
DS_{Me}	Degree of methyl substitution
DOSY NMR	Diffusion-ordered spectroscopy Nuclear Magnetic Resonance
EG	Endoglucanases
EGU	Endo-Glucanase Units

Abbreviations

EO	Ethylene oxide
EX	Exoglucanases
FTIR	Fourier Transform InfraRed spectroscopy
G	Relaxation frequency
GHs	Glycoside Hydrolases
GPC	Gel-permeation chromatography
GTs	Glycosyl Transferases
η	Viscosity of the medium
HPMC	Hydroxypropylmethylcellulose
HPO	Hydroxypropoxy
ILs	Ionic liquids
INN	International Nonproprietary Name
LCST	Temperature above a lower critical solution
LPMOs	Lytic Polysaccharide MOnooxygenases
k_B	Boltsman constant
MADIX	Macromolecular design by interchange of xanthate
MALS	Multi angle light scattering
MeO	Methoxy
MF	Microfiltration
MH	Maltoheptaose
MS	Molar substitution
MS_{HP}	Degree of hydroxypropylation or hydroxypropyl molar substitution
M_w	Weight average molar mass
MWCO	Molecular weight cut-off
NNLS	Non-Negative Least Squares
NF	Nanofiltration
NMP	Nitroxide-Mediated Polymerization
NS	Nelson-Somogyi

Abbreviations

P	Precipitate
PDI	Polydispersity index
PEA	Polyetheramine
PES	Polyethersulphone
PEM	Polyelectrolyte multilayer
PLs	Polysaccharide Lyases
PMGA	PolyGlycidylMethAcrylate
PO	Propylene oxide
PHA	Polyhydroxyalkanoates
RAFT	Reversible addition/ Fragmentation Chain Transfer Polymerization
RE	Reducing End
REG	Reducing End Group
R_H	Hydrodynamic radius
RI	Refractive Index
RIPS	Reaction induced phase separation
RO	Reverse Osmosis
ROP	Ring Opening Polymerization
ROMP	Ring Opening Metathesis Polymerization
S	Supernatant
SEC	Size-Exclusion Chromatography
SPIONs	SuperParamagnetic Iron oxide nanoparticles
T	Temperature
TEM	Transmission electron microscopy
TIPS	Temperature induced phase separation
TFNC	Thin-film nanofibrous composite
UF	Ultrafiltration
λ	Wavelength
XGO-<i>b</i>-XGO	Xiloglucoses diblock copolymers

Abbreviations

PS-*b*-PLA polystyrene-*block*-poly(lactic acid)

HPMC-*b*-PLA Hydroxypropylmethyl cellulose-*block*-poly(lactic acid)

HPMC-*b*-PO Hydroxypropylmethyl cellulose-*block*- Propylene Oxide

List of Figures

LIST OF FIGURES

Figure i. Schematic presentation of bio-based polymers based on their origin and method of production ⁴ .	2
Figure ii. Simplified HPMC structure	4
Figure iii. Schematic presentation of two routes of block copolymer preparation: (a) reductive amination and (b) thiol-en dick reaction.	5
Figure I. 1. Glycosidic bond and Acetal group in cellulose.	9
Figure I. 2. Cellulose polymer chain structure ⁹ .	10
Figure I. 3. Intra and Intermolecular hydrogen bonds in cellulose chains ⁹ .	11
Figure I. 4. Scheme of the structure of cellulose fibrils ¹⁴ .	12
Figure I. 5. Scheme of protein structures adapted from Owusu-Apenten ⁴⁸ and Darryl ⁵⁰ .	17
Figure I. 6. Chemical reactions of vegetable oils ¹¹⁵ .	21
Figure I. 7. Schematic diagrams of main types of membranes ¹²⁴ .	23
Figure I. 8. Reaction of chitosan and gluteraldehyde ¹³⁴	25
Figure I.9. Cross-section images of the composite membranes prepared from purified polysaccharide ¹³⁵ .	26
Figure I.10. Cross-sectional and overall morphology of chitosan/cellulose acetate hollow fiber membrane ¹²⁷ .	27
Figure I. 11. Schematic polyelectrolyte formation between polyanion and mPEG-g-Chitosan ¹⁴⁹ .	28
Figure I. 12. Illustration of interactions between 1,2-diols of DS-b-PGMA and the SPION iron atom ¹⁵⁰ .	29
Figure I. 13. Some possible structure organizations of block copolymers ^{153, 159-160} .	31
Figure I. 14. Aggregation morphology of linear diblock copolymers ^{165, 168} .	33
Figure I. 15. Theoretical phase diagram for diblock copolymer: S-spherical, C-cylindrical, G-gyroid, L- Lamellae, CPS- close packed sphere and disordered phase ¹⁵² .	34
Figure I. 16. Phase diagram for linear AB diblock copolymer ¹⁷²⁻¹⁷³ .	35
Figure I. 17. An example of the universality of order principle through pair forces. Left (lamellar organization) and right (hexagonal domains) in a ferrofluid a) $d = 1 \text{ cm}$ and b) $d = 4 \mu\text{m}$; in a ferromagnetic film c) and d) $d = 10 \mu\text{m}$; in a block copolymer superlattice e) $d = 40 \text{ nm}$ and f) $d = 16 \text{ nm}$ ¹⁶⁸ .	36
Figure I. 18. Self-assembled architectures of A) PS-b-PLA ¹⁷³ ; B) PS-b-PMMA ¹⁷⁴ ; C)PS-b-PMMA ¹⁷⁵ .	37
Figure I.19. A) Globular protein m-Cherry conjugation with poly(N-isopropylacrylamide) and the observed possible phases formed. B) TEM of solid state structures formed from m-Cherry-b-poly(N-isopropylacrylamide) ¹⁷² .	37
Figure I. 20. Reductive amination with cyanoborohydride ion at the reducing end of a polysaccharide chain ¹⁷⁹ .	38
Figure I. 21. Several coupling reactions between polysaccharide and other synthetic polymers: a) reductive amination, b) aminolysis of a dextran lactone-end group, c) stepwise elongation of a nylon block and d) copper(I)-catalysed azide-alkyne cycloaddition ¹⁷⁹ .	39
Figure I. 22. Controlled/living polymerizations of vinyl blocks from poly- or oligosaccharides with suitably modified end groups. Note that hydroxyl groups are not protected in the second and latter methods ¹⁷⁹ .	40

List of Figures

Figure I. 23. Ring opening polymerizations of polypeptide, polyether, polyamide and polyester from polysaccharides with suitably modified end groups ¹⁷⁹ .	41
Figure I. 24. Polymersome of poly(γ -benzyl L-glutamate) (PBLG) and hyaluronan (HYA) using click chemistry (PBLG ₂₃ -b-HYA ₁₀) ¹⁸¹ .	42
Figure I. 25. A) TEM of dextran-b-PCL material ¹⁸² and B) FEG-SEM of oligosaccharides-b-PNIPAM ¹⁸⁴ .	42
Figure I. 26. A simplified scheme of the current view on the enzymatic degradation of cellulose ²¹⁶ .	51
Figure I. 27. Schematic drawing of the glucose- binding subsites in several glycosyl hydrolases ²²¹ .	52
Figure II. 1. The molecular structure of hydroxypropylmethyl cellulose (HPMC).	68
Figure II. 2. Jeffamine® M-2005 structure (Manufacturer information).	69
Figure II. 3. Jeffamine® T-5000 structure (X+Y+Z=85) (Manufacturer information).	69
Figure II. 4. Process flow sheet of HPMC depolymerization.	71
Figure II. 5. Schematic design of the Amicon diafiltration set-up: 1) permeate; 2) stirred filtration cell; 3) pressure inlet pipe; 4) cell inflow tubing; 5) tank pressure inlet; 6) tank outflow tubing; 7) water for washing salts and low Mw compounds; 8) diafiltration tank.	72
Figure II. 6. Synthesis of 2,3,6-O-acetyl AGU.	74
Figure II. 7. Terminal aldehyde oxidation by Cu ²⁺ ions	76
Figure II. 8. Standard glucose calibration curve.	78
Figure II. 9. Standard acetyl cysteamine calibration curve.	79
Figure II. 10. Clouding point profile and the schema to consider Cp ₀ and Cp ₅₀ .	80
Figure II. 11. NMR spectrum in CDCl ₃ of acetylated K4M. Signal (a) is assigned to protons on the glucose ring, the methyl substituents, and the protons on isopropyl substituents, signal (b) to protons on the acetyl groups and signal (c) to methyl protons on isopropyl substituents.	81
Figure II. 12. Synthesis scheme of HPMC-b-PO ₂₉ -EO ₆ .	82
Figure II. 13. Synthesis scheme of (HPMC) ₃ -b-PO ₈₅ .	83
Figure II. 14. Synthesis scheme of HPMC-thiol	84
Figure II. 15. Synthesis scheme of alkene functional PLA.	85
Figure III. 1. Molecular structure of hydroxypropylmethyl cellulose (HPMC).	89
Figure III. 2. Cumulative molar mass distribution of the crude product obtained by hydrolysis of G4 using Enzyme/Substrate ratio of 180 $\mu\text{L}\cdot\text{g}^{-1}$ for 72 h.	90
Figure III. 3. Schematic description of the preparation of HPMCS and P fractions.	90
Figure III. 4. Cumulative molar mass distribution of the crude and purified S and P products obtained by hydrolysis of G4 using Enzyme/Substrate ratio of 180 $\mu\text{L}\cdot\text{g}^{-1}$ for 72 h.	91
Figure III. 5. Yield evolution of the recovered S (dashed) and P (black) polymers as a function of reaction time (enzyme concentration = 30 $\mu\text{L}\cdot\text{g}^{-1}$).	92
Figure III. 6. M _w variation of S and P fractions as a function of reaction time using 30 $\mu\text{L}\cdot\text{g}^{-1}$ enzyme concentration and K4M HPMC as starting polymer (M _w = 235 000 g.mol ⁻¹).	93

List of Figures

Figure III. 7. Evolution of the weight average molar mass of K4M-P-30 over reaction time.	96
Figure III. 8. Evolution of the weight average molar mass of K4M-S-30 over reaction time.	96
Figure III. 9. Total polymer yield over reaction time.	97
Figure III. 10. M_w variation of S and P fractions as a function of enzyme concentration after 1 h of reaction. K4M HPMC was the starting polymer ($M_w = 235\ 000\ \text{g}\cdot\text{mol}^{-1}$).	98
Figure III. 11. Yield of the two isolated fractions as a function of enzyme concentration and reaction time.	100
Figure III. 12. Effect of the enzyme concentration on M_w of (a) P fraction and (b) S fraction.	101
Figure III. 13. Effect of the reaction time on M_w of P and S fraction using a $180\ \mu\text{L}\cdot\text{g}^{-1}$ enzyme concentration.	101
Figure III. 14. Yield of the two isolated short chained fractions as a function of enzyme concentration and reaction time obtained in G4 depolymerisation.	103
Figure III. 15. M_w variation of P and S fractions as a function of time and enzyme concentration (15 to $180\ \mu\text{L}\cdot\text{g}^{-1}$) in G4 depolymerisation.	104
Figure IV. 1. Concentration profiles of K4M and G4 samples observed by SEC-MALS-RI and molar mass calculated from coupled light scattering.	116
Figure IV. 2. Log-log plot of the radius of gyration vs molar mass for K4M and G4 samples and linear regression fitting.	117
Figure IV. 3. Concentration profiles of P and S fractions yielded with Enz/K4M ratio of $180\ \mu\text{L}\cdot\text{g}^{-1}$ after 72 h of reaction observed by SEC-MALS-RI and molar mass calculated from coupled light scattering.	118
Figure IV. 4. Concentration profiles of P and S fractions yielded with Enz/G4 ratio of $180\ \mu\text{L}\cdot\text{g}^{-1}$ after 72 h of reaction observed by SEC-MALS-RI and molar mass calculated from coupled light scattering.	119
Figure IV. 5. Cumulative molar mass distribution of K4M, K4M-P-180-72, K4M-S-180-72.	119
Figure IV. 6. Log-log plot of the radius of gyration vs molar mass for K4M-P-180-72 and K4M-S-180-72 samples and linear regression fitting.	120
Figure IV. 7. Log-log plot of the radius of gyration vs molar mass for G4-P-180-72 and G4-S-180-72 samples and linear regression fitting.	121
Figure IV. 8. ^1H NMR spectra of (top) native K4M in D_2O and (bottom) of acetylated K4M in CDCl_3 .	124
Figure IV. 9. $d(\log M)/d(\log R_g)$ as a function of the DS_{Me} for the starting HPMC (K4M and G4) and the P fractions of the nine selected batches.	126
Figure IV. 10. Reducing end titration of HPMCs obtained by enzymatic and acid reaction compared to that of their parent compounds.	128
Figure IV. 11. Two ways of determining C_p from the turbidity experiments.	130
Figure IV. 12. Transmittance curves as a function of T for G4 and K4M.	131
Figure IV. 13. Transmittance curves for K4M and its short chains prepared by enzymatic depolymerisation.	132
Figure IV. 14. Transmittance curves for K4M and its short chains prepared by acidic depolymerisation.	132
Figure IV. 15. Cloud point temperatures (C_{p0}) as a function of the degree of methyl substitution DS_{Me} .	133
Figure IV. 16. Cloud point temperatures (C_{p50}) as a function of the degree of methyl substitution DS_{Me} .	133

List of Figures

Figure IV. 17. Turbidity curve profile of short chained HPMC with a Mw of about 10 000 g.mol ⁻¹ prepared by enzymatic and acid depolymerisation of K4M. _____	135
Figure V. 1. Synthesis scheme of HPMC-b-PO ₂₉ -EO ₆ . _____	141
Figure V. 2. Cumulative molar mass distribution of the starting short chained HPMC and the resulting block copolymer HPMC-b-PO ₂₉ -EO ₆ . _____	142
Figure V. 3. FTIR spectra of (A) H ₂ N-PO ₂₉ -EO ₆ , (B) HPMC (Mw=8000 g mol ⁻¹), (C) HPMC-b-PO ₂₉ -EO ₆ . _____	143
Figure V. 4. DOSY NMR spectra obtained at 298 K in DMSO-d ₆ solution of the copolymer HPMC-b-PO ₂₉ -EO ₆ . _____	143
Figure V. 5. ¹ H NMR spectra of HPMC, H ₂ N-PO ₂₉ -PEO ₆ copolymer HPMC-b-PO ₂₉ -EO ₆ in DMSO-d ₆ . _____	144
Figure V. 6. Possible morphologies of self-assembled HPMC-b-PO ₂₉ -EO ₆ . _____	144
Figure V. 7. Size distribution (black) and autocorrelation function (blue) measured by DLS for HPMC-b-PO ₂₉ -EO ₆ copolymer at a concentration of 0.3 g L ⁻¹ . _____	145
Figure V. 8. TEM image of the self-assembled nanoparticles of HPMC-b-PO ₂₉ -EO ₆ copolymer. _____	146
Figure V. 9. Plot of scattered intensity (%) as a function of HPMC-b-PO ₂₉ -EO ₆ copolymer concentration. _____	147
Figure V. 10. Plots of transmittance changes as a function of temperature for aqueous solutions (10 g L ⁻¹) for HPMC and HPMC-b-PO ₂₉ -EO ₆ . Solutions prepared in deionized water. _____	148
Figure V. 11. Synthesis scheme of (HPMC) ₃ -b-PO ₈₅ . _____	149
Figure V. 12. Average of molar mass distribution of HPMC and HPMC-b-PO ₈₆ . _____	150
Figure V. 13. FTIR spectra of (A) PO ₈₅ , (B) HPMC (Mw=8000 g.mol ⁻¹), (C) (HPMC) ₃ -b-PO ₈₅ . _____	151
Figure V. 14. DOSY NMR spectrum obtained at 298 K in DMSO-d ₆ solution of the copolymer (HPMC) ₃ -b-PO ₈₅ . _____	152
Figure V. 15. Possible self-assembly organizations of ABA-type block copolymer. _____	152
Figure V. 16. TEM images of self-assembled nano-objets of (HPMC) ₃ -b-PO ₈₅ copolymer. _____	153
Figure V. 17. Synthesis scheme of thiolation of HPMC. _____	154
Figure V. 18. Cumulative weight fraction as a function of molar mass: red line corresponds to the initial HPMC, blue line to the disulfide bonded diHPMC and black line to the HPMC-SH after reduction with DTT. _____	155
Figure V. 19. Synthesis scheme of PLA=CH ₂ . _____	155
Figure V. 20. ¹ H NMR spectrum of PLA=CH ₂ . _____	156
Figure V. 21. Synthesis scheme of PLA=CH ₂ -b-HPMC. _____	157
Figure V. 22. FTIR spectra of (A) PLA allyl, (B) HPMC, (C) HPMC-b-PLA. _____	157
Figure V. 23. DOSY NMR spectrum obtained at 298 K in DMSO-d ₆ solution of the copolymer PLLA-b-HPMC. _____	158
Figure V. 24. Possible self-organization of PLA-b-HPMC. _____	159
Figure V. 25. TEM images of self-organized architectures of PLA-b-HPMC. _____	160

List of Tables

LIST OF TABLES

Table I. 1. Industrial cellulose ethers, etherifying agents and their main application. ³⁶	15
Table I. 2. Composition/Organization copolymer structures ¹⁵¹ .	30
Table I. 3. Comparison of catalytic properties and activities of solid acid catalysts for cellulose hydrolysis to glucose.	48
Table II. 1. Specification of samples used in this research work as given by the manufacturer.	68
Table II. 2. Operating conditions for HPMC depolymerisation and list of the obtained products.	73
Table III. 1. Weight (M_w) and number (M_n) molar mass averages of the starting K4M HPMC and of the S and P polymers obtained after 1 h of reaction ($EG = 30 \mu\text{L}\cdot\text{g}^{-1}$ of K4M) named K4M-S-30-1 and K4M-P-30-1, respectively and their corresponding polydispersity index (PDI).	94
Table III. 2. Weight (M_w) and number (M_n) molar mass averages of the S and P polymers obtained with different enzyme concentrations after 1 h of reaction and corresponding yield.	98
Table III. 3. The average number of chain cleavage (z) and the mean number of P (x) and S (y) fragments per chain (rounded values for sake of clarity) calculated from equations III.1 to III.4.	99
Table III. 4. Macromolecular and substitution characteristics of the studied HPMC.	102
Table III. 5. The average number of chain cleavage (z) and the mean number of P (x) and S (y) fragments per chain (rounded values for sake of clarity) calculated from equations III.1 to III.4.	104
Table III. 6. Influence of the chain length on the enzymatic depolymerisation.	105
Table III. 7. Characteristics of P and S fractions obtained by acid depolymerisation	107
Table III. 8. Library of short chained HPMC produced by enzymatic and chemical hydrolysis.	109
Table IV. 1. Reference of the nine batches corresponding to the selected short chained HPMCs produced by enzymatic and acidic hydrolysis and reaction parameters analyzed.	115
Table IV. 2. Weight average molar mass (M_w), polydispersity index (PDI), radius of gyration (R_g) and x value of K4M and G4 HPMCs as determined by SEC-MALS-RI.	117
Table IV. 3. Macromolecular features of the nine batches corresponding to the selected short chained HPMCs produced by enzymatic and acidic hydrolysis.	122
Table IV. 4. Data on the chemical composition of the starting HPMCs and of the nine selected batches.	125
Table IV. 5. Cloud point temperatures (C_{p0} and C_{p50}) as a function of the structural features of the selected polymers.	131

GENERAL INTRODUCTION

General introduction

Polymers are macromolecules constructed by a linkage between a certain number of small molecules generally called monomers or monomer units¹. Currently, those macromolecules are recognized as synthetic and bio-based polymers, which play an essential role in everyday life^{2,3}. Synthetic polymers are derived from fossil resources (petroleum) e.g. polyethylene, polystyrene, nylon, etc., and bio-based polymers are extracted or produced from renewable resources as plants, animals, algae, microorganisms, etc.

Bio-based polymers are divided into three main categories founded on their origin and production (Figure i)⁴. *Category 1* corresponds to polymers or pre-polymers directly extracted from biomass (e.g. polysaccharide, protein, and lipids). *Category 2*, polymers produced by synthesis of bio-based monomers (e.g. polylactic acid) and *category 3* are polymers produced by microorganisms or genetically modified bacteria (e.g. polyhydroxyalkanoates (PHA)).

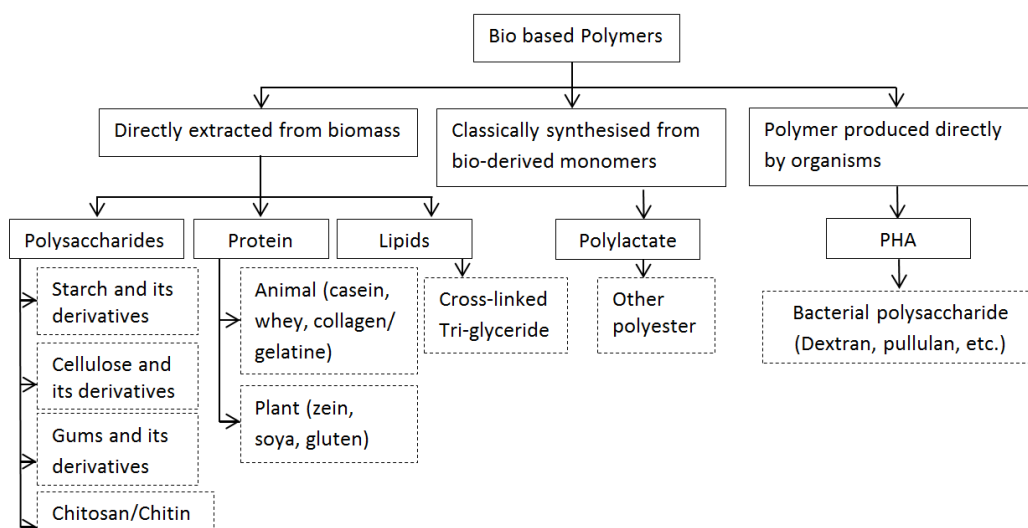


Figure i. Schematic presentation of bio-based polymers based on their origin and method of production⁴.

The high interest from several research areas on bio-based polymers is associated with their biodegradability, bioactivity, and easy availability. In contrast, petroleum-based polymers are toxic, not biodegradable, and their depletion leads to price volatility that became expensive^{5,6}. In this sense, several researchers used bio refinery concept to extract specific and functional organic compounds from renewable resources^{5,6}. Those compounds are suggested to replace synthetic polymers.

General introduction

Indeed, comparing natural and synthetic polymers, natural ones have poor thermal and mechanical properties. To enhance these properties, blends of two or more macromolecules such as natural/natural or natural/synthetic were established to create a new form of materials. These new materials are shown good mechanical properties and biocompatibility compared to those of individual polymeric components⁷.

On the other hand, during the past decades, nanoparticles have been introduced in several fields mainly for its original properties and greater surfaces area than the large particles. For example, nanoparticles are highly interesting on pharmaceutical fields. The reasons relate the protection of drugs from premature degradation, the control of drug release and the intracellular penetration^{8,9}. Therefore, the design of novel polymeric materials used for their preparation draws much attention in many research groups. These materials should be biocompatible, biodegradable, and easily functionalized^{9,10}. Thus, biopolymers such as polysaccharides are presented to fulfill all of these requirements.

In this sense, several researchers proposed to develop new techniques that lead producing refined polysaccharides, with well-defined molecular weight (M_w) and chemical composition¹¹. Besides, small fragments of polysaccharides are already used as building blocks in the preparation of nanoparticle^{12,13}.

The present study is focused on bio-polymers of category 1, more precisely on cellulose derivatives. It is very well known that cellulose is the most abundant natural polymer on the earth. Their non-solubility in water and common organic solvents has to be overcome to extend its application. Thus, cellulose derivatives such as cellulose ethers¹⁴ and cellulose esters¹⁵ have been prepared to provide solubility, flexibility, and processability.

Cellulose ethers are extensively used in many fields including applications in food, paint, textile, plastic, drug delivery, etc¹⁶. Recently, Akhlaghi et al.¹⁷ presented several polysaccharides including cellulose ethers as amphiphilic systems because they possess hydrophilic and hydrophobic moieties. The authors also revealed that the hydrophobic moieties in cellulose ethers are highly related to their properties such as thermos-responsive behaviors, high viscosity, and gel formation.

General introduction

The preparation and use of block copolymers for designing membrane materials with novel functionalities are one of the main research domains in our group. Thus, our goal in this project is to study the biotransformation of hydroxypropyl methylcellulose (HPMC, Figure ii) and the physicochemical characteristics of the obtained products in view of preparing short-chained polysaccharides that can be used further as building blocks to prepare novel polymeric architectures.

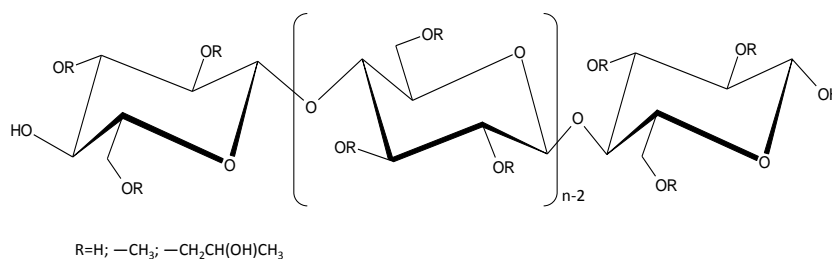


Figure ii. Simplified HPMC structure

This dissertation consists in six chapters. Chapter I presents an overview of bio sourced polymers (polysaccharide, protein and lipids (as prepolymers)), including bioconversion of biomass, their application in membrane and material field and a brief introduction of polysaccharide based block copolymers for their future and new applications.

Materials and description of experimental methods to depolymerize HPMC to prepare short-chained fragments and characterization techniques used in this study are provided in Chapter II.

Chapter III describes the enzymatic hydrolysis of HPMC using endo cellulases from *Trichoderma reesei* to produce short-chained building blocks. Herein, the experimental parameters including the nature of starting HPMC, reaction time and enzyme concentration were studied. A library of short-chained HPMC fragments with an average molar mass between 6000 and 46000 g mol⁻¹ is reported for the first time. On the other hand, HPMC fragments were also prepared by acidic hydrolysis for comparison.

Chapter IV presents the physicochemical characterization of the small fragments recovered after the partial depolymerization process (enzymatic and acidic). Chemical composition and macromolecular structure were determined by ¹H NMR and size exclusion chromatography coupled to a multi-angle light scattering detector (SEC-MALS), respectively. End group

General introduction

titration of reducing extremity was used to show their end functionality enabling further reaction for the preparation of block copolymers. HPMC exhibits phase separation ability and gelation property upon heating. The clouding point (Cp) temperature was determined by UV transmittance.

Chapter V focuses on the synthesis of block copolymers based on short HPMC chains. Two different approaches were studied. The first one consists in classical coupling of polysaccharide block and amine-terminated polymer chains through reductive amination (Figure iia). Thus, HPMC-*b*-polyether copolymers were prepared by reaction with hydrophobic Jeffamine® M-2005. In the second approach, thiol-ene click reaction was used to perform the coupling. In this case, thiolation of HPMC chains were first carried out using cysteamine by reductive amination and the obtained compounds reacted with ene-terminated polymers (Figure iib). HPMC-*b*-poly(lactic acid) (PLA) and HPMC-*b*-Jeffamine® M-2005 copolymers were prepared and characterized. Moreover, self-assembly and phase separation properties were studied by dynamic light scattering (DLS), transmission electron microscope (TEM) and UV transmittance.

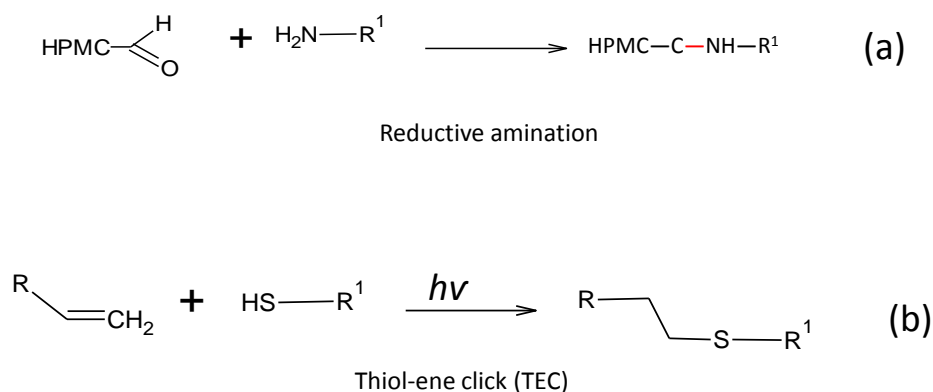


Figure iii. Schematic presentation of two routes of block copolymer preparation: (a) reductive amination and (b) thiol-ene click reaction.

Finally, Chapter VI summarizes the overall conclusions of this study and provides suggestions for future work.

REFERENCES

1. Odian, G., *La polymérisation-principes et applications*. Polytechnica: Paris, **1994**; p 823.
2. Matyjaszewski, K.; Tsarevsky, N. V., Nanostructured functional materials prepared by atom transfer radical polymerization. *Nat Chem* **2009**, *1* (4), 276-288.
3. McCrum, N. G.; Buckley, C. P.; Bucknall, C. B., *Principles of Polymer Engineering*. University Press: Oxford, **1997**; p 447.
4. Weber, C. J. *Biobased Packaging Materials for the food industry*. Frederiksberg, **2000**; p 69.
5. Imre, B.; Pukanszky, B., From natural resources to functional polymeric biomaterials. *Eur Polym J* **2015**, *68*, 481-487.
6. Zia, K. M.; Zia, F.; Zuber, M., *et al.*, Alginate based polyurethanes: A review of recent advances and perspective. *Int J Biol Macromol* **2015**, *79*, 377-87.
7. Iwasaki, N.; Yamane, S. T.; Majima, T., *et al.*, Feasibility of polysaccharide hybrid materials for scaffolds in cartilage tissue engineering: evaluation of chondrocyte adhesion to polyion complex fibers prepared from alginate and chitosan. *Biomacromolecules* **2004**, *5* (3), 828-833.
8. De Jong, W. H.; Borm, P. J., Drug delivery and nanoparticles: applications and hazards. *Int J Nanomedicine* **2008**, *3* (2), 133-49.
9. Peer, D.; Karp, J. M.; Hong, S., *et al.*, Nanocarriers as an emerging platform for cancer therapy. *Nat Nanotechnol* **2007**, *2* (12), 751-760.
10. Mizrahy, S.; Peer, D., Polysaccharides as building blocks for nanotherapeutics. *Chem Soc Rev* **2012**, *41* (7), 2623-2640.
11. Myrick, J. M.; Vendra, V. K.; Krishnan, S., Self-assembled polysaccharide nanostructures for controlled-release applications. *Nanotechnol Rev* **2014**, *3* (4), 319-346.
12. Schatz, C.; Lecommandoux, S., Polysaccharide-containing block copolymers: synthesis, properties and applications of an emerging family of glycoconjugates. *Macromol Rapid Commun* **2010**, *31* (19), 1664-84.
13. Bondalapati, S.; Ruvinov, E.; Kryukov, O., *et al.*, Rapid End-Group Modification of Polysaccharides for Biomaterial Applications in Regenerative Medicine. *Macromol Rapid Commun* **2014**, *35*, 1754-1762.
14. Collings, W. R.; De-Pree, L. Making Cellulose Ethers. US 2163869 A. June 27, **1939**.
15. Clarke, H. T.; Malm, C. J. Pcess of making cellulose esters and the products resulting there-from. US 2,084,685. July 28, **1936**.
16. Feller, R. L.; Wilt, M., *Evaluation of cellulose ethers for conservation*. J.Paul Getty Trust: USA, **1990**; p 149.
17. Akhlaghi, S. P.; Peng, B. L.; Yao, Z. L., *et al.*, Sustainable nanomaterials derived from polysaccharides and amphiphilic compounds. *Soft Matter* **2013**, *9* (33), 7905-7918.

CHAPTER I: BIBLIOGRAPHY

INTRODUCTION

As we introduced before, this research project had an objective to study the bio-transformation of hydroxypropyl methylcellulose (HPMC) and physicochemical characteristics of the obtained products in view of preparing short-chained polysaccharides that can be used further as building blocks to prepare novel polymeric architectures.

In this context, this literature search aims at giving an overview of recent studies related to bio polymers based materials within the sustainable polymer approach. This chapter is divided into four parts. First, physicochemical characteristics, availability, current and future trends in the use of bio-sourced polymers (polysaccharide, proteins, and lipids) are shown. The second part presents the application of polysaccharides in filtration and biomedical materials. Third, the formation of materials and biomaterials based on block copolymers is summarized. Finally, the methods to prepare short-chained polysaccharides which are the starting building blocks to design block copolymers are exemplified.

I.1. BIOSOURCED POLYMERS

The polymers extracted from the biomass (plants, animals, algae) correspond to the appellation of bio sourced, these are part of category 1 on biobased polymers (See Figure i). Based on their biodegradability, availability and low cost these polymers have gained a great attention in the material field. Therefore, polysaccharides, proteins, and lipids (as pre-polymer) can be used individually but also in blends and composites. Blends or composites are prepared to improve the properties and functionalities of the polymer itself, which consequently influences the materials properties and late their application.

For these reasons the study of the physical, chemical and structural features of biopolymers becomes necessary. In this section of the literature review, we will summarize the physicochemical characteristics of chemically modified biosourced polymers, beside their availability and their properties as a polymer. The first part is devoted to the presentation of polysaccharides and their derivatives (mainly cellulose and cellulose ethers), followed by proteins and finally lipids as a pre-polymer.

I.1.1. Polysaccharide and derivatives

Polysaccharides are polymeric carbohydrates composed along their chain of monosaccharides as monomers. Homopolysaccharides comprises only one type of monomer units like, for example, glucose units in cellulose. Complex structures also exist containing two or more types of monomers. Each monomer is linked by glycosidic bonds formed between the hemiacetal group of one monosaccharide and the hydroxyl group of another one (Figure I.1).

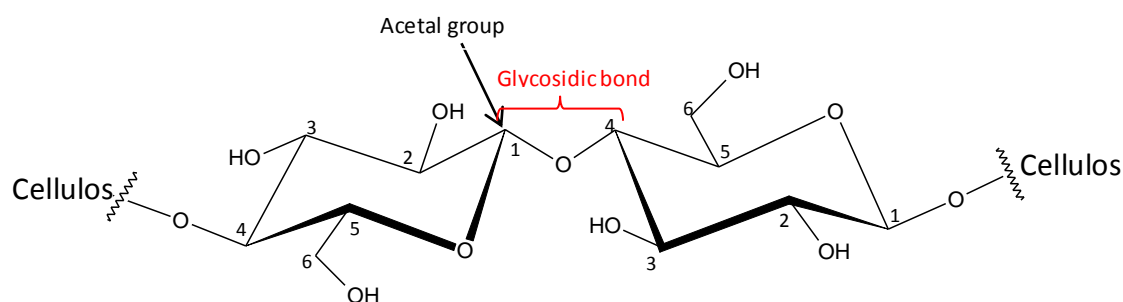


Figure I. 1. Glycosidic bond and Acetal group in cellulose.

Depending on their origin, various conformations such as helices and sheets are observed in their structure¹. As the main component of plant cell walls, polysaccharides are biodegradable and environmentally friendly materials.

In the plant kingdom, polysaccharides are recognized as an energy source (starch, guar gum) and plant support (cellulose, hemicellulose, pectin, agar and alginate). The animal kingdom also possesses polysaccharides which are recognized as support of skeleton (chitin), as physiological functions on the intercellular matrix (glycosaminoglycans) or as well as a source of energy (glycogene). Moreover, monera kingdom is used to synthesize several polysaccharides (dextran, gellan, pullulan, xanthan, scleroglucan).

Besides of their availability and low cost, those polymers present biological and chemical properties such as non-toxicity, biocompatibility, biodegradability, polyfunctionality, high chemical reactivity, chirality, chelation, and adsorption capacities². These properties have been largely demonstrated in the literature.

It was proposed that cellulosic material can be employed as reinforcing and bonding components into the fiber/thermoplastics interfaces, even in film preparation³.

Bioconversion of renewable lignocellulose materials to biofuels, provide an alternative source of energy to decrease the dependence on fossil-based materials⁴. The chemical modified polysaccharides, such as cellulose derivatives can be used to mimic many biological complexes⁵ or to prepare advanced materials⁶. These materials are proposed as delivery systems for anti-cancer drugs⁷, or as adsorbents in waste water treatment^{2,8}.

Thus, polysaccharides have become one of the most attractive biopolymers to prepare drug delivery materials, biomaterials and nanomaterials, etc. In the following section the cellulose, by far the most abundant polymer in nature and its derivatives are described.

I.1.1.1. Cellulose

Cellulose is a linear homopolymer consisting of repeat units of D-anhydroglucopyranose units (AGUs). As shown in Figure I.2, each glucopyranose unit is linked to adjacent units by β -(1-4) glucosidic bonds at the C1 and C4 positions⁹. This polymer is insoluble in water and common organic solvents due to the strong interaction between hydroxyl groups in position C3 and the ring oxygen atoms of the neighboring glucose unit and between the hydroxyl group of C6 and the oxygen bond of the glycosidic linkage¹⁰.

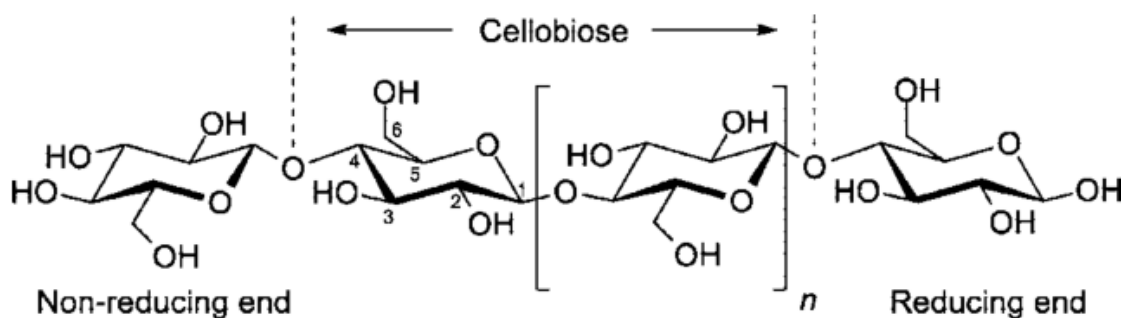


Figure I. 2. Cellulose polymer chain structure⁹.

The size of cellulose is given regarding its degree of polymerization (DP), i.e. the number of AGUs present in a single chain. However, conformational analysis of cellulose indicated that cellobiose (DP=2) rather than glucose is its basic unit¹¹. A number of 2 to 6 DP are called cello-oligosaccharides which are soluble in water, and from 7-13 are soluble oligoglucoses in hot water. A DP superior to 15 or 20 is part of insoluble glucosidic chains¹⁰.

Bibliography

There are three free hydroxyl groups per AGU at the C6, C3, and C2 in the cellulose chains¹². Adjacent AGUs are rotated approximately at 180° on its neighbor. This rotation causes cellulose to be highly symmetrical since each side of the chain has an equal number of hydroxyl groups¹⁰. On the other hand, hydroxyl groups at both ends of cellulose chain show different behaviors. One chain end of cellulose has a reducing hemiacetal group at the C1 position while the other end has an alcoholic hydroxyl (OH-) group on the C4 position⁹. The end of the chain at the C1 position is known as reducing end groups (REG), it can turn to an aldehyde which is highly reactive towards aqueous alkaline conditions¹³.

Cellulose chains are very stable and rigid due to β -(1-4)-linkers between each glucose units. Also, their stability is reinforced by intrachain hydrogen bonds between parallel chains (Figure I.3). In the natural state, about 40 to 70 cellulose chains are interconnected by hydrogen bonds between the C6 hydroxymethyl and the C3 hydroxy groups of the adjacent chains to form microfibrils⁹.

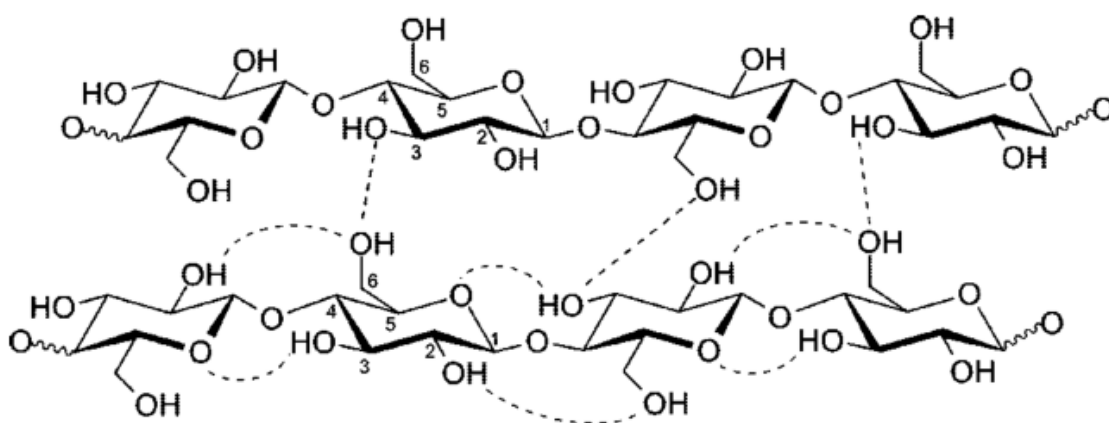


Figure I. 3. Intra and Intermolecular hydrogen bonds in cellulose chains⁹.

Cellulose microfibrils are alternated by order (crystalline) and disorder (amorphous) regions (Figure I.4)¹⁴. In the ordered regions, cellulose chains are tightly packed to form crystallites, as a result of a strong and very complex intra- and inter-molecular hydrogen bond interactions.

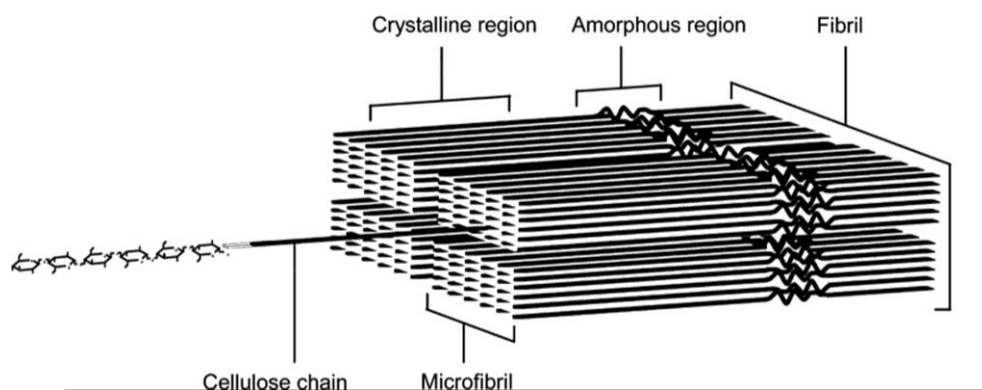


Figure I. 4. Scheme of the structure of cellulose fibrils¹⁴.

Crystalline zones in cellulose fibrils had been demonstrated by X-ray diffraction and polarized light optical microscopy¹⁵. It was shown that crystalline portions could be extracted via controlled acid hydrolysis, where amorphous regions are removed, leaving high ratio of crystals cellulose¹⁶. Several synonyms are used in literature, referring to cellulose nanocrystals: cellulose whiskers, cellulose nanowhiskers, nanocrystalline cellulose and microcrystalline cellulose. Depending on the source, the crystallinity can vary from 50-90%¹⁷.

Cellulose nanocrystal has been considered to be a potential reinforcement material in composite fabrication. However, their use has been limited by their low compatibility with the solvents and the polymeric matrix. In this sense, several methods based on surface modification were proposed^{18,19-20}.

The reactivity of cellulose was greatly enhanced by swelling treatment, acid degradation or as well mechanical grinding, which break down the crystalline conformation. On the other hand, 100 years ago, the solubility of cellulose was discovered. This finding was based on modifying free hydroxyl groups along the cellulose chain under strongly alkaline condition. Thus, cellulose nitrate and cellulose sulfate were the first two cellulose derivatives produced. To date, many other derivatives have been produced (ethers, esters, ionic, non-ionic, cationic, etc.), but only a few of them have gained commercial importance²¹.

To conclude this part, cellulose is an insoluble polymeric material, with a high percentage of completely crystalline structure whatever the source of cellulose. These intrinsic properties limit the pristine cellulose utilization in our objective of preparing short-chained

polysaccharides with DP in the range of 30 to 50. Therefore, we now propose to explore water-soluble cellulose ether derivatives.

I.1.1.2. Cellulose ethers

Cellulose ethers could consider as cellulose copolymer that containing modified AGUs, through the functionalization of lateral hydroxyl groups. The hydroxyl groups of AGUs can be partial or fully substituted. The chemical modification process is based on two steps:

a) alkaline swelling of the cellulose, a method in which the strong hydrogen bonds of micro crystalline cellulose are more or less disrupted by the formation of the so-called alkali cellulose:



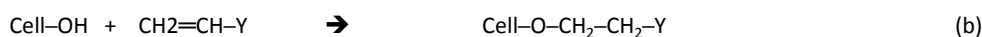
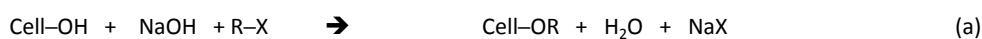
It should be noted that salinization mainly takes place at C2 and C6 position. Under strong alkaline conditions, the formed alcoholate ions are highly nucleophilic and can react with electrophilic alkyl halides or oxiranes. Besides, other methods were developed following the principles of green chemistry^{22,23,24}. However, classical method preparing alkali cellulose is preferred by the manufacturer of cellulose ethers.

b) Etherification, this reaction is expressed by the follow equation using alkyl halides:



Where: R' is an organic radical such as the methyl (CH₃-), ethyl (C₂H₅-), or a more complex structure²⁵.

Feller²⁵ also reported the preparation of mixed ethers. In this case, the reagents may be added simultaneously or in subsequent reaction steps. Thus, the author described three main industrial reaction types:



Bibliography

Reaction: a) describes the Williamson etherification where X can be a halide or sulfate. Unreacted NaOH is washed away after the reaction. b) Involve Michael-addition of Cell—OH to an activated double bond C=C by an electron-withdrawing group Y in the presence of a proton acceptor. And c) shows an alkali-catalyzed addition of an oxirane, this reaction may propagate further since new hydroxyl groups generated during the reaction²⁶. All these reactions are base catalyzed.

The average number of substituents per AGU is characterized by the degree of substitution (DS). DS values can vary between 0 and 3, however derivative products with a DS values below 0.1 and above 2 are insoluble in water²⁷. The reactivity of hydroxyl groups varies according to the reaction medium in which functionalization is done. E.g., etherification reactions in alkaline medium is C2 > C6 > C3, and C6 > C2 > C3 in non-aqueous solvents²⁸. The substituent can be of one type; or, a combination of different ether groups. Substitutions that generate new free hydroxyl functions can again be etherified and characterized by the molar substitution (MS)^{29,30}. Therefore, heterogeneous substituted cellulose derivatives can be produced. In contrast, homogeneous substituted cellulose derivative cannot be produced. The reasons are relate to the variation of the reactivity of OH groups in AGUs, as well their accessibilities in the amorphous and crystalline regions³¹.

Parameters such as chain length, type and distribution of substituent, DS, MS and its location in the AGU will determine the properties of cellulose derivatives^{26,32,33}. One of these properties is their sol-gel transition in water, which is highly related to the balance of the hydrophilic and hydrophobic substitutions³⁴.

Table I.1 provides a list of commercially available water-soluble cellulose ethers. Their properties such as thickeners, binders, film formers, water retention agent, surfactants and thermo-reversible behaviors play an important role in several industrial fields such as food, cosmetic, pharmaceutical, latex paints and construction³⁵. In our project, we are interested in polymers that exhibit thermoreversible behavior. Thus, we will focus on studying hydroxypropyl methylcellulose (HPMC).

Bibliography

Table I. 1. Industrial cellulose ethers, etherifying agents and their main application.³⁶

Cellulose Ether	Etherifying Agent	Application
Methyl Cellulose(MC)	Chloromethane	Building, Material and Surfactant
Carboxymethyl (CMC)	Chloroacetic Acid	Detergent and Food
Hydroxyethyl cellulose (HEC)	Ethylene oxide	Paint, Emulsion, Drilling
Hydroxypropyl (HPC)	Propylene Oxide	Paint an Tablets
Hydroxypropyl(methyl) (HPMC)	Propilene Oxide/Methyl	Paint, Tablets and Building

I.1.1.3. Hydroxypropylmethyl cellulose (HPMC)

This cellulose derivative also called hypromellose in INN (International Nonproprietary Name) nomenclature is a partially O-methylated and O-(2-hydroxypropylated) cellulose. There are HPMCs in various grades with different viscosities and extents of substitution. This polymer is considered as a neutral or nonionic polymer with high stability compared to ionic polymers or surfactants^{37,38}. Besides their biocompatibility and easy utilization in important formulations, HPMC presents particular interest for biomedical and healthcare applications.

HPMC has many different functions in drug formulation as a dispersing, emulsifying, foaming, solubilizing, stabilizing, suspending and thickening agent. Also, HPMC can be applied as controlled-release and sustained-release agents^{39,40}. Moreover, their aqueous solution seems presents greater clarity and fewer undissolved fibers compared with methylcellulose. On top of that, HPMC prevents droplets and agglomeration of particles to avoid coalescence effect.

Another important property of HPMC is their thermoresponsive behavior, where the polymer solubility decreases with increasing temperature above a Lower Critical Solution Temperature (LCST). LCST is the phase separation process from solution to solidification above a certain temperature in thermoresponsive hydrogels³⁴. Thus, thermoresponsive polymer shows transparent solution below the LCST temperature, and above LCST, the polymer becomes hydrophobic and insoluble leading to gel formation^{41,34}. This phenomenon is governed by the balance between hydrophilic and hydrophobic moieties in the polymer chain^{42,43}. Furthermore, the gelation of such a system is coupled to an increase in turbidity (Clouding point (Cp) temperature) due to phase separation. Therefore, depending on the

authors, C_p is defined as the intercept between the 100 % of transmittance of the transparent solution and the slope of the decrease of transmittance⁴⁴, or as the temperature at which light transmission reaches a 50% value⁴⁵, or half C_p measured when the transmittance reaches 96%⁴⁶.

Fairclough *et al.*⁴⁴ hypothesized that to raise the solubility of the polymer, water molecules at a low temperature form a cage structure around hydrophobic segments. And when the temperature increases, hydrogen bonds become weaker, and the cage structure is sufficiently disrupted at the gelation temperature that facilitate the phase separation.

In this research work, we are interested in playing with thermosensitive and gelation properties by using short-chained HPMC and subsequently by combining the prepared compounds as building blocks in block copolymer preparation.

I.1.2. Protein

Proteins are bio-sourced macromolecules which are built by monomer units called amino acids. In nature, there are 21 different amino acids. The amount and sequence govern the functional properties for each protein⁴⁷. The chemical structure in amino (NH_2) and carboxyl (COOH) groups of amino acids can be compared to synthetic polyamide that is a polymer containing monomers joined by peptide bonds. Thus, it is assumed that the protein structure could be used to form different kinds of materials like polyamides.

Their physicochemical properties are organized according to the hierarchy of the structure: primary, secondary, tertiary and quaternary structures (Figure I-5). Quaternary or native structure of proteins is stabilized by several interactions such as:

1) *electrostatic interactions*, where acidic (Aspartic acid, Glutamic acid) and basic (Lysine, Arginine, Histidine) amino acids are attracted.

2) *hydrogen bonds*, occurring when hydrogen is shared between two highly electronegative atoms ($\text{N}-\text{H}\cdots\text{O}$). The presence of high concentration of Asparagine and Glutamic acid allows a high degree of H-bond⁴⁸.

3) *disulfide bonds*, (S-S covalent bonds) arising when the SH groups of two cysteine residues are covalently linked by oxidation.

4) *hydrophobic interaction*, is particularly important for protein stability. In globular proteins, most hydrophobic amino acid residues are arranged in the interior of the structure in the native conformation, while the polar amino acids are mainly found on the surface⁴⁹.

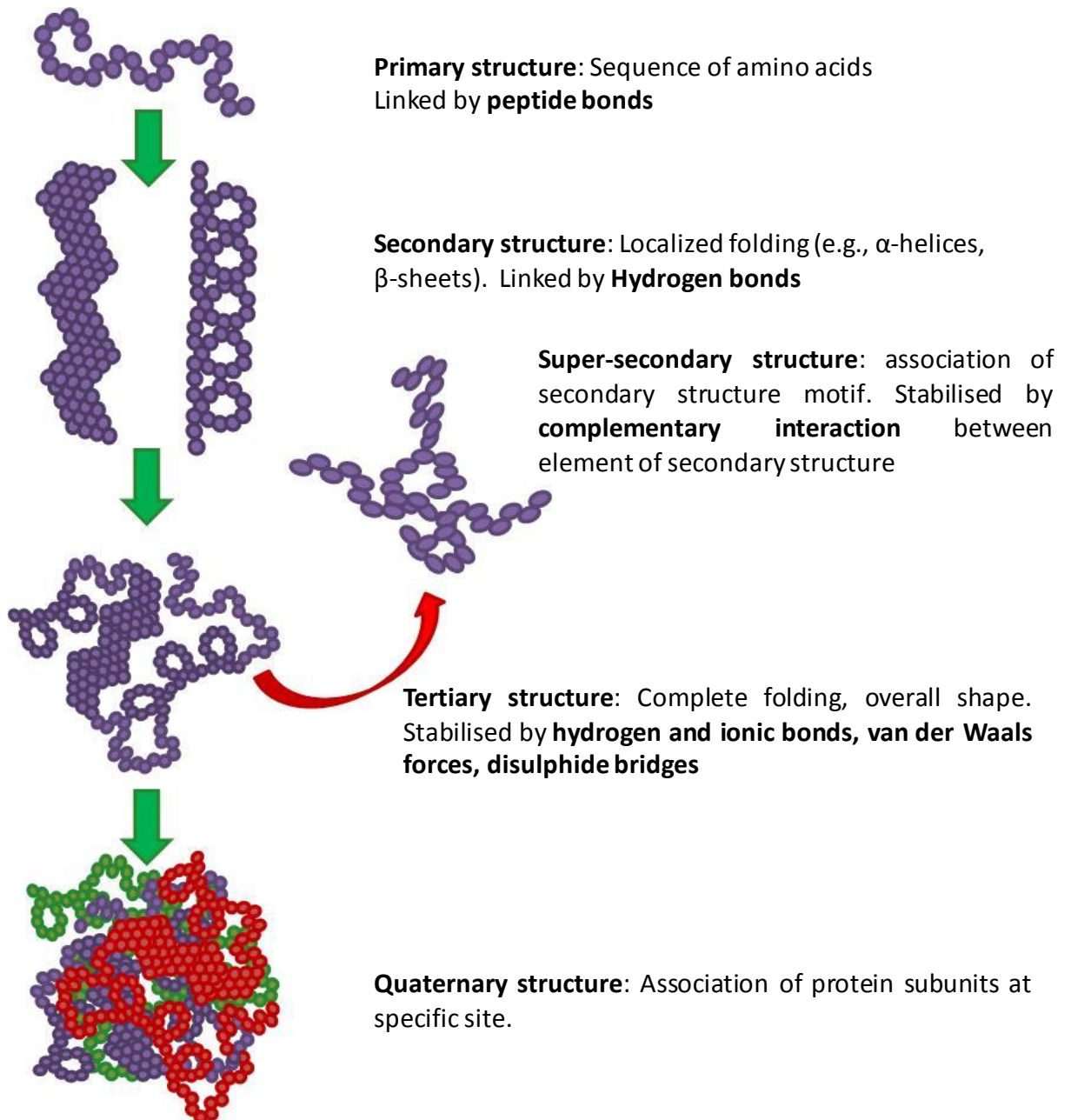


Figure I. 5. Scheme of protein structures adapted from Owusu-Apenten⁴⁸ and Darryl⁵⁰.

The native structures sometimes limit their utilization (i.e. depletion of protein structure enhances their functionality). Therefore, several mechanisms (chemical, physical, thermal,

enzymatic) have been developed to unfold proteins. These unfolding processes based on the loss of quaternary, tertiary and secondary structure are called denaturation⁵¹. Consequently, unfolded proteins expose its active sites that enhance their functional and active properties.

I.1.2.1. Functional properties

The functional properties of proteins are based on three effects:

1) **Hydration properties** related to the protein-water interactions that lead to wettability, dispersibility, swelling and solubilization. These effects play an important role in gelation, viscoelasticity and water holding capacity of proteins^{48,52}.

2) **Protein interactions** reflect the tridimensional structure formation, e.g. gel, dough, fiber, material, and biomaterial formation. The unfolding process leads exposing various interaction forces (disulfide bridges, electrostatic attractions, hydrogen bonds, hydrophobic and van der Waals) which will play an important role in the mechanism of network formation^{53,54,55}.

It should be noted that hydrophobic interaction could have adverse effects due to the possible occurrence of aggregation and precipitation phenomena.

3) **Surface properties**, based on the presence of charged groups in the protein side chain, and on the hydrophilic or/and hydrophobic amino acid sequences⁵⁶. This property gives the ability to adsorb at the oil-water interface and form stabilizing layers around oil droplets⁵⁷; this effect is recognized as emulsion⁵⁸.

I.1.2.2. Extraction process

Proteins are categorized in function of their purity during the extraction process; thus isolated protein (purity over 90 %) and concentrated protein (around 60-85 %) can be recovered⁴⁷. The Classical method is based on alkali dissolution and acid precipitation in relation to the isoelectric point^{59,60}. This process may influence the conformational and functional properties, such as stability, surface hydrophobicity, and surface/interfacial activity^{61,62}. Thereby, in the past years, the exigencies to obtain proteins with high purity and good functional properties lead to search process with a minor impact on the protein structure and more environmentally friendly^{63,64}.

I.1.2.3. Developments and uses

In the past decades, much research effort has been undertaken to use plant or animal proteins for packaging application in food industry. Thus, films and/or coatings materials have been developed mainly due to their excellent gas barrier properties. The production of those films follow three principles: 1) the rupture of intermolecular bonds that stabilize polymers, 2) the arrangement and orientation of polymer chains, and 3) the formation of three-dimensional network stabilized by new interaction^{65,66,67}.

Thus, food packaging materials are prepared using a different source of proteins. The formulation of these materials is in function to the protein concentration. The ranges are between 5-20 % of the protein and the pH value adjusted as a function of the protein type to break down the inter-chain interactions⁶⁸⁻⁷⁴. Then, heating and drying processing of the filmogenic solution give rise to a stiff and brittle film due to strong protein-protein interactions. Therefore to solve this drawback and enhance the mechanical properties of obtained films, the addition of plasticizer between 10-60 % in protein formulation was proposed⁷⁵⁻⁷⁷.

Recently, the new formulation has been developed, first to diminish the hydrophilic nature of protein film. Thus, protein was blended with certain additives such as lipids⁷⁸⁻⁸¹, polysaccharides⁸²⁻⁸⁴ and inorganic polymers^{69, 85-86}. A second approach has been proposed to improve density and mechanical properties of the film structure using cross-linking agents⁸⁷⁻⁹².

Proteins have also been applied to the development of a large variety of materials as drug coating⁹³⁻⁹⁴, biomaterial for biomedical application⁹⁵⁻⁹⁶, electrospun fibres⁹⁷⁻⁹⁸, plastic mulch film for agriculture industries⁹⁹, plants containers¹⁰⁰, foam plastic to produce automobile part¹⁰¹⁻¹⁰², membranes for ethanol permselectivity¹⁰³, dynamic materials¹⁰⁴⁻¹⁰⁶, polyelectrolyte multilayer (PEM) films¹⁰⁷, bilayer scaffolds, tissue engineering; composite gels to tissue regeneration, and nanofibrous membrane¹⁰⁸.

From the previous literature search, it appears that protein can be the choice for making biomaterials. Their thermo form and high functional properties could impart new challenge

for the material preparation, by coupling: protein-polysaccharide, protein-lipids or protein-inorganic polymer as well. Therefore, we can mention that plant or animal protein with specific polypeptides sequences could be used in new architecture building blocks synthesis.

In the same way, several authors mentioned that mimicking fibroin, keratin, and elastin structures could be a way to prepare flexible, resistant and hydrophobic materials¹⁰⁹. On the other hand, bioactive peptides with a particular sequence show biological function in living organisms. These peptides could insert into biomaterials for biomedical or cosmetics applications.

I.1.3. Polymers from lipids

Vegetable oils, from edible to drying oil are a rich source of polymer precursors that can be modified to exhibit various types of functionalities, leading to new materials with a wide range of properties from structural to functional (Figure I.6)¹¹⁰. Several research works have already been published reflecting the international efforts to use these natural products to produce novel polymers and polymer precursors enlarging the range of potential application¹¹¹⁻¹¹⁴. Triglyceride molecules can be modified through hydrolysis or transesterification by reacting unsaturations present in the fatty acid chains. This reaction leads to a large variety of functionalized molecules, with those containing epoxy or hydroxyl groups being probably the most popular choice.

Vegetable oils are categorized as a function of their iodine value which is a measure of the degree of unsaturation. Vegetable oil are then classified as “drying” (iodine value >130, “semi-drying” (100>iodine value<130) and “non-drying” (iodine value <100). Usually, drying or semi-drying oils are used in surface coatings¹¹⁵. Non-drying oils find a wide variety of industrial uses in soaps, cosmetics, lubricants, leather dressings, candles, etc.

Currently, several precursors such as epoxy, alkyd, polyurethane are commercially available for specific applications¹¹⁰.

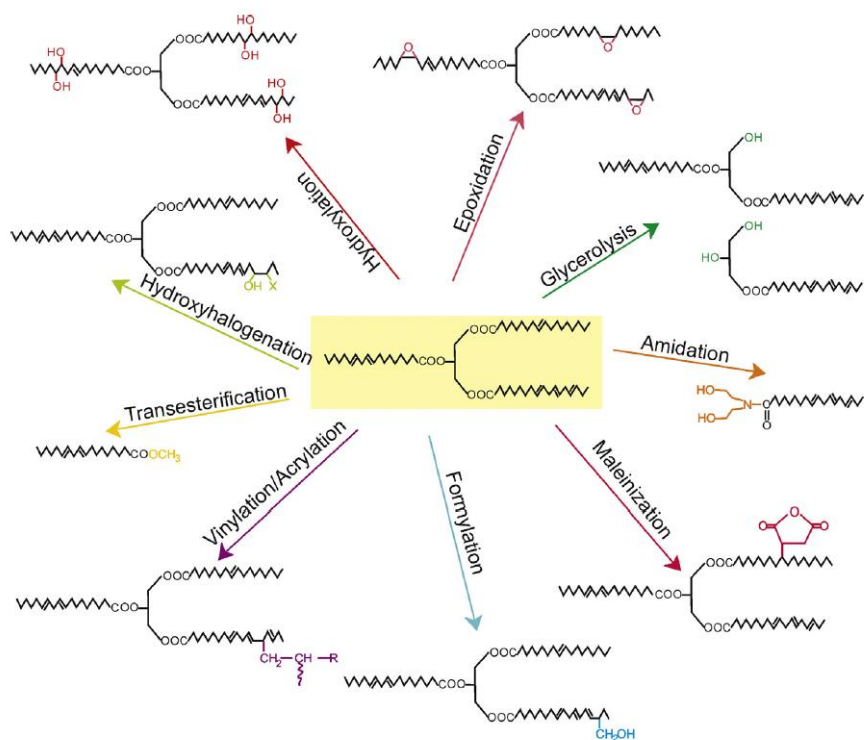


Figure I. 6. Chemical reactions of vegetable oils¹¹⁵.

I.1.3.1. Future trends/ Applications:

Plant oil has already shown their versatility as sources for polymers and precursors^{111, 116-117} or as well to form a hyperbranched structure to improve the dispersion of the carbon nanotubes (CNTs)¹¹⁰. Oil based polymers are also used to prepare composite matrices (organic or inorganic)¹¹⁸⁻¹¹⁹, thermosetting materials¹²⁰.

Applications of vegetable oil based polymeric materials are not restricted to the industrial arena and can also extend to a variety of biomedical applications as surgical sealants and glues, pharmacological patches, wound healing devices, drug carriers and scaffolds for tissue engineering¹¹⁸. The interest on vegetable oil relates to its biobased and biocompatible properties.

In principle, the production of renewable oils and monomers has been demonstrated to be technologically feasible and capable of substituting petrochemical feedstock.

CONCLUSION

Renewable resources provide variable new structures as thermosetting materials. Polysaccharide, proteins, and plant oil based polymers show their availability and reactivity functions which could be used to reach acceptable properties for the resulting thermosetting materials.

On the other hand, bio-sourced polymers have several reactive sites such as hydroxyl, acetamino or amino, aldehyde, ester, etc. These functions can be taken advantage to prepare biomaterials suitable for any given application.

I.2. POLYSACCHARIDE BASED FILTRATION AND BIOMEDICAL MATERIALS

As shown above, polysaccharides structures present a large number of hydroxyl groups and one aldehyde group at the end of their chain. These reactive groups reflect chemical stability and high reactivity of the polymer. Therefore, polysaccharides became interesting feedstock for material preparation, such as membrane filtration, and most recently into biomaterials such as tissues engineering scaffold.

The next part of our bibliography review introduces polysaccharide based membranes and biomedical materials.

I.2.1. Polysaccharide based membrane materials

Based on their excellent filmogenic and mechanical properties, polysaccharides were used for the first time by Fick in 1855, who prepared a membrane using a cellulose derivative (nitrocellulose)¹²¹. Since then, cellulosic membrane materials have been developed. Today, numerous grades of porous and dense membrane based on cellulose ester are commercially available mainly for ultrafiltration, dialysis, and reverse osmosis process.

The membrane is defined as a selective barrier between two phases¹²². A membrane can be homogeneous or heterogeneous, symmetric or asymmetric in structure, solid or liquid. It can carry positive or negative charges, be neutral or bipolar. The transport through a membrane can be affected by convection or by diffusion of individual molecules, induced by an electric field, concentration, pressure or temperature gradient. The membrane thickness may vary from as small as 10 microns to few hundred micrometers¹²³. They can be classified in

Bibliography

isotropic, anisotropic, ceramic, metal and liquid membranes. The main types of membranes are shown schematically in Figure I.7.

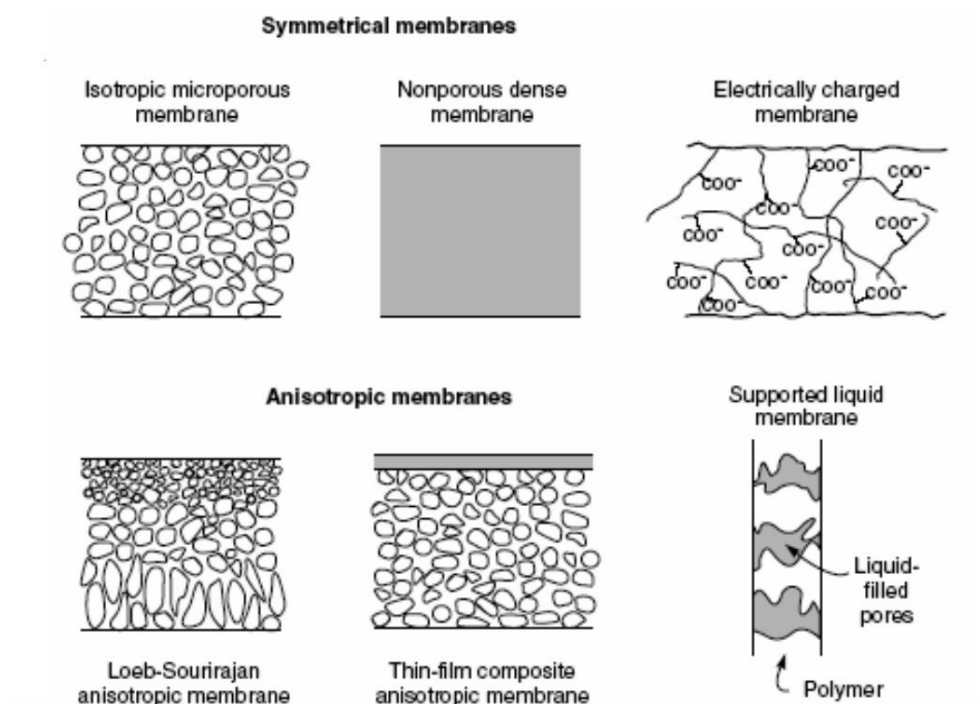


Figure I. 7. Schematic diagrams of main types of membranes¹²⁴.

According to their pore size, pressure-driven-membranes are established in typical filtration process. e.g. microfiltration (MF) with pore size range from 0.1 to 10 μm , ultrafiltration (UF) from 2 to 100 nm, nanofiltration (NF) lower than 2 nm and reverse osmosis (RO) in which there is no permanent pore size (dense membrane). In such dense membranes, the transport of molecules is described in terms of solubility and diffusivity¹²², mostly studied for gas or vapor separation.

The membrane processability and performance are highly related to the **membrane material** which refers to the substance from which the membrane itself is made and to the **morphology** of the obtained membrane. The polymeric membranes with more than 80 % of the total market can be made from synthetic or natural macromolecules. Obviously, the physical and chemical matrix properties of membrane such as the physical strength, its resistance to temperature and chemicals and its biocompatibility are in relation at the efficiency of the filtration system. On the other hand, the membrane structure, transport and separation properties are determined by techniques and conditions under which membrane is produced (porous vs. non porous, homogeneous vs. asymmetric)¹²².

Among natural biobased membrane matrix, polysaccharides offer certain advantages over existing synthetic polymers in ultrafiltration process: 1) increase in flux while maintaining the same rejection ratio; and 2) low fouling due to the smooth hydrophilic active layer, thereby reducing particulate clogging and adsorption of hydrophobic materials¹²⁵.

The membrane media is manufactured as flat sheets or as hollow fibers and then configured into membrane modules as explained below.

I.2.2. Method of membrane preparation

A number of different techniques are available to prepare membranes.¹²² Casting followed by solvent evaporation is used mostly to prepare **dense** or **nonporous membrane**. Compressing membrane material at high temperature is used to prepare **microporous membrane**. A **porous membrane** can be prepared through 1) making the composite membrane, 2) or phase inversion techniques.

1) Composite membrane can be prepared using two or more different materials. Those materials are deposited layer by layer, and their selectivity is determined by the thin top layer. Several coating procedure such as dip coating, or another type of polymerization such as plasma, interfacial, in-situ polymerization are available to prepare composite membranes.

2) Phase inversion is a process where the polymer in solution is converted in the solid phase by demixing effects. Several techniques lead to reach phase inversion process. Thus, a) temperature induced phase separation (TIPS), b) reaction induced phase separation (RIPS), and c) diffusion of non-solvent induced phase separation (DIPS) are techniques to prepare porous membrane¹²⁶.

I.2.3. Polysaccharide based flat sheet membranes

This type of membrane is prepared mainly by inversion method. A flat sheet membrane is prepared when the polymer solution is cast as a thin film on a support (glass plate or non-woven paper) with a casting knife, and then the film is immersed in a coagulation bath that contains a non-solvent for the polymer. Consequently, a phase inversion takes place¹²⁷.

Bibliography

Since a long time regenerated cellulose and its derivatives (nitrocellulose and cellulose acetate) have been used to produce membranes with different pore size going from MF to RO for such applications as desalting, water depollution, as well as separation of solutes¹²⁸. As a recent example, cellulose acetate solubilized in two nonvolatile solvents (N-methyl-2-pyrrolidone (NMP) and γ -butyrolactone) generates porous membranes by a demixing process after coagulation in water¹²⁹. Besides, composite and surface modification can result in improved membrane performances¹³⁰⁻¹³². Another recent approach consists in solubilizing cellulose in ionic liquids that allows combine two principles of green chemistry i. e. environmentally-friendly solvent and bio-renewable feedstock¹³³.

Chitosan is another polysaccharide that can be used to produce membrane. In that case, dense membranes are prepared with application in pervaporation of gas permeation. So far, chitosan based membrane has been shown to have a good permselectivity in water/ ethanol solution¹³⁴. The authors described that the addition of crosslinkers as glutaraldehyde increases the permeation rate. This effect is related to the reaction of glucosamine units with the aldehyde group of the crosslinkers agent to form a bridge between two chitosan fibrils (Figure I.8).

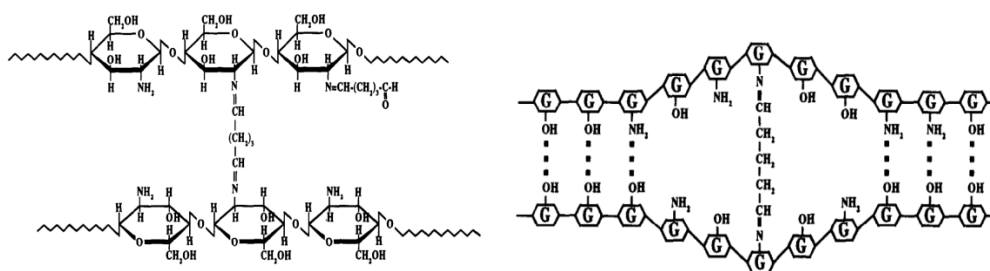


Figure I. 8. Reaction of chitosan and glutaraldehyde¹³⁴

Composite membranes were also investigated for their use in pervaporation and adsorptive process. Meireles and coworkers¹³⁵ obtained good ethanol dehydration using a composite microbial polysaccharides membrane. The authors used polyethersulphone (PES) as support for the active polysaccharide layer¹³⁵ (Figure I.9).

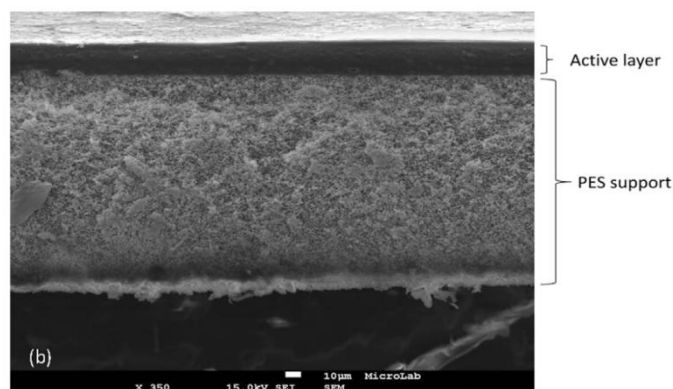


Figure I.9. Cross-section images of the composite membranes prepared from purified polysaccharide¹³⁵.

On the other hand, ultrafine cellulose nanofibers were employed to prepare new class of thin-film nanofibrous composite (TFNC) membranes⁹⁴. TFNC membrane has 10-fold higher permeation flux than commercial polyacrylonitrile membranes, for ultrafiltration of oil/water emulsion^{125,136}. Another type of composite polysaccharide membrane composed by positive chitosan, negative hyaluronic acid, and konjac glucomannan, where studied for biomedical applications¹³⁷.

I.2.4. Polysaccharide based hollow fiber

Porous hollow fibers are prepared using a viscous polymer solution which is pumped through a spinneret and at the same time, a bore liquid (mainly consisting in a polymer non-solvent) is injected through the inner tube of the spinneret. The polymer solution and the bore fluid are extruded into an external non-solvent coagulation bath to form hollow fiber¹²².

The first polysaccharide hollow fiber membrane was prepared by Pittalis *et al.*¹³⁸. This hollow fiber membrane was studied in UF and dialysis processes. In addition to the application in water treatment above-reviewed for flat-sheet membranes, hollow fibers have also been considered as an adsorptive membrane which has been developed to remove contaminants such as heavy metals and humic matters. For instance, chitosan/cellulose acetate blend hollow fiber has been studied for copper ion adsorption¹²⁷, (Figure 1.10). In that case, the $-NH_2$ group of chitosan chains act as heavy metal ion chelator.

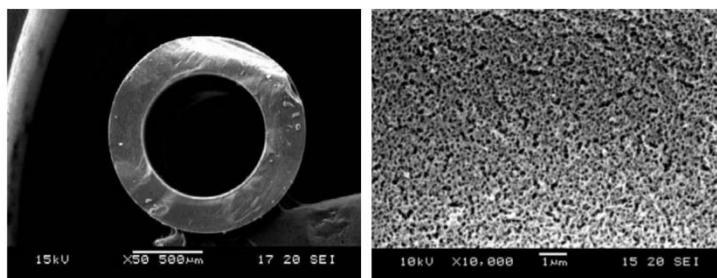


Figure I.10. Cross-sectional and overall morphology of chitosan/cellulose acetate hollow fiber membrane¹²⁷.

Those composite membranes were also showed higher efficiency for the removal of dyes compounds such as Victoria Blue (98%)¹³⁹ and high extraction efficiency (80-90 %) toward silver (Ag) and gold (Au)¹⁴⁰.

On the other hand, polysaccharide-poly(vinyl alcohol) (PVA) hydrogel graft materials were studied as a removal of toxic and carcinogenic arsenic (Ar) as well of heavy metals (Mn²⁺, Cu²⁺, Fe³⁺, Ni²⁺, and Pb²⁺) from contaminated water⁸. They also mentioned that the polysaccharide analogous showed affinities toward the metal ions according to the decreasing order: Fe³⁺ > Mn²⁺ > Cu²⁺.

1.2.5. Polysaccharide based biomedical materials

Polysaccharides are used to prepare biomedical materials due to their thermo reversible and biocompatible properties. The most studied polysaccharides in this field are cellulose derivatives, chitosan, alginate, agarose, glycosaminoglycans, gellan gum and starch¹⁴¹. These polymers are using alone or blended with other organic compounds such as protein and lipid based polymers.

A biomedical material shows an appropriate host response with minimal or no immune response and any inflammation. These materials also promote cell adhesion and proliferation in the case of tissue-engineering product¹⁴².

Following this approach, a large number of nonionic cellulose ethers e.g. hydroxypropylmethyl cellulose (HPMC) was applied as binders or coating material to protect

Bibliography

active drugs¹⁴³ or as well as to deliver anti-cancer drugs⁷. Microbial cellulose was also used for burns treatment¹⁴⁴. Polysaccharides as chitosan could also be applied for cartilage repair in clinical setting¹⁴⁵.

Furthermore, biodegradable porous scaffold made from starch and polycaprolactone were able to maintain a normal expression of endothelial cell-specific genes and proteins, indicating a potential application in vascularization process associated with bone tissue engineering¹⁴⁶. Alginate-based chitosan polymer fiber showed good adhesion capacity with chondrocytes in comparison with alginate polymer fibers¹⁴⁷.

Another important application in the biomedical field concerns nanoparticles. Nanoparticles can be classified as amphiphilic systems as they possess hydrophilic and hydrophobic moieties that are responsible for their self-organization behavior¹⁴⁸. Thus, nanosized and stable chitosan-g-PEG/heparin polyelectrolyte complex micelles were prepared by a self-assembly process¹⁴⁹ (Figure I.11). These polyelectrolytes assembly promotes the apoptotic death of cancer cells.

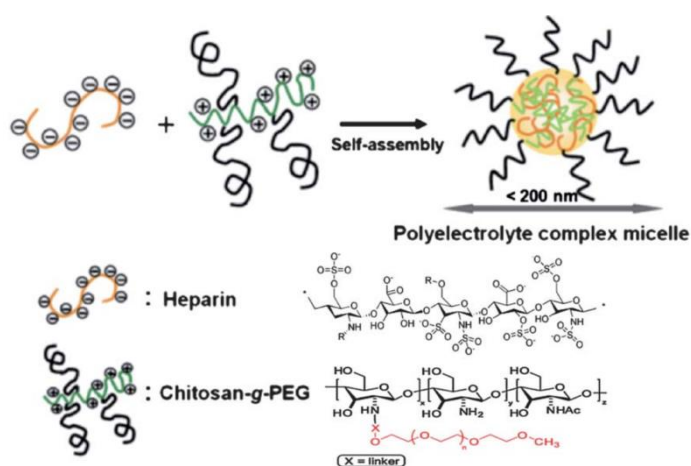


Figure I. 11. Schematic polyelectrolyte formation between polyanion and mPEG-g-Chitosan¹⁴⁹.

On the other hand, nanoparticles are used as agents for diagnosis of various diseases. Currently, dextran-coated superparamagnetic iron oxide nanoparticles (Dextran-SPION (DS-SPIONs)) are clinically available as magnetic resonance imaging contrast agent for diagnosis of various diseases. In order to prepare Dextran-SPIONs, a double hydrophilic DS-*b*-PolyGlycidylMethAcrylate (PMGA) block copolymer comprising a DS block as a ligand for

macrophage activation and a PGMA block as a robust attachment on the surface of SPIONs¹⁵⁰ (Figure I.12).

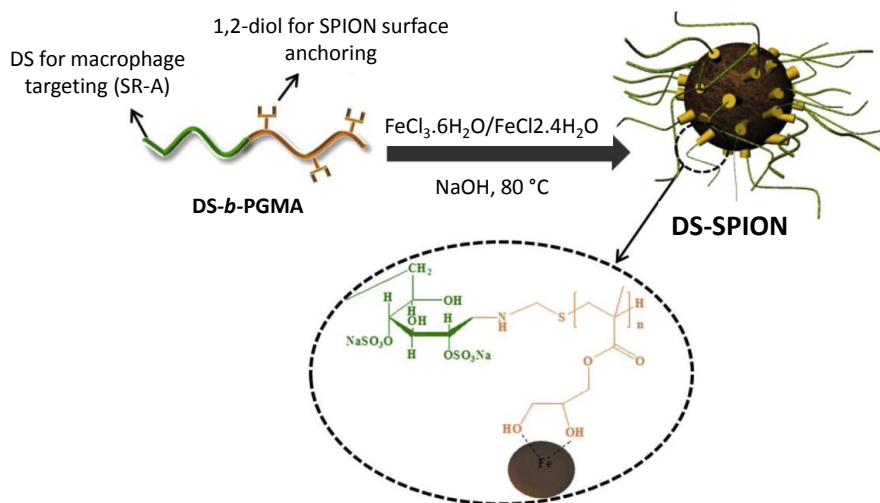


Figure I. 12. Illustration of interactions between 1,2-diols of DS-b-PGMA and the SPION iron atom¹⁵⁰.

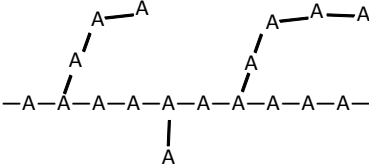
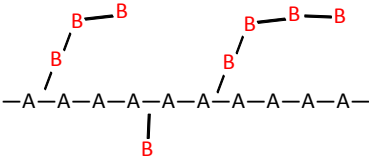
This review provides insights in potential applications of polysaccharides as a macro, micro, and nanostructure in many fields. On the behavior of biomacromolecules and amphiphilic compounds, the driving forces controlling the interaction between these two systems can be manipulated to achieve desired characteristics and physical properties.

I.3. POLYSACCHARIDE BASED BLOCK COPOLYMERS

From the structural point of view, the polymer is organized as linear and non-linear structure (Table 1.2). Linear structure is divided in four sub groups, namely homopolymer (poly(A)), block copolymer (poly(A-b-B)), alternating copolymer (poly(A-*alt*-B)) and statistical copolymer (poly(A-*stat*-B). The non-linear group includes branched homopolymer and graft copolymer (poly(A-*g*-B))¹⁵¹. It should be noted that more than two monomers can be involved generating more complicated structures.

Bibliography

Table I. 2. Composition/Organization copolymer structures ¹⁵¹.

Type	Polymer type	Nomenclature	Structure
Linear polymer	Homopolymer	poly(A)	—A—A—A—A—A—A—A—A—A—A—
	Block copolymer	poly(A- <i>b</i> -B)	—A—A—A—A—A—A—B—B—B—B—B—
	Alternating copolymer	poly(A- <i>alt</i> -B)	—A—B—A—B—A—B—A—B—A—B—
	Statistical copolymer	poly(A- <i>stat</i> -B)	—A—B—A—A—A—A—B—B—A—B—A—
Non-linear polymer	Branched polymer	—	
	Graft copolymer	poly(A- <i>g</i> -B)	

All the polymer structures shown in Table I.2, present their specific physicochemical properties. Hence, we are focusing on linear block copolymer organization.

The interest of block copolymer structures is based on their self-assembly behavior. This type of materials has emerged recently, as a very attractive method for the fabrication of functional nanostructured materials¹⁵²⁻¹⁵⁴ and as a new generation for lithography and semiconductor applications¹⁵⁵⁻¹⁵⁷. In this context, tremendous effort has been devoted during the past decades exploring engineering macromolecules of polymer chains, preparing different shapes (stars, cylindrical micelles, vesicles, etc.) and investigating the various possibility of nanostructure morphology.

In the following section, we summarize first the techniques used to synthesize block copolymers, their properties, and applications. In the second part, the use of polysaccharide as building blocks is presented.

I.3.1. Block copolymers

Block copolymers are macromolecules constructed by two or more distinct homopolymers linked end to end through covalent bonds¹⁵⁸. The number of blocks and the arrangement in their structure determine the molecular architecture (Figure I.13). Thus, two, three, and more blocks are called diblock, triblock, and multiblock. Their topology can be linear (blocks connected end-to-end) or stars (blocks connected via one of their ends at the single junction)^{153, 159}. More complicated arrangements like brushes, miktoarm stars or H-shape, are also possible¹⁶⁰. Various schematic arrangements of block copolymers are presented in Figure I.13.

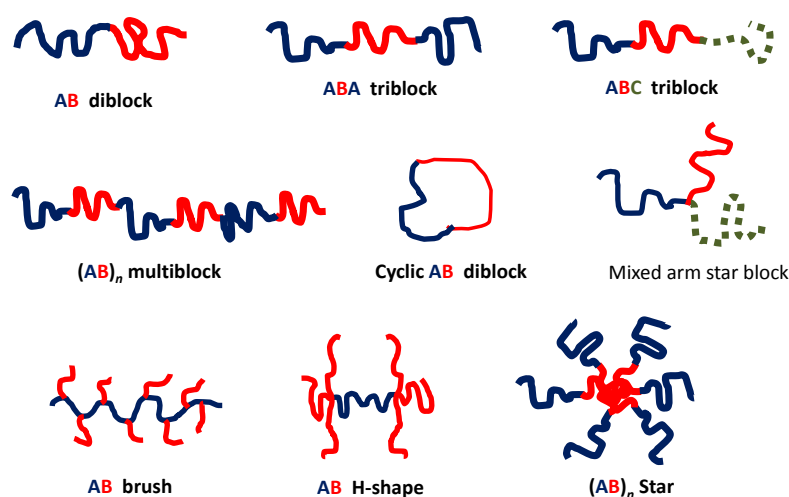


Figure I. 13. Some possible structure organizations of block copolymers^{153, 159-160}.

A number of different chemical reactions may be used to synthesize block copolymers. These include esterification, amidation, the formation of urethanes, aromatic substitution, etc. Polymerization usually proceeds by the reaction between two different functional groups, e.g. hydroxyl and carboxyl groups, or amino and aldehyde. Another more popular way consists in constructing polymers of the desired length by controlled radical polymerization.

I.3.2. Synthesis

Chain-growth polymerization has been successfully performed during the past decades through conventional ionic, radical, metal-catalyzed olefin metathesis and ring opening metathesis polymerization (ROMP) techniques^{154, 161-162}. These polymerization techniques

enable control over the polymer architecture, functionalities, and composition¹⁶³. In the 90s years, Controlled Radical Polymerization (CRP) was highly developed as a fundamental technique in polymer synthesis field by using three different approaches:

- Atom Transfer Radical Polymerization (ATRP)
- Reversible addition/ Fragmentation Chain Transfer Polymerization (RAFT)
- Nitroxide-Mediated Polymerization (NMP)

These techniques are governed by the equilibrium between a propagating radicals and dormant moieties¹⁶³. Polymers generated by CRP are used in many applications such as surface modification (commonly performed through ATRP), block copolymers for bio-applications (performed through RAFT and ATRP), and NMP techniques are used in pigment dispersion, memory devices, composite manufacturing¹⁶⁴.

A comparison between CRP techniques revealed one advantages of ATRP over RAFT and NMP techniques. ATRP could be preferred to prepare more purified block copolymers^{153, 163}. Besides, the amount of metal complex compound used as a catalytic in ATRP techniques was reduced to a few ppm. This action leads easy purification of the obtained polymers.

Currently, several controlled polymerization techniques are available to design new smart macromolecules, which can be analogs to the natural block polymers.

I.3.3. Structure of self-organization

In the following section, the self-organization of block copolymers in solution (micelles, cylindrical micelles, vesicles) and in bulk phases is described.

Self-assembly involves the formation of hydrophobic (in contact with a non-polar solvent or surface if applicable) and hydrophilic domains (in contact with water or another polar solvent or a hydrophilic surface)¹⁶⁵. Thus, well-defined amphiphilic block copolymers undergo self-assembly in aqueous solution. The morphology of block-copolymer self-assembly results from the inherent molecular curvature and their influence to packing copolymer chain¹⁶⁶.

I.3.4. Self-organization in solution

Block copolymers in a solvent that are selective for one of the block exhibit self-assembly behaviors¹⁶⁶⁻¹⁶⁷. As a consequence of their chemical conformation, diblock copolymers form a super-molecular aggregate, such as micelles, monolayer, bilayer, and vesicle organization (Figure I.14).

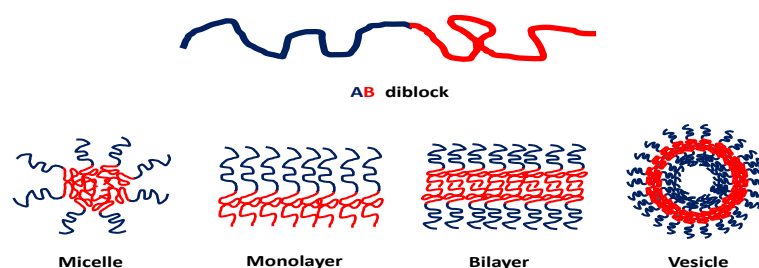


Figure I. 14. Aggregation morphology of linear diblock copolymers^{165, 168}.

The nanostructure formed by self-assembly of diblock copolymer could present a size around 5 to 100 nm¹⁵². Matyjaszewski and coworkers¹⁵³ have reported that the size and shape of nanodomains are determined by the chain architecture, M_w of each segment, their interaction parameters, and the temperature. Additionally, the M_w and M_w distribution are essential parameters for obtaining well-defined macromolecules. On the other hand, amphiphilic block self-assembly is characterized by a critical micelle concentration (CMC) that is usually lower than their low average molar mass counterparts such as surfactants.

The low CMC values and the control of M_w on each segment have led to use amphiphilic block copolymers for drug delivery. The applications of block copolymers in drug release are limited by the length of blocks, since the polymer fragments of the carrier should have a size below the renal threshold (30000 g/mol) to be sure that it is easily excreted¹⁵³.

Specific self-assembled nanostructures can be targeted according to a dimensionless “packing parameter”, p , is defined in Equation (1)

$$p = \frac{v}{a_o l_c}$$

Where v is the volume of hydrophobic chain, a_o is the optimal area of the head group, and l_c is the length of the hydrophobic tail. Therefore, packing parameter is much related to self-

assembly morphology. Thus, spherical micelles are favored when $p \leq 1/3$, cylindrical micelles when $1/3 \leq p \leq 1/2$, and vesicles or polymersomes when $1/2 \leq p \leq 1$ ¹⁶⁶.

I.3.5. Lyotropic phases/bulk phase

Leibler¹⁶⁹ has described the theory of microphase separation in block copolymers. The phase separation behavior is determined by three experimental factors: a) the degree of polymerization ($N = N_A + N_B$), b) the block copolymer composition (f) (as the overall volume fraction of the A component, $f_A = N_A/N$) and c) the Flory-Huggins interaction parameter χ , representing the strength of repulsive interaction between two blocks^{152,170-172}.

According to Bates and Fredrickson¹⁵², the microphase separation of block copolymers can be illustrated in a schematic phase diagram, in function to χN versus the block length ratio f_A (Figure I.15).

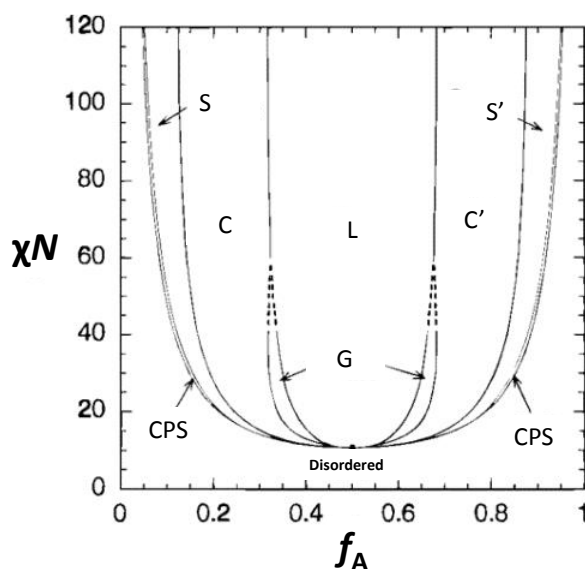


Figure I. 15. Theoretical phase diagram for diblock copolymer: S-spherical, C-cylindrical, G-gyroid, L- Lamellae, CPS- close packed sphere and disordered phase¹⁵².

Bates and Fredrickson^{152,170} and also Malstrom and Darling¹⁷²⁻¹⁷³ have represented various arrangements of microphase separation of block copolymers. Figure 1.16 shows a scheme of thermodynamically stable diblock copolymer phases. In this example, the linear A–B diblock copolymer (PS-*b*-PMMA) molecule represented at the top. The chains self-organize such that

contact between the immiscible blocks is minimized, with the structure determined primarily by the relative lengths of the two polymer blocks (f_A)¹⁷³.

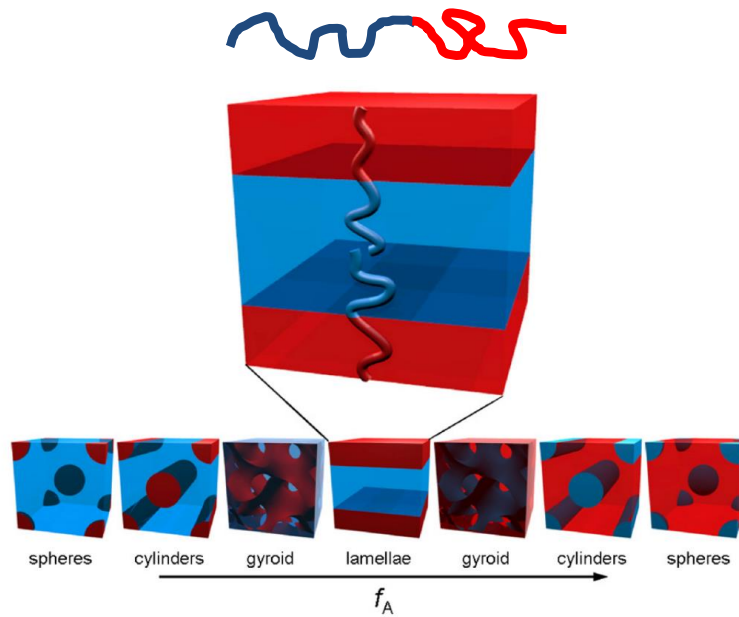


Figure I. 16. Phase diagram for linear AB diblock copolymer¹⁷²⁻¹⁷³.

I.3.6. Hierarchical self-assembly

Thermodynamic immiscibility between two distinct blocks leads to a variety of ordered nanostructures with periodicity at the scale of 10–100 nm¹⁷⁴. Ordered domains follow the principle of self-organization by attractive/repulsive pair forces¹⁶⁸. Repulsive interaction (include: incompatibility of polymers, hydrophobic interaction, and excluded volume of anisotropic molecules) are characterized by their order phase (polymorphism).

The formation of very similar ordered structures (A and B domains) in different materials as magnets, block copolymers, and liquid crystals had shown that self-mechanism is a widespread behavior (Figure I.17)¹⁶⁸.

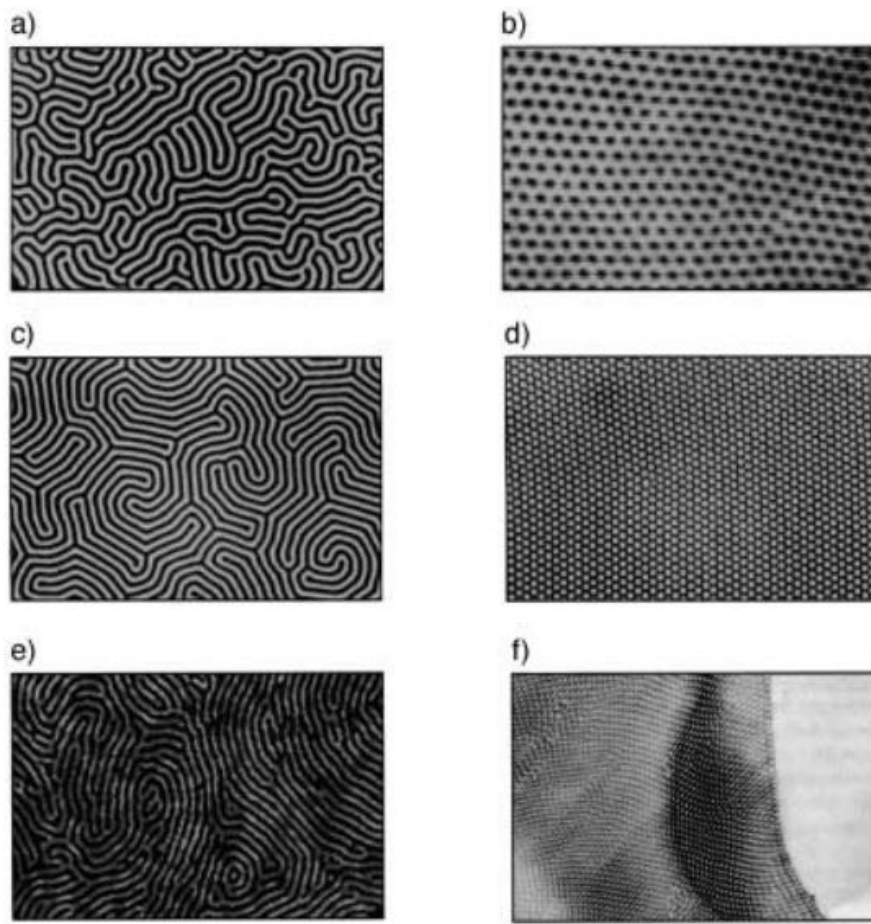


Figure I. 17. An example of the universality of order principle through pair forces. Left (lamellar organization) and right (hexagonal domains) in a ferrofluid a) $d = 1$ cm and b) $d = 4$ μm ; in a ferromagnetic film c) and d) $d = 10$ μm ; in a block copolymer superlattice e) $d = 40$ nm and f) $d = 16$ nm¹⁶⁸.

Other examples of ordered block copolymer self-assembly are reported in Figure 1.18 as monolith materials of a polystyrene-*block*-poly(lactic acid) (PS-*b*-PLA) with a gyroid morphology¹⁷³, and PS-*b*-PMMA copolymer by Park *et al.*¹⁷³, or in Figure I.19 as well as protein-*b*-poly(N-isopropylacrylamide)¹⁷².

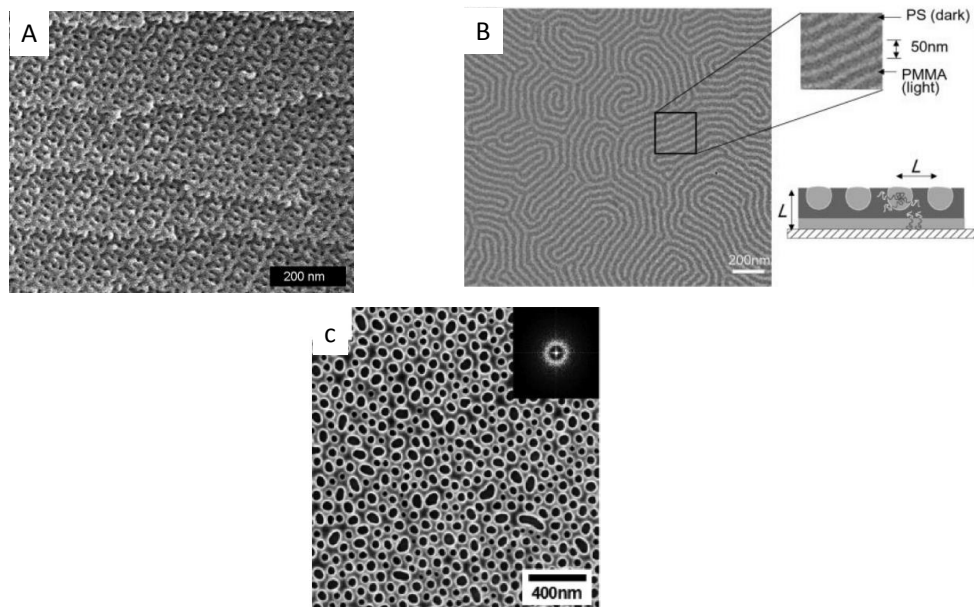


Figure I.18. Self-assembled architectures of A) PS-*b*-PLA¹⁷³; B) PS-*b*-PMMA¹⁷⁴; C) PS-*b*-PMMA¹⁷⁵.

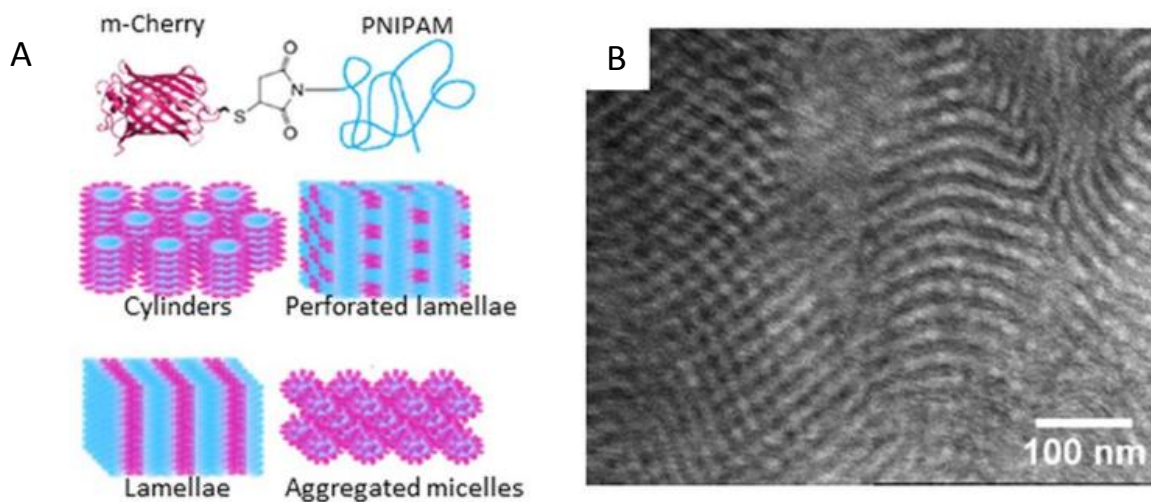


Figure I.19. A) Globular protein m-Cherry conjugation with poly(N-isopropylacrylamide) and the observed possible phases formed. B) TEM of solid state structures formed from m-Cherry-*b*-poly(N-isopropylacrylamide)¹⁷².

I.3.7. Block copolymers based on polysaccharide

The use of polysaccharides as hydrophilic moieties for amphiphilic block copolymer preparation is based on their hydrophilic nature, biocompatibility, biodegradability, and

bioactivity. To date, several research groups have focused on designing smart polymers which allow to construct intelligent nanomaterials for active intracellular delivery of anticancer drugs¹⁷⁶. In this view, carbohydrates are interesting ligands to target hepatic and cervical cancer cells¹⁷⁷, or just as nanocomposite for biomedicine¹⁷⁸.

In this part of the bibliography research work, we summarize the few publications related to polysaccharide containing block copolymers.

I.3.8. Synthesis

Schatz and Lecommandoux¹⁷⁹ have reviewed the different routes that can be used to synthesize polysaccharide based block copolymers:

- a) Enzymatic polymerization,
- b) Adding synthetic block at the reducing end of polysaccharide,
- c) End-to-End, coupling two blocks bearing antagonist functions.

The methods here mentioned imply the introduction of a reactive function at the native reducing end of polysaccharides. An example is the reductive amination that proceeds in two steps as illustrated in Figure I.20: step 1) an initial equilibrium between aldehyde and iminium group resulting from the nucleophilic addition of an amine function and step 2) the reduction of iminium in the presence of a reducing agent such as sodium cyanoborohydride (NaBH_3CN)¹⁷⁹⁻¹⁸⁰.

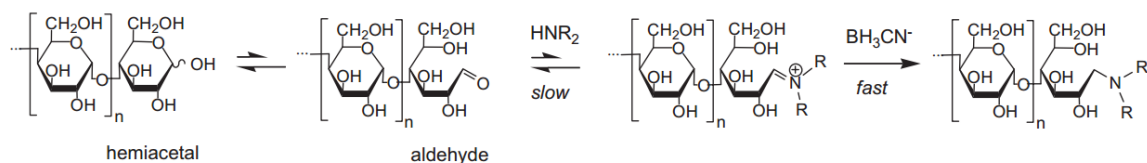


Figure I. 20. Reductive amination with cyanoborohydride ion at the reducing end of a polysaccharide chain¹⁷⁹.

Following this way, several articles have demonstrated the use of polysaccharides into block copolymer formation, either coupling them with natural biopolymers, synthetic polymers or to inorganic compounds, as well.

I.3.8.1. Block copolymers based on polysaccharides by coupling reaction

Polysaccharide-based block copolymers have been synthesized by coupling oligosaccharides or polysaccharides with another polymer block using different kinds of reactions listed in Figure I-21, including reductive amination, aminolysis of a dextran lactone-end group, stepwise elongation of a nylon block and copper(I)-catalysed click azide-alkyne cycloaddition¹⁷⁹.

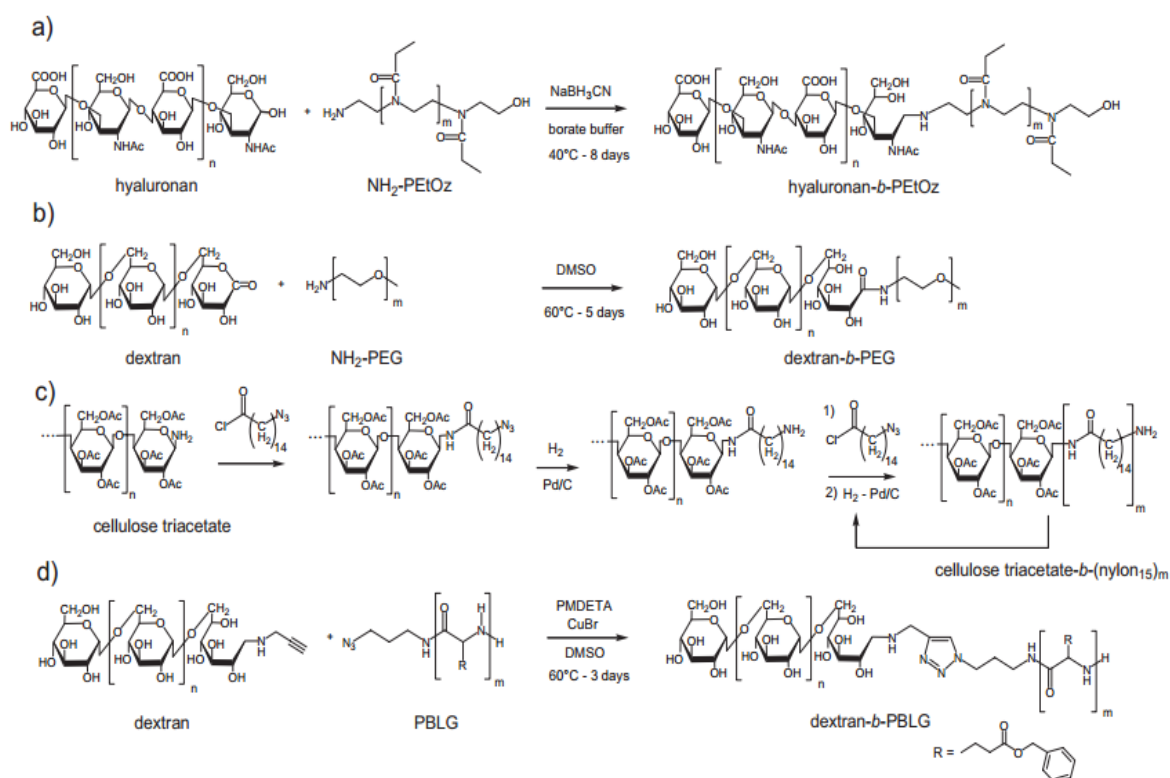


Figure I. 21. Several coupling reactions between polysaccharide and other synthetic polymers: a) reductive amination, b) aminolysis of a dextran lactone-end group, c) stepwise elongation of a nylon block and d) copper(I)-catalysed azide-alkyne cycloaddition¹⁷⁹.

I.3.8.2. Block copolymer based on polysaccharide by Controlled radical Polymerization (CRP)

CRP such as ATRP, NMP, RAFT or macromolecular design by the interchange of xanthate (MADIX) has also been applied to synthesize glycopolymers with well-defined composition as illustrated in Figure 1.22.

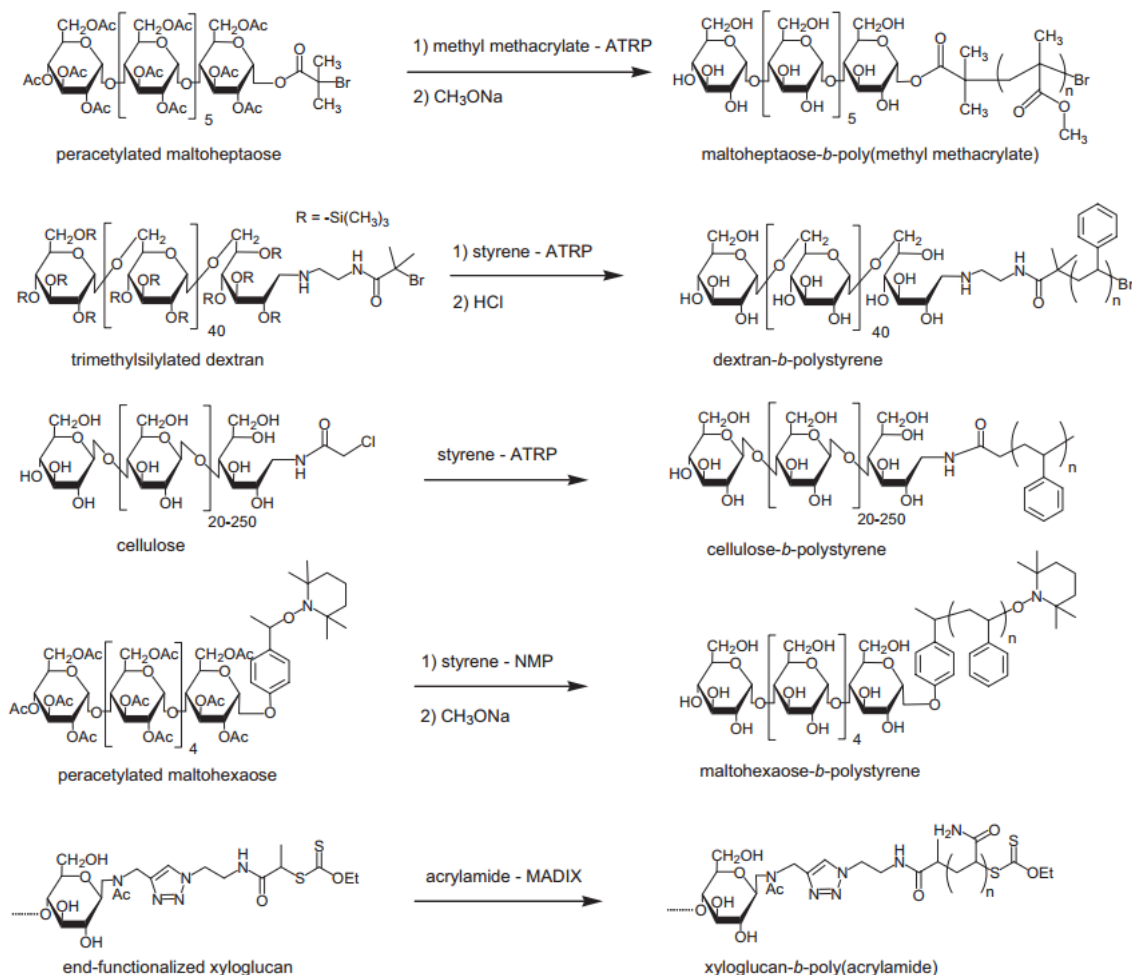


Figure I. 22. Controlled/living polymerizations of vinyl blocks from poly- or oligosaccharides with suitably modified end groups. Note that hydroxyl groups are not protected in the second and latter methods¹⁷⁹.

I.3.8.3. Block copolymer based on polysaccharides by Ring Opening Polymerization (ROP)

ROP of cyclic monomers such as lactones, lactams or cyclic ethers is also a convenient route for block copolymer synthesis. Many ROPs proceed as living polymerizations can be used to increase linearly the M_w of the polymer, with a controlled monomer and initiator ratios as presented in Figure 1.23 for polysaccharides.

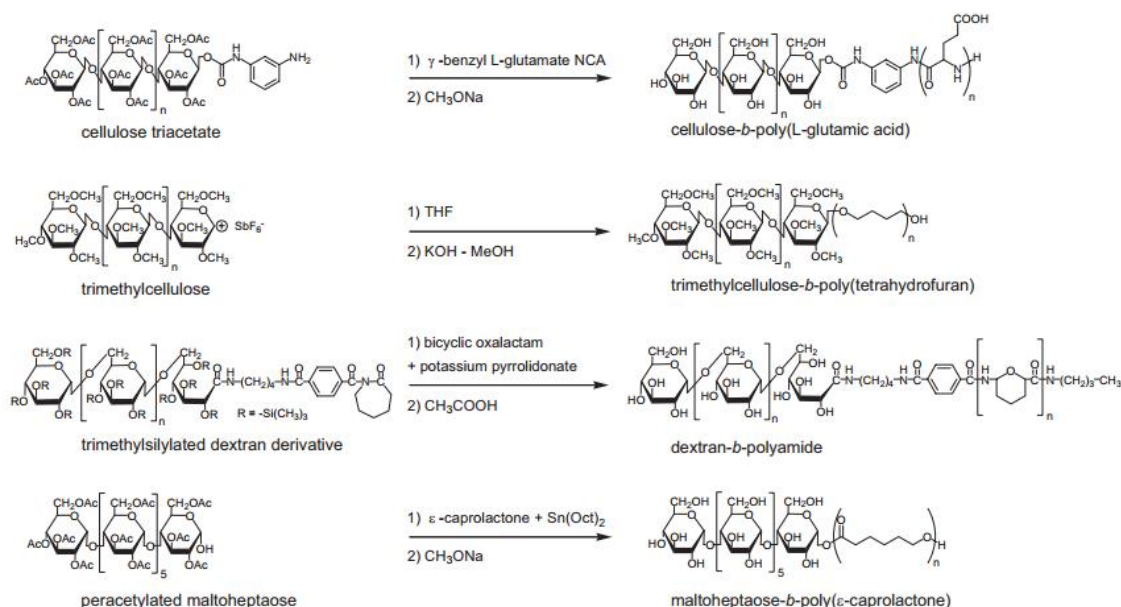


Figure I. 23. Ring opening polymerizations of polypeptide, polyether, polyamide and polyester from polysaccharides with suitably modified end groups¹⁷⁹.

Several techniques to prepare linear copolymer based on polysaccharide are presented above. Starting from this point, we will present the recent advances focusing on the self-assembly behavior of the prepared block copolymers based on the polysaccharide.

I.3.9. Self-assembly and properties

To date, only a few papers have dealt with the self-assembly properties of polysaccharide based block copolymers. Upadhyay et al.¹⁸¹, prepared polymersomes from a block copolymer obtained by coupling poly(γ -benzyl L-glutamate) (PBLG) and hyaluronan (HYA) (PBLG₂₃-*b*-HYA₁₀) using click chemistry. The self-assembly of these block copolymer showed polymersomes with a hydrodynamic radius of 220 nm (Figure I.24). In the same way, micelles obtained from Dextran-*b*-polycaprolactone (PCL) presented a size range between 20-50 nm as seen by Transmission electron microscopy (TEM) (Figure 1.25 (A))¹⁸². Self-assembly of Dextran-*b*-polypeptide gives rise to vesicle formation with 45 nm of hydrodynamic radius¹⁸³.

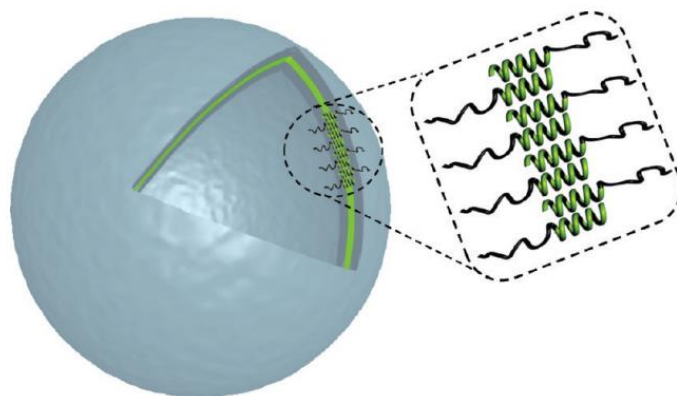


Figure I. 24. Polymersome of poly(γ -benzyl L-glutamate) (PBLG) and hyaluronan (HYA) using click chemistry (PBLG₂₃-*b*-HYA₁₀)¹⁸¹.

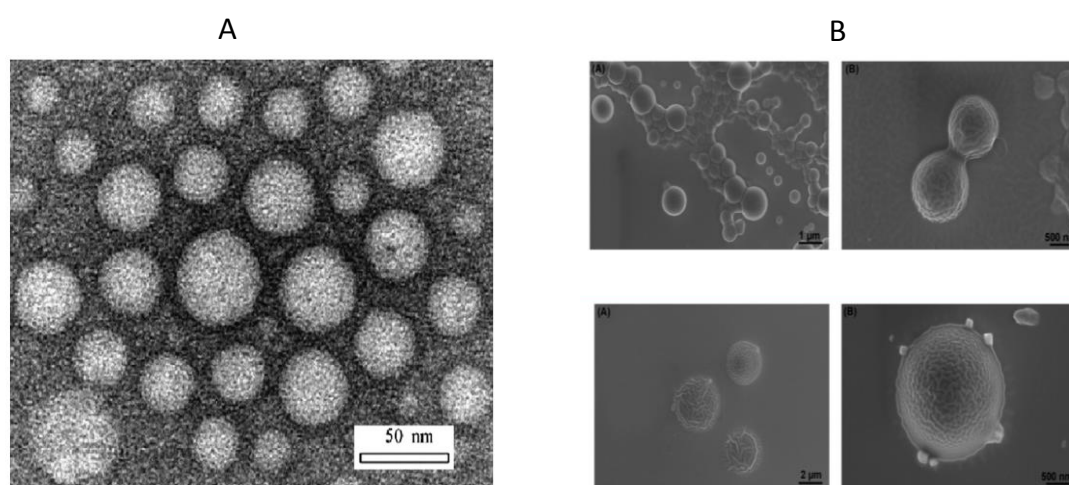


Figure I. 25. A) TEM of dextran-*b*-PCL material¹⁸² and B) FEG-SEM of oligosaccharides-*b*-PNIPAM¹⁸⁴.

Another example presented in Figure I.25 (B) shows vesicles of oligosaccharide-*b*-poly(*N*-isopropylacrylamide) (PNIPAM)¹⁸⁴ prepared by click reaction of propargyl-functionalized beta-cyclodextrin or xyloglucooligosaccharide with poly(*N*-isopropylacrylamide) (PNIPAM) having a terminal azido group. Another example is xyloglucose (XGO) diblock copolymers (XGO-*b*-XGO) which have been synthesized by click chemistry¹⁸⁵. Besides, maltoheptaose (MH) and poly(ϵ -caprolactone) were coupled to form MH-*b*-(PCL)₂ and MH-*b*-(PCL)₃ having a very narrow polydispersity index (PDI) close to 1¹⁸⁶. MH-*b*-PCL micelles exhibit a size of 9 nm determined by DLS analysis. Even though these copolymers do not involve polysaccharides, the diblock copolymers exhibit self-assembly properties in response to the temperature.

Bibliography

Bosker and coworkers¹⁸⁷, synthesized a linear block copolymer by reductive amination coupling polystyrene (PS) with amino end group and reducing end of dextran (yield of the reaction was 75-90%). It was shown that the yield decreased drastically when polysaccharide blocks with a $M_w > 6000 \text{ g.mol}^{-1}$ have been used (reaction in DMF/H₂O at 60°C during seven days). The effect of the polysaccharide block length on the yield of reductive amination has been studied in the formation of dextran terminated by hydrophobic groups¹⁸⁸. Dextran chains with M_w from 4 to 23 kg.mol⁻¹ were allowed to react with C12-C18 alkyl amine and bile acid to produce amphiphilic dextran. The low average molar mass fragments showed high conversion values of 95-98 %, using a molar ratio reducing end group/primary amine/NaBH₃CN of 1/10/15¹⁸⁸. Moreover, the authors showed that the critical aggregation concentration (CAC) values decrease with increasing monoalkyl chain length and decreasing dextran block length. The hydrodynamic radius of these micelles showed a range of 20-30 nm. This amphiphilic block copolymer was proposed to drug delivery systems, antimicrobial agents or surface active agents.

Pursuing the same objective, Jeong *et al.*¹⁸⁹ prepared diblock hydrophilic copolymers using dextran with 17 kg.mol⁻¹ and a methoxy poly(ethylene glycol) N-hydroxy succinimide (mPEG-NHS) of 2 kg.mol⁻¹ blocks. The reaction was performed in two steps:

- First, the functionalization of dextran by reductive amination. To do that, dextran and NaBH₃CN were first mixed for 24h at room temperature. Then, the addition of hexamethylene diamine in excess allows preparing Dextran-NH₂ (yield 95%) in DMSO at room temperature for another 24h.
- The coupling of the two blocks was carried out in the second step, where aminated dextran and mPEG-NHS is dissolved and stirred in DMSO for 24 h at room temperature. The block copolymer dextran-*b*-mPEG was isolated with a yield of 85%.

Another approach has been described to design the same type of block copolymer namely dextran-*b*-PEG using the oxime click reaction with a yield of 95% within 24h¹⁹⁰.

The thio derivatives of polysaccharides are interesting intermediates for block copolymer preparation. Sun *et al.*¹⁹¹ synthesized Dextran-S-S-PCL copolymer for triggered release of doxorubicin (DOX) *in vitro*. It was shown that thiol dextran (dextran-SH) can be

Bibliography

functionalized with a 100 % yield as revealed by the Ellman test. Petrelli *et al.*¹⁹² studied the formation of amphiphilic block copolymer based on thiol-oligosaccharides and maleimide-Polystyrene (PS) (Oligosaccharide-*b*-PS) by click reaction. The authors also mentioned that metal free thiol-maleimide click addition is a viable alternative to the copper(I)-catalyzed azide-alkyne cycloaddition (CuAAC) reaction. The oligosaccharide block copolymer resulted from those reactions form micelles or aggregates with 16-28 nm of size.

Dextran-*b*-poly(vinyl acetate) was prepared for uses as a steric stabilizer by batch emulsion polymerization of vinyl acetate¹⁹³. The amphiphilic block copolymers efficiently stabilize the latex particles as solid content as high as 27 % can be obtained. Kamitakahara's group has also published the synthesis of amphiphilic block copolymers (*A-b-B*) based on cellulose triacetate and nylon-15¹⁹⁴.

On the other hand, polysaccharide blocks are also interesting materials for surface modification, which are profitable for various technologies, such as super hydrophobic/hydrophilic, antibacterial, and biosensors surfaces. For example, Thébault and coworkers¹⁹⁵ modified gold surfaces by grafting polysaccharides functionalized with thiol groups (pullulan-SH). Other polysaccharides as derivative of cellulose were also used for surface modification¹⁹⁶.

CONCLUSION

Advances in polymer engineering have led to the synthesis of a polysaccharide containing block copolymers with unique physical and biological properties. The benefits, incorporating bio based blocks (polysaccharides or peptides) into copolymer designs arise from the fundamental properties to adopt ordered conformations and to undergo self-assembly, providing control over structure formation at various length scales when compared to conventional block copolymers.

I.4. DEPOLYMERIZATION OF CELLULOSE AND DERIVATIVES

Following the biorefinery concept, depolymerisation of carbohydrate based biopolymers is a preliminary and required step from which fine chemicals, transportation fuel, and platform molecules can be more easily produced.

To date, complete degradation of cellulosic polymers into AGUs was extensively studied to yield a raw material that can be useful for biofuel and chemical production. On the other hand, partial degradation leading to small cellulose fragments to construct new biomolecules has been much less studied. In this sense, different ways of cellulose depolymerisation including mechanical, chemical and thermochemical methods as well as enzymatic hydrolysis are studied.

I.4.1. Methods for biopolymer degradation

Development and optimization of existing degradation methods have been mostly investigated for highly packed crystalline biopolymers e.g. cellulose and chitosan. Those methods follow two steps:

- a) *Pretreatment process*, used to disrupt hydrogen interactions present in crystalline regions. This process increases the free volumes and thereby the accessibility to catalysts.
- b) *Hydrolysis reaction* where glycosidic bonds on the polymer backbone are cleaved.

I.4.2. Pretreatment processes

The pretreatment processes can be divided in two, physical and chemical:

Physical pretreatment, includes chipping, grinding, milling and thermal methods¹⁹⁷⁻¹⁹⁹. The authors consider that these methods are effective for reducing particle size and crystallinity of biopolymers. However they are less efficient and consume more energy than chemical pretreatment methods.

Chemicals treatments, including mineral acids (sulphuric, hydrochloric, nitric and phosphoric acid) and bases (NaOH and KOH), are used at various concentrations. Acid treatment mainly breaks the inter- and intra-molecular bonds within cellulose micro fibrils. Alkali is used mostly to swell the cellulose structure by formation of alcoholate salts (see section I.1.1.2) generating amorphous cellulose. However, the chemicals used for pretreatment are corrosive and not considered environmentally friendly. In this context, organic acids such as maleic, fumaric, oxalic acid have been suggested¹⁹⁹.

Other solvents such as LiCl/N,N-dimethylacetamide (LiCl/DMAc), NaOH/urea, cadoxen (cadmium ethylenediamine solvent) and dimethyl sulphoxide/ tetrabutylammonium fluoride trihydrate (DMSO/TBAF) are able to dissolve crystalline cellulose²⁰⁰.

Ionic liquids (ILs) are organic salts with melting temperatures below 118°C¹⁶⁰. ILs are currently the best solvent to dissolve cellulose. Their efficiency is attributing to the thermal stability and non-volatile properties. Thus, solutions containing up to 10 wt % of cellulose can be formed viscous pastes in chloride-containing ILs^{199,201}. However, their availability and its high prices limit their utilization in large scales.

The mecanocatalytic process is another method recently proposed to enhance the degradation of the cellulosic polymer. This reaction is based on the combination of acid-catalysis with mechanical forces. Full conversion of cellulosic polymer in water soluble product was obtained impregnating cellulose with HCl or H₂SO₄ followed by two hours of milling process²⁰².

Several pretreatment processes were available to facilitate the hydrolysis of glycosidic bonds in the polysaccharide structure. The selection of one of them is determined as a function of the following degradation process.

I.4.3. Depolymerisation methods

I.4.3.1. Depolymerisation by liquid acid

The catalytic action of liquid acids over cellulosic materials is in function of their concentration and process parameters (temperature, reaction time, pressure, etc.). For instance, the cellulose structure is completely hydrolyzed in 12 M HCl solution at room temperature. Even lower concentrations (6 – 7 M HCl) can be effective in the presence of CaCl₂ and LiCl as additives²⁰³. A concentration of 63.5 % of H₂SO₄ generates cellulose nanocrystals having a length between 200 and 400 nm within 2 hours of reaction¹⁸.

Current strategies for the hydrolysis of cellulose with acids are mainly accomplished with the two acids mentioned above. Although homogeneous-based processes are efficient, the mineral acid systems still suffer from major problems in product/catalyst separation, reactor corrosion, catalyst recycling and the treatment of waste effluent. For example, in the H₂SO₄

based system, the acid in the reaction mixture has to be neutralized with a mixture of CaO/CaSO₄, which forms a lot of gypsum as waste. For the HCl system, it is difficult to reuse the acid liquor while the hydrofluoric acid (HF) system is very toxic when utilized in large-scale process²⁰³.

I.4.3.2. Depolymerisation by solid acids

Solid acid catalysts showed various advantages over liquid acid catalysts, ease of product separation, recyclability, less damage to the reactor. Besides, the use of solid acid catalysts can reduce the pollutants which will have a minimal impact on the environment²⁰³.

A solid acid catalyst is defined as solid which can donate protons or accept electrons during reactions. The catalytic function for a solid acid catalyst is derived from its acidic centers, existing mainly on its surface. Accordingly, solid acids with Brønsted acid sites can catalyze biomass²⁰⁴. However, it is also necessary to mention that the solid catalytic activities decrease when water is present. Moreover, most solid acids do not function effectively for cellulose hydrolysis because the surfaces of these solids do not have strong acid sites or cannot allow close contact of β-1,4-glucans.

A number of solid acid catalysts have been proposed in Table 1.3, most of them need pretreatment process and high reaction temperature¹⁹⁹.

Bibliography

Table I. 3. Comparison of catalytic properties and activities of solid acid catalysts for cellulose hydrolysis to glucose.

Catalyst	Amount	Amount of acid sites (mmol/g)	Substrate	Amount	Pretreatment method	Water amount	Reaction temperature (°C)	Reaction time (h)	Glucose yield (%)	Selectivity
HSM-5B	0.2 wt%	0.3	Cellulose	1 wt %	–	–	175	0.5	33.7	74.4
H-ZSM5	50 mg	–	Cellulose	45 mg	Milling	5 mL	150	24	12	–
HY	10 mg	–	Cellulose	100 mg	[BMIm][Cl]	10 mg	(240 W)	0.12	35	76
γ -Al ₂ O ₃	1.5 g	0.05	Cellulose	1.5 g	–	15 mL	150	3	–	–
Layered HNbMoO ₆	0.2 g	1.9	Cellulose	1.0 g	–	10 mL	100	18	41	–
HT-OH _{Ca}	0.5 g	1.17	Cellulose	0.45	Milling	150 mL	150	24	40	85
Nafion-50	0.1 g	–	Cellulose	0.2 g	[BMIm][Cl]	20 mL	160	4	35	–
Sulfated ZrNDSBA-15	50 mg	–	Cellulose	250 mg	–	50 mL	160	1.5	55	65
FeCl ₃ /Silica	0.47 g	–	Cellulose	2.0 g	[BMIm][Cl]	30 mL	130	24	3	–
FeCl ₃ /Silica	0.47 g	–	Cellulose	2.0 g	[BMIm][Cl]	30 mL	190	24	9	–
Amberlyst-15	50 mg	1.8	Cellulose	45 mg	Miling	5 mL	150	24	25	–
Amberlyst-15	1.5 g	4.4	Cellulose	1.5 g	–	15 mL	150	3	15	–
Dowex 50wx8-100 ion-exchange resin	26 mg	–	Cellulose	50 mg	[EMIm][Cl]	270 mg	110	4	83	–
AC-SO ₃ H	50 mg	1.25	Cellulose	45 mg	Milling	5 mL	150	24	40	95
AC-SO ₃ H-250	0.3 g	2.23	Cellulose	0.27	–	27 mL	150	24	62	74
Fe ₃ O ₄ -SBA-SO ₃ H	1.5 g	1.09	Cellulose	1.0 g	–	15 mL	120	1	98	–
Fe ₃ O ₄ -SBA-SO ₃ H	1.5 g	1.09	Cellulose	1.0 g	[BMIm][Cl]	15 mL	150	3	50	–
Fe ₃ O ₄ -SBA-SO ₃ H	1.5 g	1.09	Starch	1.0 g	–	15 mL	150	3	95	–
Fe ₃ O ₄ -SBA-SO ₃ H	1.5 g	1.09	Corn cob	1.0 g	–	15 mL	150	3	45 ^a	–
PCPs-SO ₃ H	0.2 g	1.8	Cellulose	25 mg	–	2.0 g	120	3	1.4	27
Ru-CMKs	50 mg	–	Cellulose	324 mg	–	40 mL	230	24	34	51
Cellulase-MSNs	4.5 mg	–	Cellulose	15 mg	–	–	50	24	90	–
HPA	0.08 mmol	–	Cellulose	0.1 g	–	5 mL	180	2	51	90
Cs-HPA	0.07 mmol	–	Cellulose	0.1 g	–	7 mL	170	8	39	89
Micellar HPA	0.07 mmol	–	Cellulose	0.1 g	–	7 mL	170	8	60	85

Activated hydrotalcite (HT-OH_{Ca}); Sulfonated activated-carbon (AC-SO₃H); Sulfonic group functionalized magnetic SBA-15 catalyst (Fe₃O₄-SBA-SO₃H); Ru-mesoporous carbon materials (Ru-CMKs); Cellulase immobilized mesoporous silica nanocatalysts (Cellulase-MSNs); Porous coordination polymers decorated with sulfonic acid functional groups (PCPseSO₃H); Heteropoly acid H₃PW₁₂O₄₀(HPA)¹⁹⁹.

1.4.3.3. Depolymerisation by Advanced Oxidation Process (AOPs)

Advanced oxidation processes (AOPs) are oxidation techniques usually operating at ambient or near ambient temperature and pressure. These techniques are based on the production of OH[•] radicals that attack the most of the organic molecules²⁰⁵. Technologies, such as ozonation, peroxone, non-thermal plasma, fenton, photo-fenton, UV/O₃, UV/H₂O₂ and UV/ZnO, have been developed and described by many researchers to degrade organic compounds in wastewater and have been growing in importance during the past decade²⁰⁶.

The coupling of ultrasound irradiation with AOPs or Sono catalysts (Rutile-TiO₂, Anatase-TiO₂, montmorillonite, Fe₃O₄ and ZnO) was investigated to degrade cellulose derivative. Thus, a polymer with a M_w around $1,3 \times 10^5$ g.mol⁻¹ was reduced to a M_w of 45 000 g.mol⁻¹ that seems to be the limit for a depolymerisation using the Sono catalysis method²⁰⁷.

In a similar way, ultrasonic irradiation was studied for water soluble polysaccharide degradation²⁰⁸⁻²¹¹. As found for sonication, the depolymerisation using ultrason method is limited to molar masses between 35 000 to 40 000 g.mol⁻¹; larger time of irradiation did not diminish these values.

I.4.4. Enzymatic depolymerisation

Enzymatic degradation is known as a more selective method than conventional chemical catalysis. This selectivity is often optional (i.e., regioselectivity) or chiral (i.e., stereoselectivity). Enzymatic hydrolysis is also acid catalysis that requires two critical residues: a proton donor and nucleophile/base²¹². Therefore, their high selectivity has some key benefits including reduced side reactions and effective environmentally friendly process. In addition to their selectivity, other factors make these catalysts potentially useful to degrade bio-sourced polymers, including type of enzyme and operating conditions (pH, temperature, stirring, etc.)²¹³.

I.4.4.1. Enzyme

Enzymes for catalysis, biosynthesis or modification of carbohydrates and glycol-conjugates are classified into five groups by Carbohydrate Active enZyme database (CAZY; <http://www.cazy.org>):

- a) Glycoside Hydrolases (GHs): hydrolysis and rearrangement of glycosidic bonds
- b) Glycosyl Transferases (GTs): formation of glycosidic bonds
- c) Polysaccharide Lyases (PLs): non-hydrolytic cleavage of glycosidic bonds
- d) Carbohydrate Esterases (CEs): hydrolysis of carbohydrate esters
- e) Auxiliary Activities (AAs): redox enzymes that act in conjunction with CAZymes.

Here, we will focus on **Glycoside hydrolases (GHs)** as a bio catalyst for polysaccharides. GHs are enzymes that can cleave glycosidic bonds in polysaccharide chains, leading to the formation of hemiacetal or hemiketal at the end of the chain²¹⁴.

Glycoside hydrolases (GHs) are divided into two groups following their function at the synergistic action: Endoglucases and Exoglucanases²¹⁴⁻²¹⁵.

Bibliography

Endoglucanases (EGs), specific enzymes that cleave randomly on internal bonds inside the polysaccharide chain. Their catalytic behaviors depend on factors such as temperature, pH, and the substrate. This enzyme produces fragments of polysaccharides.

Exoglucanases (EX), enzymes that include cellobiohydrolases (CBHs). Their catalytic action takes place at the reducing and non-reducing ends. This enzyme produces mostly cellobioses.

β -glucosidases (BGs), which hydrolyze cellobiose to produce glucose units.

The GHs enzymes have high efficiency only in amorphous domain where the complexation enzyme/polymer is more easily in comparison with the crystalline polysaccharides. Therefore, pretreatment to disrupt crystalline regions is essential for cellulose degradation.

Another group of enzymes has been recently discovered by Dimaragone and Topakas²¹⁶, which are called Lytic Polysaccharide MOnooxygenases (LPMOs). Interestingly, they are capable to interact with polysaccharide chains in the crystalline state. LPMOs are also sub-classified in function of their catalytic preferences:

LPMO-1: releases reducing end oxidized product,

LPMO-2: acts at the non-reducing end of the glucose moiety,

LPMO-3: is less specific, releasing both C1 and C4-oxidized celooligomers

The catalytic activity of these enzymes is dependent on an external electron donor as well as molecular oxygen and presence of copper ions for their proper functioning.

The Figure 1.26 summarizes the enzymatic degradation of cellulose structure, where the crystalline part is attacked by LPMOs. Endoglucanases (EG) are active on amorphous segments and exoglucanases (cellobiohydrolases) initiate the process in crystalline part by cleavage through chain ends. Cellobiose dehydrogenase (CDH) is a potential electron donor for LPMOs. Finally, β -glucosidase converts cellobioses in AGUs.

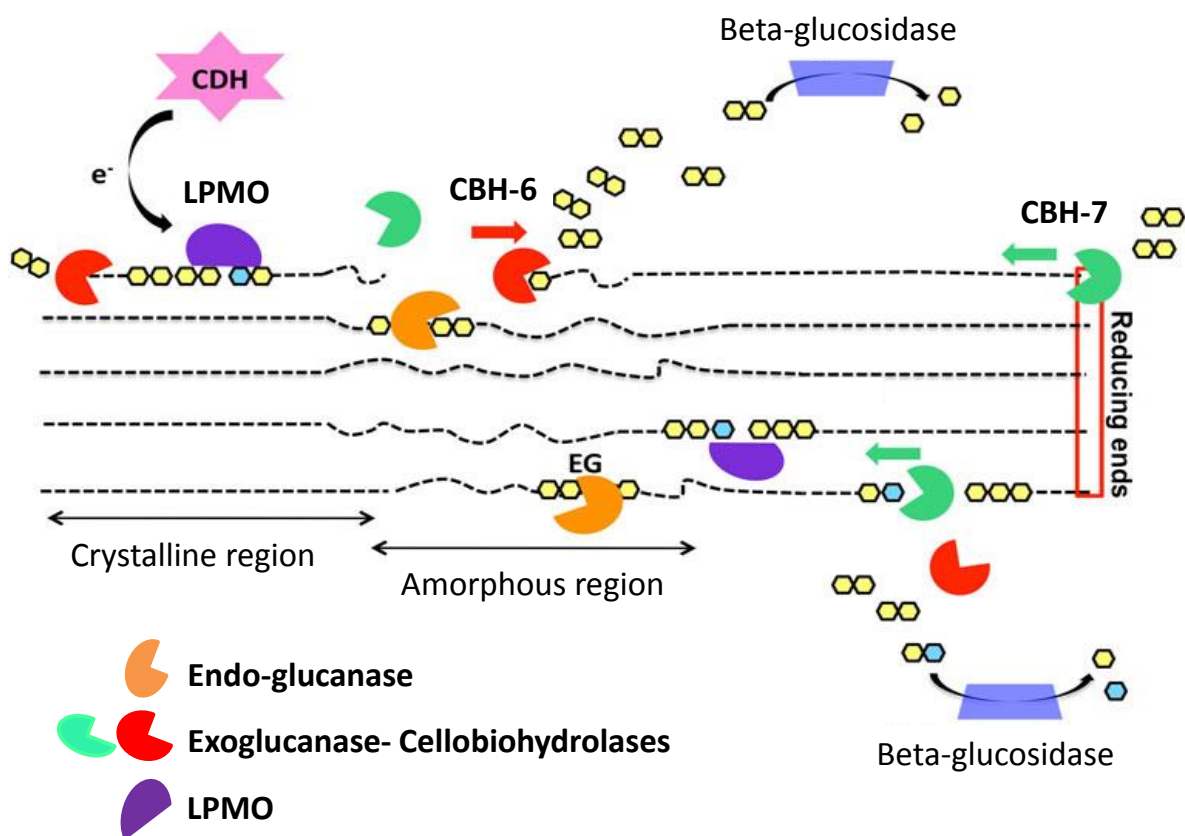


Figure I. 26. A simplified scheme of the current view on the enzymatic degradation of cellulose²¹⁶.

I.4.4.2. Mechanism of hydrolysis

Enzymatic depolymerisation of cellulosic material follows three steps²¹⁷.

- Adsorption of enzyme into polymer surface,
- Cleavage of glycosidic bonds,
- Desorption of enzyme.

The factors which influence enzymatic hydrolysis process are:

- Availability of active sites where enzyme can adsorb. In general, adsorption of one enzyme needs around 5-8 AGUs. A nomenclature exists to demarcate substrate binding by glycosidase (Figure I.27). Therefore, it is clear that amorphogenesis in crystalline polymers is necessary before addition of enzymes²¹⁸. In the same way, the sequences of unsubstituted or partially

Bibliography

substituted AGUs in cellulose derivatives are required to achieve degradation²¹⁹⁻²²⁰.

- Concentration [Substrate: Enzyme]: this parameter is related to the affinity and activity of the enzyme.
- Physical and chemical environmental (temperature and ionic strength) must be appropriate for good enzyme functioning.

In the case of LPMOs, amorphogenesis is not necessary as explained above. However, concentration and operating conditions, including the presence of external electron donor as well molecular oxygen and copper ions, must be fulfilled. On the other hand, Lynd *et al.*²¹⁵ mentioned that enzyme-cellulose complexes are a pre-requisite for cellulose hydrolysis. This effect is described by the adsorption of cellulases into cellulose chains, which could reach constant values in ≤ 90 minutes whereas complete hydrolysis of cellulose usually requires a day or more.

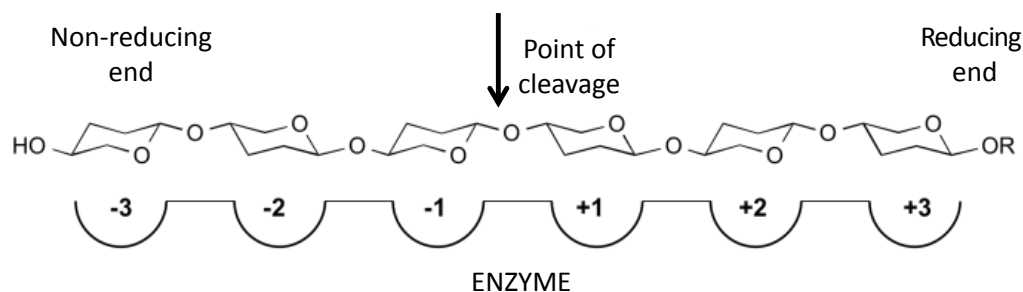


Figure I. 27. Schematic drawing of the glucose-binding subsites in several glycosyl hydrolases²²¹.

Degradation of cellulose is achieved by adding an enzyme in a reactor. Experimentally, a cocktail of enzymes is applied to yield the complete depolymerisation. The most commonly used commercial enzyme cocktails are produced by the fungus *Trichoderma reesei* (*Hypocrea jecorina*) and the depolymerisation process usually takes place at pH 4.5 - 5.0 and temperatures in the range of 40 to 50°C^{222,223,224}. Thus, enzymes mostly used to cellulose hydrolysis are called cellulases.

The major advantages of enzymes in polymer modification compared with chemical methods are milder reaction conditions and highly specific nondestructive transformation.

Bibliography

Today enzymatic hydrolysis methods are used 1) to produce AGUs to prepare biofuel and other chemicals, 2) to determine chain structure in cellulose derivative including the variation of the degree and molar substitution, as well its distribution, 3) to investigate drug release from polysaccharide matrix.

So far any research groups have been interested in the partial degradation of HPMC, with the objective of producing short chained polymers. Those short fragments could be used as building blocks: first, for copolymer design and second, to create a new generation of materials. In this sense, our objective is based on the study of partial depolymerization of HPMC and the use of the obtained short fragments to design new block copolymer architectures. Thus, this work should introduce new valuable compounds into the biorefinery's portfolio.

CONCLUSION

It is clear that many methods are available for converting biomass into the new platform for bio-refinery processes. These methods should be the most versatile, economical and friendly with the environment. The choices can also be influenced by the type of product that we should produce. Therefore, the availability of several biopolymers and bio refinery methods can be used as response at the new demands of specific polymer preparation.

REFERENCES

1. Tsai, S. C., *Biomacromolecules: Introduction to Structure, Function and Informatics*. John Wiley & Sons: New Jersey, **2006**, p. 708.
2. Crini, G., Recent developments in polysaccharide-based materials used as adsorbents in wastewater treatment. *Prog Polym Sci* **2005**, *30* (1), 38-70.
3. Samir, M. A. S. A.; Alloin, F.; Dufresne, A., Review of recent research into cellulosic whiskers, their properties and their application in nanocomposite field. *Biomacromolecules* **2005**, *6* (2), 612-626.
4. Berlin, A.; Balakshin, M.; Gilkes, N., *et al.*, Inhibition of cellulase, xylanase and beta-glucosidase activities by softwood lignin preparations. *J Biotechnol* **2006**, *125* (2), 198-209.
5. Gradwell, S. E.; Renneckar, S.; Esker, A. R., *et al.*, Surface modification of cellulose fibers: towards wood composites by biomimetics. *Cr Biol* **2004**, *327* (9-10), 945-953.
6. Metaxa, A. F.; Efthimiadou, E. K.; Boukos, N., *et al.*, Polysaccharides as a source of advanced materials: Cellulose hollow microspheres for drug delivery in cancer therapy. *J Colloid Interf Sci* **2012**, *384*, 198-206.
7. Posocco, B.; Dreussi, E.; de Santa, J., *et al.*, Polysaccharides for the Delivery of Antitumor Drugs. *Materials* **2015**, *8* (5), 2569-2615.
8. Chowdhury, M. N. K.; Ismail, A. F.; Beg, M. D. H., *et al.*, Polyvinyl alcohol/polysaccharide hydrogel graft materials for arsenic and heavy metal removal. *New J Chem* **2015**, *39* (7), 5823-5832.
9. Pinkert, A.; Marsh, K. N.; Pang, S., *et al.*, Ionic liquids and their interaction with cellulose. *Chem Rev* **2009**, *109* (12), 6712-28.
10. Zhang, Y. H. P.; Lynd, L. R., Toward an aggregated understanding of enzymatic hydrolysis of cellulose: Noncomplexed cellulase systems. *Biotechnol Bioeng* **2004**, *88* (7), 797-824.
11. Ramos, L. P., The chemistry involved in the steam treatment of lignocellulosic materials. *Quim Nova* **2003**, *26* (6), 863-871.
12. Klemm, D.; Heublein, B.; Fink, H. P., *et al.*, Cellulose: Fascinating biopolymer and sustainable raw material. *Angew Chem Int Edit* **2005**, *44* (22), 3358-3393.
13. Testova, L.; Nieminen, K.; Penttila, P. A., *et al.*, Cellulose degradation in alkaline media upon acidic pretreatment and stabilisation. *Carbohydr Polym* **2014**, *100*, 185-94.
14. Desvaux, M., *Clostridium cellulolyticum*: model organism of mesophilic cellulolytic clostridia. *Fems Microbiol Rev* **2005**, *29* (4), 741-764.
15. Park, S.; Baker, J. O.; Himmel, M. E., *et al.*, Cellulose crystallinity index: measurement techniques and their impact on interpreting cellulase performance. *Biotechnol Biofuels* **2010**, *3*.
16. Lee, J. H.; Park, S. H.; Kim, S. H., Preparation of cellulose nanowhiskers and their reinforcing effect in polylactide. *Macromol Res* **2013**, *21* (11), 1218-1225.
17. Hon, D. N. S., Cellulose - a Random-Walk Along Its Historical Path. *Cellulose* **1994**, *1* (2), 1-25.
18. Habibi, Y.; Lucia, L. A.; Rojas, O. J., Cellulose Nanocrystals: Chemistry, Self-Assembly, and Applications. *Chem Rev* **2010**, *110* (6), 3479-3500.
19. Lin, N.; Dufresne, A., Nanocellulose in biomedicine: Current status and future prospect. *Eur Polym J* **2014**, *59*, 302-325.

Bibliography

20. Hasani, M.; Cranston, E. D.; Westman, G., *et al.*, Cationic surface functionalization of cellulose nanocrystals. *Soft Matter* **2008**, *4* (11), 2238-2244.
21. Mischnick, P.; Heinrich, J.; Gohdes, M., *et al.*, Structure analysis of 1,4-glucan derivatives. *Macromol Chem Phys* **2000**, *201* (15), 1985-1995.
22. Cheng, G.; Varanasi, P.; Li, C. L., *et al.*, Transition of Cellulose Crystalline Structure and Surface Morphology of Biomass as a Function of Ionic Liquid Pretreatment and Its Relation to Enzymatic Hydrolysis. *Biomacromolecules* **2011**, *12* (4), 933-941.
23. Peng, H. D.; Li, H. Q.; Luo, H., *et al.*, A novel combined pretreatment of ball milling and microwave irradiation for enhancing enzymatic hydrolysis of microcrystalline cellulose. *Bioresource Technol* **2013**, *130*, 81-87.
24. Wu, L.; Lee, S. H.; Endo, T., Effect of dimethyl sulfoxide on ionic liquid 1-ethyl-3-methylimidazolium acetate pretreatment of eucalyptus wood for enzymatic hydrolysis. *Bioresource Technol* **2013**, *140*, 90-96.
25. Feller, R. L.; Wilt, M., *Evaluation of cellulose ethers for conservation*. J. Paul Getty Trust: USA, **1990**, p. 149.
26. Varshney, V. K.; Naithani, S., Chemical Functionalization of Cellulose Derived from Nonconventional Sources. In *Cellulose Fibers: Bio- and Nano-Polymer Composites*, Verlag Berling Heilderberg: London, **2011**, p. 43.
27. Melander, C. New Methods for Enzyme Hydrolysis, Analysis, and Characterization of Modified Cellulose. Ph.D. Thesis, Lund University, Lund, **2006**.
28. Heinze, T.; Liebert, T., Unconventional methods in cellulose functionalization. *Prog Polym Sci* **2001**, *26* (9), 1689-1762.
29. Ho, F. F. L.; Ward, G. A.; Kohler, R. R., Determination of Molar Substitution and Degree of Substitution of Hydroxypropyl Cellulose by Nuclear Magnetic-Resonance Spectrometry. *Anal Chem* **1972**, *44* (1), 178-&.
30. Fitzpatrick, F.; Schagerlof, H.; Andersson, T., *et al.*, NMR, cloud-point measurements and enzymatic depolymerization: Complementary tools to investigate substituent patterns in modified celluloses. *Biomacromolecules* **2006**, *7* (10), 2909-2917.
31. El Seoud, O. A.; Nawaz, H.; Areas, E. P., Chemistry and applications of polysaccharide solutions in strong electrolytes/dipolar aprotic solvents: an overview. *Molecules* **2013**, *18* (1), 1270-313.
32. Adden, R.; Muller, R.; Mischnick, P., Analysis of the substituent distribution in the glucosyl units and along the polymer chain of hydroxypropylmethyl celluloses and statistical evaluation. *Cellulose* **2006**, *13* (4), 459-476.
33. Schagerlof, H.; Johansson, M.; Richardson, S., *et al.*, Substituent distribution and clouding behavior of hydroxypropyl methyl cellulose analyzed using enzymatic degradation. *Biomacromolecules* **2006**, *7* (12), 3474-81.
34. Jain, S.; Sandhu, P. S.; Malvi, R., *et al.*, Cellulose Derivatives as Thermoresponsive Polymer: An Overview. *J Appl Pharm Sci* **2013**, *3* (12), 139.
35. Rowe, R. C.; Sheskey, P. J.; Owen, S. C., *Handbook of Pharmaceutical Excipients*. Pharmaceutical Press: Great Britain, **2006**, p. 832.
36. Feller, R. L.; Wilt, M., *Evaluation of cellulose ethers for conservation*. USA, **1990**.
37. Sepassi, S.; Goodwin, D. J.; Drake, A. F., *et al.*, Effect of polymer molecular weight on the production of drug nanoparticles. *J Pharm Sci* **2007**, *96* (10), 2655-2666.
38. Werawatganone, P.; Wurster, D. E., Determination of the hydrolysis kinetics of alpha-naphthyl acetate in micellar systems and the effect of HPMC (catalyst present). *J Pharm Sci* **2007**, *96* (2), 448-458.

Bibliography

39. Viriden, A.; Wittgren, B.; Larsson, A., Investigation of critical polymer properties for polymer release and swelling of HPMC matrix tablets. *Eur J Pharm Sci* **2009c**, *36* (2-3), 297-309.
40. Viriden, A.; Larsson, A.; Schagerlof, H., *et al.*, Model drug release from matrix tablets composed of HPMC with different substituent heterogeneity. *Int J Pharm* **2010a**, *401* (1-2), 60-7.
41. Klouda, L.; Mikos, A. G., Thermoresponsive hydrogels in biomedical applications. *Eur J Pharm Biopharm* **2008**, *68* (1), 34-45.
42. Taylor, L. D.; Cerankowski, L. D., Preparation of Films Exhibiting a Balanced Temperature-Dependence to Permeation by Aqueous-Solutions - Study of Lower Consolute Behavior. *J Polym Sci Pol Chem* **1975**, *13* (11), 2551-2570.
43. Sarkar, N., Thermal Gelation Properties of Methyl and Hydroxypropyl Methylcellulose. *J Appl Polym Sci* **1979**, *24* (4), 1073-1087.
44. Fairclough, J. P. A.; Yu, H.; Kelly, O., *et al.*, Interplay between Gelation and Phase Separation in Aqueous Solutions of Methylcellulose and Hydroxypropylmethylcellulose. *Langmuir* **2012**, *28* (28), 10551-10557.
45. Sarkar, N.; Walker, L. C., Hydration Dehydration Properties of Methylcellulose and Hydroxypropylmethylcellulose. *Carbohydr Polym* **1995**, *27* (3), 177-185.
46. Viriden, A.; Wittgren, B.; Andersson, T., *et al.*, Influence of substitution pattern on solution behavior of hydroxypropyl methylcellulose. *Biomacromolecules* **2009a**, *10* (3), 522-9.
47. Rodrigues, I. M.; Coelho, J. F. J.; Carvalho, M. G. V. S., Isolation and valorisation of vegetable proteins from oilseed plants: Methods, limitations and potential. *J Food Eng* **2012**, *109* (3), 337-346.
48. Owusu-Apenten, R. K., *Introduction To Food Chemistry*. CRC Press: USA, **2005**, p. 272.
49. Koolman, J.; Roehm, K. H., *Color Atlas of Biochemistry*. Thieme: New York **2005**, p. 476.
50. Darryl, L. Protein. <http://www.genome.gov/Glossary/resources/protein.pdf>. Accessed: **Novembre, 2012**.
51. De Graaf, L. A., Denaturation of proteins from a non-food perspective. *J Biotechnol* **2000**, *79* (3), 299-306.
52. Ingadottir, B. The use of acid and alkali-aided protein solubilization and precipitation methods to produce functional protein ingredients from tilapia. Master Thesis, University of Florida, Florida, **2004**.
53. Kamerzell, T. J.; Esfandiary, R.; Joshi, S. B., *et al.*, Protein-excipient interactions: Mechanisms and biophysical characterization applied to protein formulation development. *Adv Drug Deliver Rev* **2011**, *63* (13), 1118-1159.
54. Ramos, O. L.; Pereira, J. O.; Silva, S. I., *et al.*, Effect of composition of commercial whey protein preparations upon gelation at various pH values. *Food Res Int* **2012**, *48* (2), 681-689.
55. Avanza, M.; Puppo, M. C.; Anon, M. C., Rheological characterization of amaranth protein gels. *Food Hydrocolloid* **2005**, *19* (5), 889-898.
56. Gomez-Guillen, M. C.; Gimenez, B.; Lopez-Caballero, M. E., *et al.*, Functional and bioactive properties of collagen and gelatin from alternative sources: A review. *Food Hydrocolloid* **2011**, *25* (8), 1813-1827.

Bibliography

57. Karaca, A. C.; Low, N.; Nickerson, M., Emulsifying properties of chickpea, faba bean, lentil and pea proteins produced by isoelectric precipitation and salt extraction. *Food Res Int* **2011**, *44* (9), 2742-2750.
58. Cabra, V.; Arreguin, R.; Farres, A., Emulsifying properties of protein. *Bol. Soc. Quim. Méx.* **2008**, *2*, 80-89.
59. Tsaliki, E.; Pegiadou, S.; Doxastakis, G., Evaluation of the emulsifying properties of cottonseed protein isolates. *Food Hydrocolloid* **2004**, *18* (4), 631-637.
60. Liu, S.; Gibb, B. C., Solvent denaturation of supramolecular capsules assembled via the hydrophobic effect. *Chem Commun* **2011**, *47* (12), 3574-6.
61. Yin, S. W.; Tang, C. H.; Wen, Q. B., *et al.*, The relationships between physicochemical properties and conformational features of succinylated and acetylated kidney bean (*Phaseolus vulgaris* L.) protein isolates. *Food Res Int* **2010**, *43* (3), 730-738.
62. Kristinsson, H. G.; Hultin, H. O., Effect of low and high pH treatment on the functional properties of cod muscle proteins. *J Agr Food Chem* **2003**, *51* (17), 5103-5110.
63. Lestari, D.; Mulder, W. J.; Sanders, J. P. M., *Jatropha* seed protein functional properties for technical applications. *Biochem Eng J* **2011**, *53* (3), 297-304.
64. Cookman, D. J.; Glatz, C. E., Extraction of protein from distiller's grain. *Bioresource Technol* **2009**, *100* (6), 2012-2017.
65. Cuq, B.; Gontard, N.; Aymard, C., *et al.*, Relative humidity and temperature effects on mechanical and water vapor barrier properties of myofibrillar protein-based films. *Polym Gels Netw* **1997**, *5* (1), 1-15.
66. Guennadios, *Protein-Based Films and Coatings*. CRC Press New York, **2002**, p. 672.
67. Han, H. J.; Gennadios, A., Edible films and coatings: a review. In *Innovations in Food Packaging*, Academic Press: Winnipeg, **2005**, p. 503.
68. Roy, S.; Gennadios, A.; Weller, C. L., *et al.*, Water vapor transport parameters of a cast wheat gluten film. *Ind Crop Prod* **2000**, *11* (1), 43-50.
69. Mascheroni, E.; Chalier, P.; Gontard, N., *et al.*, Designing of a wheat gluten/montmorillonite based system as carvacrol carrier: Rheological and structural properties. *Food Hydrocolloid* **2010**, *24* (4), 406-413.
70. MujicaPaz, H.; Gontard, N., Oxygen and carbon dioxide permeability of wheat gluten film: Effect of relative humidity and temperature. *J Agr Food Chem* **1997**, *45* (10), 4101-4105.
71. Guillaume, C.; Pinte, J.; Gontard, N., *et al.*, Wheat gluten-coated papers for bio-based food packaging: Structure, surface and transfer properties. *Food Res Int* **2010**, *43* (5), 1395-1401.
72. Irissin-Mangata, J.; Bauduin, G.; Boutevin, B., *et al.*, New plasticizers for wheat gluten films. *Eur Polym J* **2001**, *37* (8), 1533-1541.
73. Tanada-Palmu, P.; Helen, H.; Hyvonen, L., Preparation, properties and applications of wheat gluten edible films. *Agr Food Sci Finland* **2000**, *9* (1), 23-35.
74. Cho, S. Y.; Lee, S. Y.; Rhee, C., Edible oxygen barrier bilayer film pouches from corn zein and soy protein isolate for olive oil packaging. *Lwt-Food Sci Technol* **2010**, *43* (8), 1234-1239.
75. Coppola, M.; Djabourov, M.; Ferrand, M., Unified phase diagram of gelatin films plasticized by hydrogen bonded liquids. *Polymer* **2012**, *53* (7), 1483-1493.
76. Thomazine, M.; Carvalho, R. A.; Sobral, P. I. A., Physical properties of gelatin films plasticized by blends of glycerol and sorbitol. *J Food Sci* **2005**, *70* (3), E172-E176.

Bibliography

77. Krochta, J. M., Proteins as raw materials for films and coatings: definitions, current status, and oportunities. In *PROTEIN-BASED FILMS and COATINGS*, CRC Press: London, **2002**, pp 1-32.
78. Fabra, M. J.; Talens, P.; Chiralt, A., Tensile properties and water vapor permeability of sodium caseinate films containing oleic acid-beeswax mixtures. *J Food Eng* **2008**, *85* (3), 393-400.
79. Fabra, M. J.; Talens, P.; Chiralt, A., Water sorption isotherms and phase transitions of sodium caseinate-lipid films as affected by lipid interactions. *Food Hydrocolloid* **2010**, *24* (4), 384-391.
80. Monedero, F. M.; Fabra, M. J.; Talens, P., *et al.*, Effect of calcium and sodium caseinates on physical characteristics of soy protein isolate-lipid films. *J Food Eng* **2010**, *97* (2), 228-234.
81. Pereda, M.; Aranguren, M. I.; Marcovich, N. E., Caseinate films modified with tung oil. *Food Hydrocolloid* **2010**, *24* (8), 800-808.
82. Oses, J.; Fabregat-Vazquez, M.; Pedroza-Islas, R., *et al.*, Development and characterization of composite edible films based on whey protein isolate and mesquite gum. *J Food Eng* **2009**, *92* (1), 56-62.
83. Yoo, S.; Krochta, J. M., Whey protein-polysaccharide blended edible film formation and barrier, tensile, thermal and transparency properties. *J. Sci. Food Agr* **2011**, *91* (14), 2628-2636.
84. Di Pierro, P.; Sorrentino, A.; Mariniello, L., *et al.*, Chitosan/whey protein film as active coating to extend Ricotta cheese shelf-life. *Lwt-Food Sci Technol* **2011**, *44* (10), 2324-2327.
85. Lee, M. K.; Lee, S. Y., The Quality Characteristics of Soy Wan-Jas Made with Different Proteolytic Enzyme Treated Textured Soy Proteins. *J Korean Soc Appl Biol Chem* **2009**, *52* (6), 708-715.
86. Tunc, S.; Angellier, H.; Cahyana, Y., *et al.*, Functional properties of wheat gluten/montmorillonite nanocomposite films processed by casting. *J Membrane Sci* **2007**, *289* (1-2), 159-168.
87. Chambi, H.; Grosso, C., Edible films produced with gelatin and casein cross-linked with transglutaminase. *Food Res Int* **2006**, *39* (4), 458-466.
88. Giancone, T.; Torrieri, E.; Di Pierro, P., *et al.*, Role of constituents on the network formation of hydrocolloid edible films. *J Food Eng* **2008**, *89* (2), 195-203.
89. Cao, N.; Fu, Y. H.; He, J. H., Mechanical properties of gelatin films cross-linked, respectively, by ferulic acid and tannin acid. *Food Hydrocolloid* **2007**, *21* (4), 575-584.
90. Ou, S. Y.; Wang, Y.; Tang, S. Z., *et al.*, Role of ferulic acid in preparing edible films from soy protein isolate. *J Food Eng* **2005**, *70* (2), 205-210.
91. Bigi, A.; Cojazzi, G.; Panzavolta, S., *et al.*, Mechanical and thermal properties of gelatin films at different degrees of glutaraldehyde crosslinking. *Biomaterials* **2001**, *22* (8), 763-768.
92. Bigi, A.; Cojazzi, G.; Panzavolta, S., *et al.*, Stabilization of gelatin films by crosslinking with genipin. *Biomaterials* **2002**, *23* (24), 4827-4832.
93. Bourtoom, T., Edible films and coatings: characteristics and properties. *Int Food Res J* **2008**, *15* (3), 237-248
94. Falguera, V.; Quintero, J. P.; Jimenez, A., *et al.*, Edible films and coatings: Structures, active functions and trends in their use. *Trends Food Sci Tech* **2011**, *22* (6), 292-303.

Bibliography

95. Li, F. Y.; Wang, R. M.; He, Y. F., *et al.*, Keratin films from chicken feathers for controlled drug release. *J Control Release* **2011**, *152*, E92-E93.
96. Jonker, A. M.; Lowik, D. W. P. M.; van Hest, J. C. M., Peptide- and Protein-Based Hydrogels. *Chem Mater* **2012**, *24* (5), 759-773.
97. Neo, Y. P.; Ray, S.; Easteal, A. J., *et al.*, Influence of solution and processing parameters towards the fabrication of electrospun zein fibers with sub-micron diameter. *J Food Eng* **2012**, *109* (4), 645-651.
98. Li, Y.; Lim, L. T.; Kakuda, Y., Electrospun Zein Fibers as Carriers to Stabilize (-)-Epigallocatechin Gallate. *J Food Sci* **2009**, *74* (3), C233-C240.
99. Ali, Y.; Ghorpade, V.; Weber, A., *et al.* Method for mulching an agricultural soil bed using a biodegradable protein material, and a mulched agricultural crop growing plot produced thereby. US 6672001 B1, September, **2004**.
100. Helgeson, M. S.; Graves, W. R.; Grewell, D., *et al.*, Zein-based Bioplastic Containers Alter Root-zone Chemistry and Growth of Geranium. *J. Environ. Hort* **2010**, *28* (2), 74-80.
101. Innovativeindustry.net Cars Made From Renewable Materials. www.innovativeindustry.net/cars-made-from-renewable-materials. Accessed: **October 2015**.
102. Van Beilen, J. B.; Poirier, Y., Plants as factories for bioplastics and other novel biomaterial. In *Plant Biotechnology and Agriculture: Prospects for the 21st Century*, Academic Press: USA, **2012**, p. 481.
103. Ma, Y.; Li, X.; Jia, P., *et al.*, Preparation of zein-based membranes and their pervaporation for ethanol aqueous solution. *Desalination* **2012**, *299*, 70-78.
104. Bratzel, G.; Buehler, M. J., Sequence-structure correlations in silk: Poly-Ala repeat of *N. clavipes* MaSp1 is naturally optimized at a critical length scale. *J Mech Behav Biomed Mater* **2012**, *7* (0), 30-40.
105. Kundu, S. C.; Kundu, B.; Talukdar, S., *et al.*, Invited review nonmulberry silk biopolymers. *Biopolymers* **2012**, *97* (6), 455-467.
106. Higgins, M. J.; Molino, P. J.; Yue, Z. L., *et al.*, Organic Conducting Polymer-Protein Interactions. *Chem Mater* **2012**, *24* (5), 828-839.
107. Gribova, V.; Auzely-Velty, R.; Picart, C., Polyelectrolyte Multilayer Assemblies on Materials Surfaces: From Cell Adhesion to Tissue Engineering. *Chem Mater* **2012**, *24* (5), 854-869.
108. Silva, N. H. C. S.; Vilela, C.; Marrucho, I. M., *et al.*, Protein-based materials: from sources to innovative sustainable materials for biomedical applications. *J Mater Chem B* **2014**, *2* (24), 3715-3740.
109. Hu, X.; Cebe, P.; Weiss, A. S., *et al.*, Protein-based composite materials. *Mater Today* **2012**, *15* (5), 208-215.
110. Mosiewicki, M. A.; Aranguren, M. I., A short review on novel biocomposites based on plant oil precursors. *Eur Polym J* **2013**, *49* (6), 1243-1256.
111. Meier, M. A.; Metzger, J. O.; Schubert, U. S., Plant oil renewable resources as green alternatives in polymer science. *Chem Soc Rev* **2007**, *36* (11), 1788-802.
112. Guner, F. S.; Yagci, Y.; Erciyas, A. T., Polymers from triglyceride oils. *Prog Polym Sci* **2006**, *31* (7), 633-670.
113. Khot, S. N.; Lascala, J. J.; Can, E., *et al.*, Development and application of triglyceride-based polymers and composites. *J Appl Polym Sci* **2001**, *82* (3), 703-723.

Bibliography

114. Miao, S. D.; Wang, P.; Su, Z. G., *et al.*, Vegetable-oil-based polymers as future polymeric biomaterials. *Acta Biomater* **2014**, *10* (4), 1692-1704.
115. Sharmin, E.; Zafar, F.; Akram, D., *et al.*, Recent advances in vegetable oils based environment friendly coatings: A review. *Ind Crop Prod* **2015**, *76*, 229.
116. Montero de Espinosa, L.; Meier, M. A. R., Plant oils: The perfect renewable resource for polymer science. *Eur Polym J* **2011**, *47* (5), 852.
117. Moreno, M.; Goikoetxea, M.; de la Cal, J. C., *et al.*, From Fatty Acid and Lactone Biobased Monomers Toward Fully Renewable Polymer Latexes. *J Polym Sci Pol Chem* **2014**, *52* (24), 3543-3549.
118. Henna, P. H.; Kessler, M. R.; Larock, R. C., Fabrication and Properties of Vegetable-Oil-Based Glass Fiber Composites by Ring-Opening Metathesis Polymerization. *Macromol Mater Eng* **2008**, *293* (12), 979-990.
119. Lligadas, G.; Ronda, J. C.; Galia, M., *et al.*, Renewable polymeric materials from vegetable oils: a perspective. *Mater Today* **2013**, *16* (9), 337-343.
120. Raquez, J. M.; Deleglise, M.; Lacrampe, M. F., *et al.*, Thermosetting (bio)materials derived from renewable resources: A critical review. *Prog Polym Sci* **2010**, *35* (4), 487-509.
121. Singh, R., *Membrane Technology and Engineering for Water Purification*. 2nd ed.; Butterworth-Heinemann: Oxford, **2014**, p. 424.
122. Mulder, *Basic Principles of Membrane Thechnology*. Kluwer Academic: Netherlands, **1996**, p. 564.
123. Ravanchi, M. T.; Kaghazchi, T.; Kargari, A., Application of membrane separation processes in petrochemical industry: a review. *Desalination* **2009**, *235* (1-3), 199-244.
124. Baker, R. W., *Membrane technology and applications*. . A John Wiley & Sons: California, **2000**, p. 571.
125. Ma, H. Y.; Burger, C.; Hsiao, B. S., *et al.*, Ultrafine Polysaccharide Nanofibrous Membranes for Water Purification. *Biomacromolecules* **2011**, *12* (4), 970-976.
126. Kools, W. F. Membrane Formation By Phase Inversion in multicomponent Polymer System. Ph.D. Thesis, Twente University, Twente, **1998**.
127. Chunxiu, L. Development of Chitosan-Based blend hollow fiber membranes for adsorptive separation in environmental engineering and bioengineering. Ph.D. Thesis, National university of Singapore, Singapore, **2006**.
128. Lonsdale, H. K., The Growth of Membrane Technology. *J Membrane Sci* **1982**, *10* (2-3), 81-181.
129. Li, Z. S.; Ren, J. Z.; Fane, A. G., *et al.*, Influence of solvent on the structure and performance of cellulose acetate membranes. *J Membrane Sci* **2006**, *279* (1-2), 601-607.
130. Ferjani, E.; Roudesli, S.; Deratani, A., Desalination of brackish water from Tunisian Sahel using composite polymethylhydrosiloxane-cellulose acetate membranes. *Desalination* **2004**, *162* (1-3), 103-109.
131. Haddad, R.; Ferjani, E.; Roudesli, M. S., *et al.*, Properties of cellulose acetate nanofiltration membranes. Application to brackish water desalination. *Desalination* **2004**, *167* (1-3), 403-409.
132. Lajimi, R. H.; Ben Abdallah, A.; Ferjani, E., *et al.*, Change of the performance properties of nanofiltration cellulose acetate membranes by surface adsorption of polyelectrolyte multilayers. *Desalination* **2004**, *163* (1-3), 193-202.

Bibliography

133. Zhu, S. D.; Wu, Y. X.; Chen, Q. M., *et al.*, Dissolution of cellulose with ionic liquids and its application: a mini-review. *Green Chem* **2006**, *8* (4), 325-327.
134. Uragami, T.; Matsuda, T.; Okuno, H., *et al.*, Structure of Chemically-Modified Chitosan Membranes and Their Characteristics of Permeation and Separation of Aqueous-Ethanol Solutions. *J Membrane Sci* **1994**, *88* (2-3), 243-251.
135. Meireles, I. T.; Portugal, C.; Alves, V. D., *et al.*, Impact of biopolymer purification on the structural characteristics and transport performance of composite polysaccharide membranes for pervaporation. *J Membrane Sci* **2015**, *493*, 179-187.
136. Ma, H. Y.; Burger, C.; Hsiao, B. S., *et al.*, Fabrication and characterization of cellulose nanofiber based thin-film nanofibrous composite membranes. *J Membrane Sci* **2014**, *454*, 272-282.
137. Li, N.; Zhao, M.; Ye, B., *et al.*, Fabrication of Asymmetric Polysaccharide Composite Membranes as Guided Bone Regeneration Materials. *J. Adv. Biomed. Eng. Techno.* **2015**, *2*, 51-61.
138. Pittalis, F.; Bartoli, F.; Giovannoni, S., *et al.* Process for the preparation of chitosan fibers. US 4464321 A, **1984**.
139. Karim, Z.; Mathew, A. P.; Grahn, M., *et al.*, Nanoporous membranes with cellulose nanocrystals as functional entity in chitosan: Removal of dyes from water. *Carbohydr Polym* **2014**, *112*, 668-676.
140. Mahanta, N.; Leong, W. Y.; Valiyaveetil, S., Isolation and characterization of cellulose-based nanofibers for nanoparticle extraction from an aqueous environment. *J Mater Chem* **2012**, *22* (5), 1985-1993.
141. Oliveira, J. T.; Reis, R. L., Polysaccharide-based materials for cartilage tissue engineering applications. *J Tissue Eng Regen M* **2011**, *5* (6), 421-436.
142. Imre, B.; Pukanszky, B., From natural resources to functional polymeric biomaterials. *Eur Polym J* **2015**, *68*, 481-487.
143. Klein, S., Polysaccharides in Oral Drug Delivery - Recent Applications and Future Perspectives. *Acs Sym Ser* **2009**, *1017*, 13-30.
144. Freitas, F.; Alves, V. D.; Reis, M. A., *et al.*, Microbial Polysaccharide- Based Membranes: Current and Future Applications. *J Appl Polym Sci* **2014**, *131* (6).
145. Suh, J. K.; Matthew, H. W., Application of chitosan-based polysaccharide biomaterials in cartilage tissue engineering: a review. *Biomaterials* **2000**, *21* (24), 2589-98.
146. Santos, M. I.; Fuchs, S.; Gomes, M. E., *et al.*, Response of micro- and macrovascular endothelial cells to starch-based fiber meshes for bone tissue engineering. *Biomaterials* **2007**, *28* (2), 240 - 248.
147. Iwasaki, N.; Yamane, S. T.; Majima, T., *et al.*, Feasibility of polysaccharide hybrid materials for scaffolds in cartilage tissue engineering: evaluation of chondrocyte adhesion to polyion complex fibers prepared from alginate and chitosan. *Biomacromolecules* **2004**, *5* (3), 828-833.
148. Akhlaghi, S. P.; Peng, B. L.; Yao, Z. L., *et al.*, Sustainable nanomaterials derived from polysaccharides and amphiphilic compounds. *Soft Matter* **2013**, *9* (33), 7905-7918.
149. Bae, K.; Moon, C.; Lee, Y., *et al.*, Intracellular Delivery of Heparin Complexed with Chitosan-g-Poly(Ethylene Glycol) for Inducing Apoptosis. *Pharm Res* **2009**, *26* (1), 93-100.
150. You, D. G.; Sarayanakumar, G.; Son, S., *et al.*, Dextran sulfate-coated superparamagnetic iron oxide nanoparticles as a contrast agent for atherosclerosis imaging. *Carbohydr Polym* **2014**, *101*, 1225-1233.

Bibliography

151. Gedde, U. W., A brief introduction to polymer science. In *Polymer physics*. Springer Science & Business Media: USA, **1995**, p. 298.
152. Bates, F. S.; Fredrickson, G. H., Block Copolymers—Designer Soft Materials. *Phys Today* **1999**, *52*(2), 32-38.
153. Matyjaszewski, K.; Tsarevsky, N. V., Nanostructured functional materials prepared by atom transfer radical polymerization. *Nat Chem* **2009**, *1* (4), 276-288.
154. Schacher, F. H.; Rugar, P. A.; Manners, I., Functional Block Copolymers: Nanostructured Materials with Emerging Applications. *Angew Chem* **2012**, *51* (32), 7898-7921.
155. Hawker, C. J.; Russell, T. P., Block copolymer lithography: Merging "bottom-up" with "top-down" processes. MRS BULLETIN: 2005; Vol. 30, pp 952-966.
156. Stoykovich, M. P.; Nealey, P. F., Block copolymers and conventional lithography. *Mater Today* **2006**, *9* (9), 20-29.
157. Jeong, S.-J.; Kim, J. Y.; Kim, B. H., *et al.*, Directed self-assembly of block copolymers for next generation nanolithography. *Mater Today* **2013**, *16* (12), 468-476.
158. Kim, H. C.; Park, S. M.; Hinsberg, W. D., Block copolymer based nanostructures: materials, processes, and applications to electronics. *Chem Rev* **2010**, *110* (1), 146-77.
159. Hamley, I. W., Introduction to Block Copolymer. In *Developments in Block Copolymer Science and Technology*. John Wiley & Sons: England, **2004**, p. 380.
160. Iatrou, H.; Avgeropoulos, A.; Hadjichristidis, N., Synthesis of Model Super H-Shaped Block-Copolymers. *Macromolecules* **1994**, *27* (21), 6232-6233.
161. Lutz, J. F., 1,3-dipolar cycloadditions of azides and alkynes: A universal ligation tool in polymer and materials science. *Angew Chem Int Edit* **2007**, *46* (7), 1018-1025.
162. Opsteen, J. A.; van Hest, J. C. M., Modular synthesis of block copolymers via cycloaddition of terminal azide and alkyne functionalized polymers. *Chem Commun* **2005**, (1), 57-59.
163. Braunecker, W. A.; Matyjaszewski, K., Controlled/living radical polymerization: Features, developments, and perspectives. *Prog Polym Sci* **2007**, *32* (1), 93-146.
164. Grajales, S., Controlled Radical Polymerization Guide ATRP/RAFT/NMP. SIGMA-ALDRICH: St. Louis, 2012; p 52.
165. Lindman, B.; Alexandridis, P., Amphiphilic molecules: small and large. In *Amphiphilic Block Copolymers: Self-Assembly and Applications*, Elsevier Science B.V.: Amsterdam, **2000**, p. 448.
166. Blanazs, A.; Armes, S. P.; Ryan, A. J., Self-Assembled Block Copolymer Aggregates: From Micelles to Vesicles and their Biological Applications. *Macromol Rapid Commun* **2009**, *30* (4-5), 267-277.
167. Chu, B., Structure and Dynamics of Block-Copolymer Colloids. *Langmuir* **1995**, *11* (2), 414-421.
168. Forster, S.; Plantenberg, T., From self-organizing polymers to nanohybrid and biomaterials. *Angew Chem Int Edit* **2002**, *41* (5), 689-714.
169. Leibler, L., Theory of Microphase Separation in Block Copolymers. *Macromolecules* **1980**, *13* (6), 1602-1617.
170. Bates, F. S.; Fredrickson, G. H., BLOCK COPOLYMER THERMODYNAMICS: Theory and Experiment. *Annu. Rev. Phys. Chem.* **1990**, *41*, 525-527.
171. Hardy, C. G.; Tang, C. B., Advances in square arrays through self-assembly and directed self-assembly of block copolymers. *J Polym Sci Pol Phys* **2013**, *51* (1), 2-15.

Bibliography

172. Malmstrom, J.; Travas-Sejdic, J., Block Copolymers for Protein Ordering. *J Appl Polym Sci* **2014**, *131* (14).
173. Darling, S. B., Directing the self-assembly of block copolymers. *Prog Polym Sci* **2007**, *32* (10), 1152-1204.
174. Lopes, W. A.; Jaeger, H. M., Hierarchical self-assembly of metal nanostructures on diblock copolymer scaffolds. *Nature* **2001**, *414* (6865), 735-738.
175. Park, S.-M.; Craig, G. S. W.; La, Y.-H., *et al.*, Square Arrays of Vertical Cylinders of PS-*b*-PMMA on Chemically Nanopatterned Surfaces. *Macromolecules* **2007**, *40* (14), 5084-5094.
176. Yang, H.-K.; Zhang, L.-M., New amphiphilic glycopolyptide conjugate capable of self-assembly in water into reduction-sensitive micelles for triggered drug release. *M Mater Sci Eng C* **2014**, *41*, 36-41.
177. Nicolas, J.; Mura, S.; Brambilla, D., *et al.*, Design, functionalization strategies and biomedical applications of targeted biodegradable/biocompatible polymer-based nanocarriers for drug delivery. *Chem Soc Rev* **2013**, *42* (3), 1147-1235.
178. Zheng, Y. Y.; Monty, J.; Linhardt, R. J., Polysaccharide-based nanocomposites and their applications. *Carbohydr Res* **2015**, *405*, 23-32.
179. Schatz, C.; Lecommandoux, S., Polysaccharide-containing block copolymers: synthesis, properties and applications of an emerging family of glycoconjugates. *Macromol Rapid Commun* **2010**, *31* (19), 1664-84.
180. Borch, R. F.; Bernstei.Md; Durst, H. D., Cyanohydrinborate Anion as a Selective Reducing Agent. *J Am Chem Soc* **1971**, *93* (12), 2897-&.
181. Upadhyay, K. K.; Le Meins, J. F.; Misra, A., *et al.*, Biomimetic doxorubicin loaded polymersomes from hyaluronan-block-poly(γ -benzyl glutamate) copolymers. *Biomacromolecules* **2009**, *10* (10), 2802-8.
182. Liu, J. Y.; Zhang, L. M., Preparation of a polysaccharide-polyester diblock copolymer and its micellar characteristics. *Carbohydr Polym* **2007**, *69* (1), 196-201.
183. Schatz, C.; Louguet, S.; Le Meins, J. F., *et al.*, Polysaccharide-block-polypeptide Copolymer Vesicles: Towards Synthetic Viral Capsids. *Angew Chem Int Edit* **2009**, *48* (14), 2572-2575.
184. Otsuka, I.; Travelet, C.; Halila, S., *et al.*, Thermoresponsive Self-Assemblies of Cyclic and Branched Oligosaccharide-block-poly(N-isopropylacrylamide) Diblock Copolymers into Nanoparticles. *Biomacromolecules* **2012**, *13* (5), 1458-1465.
185. Gauche, C.; Soldi, V.; Fort, S., *et al.*, Xyloglucan-based diblock co-oligomer: Synthesis, self-assembly and steric stabilization of proteins. *Carbohydr Polym* **2013**, *98* (2), 1272-1280.
186. Isono, T.; Otsuka, I.; Kondo, Y., *et al.*, Sub-10 nm Nano-Organization in AB₂- and AB₃-Type Miktoarm Star Copolymers Consisting of Maltoheptaose and Polycaprolactone. *Macromolecules* **2013**, *46* (4), 1461-1469.
187. Bosker, W. T. E.; Agoston, K.; Stuart, M. A. C., *et al.*, Synthesis and interfacial behavior of polystyrene-polysaccharide diblock copolymers. *Macromolecules* **2003**, *36* (6), 1982-1987.
188. Nichifor, M.; Mocanu, G.; Stanciu, M. C., Micelle-like association of polysaccharides with hydrophobic end groups. *Carbohydr Polym* **2014**, *110*, 209-218.
189. Jeong, Y. I.; Kim, D. G.; Kang, D. H., Synthesis of Dextran/Methoxy Poly(ethylene glycol) Block Copolymer. *J Chem-Ny* **2013**, 1-7.

Bibliography

190. Novoa-Carballal, R.; Muller, A. H. E., Synthesis of polysaccharide-b-PEG block copolymers by oxime click. *Chem Commun* **2012**, *48* (31), 3781-3783.
191. Sun, H.; Guo, B.; Li, X., *et al.*, Shell-Sheddable Micelles Based on Dextran-SS-Poly(ϵ -caprolactone) Diblock Copolymer for Efficient Intracellular Release of Doxorubicin. *Biomacromolecules* **2010**, *11* (4), 848-854.
192. Petrelli, A.; Borsali, R.; Fort, S., *et al.*, Oligosaccharide-based block copolymers: Metal-free thiol-maleimide click conjugation and self-assembly into nanoparticles. *Carbohydr Polym* **2015**, *124*, 109-116.
193. Bernard, J.; Save, M.; Arathoon, B., *et al.*, Preparation of a xanthate-terminated dextran by click chemistry: Application to the synthesis of polysaccharide-coated nanoparticles via surfactant-free ab initio emulsion polymerization of vinyl acetate. *J Polym Sci Pol Chem* **2008**, *46* (8), 2845-2857.
194. Kamitakahara, H.; Nakatsubo, F., Synthesis of diblock copolymers with cellulose derivatives. 1. Model study with azidoalkyl carboxylic acid and cellobiosylamine derivative. *Cellulose* **2005**, *12* (2), 209-219.
195. Hoypierres, J.; Dulong, V.; Rihouey, C., *et al.*, Two Methods for One-Point Anchoring of a Linear Polysaccharide on a Gold Surface. *Langmuir* **2015**, *31* (1), 254-261.
196. Lafarge, J.; Kebir, N.; Schapman, D., *et al.*, Design of bacteria repellent PVC surfaces using the click chemistry. *Cellulose* **2013**, *20* (6), 2779-2790.
197. Chang, V. S.; Holtzapple, M. T., Fundamental factors affecting biomass enzymatic reactivity. *Appl Biochem Biotech* **2000**, *84-6*, 5-37.
198. Kelsey, R. G.; Shafizadeh, F., Enhancement of Cellulose Accessibility and Enzymatic-Hydrolysis by Simultaneous Wet Milling. *Biotechnol Bioeng* **1980**, *22* (5), 1025-1036.
199. Guo, F.; Fang, Z.; Xu, C. C., *et al.*, Solid acid mediated hydrolysis of biomass for producing biofuels. *Prog Energ Combust* **2012**, *38* (5), 672-690.
200. Ramos, L. A.; Frollini, E.; Heinze, T., Carboxymethylation of cellulose in the new solvent dimethyl sulfoxide/tetrabutylammonium fluoride. *Carbohydr Polym* **2005**, *60* (2), 259-267.
201. Swatloski, R. P.; Spear, S. K.; Holbrey, J. D., *et al.*, Dissolution of cellose with ionic liquids. *J Am Chem Soc* **2002**, *124* (18), 4974-4975.
202. Schuth, F.; Rinaldi, R.; Meine, N., *et al.*, Mechanocatalytic depolymerization of cellulose and raw biomass and downstream processing of the products. *Catal Today* **2014**, *234*, 24-30.
203. Huang, Y. B.; Fu, Y., Hydrolysis of cellulose to glucose by solid acid catalysts. *Green Chem* **2013**, *15* (5), 1095-1111.
204. Chambon, F.; Rataboul, F.; Pinel, C., *et al.*, Cellulose hydrothermal conversion promoted by heterogeneous Bronsted and Lewis acids: Remarkable efficiency of solid Lewis acids to produce lactic acid. *Appl Catal B-Environ* **2011**, *105* (1-2), 171-181.
205. Andreozzi, R.; Caprio, V.; Insola, A., *et al.*, Advanced oxidation processes (AOP) for water purification and recovery. *Catal Today* **1999**, *53* (1), 51-59.
206. Wang, J.; Jiang, Z.; Zhang, Z. H., *et al.*, Sonocatalytic degradation of acid red B and rhodamine B catalyzed by nano-sized ZnO powder under ultrasonic irradiation. *Ultrason Sonochem* **2008**, *15* (5), 768-774.
207. Taghizadeh, M. T.; Seifi-Aghjekohal, P., Sonocatalytic degradation of 2-hydroxyethyl cellulose in the presence of some nanoparticles. *Ultrason Sonochem* **2015**, *26*, 265-272.

Bibliography

208. Poinot, T.; Benyahia, K.; Govin, A., *et al.*, Use of ultrasonic degradation to study the molecular weight influence of polymeric admixtures for mortars. *Constr Build Mater* **2013**, *47*, 1046-1052.
209. Goodwin, D. J.; Picout, D. R.; Ross-Murphy, S. B., *et al.*, Ultrasonic degradation for molecular weight reduction of pharmaceutical cellulose ethers. *Carbohydr Polym* **2011**, *83* (2), 843-851.
210. Prajapat, A. L.; Gogate, P. R., Intensification of depolymerization of aqueous guar gum using hydrodynamic cavitation. *Chem Eng Process* **2015**, *93*, 1-9.
211. Yan, J. K.; Pei, J. J.; Ma, H. L., *et al.*, Effects of ultrasound on molecular properties, structure, chain conformation and degradation kinetics of carboxylic curdlan. *Carbohydr Polym* **2015**, *121*, 64-70.
212. Davies, G.; Henrissat, B., Structures and Mechanisms of Glycosyl Hydrolases. *Structure* **1995**, *3* (9), 853-859.
213. Dordick, J. S., *Biocatalysts for Industry*. Springer US: NY, **1991**, p. 330.
214. Withers, S.; Spencer, W. Glycoside hydrolases. http://www.cazypedia.org/index.php/Glycoside_hydrolases. Accessed: **September, 2015**.
215. Lynd, L. R.; Weimer, P. J.; van Zyl, W. H., *et al.*, Microbial cellulose utilization: Fundamentals and biotechnology (vol 66, pg 506, 2002). *Microbiol Mol Biol R* **2002**, *66* (4), 739-739.
216. Dimarogona, M.; Topakas, E.; Christakopoulos, P., Recalcitrant polysaccharide degradation by novel oxidative biocatalysts. *Appl Microbiol Biot* **2013**, *97* (19), 8455-8465.
217. Sun, Y.; Cheng, J. Y., Hydrolysis of lignocellulosic materials for ethanol production: a review. *Bioresource Technol* **2002**, *83* (1), 1-11.
218. Coughlan, M. P., Cellulose Hydrolysis - the Potential, the Problems and Relevant Research at Galway. *Biochem Soc T* **1985**, *13* (2), 405-406.
219. Karlsson, J.; Momcilovic, D.; Wittgren, B., *et al.*, Enzymatic degradation of carboxymethyl cellulose hydrolyzed by the endoglucanases Cel5A, Cel7B, and Cel45A from *Humicola insolens* and Cel7B, Cel12A and Cel45Acore from *Trichoderma reesei*. *Biopolymers* **2002**, *63* (1), 32-40.
220. Momcilovic, D.; Schagerlof, H.; Rome, D., *et al.*, Derivatization using dimethylamine for tandem mass spectrometric structure analysis of enzymatically and acidically depolymerized methyl cellulose. *Anal Chem* **2005**, *77* (9), 2948-2959.
221. Davies, G. J.; Wilson, K. S.; Henrissat, B., Nomenclature for sugar-binding subsites in glycosyl hydrolases. *Biochem J* **1997**, *321*, 557-559.
222. Horn, S.; Vaaje-Kolstad, G.; Westereng, B., *et al.*, Novel enzymes for the degradation of cellulose. *Biotechnol Biofuels* **2012**, *5* (45).
223. Margolles-Clark, E.; Ilmen, M.; Penttila, M., Expression patterns of ten hemicellulase genes of the filamentous fungus *Trichoderma reesei* on various carbon sources. *J Biotechnol* **1997**, *57* (1-3), 167-179.
224. Saloheimo, M.; Paloheimo, M.; Hakola, S., *et al.*, Swollenin, a *Trichoderma reesei* protein with sequence similarity to the plant expansins, exhibits disruption activity on cellulosic materials. *Eur J Biochem* **2002**, *269* (17), 4202-4211.

CHAPTER II: METHODS AND MATERIALS

INTRODUCTION

The properties of modified cellulose depend on several factors such as average molar mass, molar mass distribution, the degree of substitution, chemical nature of substitution and their distribution on the monomer units and also along the polymer chain. Currently, there is no single analytical technique that can provide information on all these aspects of modified cellulose. Instead, a combination of analytical techniques has to be employed to obtain physicochemical information of polymers.

In this chapter, we provide information about materials and analytic techniques used to prepare and characterize small fragments of polysaccharides and block copolymers. This chapter is organized into three parts; the first one presents the material and chemical products. The second part describes the methods of sample preparations, and the third will refer to the techniques of characterization.

II.1. Material and Chemical products

II.1.1. HPMC

White powder of HPMC samples was kindly provided by Shin-Etsu Tylose GmbH & Company – Germany and Dow Colorcon Limited – France. Specifications given by the manufacturers are gathered in Table II.1.

HPMC was preferred over other soluble polymers because it showed a good biocompatibility and thermoreversible gelation property, that makes it interesting in material field. The distribution and percentage of their substituents as Methoxy (MeO) and Hydroxypropyl (HPO) groups found in the HPMC backbone (Figure II.1) are given in Table II.1 (Manufacturer specification).

Methods and Materials

Table II. 1. Specification of samples used in this research work as given by the manufacturer.

Company	Sample Name	Code	MeO (%)	HPO (%)	Viscosity (mPa.s) (2% in water, 20°C)
ShinEtsu	Tylose MOBS 50 G4	G4	28-30	7-12	40-60*
	Metolose 90SH-100SR	90SH	19-24	4-12	104000
Dow	Methocel K4M	K4M	19-24	7-12	3600
Colorcon	Methocel K15M	K15M	19-24	7-12	13486

*Polymer was dispersed in pH=6 solution, which was adjusted with NaOH and HCl.

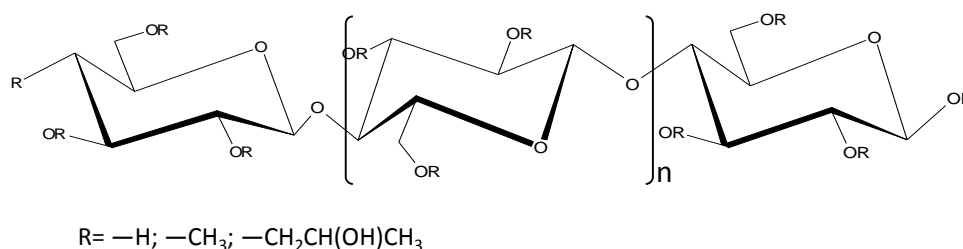


Figure II. 1. The molecular structure of hydroxypropylmethyl cellulose (HPMC).

II.1.2. Enzymes

Cellulase from *Trichoderma reesei* ATCC 26921 in aqueous solution, with the enzymatic activity of ≥ 700 Endo-Glucanase Units (EGU)/g and density of approximately 1.2 g/ml, was purchased from Sigma-Aldrich.

II.1.3. Citrate-phosphate buffer preparation:

Citrate-phosphate buffer was used for the purpose of maintaining intracellular and extracellular pH within a very narrow range¹. In this work, the expected objective is to allow the glycosidic bond cleavage by enzyme action proceed under optimal conditions (pH=5).

Thus: A and B solutions were prepared as follows:

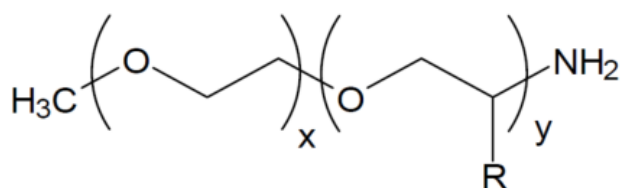
- 0.1 M solution of citric acid monohydrate ($\text{C}_6\text{H}_8\text{O}_7 \cdot \text{H}_2\text{O}$; M_w 210.14 g/mol) (10.50 g in 500 ml of Milli-Q® water).
- 0.2 M solution of dibasic sodium phosphate dodecahydrate ($\text{Na}_2\text{HPO}_4 \cdot 12\text{H}_2\text{O}$) (35.80g in 500 ml of Milli-Q® water).

Then 121,5 ml of A + 128 ml of B were diluted to a total volume of 500 ml of Milli-Q® water to reach pH=5.

II.1.4. Jeffamine® Polyetheramines:

Two polyetheramine (PEA) samples were kindly offered by Huntsman- France Company. These samples contain primary amino group attached to the end of a polyether backbone. Polyether backbone is based on either propylene oxide (PO), ethylene oxide (EO), or mixed PO/EO. Monoamine (M-2005) and Triamines (T-5000) were used in this work.

M-2005, Jeffamine® M-2005 polyetheramine is monoamine chain with an average molar mass of $2000 \text{ g}\cdot\text{mol}^{-1}$, composed by PO/EO ratio about 29/6 (Figure II.2). The content in PO is higher than that in EO, consequently Jeffamine® M-2005 is a hydrophobic compound.



R = H for (EO), or CH_3 for (PO)

Figure II. 2. Jeffamine® M-2005 structure (Manufacturer information).

T-5000, Jeffamine® T-5000 has three amines with an average molar mass of $5000 \text{ g}\cdot\text{mol}^{-1}$. Its structure is shown in Figure II.3. It is prepared by reaction of propylene oxide (PO) with a triol initiator, followed by amination of the terminal hydroxyl groups.

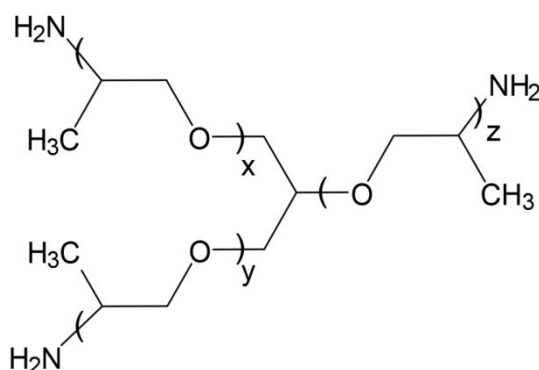


Figure II. 3. Jeffamine® T-5000 structure ($X+Y+Z=85$) (Manufacturer information).

II.2. Methods of sample preparation

II.2.1. Short chains of hydroxypropyl methylcellulose (HPMC)

II.2.1.1. Hydrolysis process

Here, we describe three steps that allow producing small fragments of HPMC. The first consist in the dissolution of polymer that leads prepare a homogeneous solution. The second correspond to cleavage of glycosidic bonds. Finally, the purification process precedes the recovery of short chained HPMC.

HPMC dissolution, was performed by first dispersing the powder in hot citrate phosphate buffer (CPB), followed by cooling of the obtained suspension. 1 g of HPMC was dispersed by mixing thoroughly with 1/5 to 1/3 of a required volume of hot CPB for 15 min at 80°C. The floats on the surface of hot CPB were gradually dispersed to form an evenly slurry. Then, the rest of CPB has added to a total volume 100 mL. The suspension was stirred over-night at room temperature to ensure complete HPMC dissolution.

Depolymerization, was achieved according to two routes: enzymatic and acid catalysis.

Enzymatic depolymerisation, the polymer solution was heated to 47 °C before enzyme addition and kept at this temperature for the whole reaction time. Different amounts of enzyme and reaction time are used in our study as given in Table 2.2. The reaction was stopped by heating the solution at 85 °C and stirring vigorously for 15 min. Then, the stirring was stopped, and the solution allowed standing at 85°C for 15 min more. Owing to the thermosensitivity, phase separation took place during the enzyme inactivation step. Consequently, the suspension was decanted into two fractions: the water soluble supernatant “S” and the precipitate “P”. After hot filtration, “P” and “S” fraction were separated. The “P” fraction was dissolved in cold water, and both fractions were kept at 4°C (Figure II.4).

Acid depolymerisation, was implemented to compare the fragments generated by enzymatic depolymerization with those from acidic one. Thus, 1 g of HPMC was dissolved under stirring (200 rpm) in 100 ml of 0.6 M of HCl at 85 °C for one h. The reaction mixture was then decanted and hot filtered into the supernatant “S” and precipitate “P” fractions,

Methods and Materials

which were recovered according to the same procedure followed for enzymatic depolymerization (Figure II.4). Acid hydrolyzed products were neutralized using 1M NaOH and cooled at room temperature.

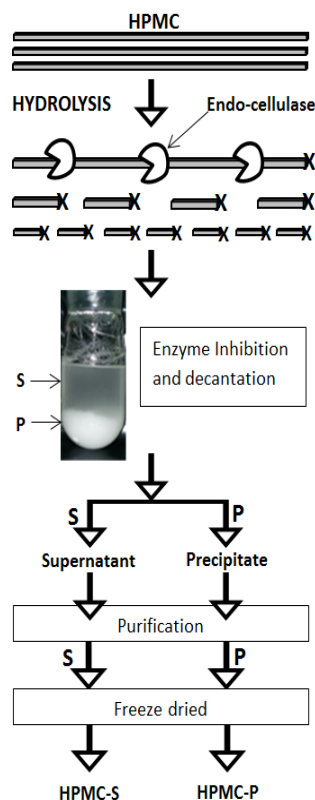


Figure II. 4. Process flow sheet of HPMC depolymerization.

Purification procedure, the objective of purification is to discard salts coming from CPB and acid neutralization, glucose units and oligosaccharides that could be produced during the hydrolysis reaction. This step was achieved by performing ultrafiltration (UF) in the diafiltration mode that is a fast and efficient method for desalting solutions and removing low M_w compounds ². A disk (76 mm) of UF GK membrane (polyamine/polysulphone material) with a molecular weight cut-off (MWCO) of 3000 g.mol⁻¹ supported by a disk of oven paper (AHLSTROM grade 3329), was placed in an Amicon stirred cell (model 8400). Fraction to be purified in 300 mL pure water was poured into the cell and washing at constant volume (continuous diafiltration) was carried out at room temperature under 3 bar of pressure (Figure II.5.). The continuous diafiltration was stopped when the filtrate solution reaches neutrality. The retentate volume was concentrated to 100 mL and freeze dried.

Methods and Materials

Fractions “S” and “P” were recovered as white fibers and stored in a dry condition before characterization. Table II-2 lists the nomenclature of the obtained products.

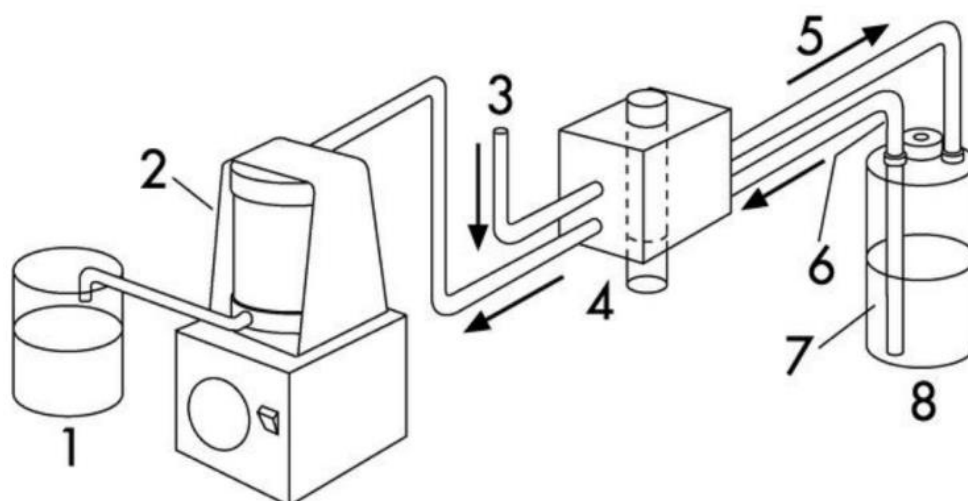


Figure II. 5. Schematic design of the Amicon diafiltration set-up: 1) permeate; 2) stirred filtration cell; 3) pressure inlet pipe; 4) cell inflow tubing; 5) tank pressure inlet; 6) tank outflow tubing; 7) water for washing salts and low M_w compounds; 8) diafiltration tank.

Methods and Materials

Table II. 2. Operating conditions for HPMC depolymerisation and list of the obtained products.

Starting HPMC	Depolymerisation method		Reaction Time (h)	Hydrolyzed product
	Enzyme:HPMC ratio ($\mu\text{L.g}^{-1}$)	Acidic		
K4M	30	—	1	KM-P-30-1; KM-S-30-1
			24	KM-P-30-24; KM-S-30-24
			72	KM-P-30-72; KM-S-30-72
	50	—	1	KM-P-50-1; KM-S-50-1
			24	KM-P-50-24; KM-S-50-24
			72	KM-P-50-72; KM-S-50-72
	180	—	1	KM-P-180-1; KM-S-180-1
			24	KM-P-180-24; KM-S-180-24
			72	KM-P-180-72; KM-S-180-72
—	HCl 0.6 M	1	KM-P-AC; KM-S-AC	
G4	15	—	1	G4-P-15-1; G4-S-15-1
			24	G4-P-15-24; G4-S-15-24
			72	G4-P-15-72; G4-S-15-72
	30	—	1	G4-P-30-1; G4-S-30-1
			24	G4-P-30-24; G4-S-30-24
			72	G4-P-30-72; G4-S-30-72
	50	—	1	G4-P-50-1; G4-S-50-1
			24	G4-P-50-24; G4-S-50-24
			72	G4-P-50-72; G4-S-50-72
	180	—	1	G4-P-180-1; G4-S-180-1
			24	G4-P-180-24; G4-S-180-24
			72	G4-P-180-72; G4-S-180-72
—	HCl 0.6 M	1	G4-P-AC; G4-S-AC	
K15M	180	—	1	K15M-P-15-1; K15M-S-15-1
			24	K15M-P-15-24; K15M-S-15-24
			72	K15M-P-15-72; K15M-S-15-72
90SH	180	—	1	90SH-P-15-1; 90SH-S-15-1
			24	90SH-P-15-24; 90SH-S-15-24
			72	90SH-P-15-72; 90SH-S-15-72

II.2.1.2. Acetylation of free hydroxyl groups in HPMC

Acetylation is a chemical reaction that is called ethanoylation in the IUPAC nomenclature. The reaction involves replacement of hydrogen atom in hydroxyl functional group by an acetyl group (Figure II.6). Acetic anhydride is used with a basic catalyst, such as pyridine. This combination promotes smooth reactions and has great solvent power. Pyridine acts as an acceptor for the acid by-product formed in the reaction. In our work, acetylation of HPMC samples was performed to determine the average substitution degree of AGUs along the cellulosic chain defined as the degree of methyl substitution (DS_{Me}) and hydroxypropyl molar substitution (MS_{HP}).

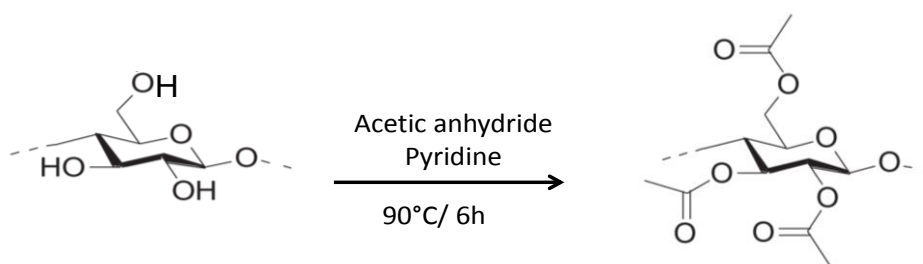


Figure II. 6. Synthesis of 2,3,6-O-acetyl AGU.

Thus, both the starting and the depolymerized HPMC samples were acetylated according to a modified version of the procedure previously described by Fitzpatrick *et al.*³. 75 mg of HPMC was mixed with 2.5 mL of acetic anhydride and 0.75 mL of pyridine, and the solution was stirred for 6 h at 90°C in a closed vial with a stopper. After the reaction, the solution was dialyzed in distilled water, using dialysis tubing with a MWCO of 12 000 g. mol⁻¹. The sample was freeze dried and recovered as a cotton fiber.

II.3. Characterization methods

II.3.1. Size-Exclusion Chromatography (SEC)

Size-Exclusion Chromatography (SEC) also referred to as gel-filtration or gel-permeation chromatography (GPC), is a very powerful separation technique. In an ideal case, the molecules are separated according to their hydrodynamic volume (volume of a polymer coil when it is dissolved in a given solvent) and eluted from the SEC column in order of decreasing size.

SEC multi-angle light scattering (MALS) in combination with refractive index (RI) detection allows the direct determination of the molar mass by an absolute method. Normally calibration standards are not required, as the MALS and RI detectors give signals proportional to molar mass and concentration, respectively⁴. MALS involves measuring the amount of light scattered by a solution at many angles relative to that of the incident laser beam.

Samples preparation: 5mg of both started and hydrolyzed samples were dispersed in the mobile phase (10mM of NaCl with 0.02 % NaN₃) and stirred for 24 hours at the room temperature. The solutions were filtered using PTFE filter (Millipore®; 0,45µm). The filtrate solutions were injected through a 100 µL loop (Rheodyne injector 7725) and eluted on a TSK-

Methods and Materials

GEL GMPWXL 7.8, 300 mm column (TosoHaas Bioseparation Specialists, Stuttgart, Germany) with a flow rate of 0.5 mL/min (Waters pump 515). A MALS detector (Dawn[®] DSP, Wyatt Technology Co, Santa Barbara, CA, USA) coupled with a refractive index detector (Optilab Wyatt Technology Co), was used to obtain on-line determination of the absolute molar mass. Each elution fraction of about 0.01 mL enables to calculate the weight average molar mass and the molar distribution (polydispersity index, PDI) for the obtained SEC profiles.

The refractive index increment (dn/dc) value taken for calculation was 0.137 mL/g. The data analysis was recovered and analyzed using Astra 4 (Wyatt Technology Co).

II.3.2. Dynamic Light Scattering (DLS)

DLS is also referred as Photon Correlation Spectroscopy or Quasi-Elastic Light Scattering. Dynamic light scattering is a non-invasive technique for measuring the size of colloids (particles and macromolecules) in a solvent. Brownian motion is the random movement of particles due to collisions caused by bombardment of the solvent molecules that surround them. The scattering intensity observed when light hits colloids, fluctuates over time due to their movement. From this information, the technique can measure the speed at which the objects diffuse due to Brownian motion. Particle and macromolecule size are given in terms of hydrodynamic radius.

This experiment was performed with a Malvern Instrument Nano-ZS equipped with a He-Ne laser ($\lambda=632.8$ nm). Polymer solutions at 1.0 mg/mL were filtered through a 0.45 μm PTFE micro filter before measurements. The correlation was analyzed via the general purpose method (NNLS) to obtain the distribution of diffusion coefficients (D) of the solutes. The apparent equivalent hydrodynamic radius (R_H) was determined from the cumulate method using the Stoke-Einstein equation:

$$R_H = \frac{k_B T}{6\pi\eta G} q^2 = \frac{k_B T}{6\pi\eta D_o}$$

Where k_B is Boltzman constant, T is temperature, G is the relaxation frequency, q is the wave vector, η is the viscosity of the medium, and D_o is the translation diffusion coefficient at finite dilution. Mean radius values were obtained from triplicate runs. Standard deviations were evaluated from hydrodynamic radius distribution.

II.3.3. Reducing end titration

Reducing end (RE) is a free aldehyde group that can be found at one end of polysaccharide chains. Several sensitive and precise assays of reducing sugars have been developed on redox reactions involving electron transfers from the aldehyde/hemiacetal functionality to oxidized metal ions such as copper sulfate (Figure II.7). Reduced cation concentrations are monitored spectrophotometrically as complexes with various chromogenic chelators such as sodium salt of 2,2'-bichinoninate acid (BCA), arsenic molybdate, phenol, 4-hydroxybenzoic acid hydrazide, etc.

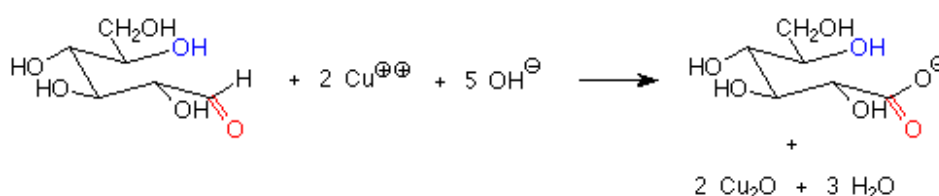


Figure II. 7. Terminal aldehyde oxidation by Cu^{2+} ions

Dinitrosalicylic acid is another available reagent that allows determining aldehyde in reducing sugars through the reduction of one nitro group into an amino group.

In this work the RE analysis was used to demonstrate the reactivity of purified hydrolyzed fractions, and not to follow enzymatic activity. The chosen titration method was Nelson-Somogyi assays which are explained in detailed below.

Nelson-Somogyi (NS) assay is based on the alkaline copper reagent of Somogyi (1952)⁵ and the color reagent of Nelson (1944)⁶. The assay involves the reduction of Cu^{2+} to Cu^+ by the RE and the formation of colored compound – arsenomolybdate. The main advantages of NS assay is the low interference with the cellulase protein⁷. However, Nelson's reagent contains arsenic which is known for its high toxicity that causes a serious environmental problem. Titration was carried out following the experience of Andersen's protocol⁸.

Reagent solutions: Alkali reagent (A) was prepared by dissolving 12 g of potassium sodium tartrate, 24 g of sodium carbonate, 16 g of sodium hydrogen carbonate, 144 g of sodium sulfate and 4 g of sodium benzoate in 500 mL of deionized water. The solution was heated

Methods and Materials

until all chemicals were dissolved. The final volume was adjusted to 800 mL with deionized water. This solution can be stored at room temperature.

Copper reagent (B) was prepared by dissolving 4 g of copper sulfate pentahydrate and 36 g of sodium sulfate in 150 mL of deionized water. The solution was heated until all chemicals were dissolved. The final volume was adjusted to 200 mL with deionized water. This solution can be stored at room temperature.

Color reagent (C) 25 g of ammonium molybdate was dissolved in 450 mL of deionized water. 21 mL of concentrated sulfuric acid was added to the molybdate solution. 3 g of sodium arsenate dibasic heptahydrate was dissolved in 25 mL of deionized water. Finally, C reagent was obtained by mixing the acidic molybdate solution with the arsenate solution. The solution was kept in a brown bottle and was incubated at 37°C during two days before use.

Sample solution: 10 mg mL⁻¹ of started and purified hydrolyzed samples were dispersed in deionized water and stirred over night at room temperature. Solutions of glucose with concentrations from 0 to 120 µM were run as standards (Figure II.8).

Titration: 500 µL of the sample or standard solution were mixed with 80 µL of (A) and 20 µL of (B) in an eppendorf tube. The mixture was thoroughly mixed before being heated at 100°C for 10 min and then cooled in an ice/water bath for 5 min. 100 µL of (C) were evenly mixed with the previous solution, and 950 µL of deionized water was added. The absorbance at 620 nm was read after 15 min of storage.

Note: The solution of high M_w HPMC (commercial samples) showed the formation of suspended solids when added to (C). Consequently, a centrifugation for 5 min at 11K RPM was done before reading the absorbance.

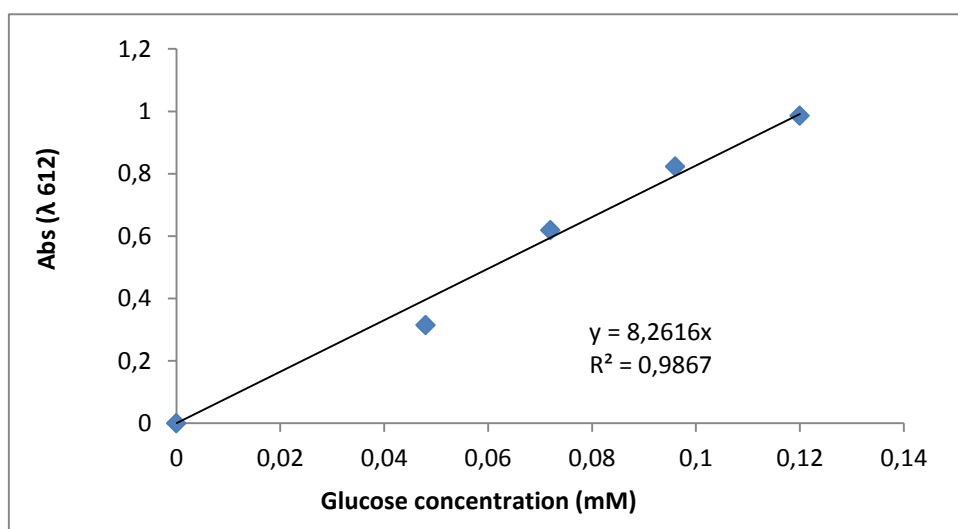


Figure II. 8. Standard glucose calibration curve.

II.3.4. Titration of thiol group using Ellman's reaction

Ellman's reagent (5,5'-dithio-bis-[2-nitrobenzoic acid], DTNB)⁹ is used to estimate sulfhydryl groups in a sample by comparing it to a standard curve of a sulfhydryl-containing compound such as cysteine¹⁰. This assay is used to determine the amount of SH groups at the extremity of functionalized polysaccharide chain obtained by reaction between reducing end and the amino group of cysteamine.

Reagent solutions:

DTNB solution: was prepared with a final concentration 2mM of 5,5'-dithio-bis-[2-nitrobenzoic acid] (DTNB) of 50 mM sodium acetate and kept refrigerated.

TRIS buffer solution (TBS), pKa = 8.06: 2-amino-2-hydroxyméthyl-1,3-propanediol was used to prepare 1M TRIS and adjusted to pH=8.

Standard solution: was prepared using acetyl cysteine (0-70 μ M) for calibration (Figure II.9).

Samples: 20 mg of thiolated polysaccharide were dispersed in 1ml of 50mM sodium acetate.

Titration: The following solutions were added in an assay tube: 100 μ L of DTNB, 200 μ L of TBS, 1680 μ L of deionized water and finally 20 μ L of sample. The solution was thoroughly

Methods and Materials

mixed with vortex and incubated for 5min at room temperature. The absorbance was measured at 412 nm.

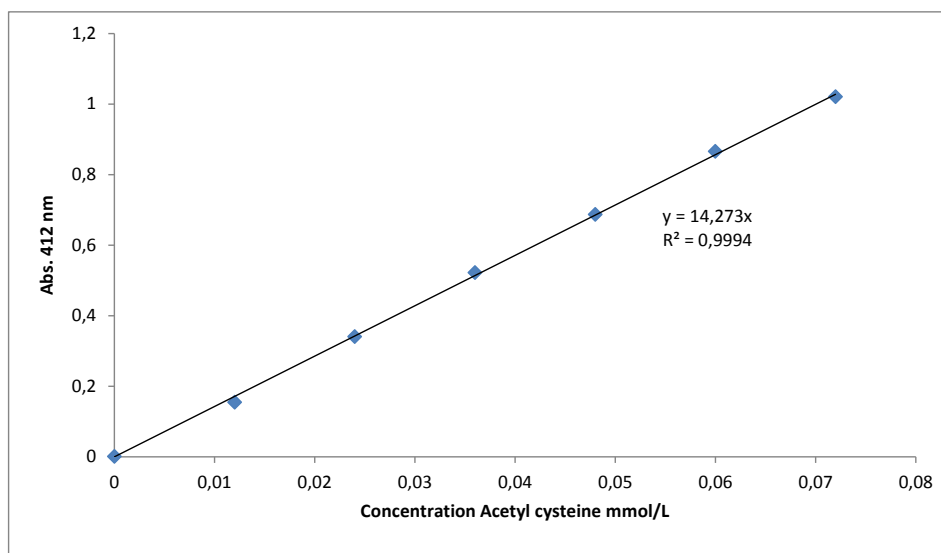


Figure II. 9. Standard acetyl cysteamine calibration curve.

II.3.5. Cloud Point (Cp)

Cp is the phase separation from solution and solidification above a certain temperature e.g. thermoresponsive hydrogel¹¹. Thermoresponsive hydrogels shows a transparent solution below the Cp temperature. In contrast above the Cp, the polymer becomes hydrophobic and insoluble. These phenomena are governed by the balance of hydrophilic and hydrophobic moieties on the polymer chain¹². Ibett and coworkers in 1992, defined cloud point as the temperature at which visual clarity was lost¹³. Other authors defined as the temperature at which light transmission reaches 50 %¹⁴. In this work, we considered both Cp_o as onset Cp (determined by extrapolation of the linear region of 100% of transmittance and the tangent line of the inflection point) and Cp_{50} as average Cp (considered when the transmittance reach the 50 % of transmittance (Figure II.10).

The cloud temperature of starting and hydrolyzed polymers was measured by the diminution of the transmittance of polarized light. UV-Vis Perkin Elmer/LAMDA 35 Spectrophotometer and Temp Lab software were used to recover data. The temperature ramp was fixed at 0.2 °C /min between 50 to 85 °C, and the wavelength at 600 nm. The sample solutions were prepared at 2 % of concentration using deionized water, stirred for 24 hours and kept at 5°C overnight before analysis.

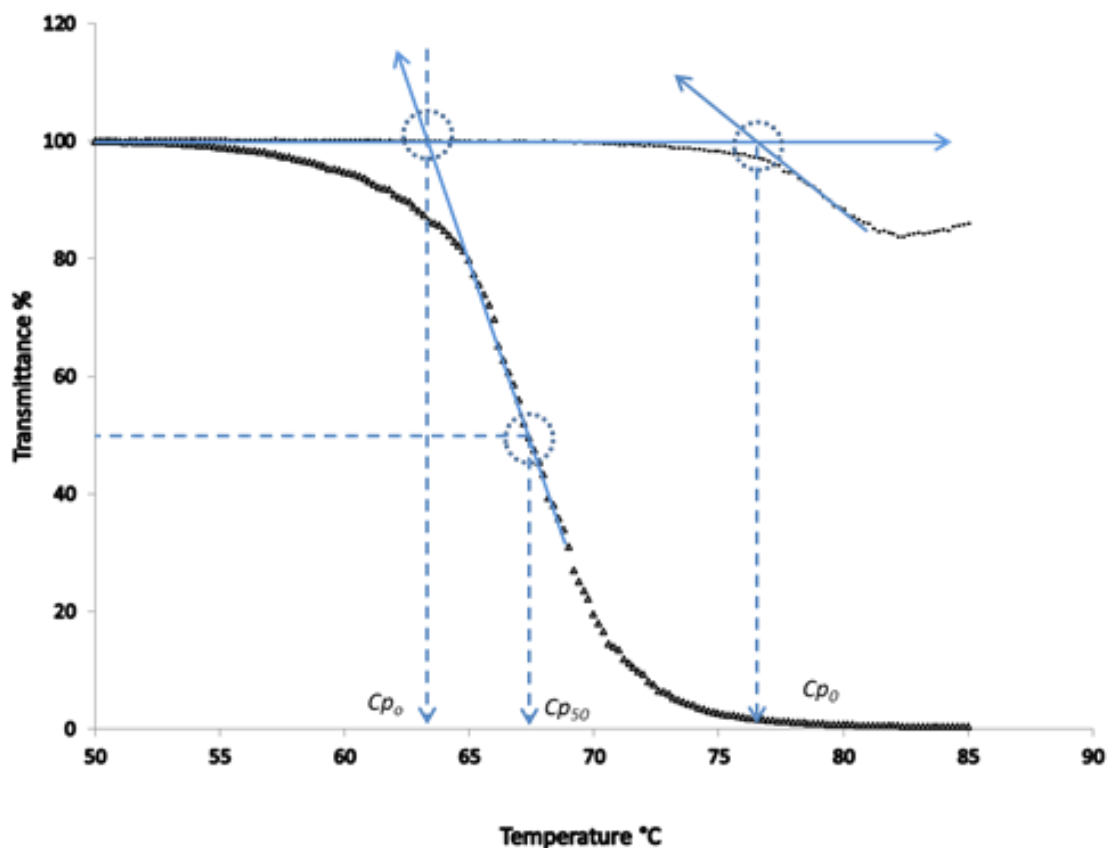


Figure II. 10. Clouding point profile and the schema to consider Cp_0 and Cp_{50} .

II.3.5. Fourier transforms infrared spectroscopy (FT-IR)

An infrared spectrum represents a fingerprint of a sample with absorption peaks which correspond to the frequencies of vibrations between the bonds and the atoms making up the material. FT-IR spectra were recorded on a Nicolet NEXUS spectrometer with a DTGS detector at 4 cm^{-1} resolution. The spectra were recorded in air atmosphere, and 64 scans were taken per sample. The sample preparations consisted in mixing 2-2.5 mg of solid sample with 200 mg of spectral grade potassium bromide (KBr). The mixture was ground and pressed to form a transparent disk.

II.3.7. Nuclear magnetic resonance (NMR) spectroscopy

The ^1H NMR spectra of acetylated samples were acquired with Bruker Avance 250 (250 MHz) spectrometer in deuterated chloroform (CDCl_3) at $50\text{ }^\circ\text{C}$ to determine the degree of methylation (DS_{Me}) and of hydroxypropyl action (MS_{HP}) of acetylated samples.

Methods and Materials

DS_{Me} and MS_{HP} values were calculated from the integration of the different NMR signals as detailed on Figure II.11. This method was described by Fitzpatrick³. The spectra were collected using oversampling with UNISON as software.

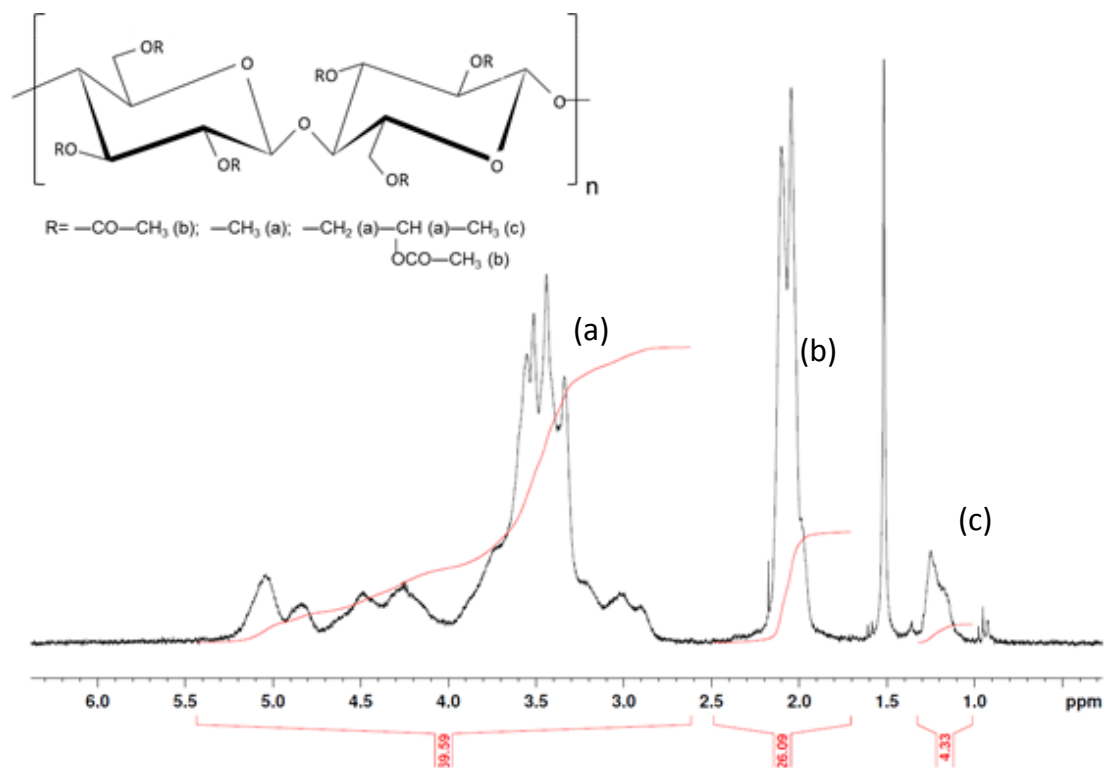


Figure II. 11. NMR spectrum in $CDCl_3$ of acetylated K4M. Signal (a) is assigned to protons on the glucose ring, the methyl substituents, and the protons on isopropyl substituents, signal (b) to protons on the acetyl groups and signal (c) to methyl protons on isopropyl substituents.

The sum of the integrations (a) + (b) was normalized to 16 protons (7 coming from the glucose ring and 9 coming from the substituents).

$$x = \frac{16}{(a+b)} \quad \text{Eq. II.1}$$

The degree of methylation was calculated by:

$$DS_{Me} = \frac{(xa-xb-7)}{3} \quad \text{Eq.II.2}$$

The hydroxypropyl molar substitution was obtained from:

$$MS_{HP} = \frac{xc}{3} \quad \text{Eq.II.3}$$

II.3.8. Synthesis of block copolymer

Linear diblock copolymer was synthesized following two procedures:

1) end-to-end coupling, consists in reacting the native terminal aldehyde end group of the polysaccharide chain with a α -amino functional polymer chain, through a reductive amination process in the presence of sodium cyanoborohydride. Thus, Jeffamine® M-2005 (PO₂₉-EO₆) and T-5000 (PO₈₅) were coupled with short HPMC chains.

HPMC-*b*-PO₂₉-EO₆: 1 g of HPMC ($M_w=8000 \text{ g mol}^{-1}$, 0.125 mmol) and NaCNBH₃ (0.2 g, 3mmol) was dissolved in 50 mL of DMSO/NaCl 10mM (3/1 v/v) at 60°C. After one day of reaction, Jeffamine® M-2005 was added ($M_w= 2000 \text{ g mol}^{-1}$, 0.615 g, 0.30 mmol) to the solution. The mixture was stirred at 60 °C for five days (Figure II.12). The resulting solution was dialyzed for four days in distilled water, using dialysis tubing with MWCO of 3000 g mol^{-1} . The samples were freeze dried and recovered as a powder.

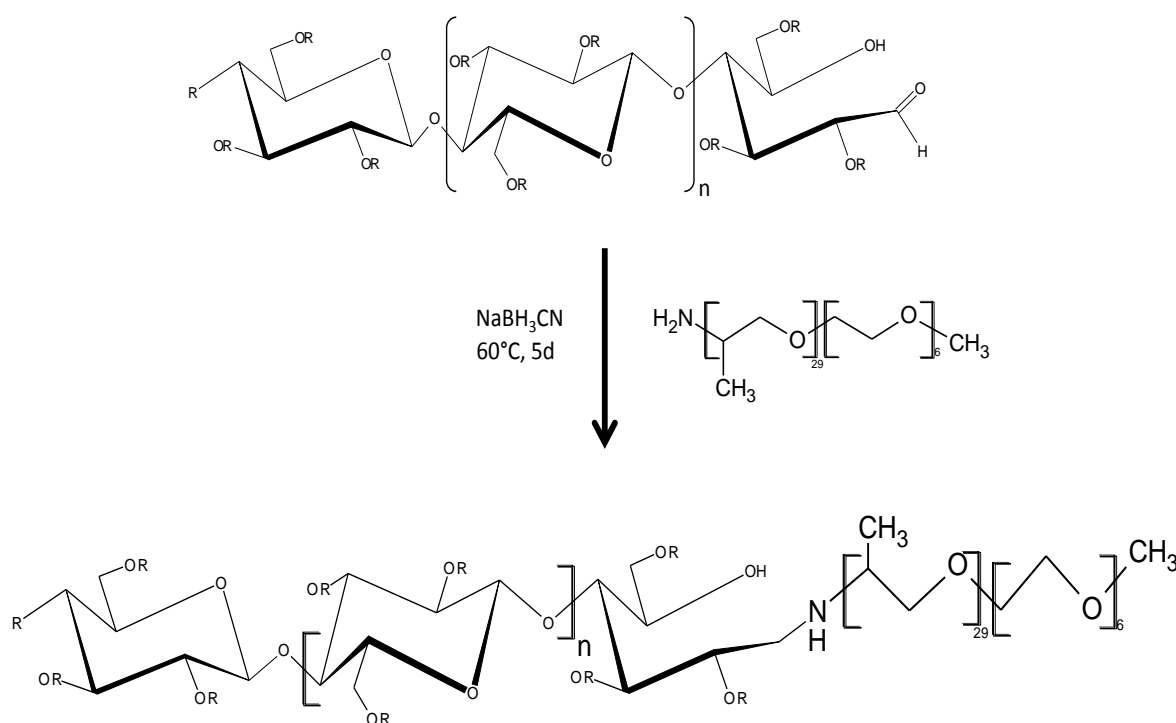


Figure II. 12. Synthesis scheme of HPMC-*b*-PO₂₉-EO₆.

(HPMC)₃-*b*-PO₈₆: 1 g of HPMC ($M_w=8000 \text{ g. mol}^{-1}$, 0.125 mmol) and NaCNBH₃ (0.008 g, 0.125mmol) was dissolved in 50 mL of DMSO/NaCl 10mM (3/1 v/v) at 60°C. After one day

Methods and Materials

of reaction, Jeffamine[®] T-5000 was added ($M_w = 5000 \text{ g. mol}^{-1}$, 0.06 g, 0.0125 mmol) to the solution. The mixture was stirred at 60 °C for five days (Figure II.13). The resulting solution was purified, using dialysis tubing with MWCO of $12000 \text{ g. mol}^{-1}$. The samples were freeze dried and recovered as a powder.

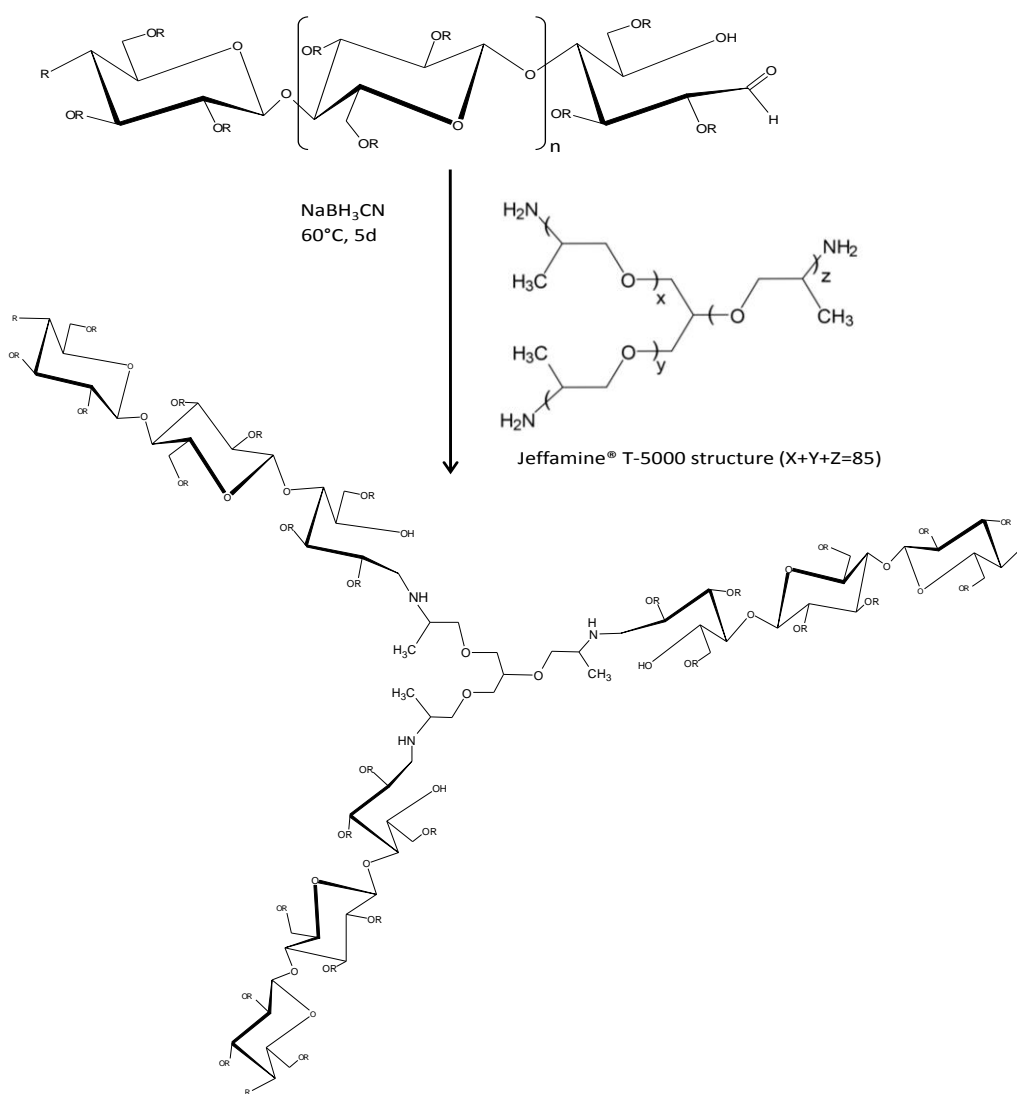


Figure II. 13. Synthesis scheme of (HPMC)₃-b-PO₈₅.

2) The second procedure to synthesize linear AB block copolymer based on polysaccharides consist to introduce thiol group at the reducing end of HPMC by reductive amination reaction (same procedure than 1) as a shown in Figure II.14. These new functional groups can be reacted with other types of alkyne terminated polymers by the way of thiol-ene click reaction.

Methods and Materials

Thiol-HPMC preparation. In brief 1 g of HPMC with an weight average molar mass of 8000 g mol⁻¹ (0.125 mmol) and NaCNBH₃ (0.2 g, 3mmol) were solubilized in 50 ml of DMSO/NaCl 10mM (3/1 v/v) at 60°C. After that, cysteamine (0.1 g, 1.25mmol) was added, and the mixture was stirred for six days at 60 °C.

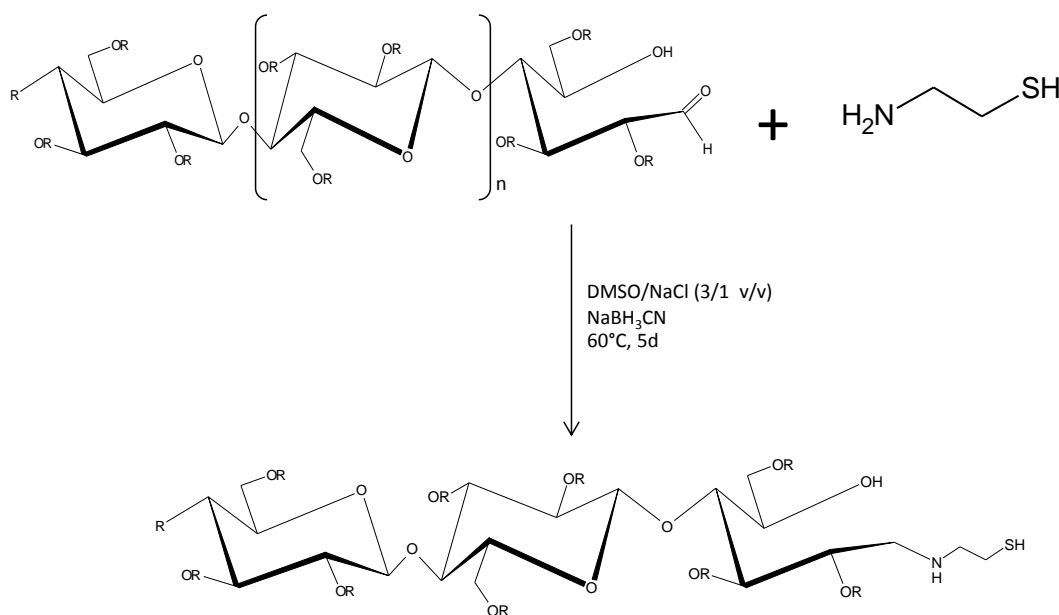


Figure II. 14. Synthesis scheme of HPMC-thiol

PLA alkene synthesis. Ring opening polymerization (ROP) was carried out in solution using standard Schlenk technique under an inert atmosphere of nitrogen. L-lactide (7,2 g, 50 mmol), allyl alcohol (0, 212 g, 3,6 mmol), catalyst tin(II) 2-ethylhexanoate (Sn(Oct)₂) (0,2 g, 0,49 mmol) and 30 ml of toluene were used (Figure II.15). Anhydrous toluene (20mL) and L-lactide were added in an oven dried Schlenk tube fitted with a rubber septum, followed by addition of allyl alcohol and a catalyst dispersed in 10 ml of anhydrous toluene. The solution was further degassed by three freeze-pump-thaw cycles. The resulting mixture was stirred at 80 °C for 15 h. After cooling down to the room temperature, the reaction mixture was poured into cold diethyl ether. The precipitate was then collected by filtration and drying in vacuum.

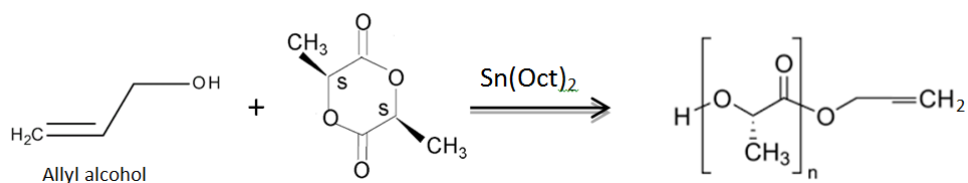


Figure II. 15. Synthesis scheme of alkene functional PLA.

II.3.9. Synthesis of HPMC-*b*-PLA, via UV- initiated thiol-ene click reaction

The UV-initiated thiol-ene click reaction of HPMC-SH homopolymer with alkene-terminated PLA in DMSO was carried out in a Dinics Uv-Chamber M3. The reactor was equipped with a PL-L 36W/01/4P Hg lamp at room temperature (26 °C). HPMC-SH homopolymer ($M_w = 8000 \text{ g mol}^{-1}$, 1 g, 0.14 mmol), PLA ($M_w = 3000 \text{ g mol}^{-1}$, 0.125 g, 0.041 mmol), DMPA (18 mg, 0.069 mmol) and DMSO (10mL) were introduced into falcon tube and vigorously stirred. The reaction mixture was poured into petri plate and subjected to UV irradiation for 10 h under slow stirring during all reaction time. The resulting HPMC-*b*-PLA copolymer was precipitated in excess acetonitrile. The solid copolymer was recovered by centrifugation at 4000 rpm for 15min and drying in a vacuum oven overnight at 35 °C.

REFERENCES

1. Mohan, C., *Buffers. A guide for the preparation and use of buffers in biological systems*. Calbiochem: Darmstadt, Germany, **2003**, p. 1-37.
2. Schwartz, L. *Diafiltration: A Fast, Efficient Method for Desalting or Buffer Exchange of Biological Samples*; Pall Corporation: PN 33289: USA, **2003**, p. 6.
3. Fitzpatrick, F.; Schagerlof, H.; Andersson, T., *et al.*, NMR, cloud-point measurements and enzymatic depolymerization: Complementary tools to investigate substituent patterns in modified celluloses. *Biomacromolecules* **2006**, *7* (10), 2909-2917.
4. Chen, M. H.; Wyatt, P. J., The measurement of mass and size distributions, conformation, and branching of important food polymers by MALS following sample fractionation. *Macromol Symp* **1999**, *140*, 155-163.
5. Somogyi, M., Notes on sugar determination. *J. Biol. Chem.* **1951**, *195*:19-23.
6. Nelson, N., A Photometric adaptation of the Somogyi method fo the determination for the determination of glucose. *J. Biol. Chem.* **1944**, *153*: 375-380.
7. Zhang, Y. H. P.; Himmel, M. E.; Mielenz, J. R., Outlook for cellulase improvement: Screening and selection strategies. *Biotechnol Adv* **2006**, *24* (5), 452-481.
8. Anderses, N. Enzymatic Hydrolysis of Cellulose. Technical university of Denmark, Copenhagen, **2007**.
9. Ellman, G. L., Tissue sulfhydryl groups. *Arch. Biochem. Biophys* **1958**, *74*, 443.
10. Bulaj, G.; Kortemme, T.; Goldenberg, D. P., Ionization-reactivity relationships for cysteine thiols in polypeptides. *Biochemistry* **1998**, *37* (25), 8965-8972.
11. Schagerlof, H.; Johansson, M.; Richardson, S., *et al.*, Substituent distribution and clouding behavior of hydroxypropyl methyl cellulose analyzed using enzymatic degradation. *Biomacromolecules* **2006**, *7* (12), 3474-81.
12. Taylor, L. D.; Cerankowski, L. D., Preparation of Films Exhibiting a Balanced Temperature-Dependence to Permeation by Aqueous-Solutions - Study of Lower Consolute Behavior. *J Polym Sci Pol Chem* **1975**, *13* (11), 2551-2570.
13. Ibbett, R. N.; Philp, K.; Price, D. M., ¹³C n.m.r. Studies of the thermal behaviour of aqueous solutions of cellulose ethers. *Polymer* **1992**, *33* (19), 4087-4094.
14. Sarkar, N., Thermal Gelation Properties of Methyl and Hydroxypropyl Methylcellulose. *J Appl Polym Sci* **1979**, *24* (4), 1073-1087.

CHAPTER III: DEPOLYMERISATION OF HYDROXYPROPYL METHYL CELLULOSE

Depolymerisation of hydroxypropyl methyl cellulose

INTRODUCTION

The preparation of smart nano- or macro-structure materials requires well defined molecules. In this context, depolymerisation of biopolymers including polysaccharides, proteins and lignin is an intense field of research to yield high-value chemicals from renewable resources¹⁻³. Most studies aim at producing low average molar mass compounds as platform molecules to replace fossil-based analogues. A complete depolymerisation is required with the notable exception of protein hydrolysis for which bioactive peptides is often sought. By contrast, our work is focused on partial depolymerisation to prepare mono-functional fragments with a low degree of polymerization (DP) that can react further as building blocks for the construction of more complex molecular architectures.

The cellulose backbone associated to an amphiphilic nature linked to the alkyl substitution gives to cellulose ether derivatives properties such as water retention, thickening and emulsifying activity. Also, their biocompatibility and harmlessness make them attractive candidates for biomedical applications⁴⁻⁵. Depolymerisation of polysaccharides can be achieved by physical, chemical and enzymatic catalysis techniques. Irradiation of cellulose and its derivatives by the electron beam and γ -ray has been studied since a long time for many purposes as sterilisation, graft modification and degradation⁶. However, it has been found that the depolymerisation efficiency decreases with the irradiation dose and the extent of substitution so that, even for large doses, the weight average molar mass (M_w) reaches a steady state of about 20 – 40 kg.mol⁻¹⁷. More recently, ultrasonic irradiation has been applied for the same purpose⁸⁻¹⁰. Interestingly, a range of cellulose ethers with varying M_w can be produced depending on the irradiation duration and the power source. Again, it was found almost the same limiting M_w of about 30 – 40 kg.mol⁻¹ independent of the starting material characteristics⁸. Therefore, the vast majority of depolymerisation studies involve acid and enzyme catalysis.

Conventional hydrolysis of polysaccharides catalysed by mineral acid has been extensively studied, and several industrial processes have been proposed for production of sugars from cellulose¹¹. The reaction is generally fast at high temperature. The chain scission takes place statistically, and it was shown that partial acidic hydrolysis of xylan led to a mixture of products with varying degrees of polymerisation¹². On the other hand, enzymatic

Depolymerisation of hydroxypropyl methyl cellulose

hydrolysis proceeds smoothly and selectively. Two main groups of cellulases can be considered for cellulose depolymerisation: endoglucanases (EG) catalysing random cleavage within the chains and exoglucanases (EX) catalysing depolymerisation from the chain ends¹. So far, most of the studies were done on the enzymatic hydrolysis of cellulose derivatives have been performed to determine their structural features, including the degree and position of substitution on the glycosyl unit, and the distribution along the chain¹³⁻¹⁶.

Hydroxypropylmethyl cellulose (HPMC) (Figure III.1) has wide applications in pharmaceuticals, cosmetics, food, etc. However, this polymer is not commercially available in M_w range down to about $20 \text{ kg}\cdot\text{mol}^{-1}$ ¹⁷. To the best of our knowledge, no studies have been reported dealing with the preparation of shorter polymers of cellulose ethers.

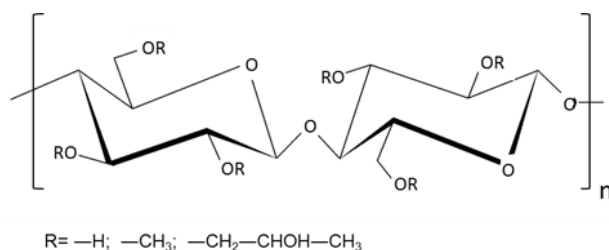


Figure III. 1. Molecular structure of hydroxypropylmethyl cellulose (HPMC).

RESULTS AND DISCUSSION

III.1. Enzymatic HPMC depolymerisation

III.1.1. Procedure

Enzymatic hydrolysis with HPMC as a substrate was undertaken to prepare small fragments of polysaccharides. Molar mass distribution and average molar mass values of started and hydrolyzed samples were monitored by SEC-MALS-RI. Figure III.2 shows the cumulative distribution of molar mass of the product obtained by hydrolysis of G4 (starting $M_w = 85\,000 \text{ g}\cdot\text{mol}^{-1}$; see chapter II). It is clear that this product contains at least two main fractions having roughly M_w values higher and lower than $10\,000 \text{ g}\cdot\text{mol}^{-1}$.

Depolymerisation of hydroxypropyl methyl cellulose

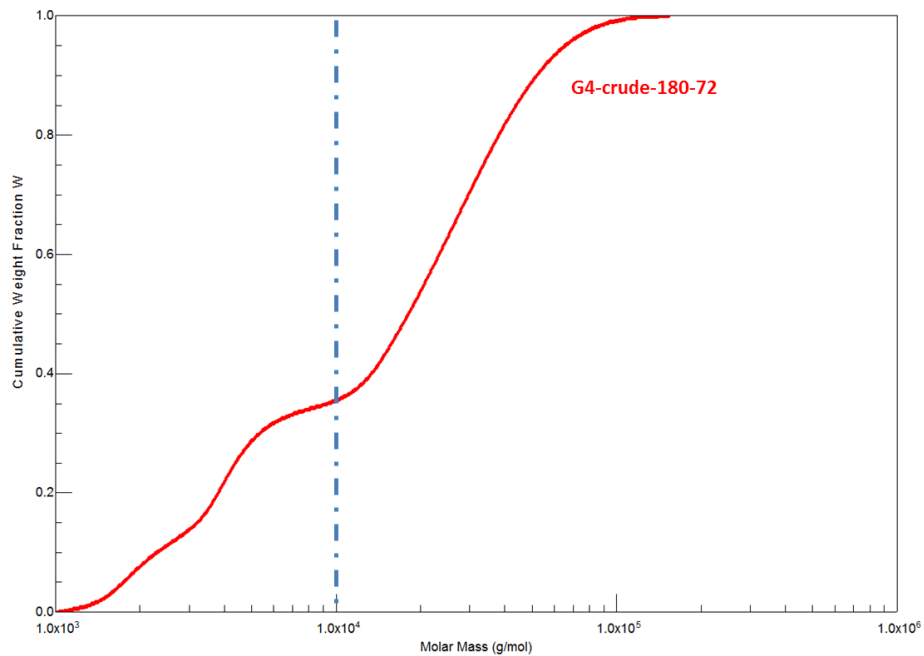


Figure III. 2. Cumulative molar mass distribution of the crude product obtained by hydrolysis of G4 using Enzyme/Substrate ratio of $180 \mu\text{L.g}^{-1}$ for 72 h.

As explained in Chapter II, a fractionation procedure was applied to the crude hydrolysate. Two distinct polymers named S and P fractions were recovered after phase separation during the enzyme inactivation step at 85°C corresponding to the soluble and precipitated fraction, respectively (Fig. III.3).

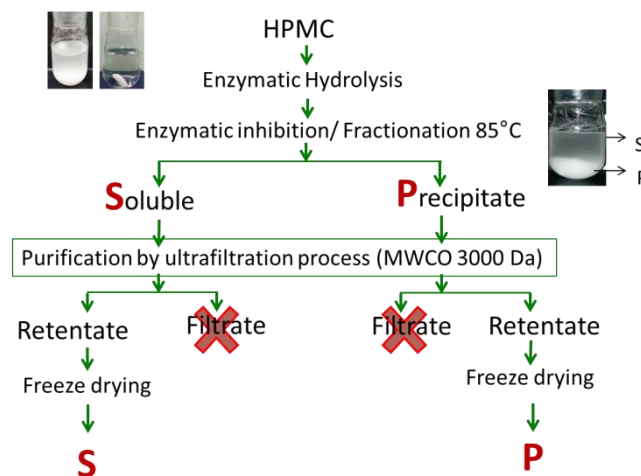


Figure III. 3. Schematic description of the preparation of HPMC S and P fractions.

Depolymerisation of hydroxypropyl methyl cellulose

Figure III.4 illustrates the SEC curves of the crude product and the fractions. The fractionation appeared successful in terms of molar distribution.

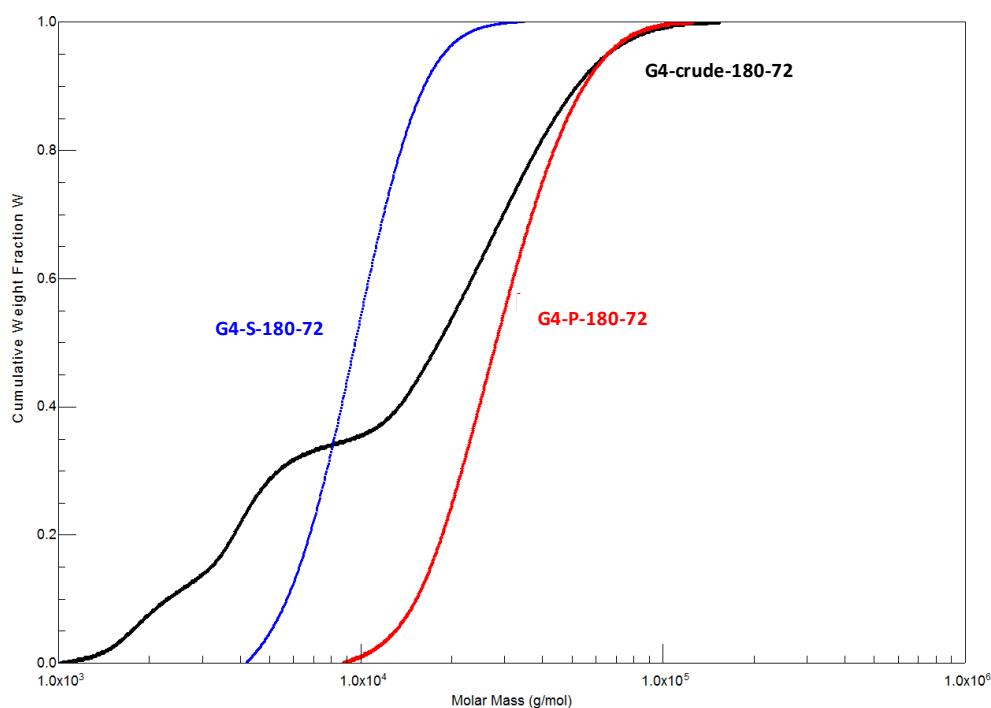


Figure III. 4. Cumulative molar mass distribution of the crude and purified S and P products obtained by hydrolysis of G4 using Enzyme/Substrate ratio of $180 \mu\text{L.g}^{-1}$ for 72 h.

It has to be noted that a deeper insight regarding the SEC-MALS-RI data can be found in Chapter IV. The depolymerisation performance was then characterized by the yield of isolated S and P fractions and, on the other hand, the respective M_w of the short HPMC chains. Parameters such as reaction time and enzyme concentration were varied to optimise the production of HPMC polymers with M_w below $20\,000 \text{ g.mol}^{-1}$.

III.1.2. Effect of reaction time on the depolymerisation efficiency

In this section, the effect of the reaction time between 1 to 96 h was examined keeping the concentration enzyme constant at $30 \mu\text{l/g}$ of HPMC. For this study, the starting HPMC was K4M from Dow Colorcon ($M_w = 235\,000 \text{ g.mol}^{-1}$).

Figure III.5 presents the yield of recovered S and P products as a function of the reaction time. The complement to 100 % of the global yield that is the sum of the S and P yields, can

Depolymerisation of hydroxypropyl methyl cellulose

be attributed to the loss of low M_w hydrolyzed compounds that pass through the UF membrane.

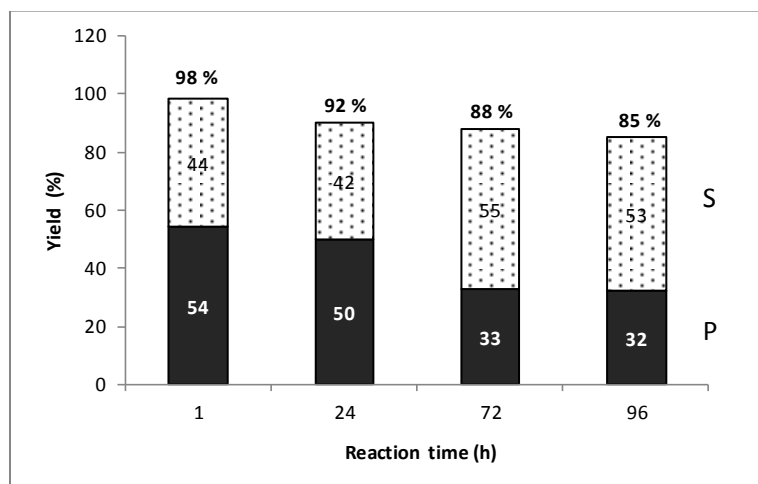


Figure III. 5. Yield evolution of the recovered S (dashed) and P (black) polymers as a function of reaction time (enzyme concentration = $30 \mu\text{L.g}^{-1}$).

As seen on Figure III.5, the yield of P fraction decreases as the depolymerisation proceeds and levels off to about 30 % at higher reaction times. During the same time, the yield of S fraction increases with an optimum value of about 55 % after 72 h.

Figure III.6 presents the variation of M_w for the two isolated polymers as a function of reaction time. The same trend of variation can be seen whatever the considered fraction: a sharp drop of M_w is observed during the first hour of reaction followed by a gradual M_w reduction.

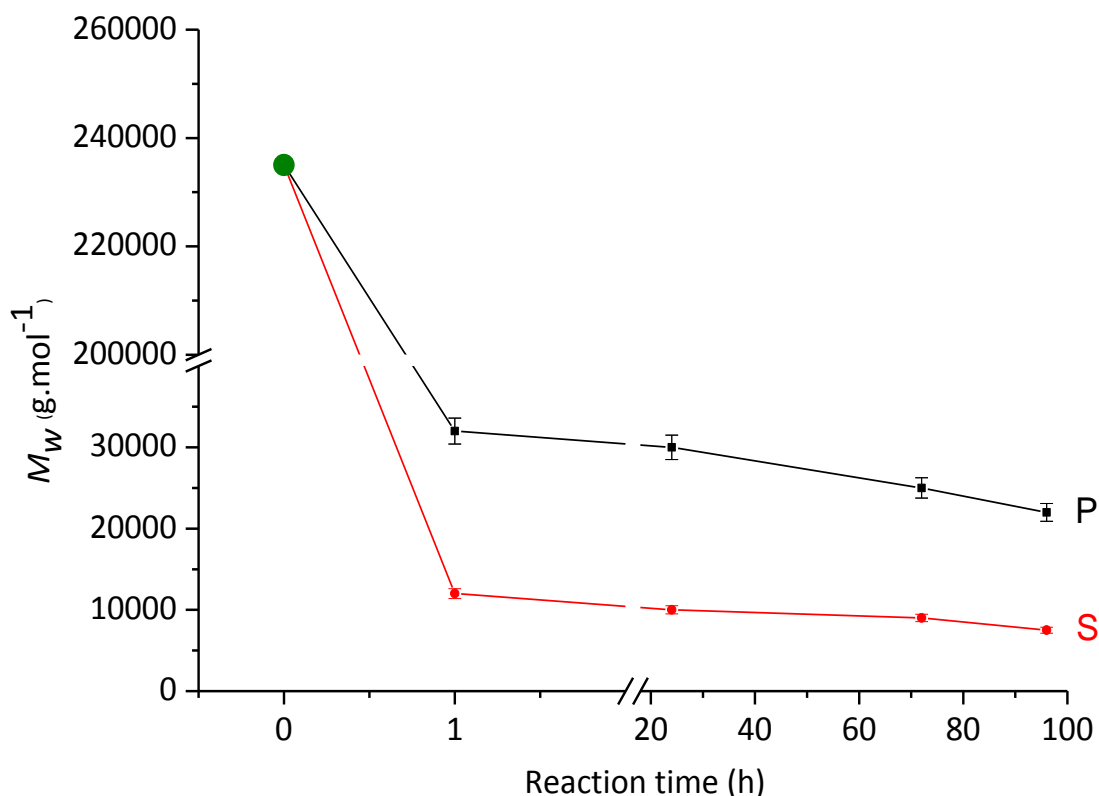


Figure III. 6. M_w variation of S and P fractions as a function of reaction time using $30 \mu\text{L.g}^{-1}$ enzyme concentration and K4M HPMC as starting polymer ($M_w = 235\,000 \text{ g.mol}^{-1}$).

Adsorption of endoglucanase (EG) onto the cellulosic chain needs at least five unmodified AGUs¹⁸⁻¹⁹. On the other hand, exoglucanase (EX) enzyme attacks by the chain extremity (see the mechanism of cellulosic chain hydrolysis depicted in Figure I.26). Indeed, cellulase from *Trichoderma reesei* used in this study is a cocktail mainly containing EG enzymes with a fraction of EX enzymes²⁰⁻²². It is then supposed that the depolymerisation of HPMC was the result of a combined effect of EG and EX enzymes. After one h of reaction, the global yield of polymers is almost 100 % (Figure III.5) meaning that only a very small fraction of low average molar mass compounds was formed. Consequently, it was assumed that the observed M_w reduction during this period is only due to EG action that randomly cleaves the cellulosic chain.

Depolymerisation of hydroxypropyl methyl cellulose

From this point, the following nomenclature was chosen to name the different HPMC products: WW-XX-YY-ZZ where WW stands for the starting HPMC, XX for the P or S fraction, YY for the enzyme concentration and ZZ for the reaction time.

The average number of domains (z) along the chain where EG can cleave the starting K4M HPMC was calculated by the following equations:

$$\frac{(z+1)}{M_n^0} = \frac{0.54}{M_n^P} + \frac{0.44}{M_n^S} \quad (\text{Eq. III.1})$$

where M_n^0 , M_n^P and M_n^S denote the number average molar mass of the starting HPMC, and of the resulting P and S polymers, respectively; 0.54 and 0.44 were the mass fraction obtained of each fractions after 1 h of reaction; and $(z + 1)$ is the mean number of fragments produced during the reaction. The first term of this equation stands for the total number of molecules in 1 g and the second term is the sum of molecules coming from both fractions.

Table III.1 displays the molar mass averages and the polydispersity index ($PDI = M_w/M_n$) of K4M, the S (K4M-S-30-1) and P (K4M-P-30-1) polymers obtained after 1 h of reaction using an enzyme concentration of $30 \mu\text{L.g}^{-1}$ of starting HPMC.

Table III. 1. Weight (M_w) and number (M_n) molar mass averages of the starting K4M HPMC and of the S and P polymers obtained after 1 h of reaction (EG = $30 \mu\text{L.g}^{-1}$ of K4M) named K4M-S-30-1 and K4M-P-30-1, respectively and their corresponding polydispersity index (PDI).

HPMC	M_w (g.mol ⁻¹)	M_n (g.mol ⁻¹)	PDI
K4M	235 000 ± 2 000	78 000 ± 1 000	3.0 ± 0.1
K4M-P-30-1	31 000 ± 600	24 000 ± 500	1.3 ± 0.1
K4M-S-30-1	11 000 ± 300	7 000 ± 250	1.6 ± 0.1

It should be noted that the fractionation step by precipitation seems to be more efficient than UF since PDI of K4M-P-30-1 is lower than that of K4M-S-30-1.

The resolution of equation III.1 using the values reported in Table III.1 gives a total number of chain cleavages:

$$z = 5.7 \quad (\text{Eq. III.2})$$

Depolymerisation of hydroxypropyl methyl cellulose

meaning that there are about 6 domains comprising at least 5 unmodified AGUs along the K4M chain where EG can readily adsorb. It is obvious that this calculation is only indicative and must be validated by structural investigations involving complete fragment hydrolysis and analysis of the resulting sugars. However, this kind of study lies out of the scope for our work.

Equation III.3 shows the mass conservation assuming again that the conversion into the low average molar mass is negligible (ε) with respect to the polymer production (supposed to be true for total polymer yield $\geq 95\%$). It allows us to calculate the mean number x and y of P and S fragments, respectively.

$$M_n^0 = x.M_n^P + y.M_n^S + \varepsilon \quad (\text{Eq. III.3})$$

with,
$$x + y = z + 1 \quad (\text{Eq. III.4})$$

It comes by combining equations III.2, III.3 and III.4 that x is equal to 1.9 and y to 4.8. It can be then concluded that the initial K4M chain was cleaved into approximately 2 P fragments and 5 S fragments when using $30 \mu\text{L.g}^{-1}$ of starting HPMC, after 1 h of reaction.

Figures III.7 and III.8 shown the gradual decrease of M_w for K4M-P-30 and K4M-S-30 between 24 h and 96 h of reaction. It can be now observed that M_w decreases linearly in both cases with a respective hydrolysis rate of $125 \text{ g.mol}^{-1}.\text{h}^{-1}$ and $21 \text{ g.mol}^{-1}.\text{h}^{-1}$ for K4M-P-30 and K4M-S-30. These data seem to indicate that depolymerisation of HPMC during this period resulted from EX action as only low M_w compounds were released especially in the case of K4M-S-30.

Depolymerisation of hydroxypropyl methyl cellulose

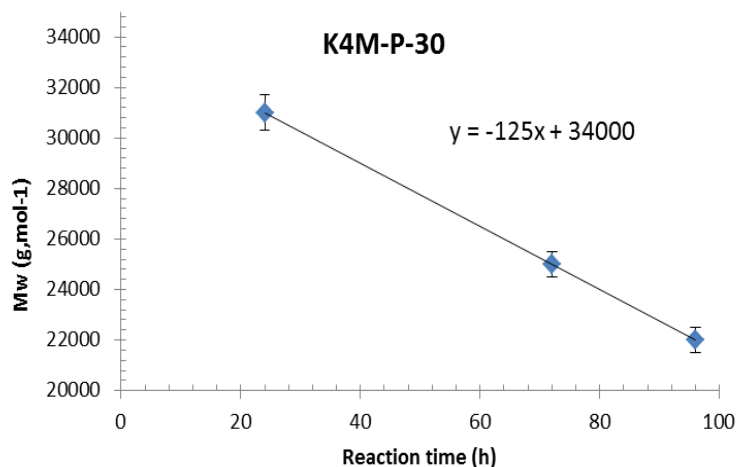


Figure III. 7. Evolution of the weight average molar mass of K4M-P-30 over reaction time.

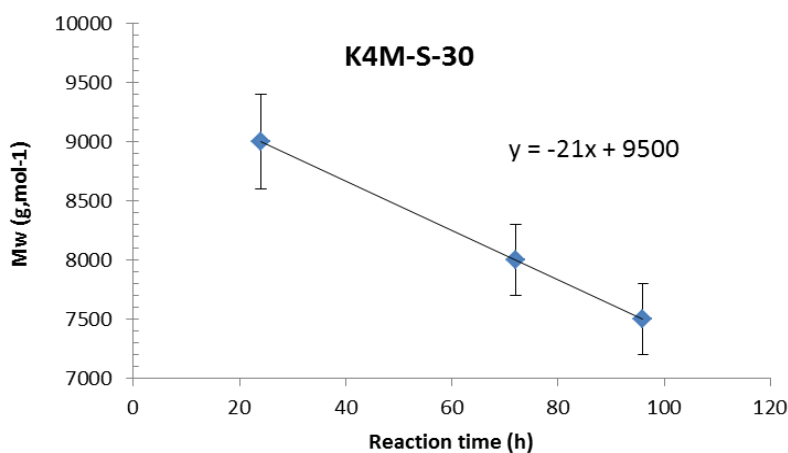


Figure III. 8. Evolution of the weight average molar mass of K4M-S-30 over reaction time.

Although the change in M_w is not very significant in the case of K4M-S-30 inherent to the accuracy of measurements by SEC-MALS-RI (in our conditions), the previous assumption is supported by the variation of the global yield in polymer over time (Fig. III.9). The low molecular weight fraction produced by EX catalysis increased with the reaction time, to reach 17 % of the initial mass after 4 days of reaction. Therefore, after 1 h of reaction, the M_w reduction can be assumed to take mainly place at chain extremities.

Depolymerisation of hydroxypropyl methyl cellulose

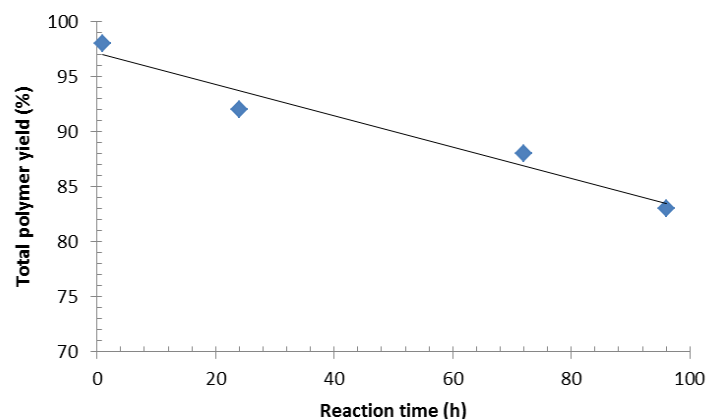


Figure III. 9. Total polymer yield over reaction time.

In conclusion of this part, the S fraction was demonstrated to give short-chained HPMC with the targeted M_w while the P fraction gave HPMC with M_w higher than $20\,000\text{ g.mol}^{-1}$. Moreover, it was observed that the chain length can be easily tuned by extending the reaction time. In fact, the enzymatic catalyst used in this work contained a small amount of EX enzyme. We believe that EX enzyme is responsible for incremental chain length reduction when EG enzyme could not cleave the chain due to the lack of adsorption sites. Thus, for instance, experimental conditions using $30\ \mu\text{L.g}^{-1}$ of enzyme cocktail and a reaction time of 3 days enabled to prepare HPMC with M_w of $8\,000\text{ g.mol}^{-1}$ in a good yield (55 %). This main conclusion raises now the question of whether other conditions as an increase of the enzyme concentration or change of starting HPMC might lead to increase shorter HPMC yields.

III.1.3. Effect of the enzyme concentration on the depolymerisation efficiency

The effect of enzyme concentration on the yield and M_w of short chained fragments obtained after K4M depolymerisation was investigated in the range 15 to $180\ \mu\text{L.g}^{-1}$. Figure III.10 shows the M_w change as a function of enzyme concentration for the P and S fractions isolated after 1h.

Depolymerisation of hydroxypropyl methyl cellulose

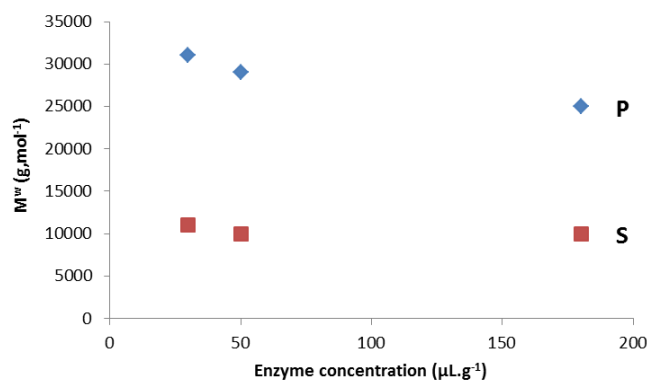


Figure III. 10. M_w variation of S and P fractions as a function of enzyme concentration after 1 h of reaction. K4M HPMC was the starting polymer ($M_w = 235\,000\text{ g.mol}^{-1}$).

As expected, a drastic drop of M_w is observed after 1 h of reaction, and the obtained M_w values level off at 25 000 and 10 000 g.mol^{-1} for P and S polymers, respectively. Again, it is assumed that the chain cleavage at this stage occurred by EG action. The average number of chain cleavages (z) and of P and S fragments per chain (x and y , respectively) can be calculated using equation III.1 to 4. Table III.2 gathers the data needed for calculation and Table III.3 the calculated z , x and y parameters.

Table III. 2. Weight (M_w) and number (M_n) molar mass averages of the S and P polymers obtained with different enzyme concentrations after 1 h of reaction and corresponding yield.

Fraction	K4M-P-YY-1			K4M-S-YY-1			
	Enzyme concentration ($\mu\text{L.g}^{-1}$)	M_w g.mol^{-1}	M_n g.mol^{-1}	Yield (%)	M_w g.mol^{-1}	M_n g.mol^{-1}	Yield (%)
	30	31 000	24 000	54	11 000	7 000	44
	50	29 000	21 000	48	10 000	6 000	50
	180	25 000	18 000	45	10 000	6 000	50

As expected from the M_w data reported in Figure III.8, the average number of chain cleavages reaches a plateau of 6 to 7 whatever the enzyme concentration. On the other hand, it appears that the mean number of P and S fragments per chain did not change with the amount of catalyst taking into account the approximations done into the calculation. This result means that the adsorption sites giving rise to the short chains are readily available

Depolymerisation of hydroxypropyl methyl cellulose

to the EG adsorption. In other words, the adsorption step is independent of the catalyst concentration provided that a minimum amount (about $30 \mu\text{L.g}^{-1}$) was added. Interestingly, the same values can be reached using a $15 \mu\text{L.g}^{-1}$ concentration for 72 h. It is important to note that the EX amount in this case seems to be too low to give a large quantity of low molecular weight compounds since the total polymer yield was almost quantitative.

Table III. 3. The average number of chain cleavage (z) and the mean number of P (x) and S (y) fragments per chain (rounded values for sake of clarity) calculated from equations III.1 to III.4.

Polymer	z	x	y
K4M-XX-15-24 ^{a)}	4.0	1.5	3.5
K4M-XX-15-72 ^{b)}	7.0	2.0	6.0
K4M-XX-30-1	6.0	2.0	5.0
K4M-XX-50-1	7.0	2.0	6.0
K4M-XX-180-1	7.0	2.0	6.0

a) M_n^P and $M_n^S = 29\ 000$ and $10\ 000 \text{ g.mol}^{-1}$; yield (P) and yield (S) = 53 and 45 %.

b) M_n^P and $M_n^S = 21\ 000$ and $6\ 500 \text{ g.mol}^{-1}$; yield (P) and yield (S) = 52 and 47 %.

Again, these data are only indicative and must be confirmed by a detailed structural study which is out of scope for our work.

At this point, it is interesting to investigate the evolution of the yield and M_w over time to examine the action of EX enzyme in various concentrations. Figure III.11 presents the yields obtained for the two isolated fractions as a function of reaction time for the different conditions of enzyme concentration.

The same trend is observed whatever the enzyme concentration used. After 1 h of reaction, each fraction was obtained in approximately 50 % yield. For longer times, P fractions decreased while S ones increased. At the same time, the total polymer yield (P + S) declined. As mentioned before, this result can be interpreted by a mass loss of low average molar mass compounds. The latter effect is more marked with higher enzyme concentration ($180 \mu\text{L.g}^{-1}$) to reach 67 % for 4 days of reaction.

Depolymerisation of hydroxypropyl methyl cellulose

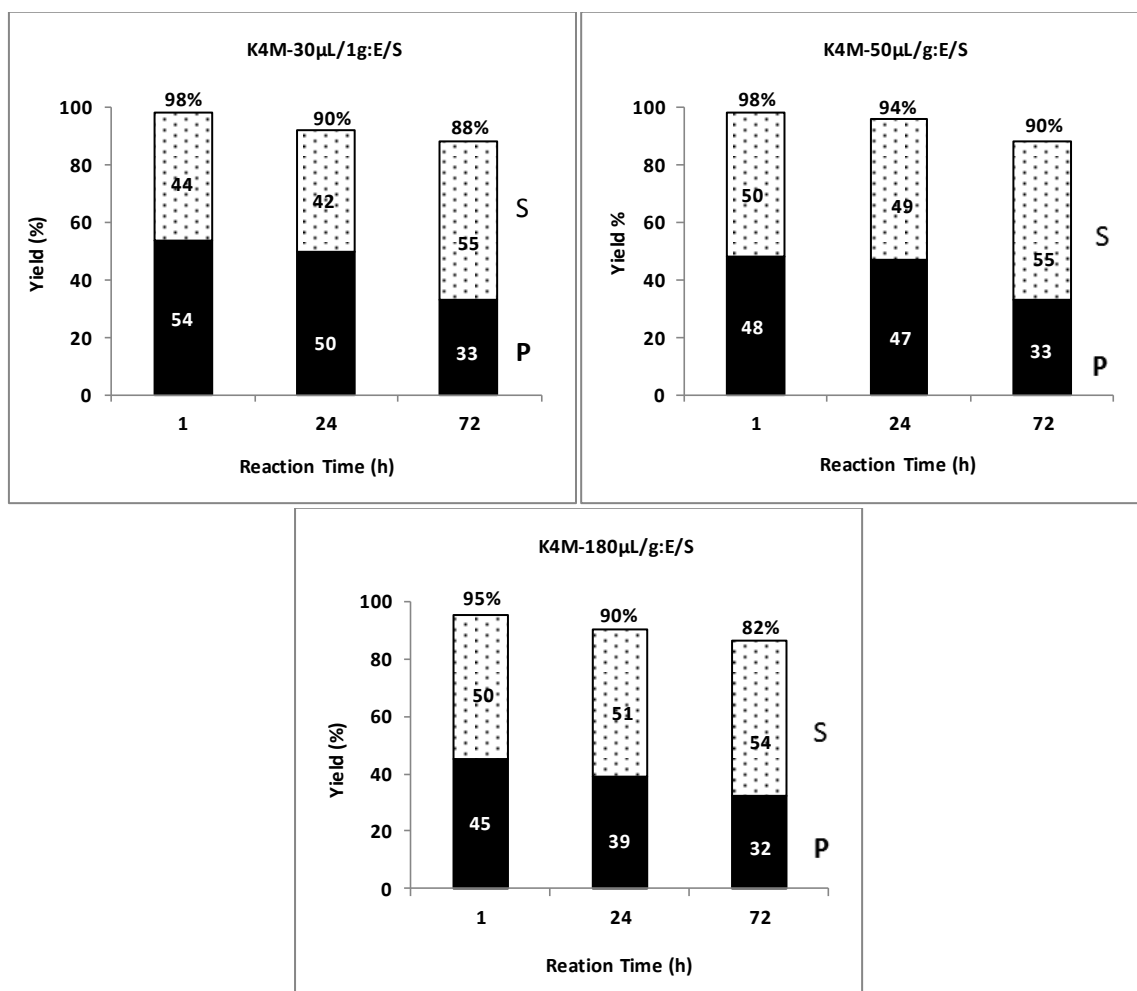


Figure III. 11. Yield of the two isolated fractions as a function of enzyme concentration and reaction time.

The effect of reaction time (1 and 3 days) and enzyme concentration on M_w are presented in the case of P fraction in Figure III.12a and of S fraction in Figure III.12b. These diagrams show the same trend as that depicted in Figure III.10 for M_w obtained after 1 h reaction. As expected, the increase of catalyst concentration allows speeding up the long-term depolymerisation due to the slow attack of EX enzyme. Thus, lower M_w was obtained faster with the higher enzyme concentration. For instance, it can be seen in Figure III.12a that the same M_w in P fraction was attained after 24 h and 72h with catalyst concentration of 180 and 50 $\mu\text{L}\cdot\text{g}^{-1}$, respectively. By contrast, this effect is much less marked for fraction S even if lower M_w was always observed with an 180 $\mu\text{L}\cdot\text{g}^{-1}$ concentration.

Depolymerisation of hydroxypropyl methyl cellulose

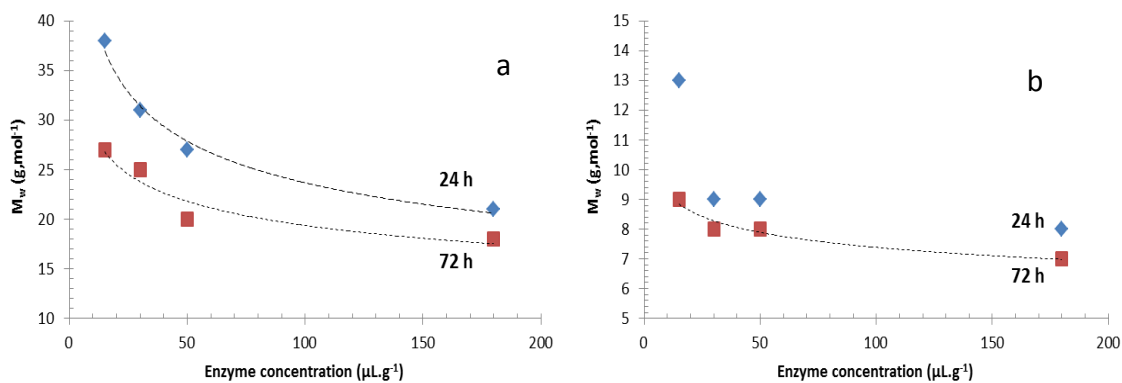


Figure III. 12. Effect of the enzyme concentration on M_w of (a) P fraction and (b) S fraction.

Finally, the effect of the reaction time is shown in Figure III.13 for the higher enzyme concentration for both fractions to investigate the activity of EX enzyme as done in Figures III.7 and 8 for a $30 \mu\text{L.g}^{-1}$ concentration.

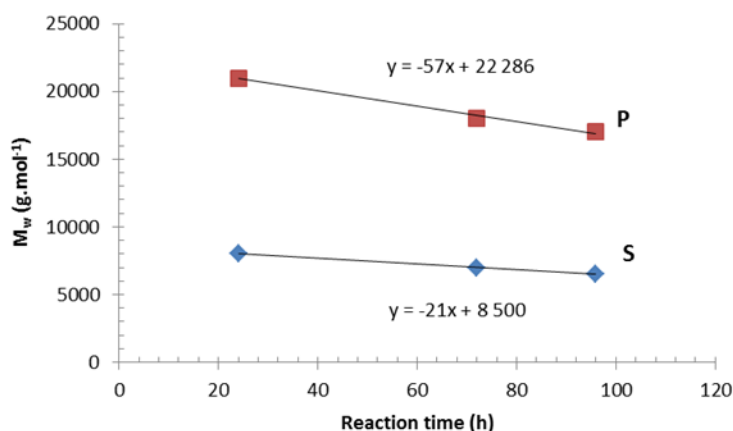


Figure III. 13. Effect of the reaction time on M_w of P and S fraction using a $180 \mu\text{L.g}^{-1}$ enzyme concentration.

Again, a linear relationship is found between the M_w reduction and the reaction time. Surprisingly, the slope observed for the P fraction ($57 \text{ g.mol}^{-1}.\text{h}^{-1}$) is low compared to that in Figure III.7 ($125 \text{ g.mol}^{-1}.\text{h}^{-1}$) determined for the $30 \mu\text{L.g}^{-1}$ concentration. This result might be explained by irreversible adsorption or partial enzyme deactivation due to self- and production inhibition¹⁸. By contrast, the same hydrolysis rate ($21 \text{ g.mol}^{-1}.\text{h}^{-1}$) can be seen for the S fragments indicating that the gradual chain shortening in the latter case seems to be independent of the enzyme concentration.

In conclusion, a raise of the enzymatic catalyst concentration enables to have faster access to shorter chains. For example, $8\,000 \text{ g.mol}^{-1}$ HPMC could be obtained after only 24 h with a

Depolymerisation of hydroxypropyl methyl cellulose

180 $\mu\text{L.g}^{-1}$ concentration whereas it took about 3 days with a 30 $\mu\text{L.g}^{-1}$ concentration. A compromise should be then found between reaction time and catalyst amount.

On the other hand, it was found the same incremental hydrolysis rate whatever the enzyme concentration in the case of S fraction. However, it is not clear if there is a limitation on the M_w reduction by EX enzyme that is if higher enzyme concentration and/or longer reaction time may produce HPMCs with shorter chain length. For instance, it should take about 11 days of reaction to obtain short HPMC chains having M_w of 3000 g.mol^{-1} using a 180 $\mu\text{L.g}^{-1}$ concentration if the EX enzyme keeps the same activity of 21 $\text{g.mol}^{-1}.\text{h}^{-1}$.

III.1.4. Influence of the HPMC source and chain length on the depolymerisation efficiency

In this section, the influence of the starting HPMC nature was investigated following the same procedure as that previously used for K4M hydrolysis. Indeed, several factors including the chain length, the degree of substitution and the substituent distribution along the chain can affect the depolymerisation reaction and thereby the characteristics of samples produced.

Table III.4 summarizes the characteristics of the four selected HPMC samples obtained from two different sources: K4M, K15M from Dow Colorcon and G4, 90SH from Shin-Etsu (see Chapter II). As it can be seen, the M_w varied from 85 000 to 780 000 g.mol^{-1} . On the other hand, G4 had a degree of substitution higher than the other samples. It was assumed that the short HPMC chains originated from depolymerisation of these samples should show highly contrasting thermo sensitive and gelation behaviors as revealed by Shagerlof *et al.*²³ (described in Chapter IV).

Table III. 4. Macromolecular and substitution characteristics of the studied HPMC.

Sample	Manufacturer	M_w (g.mol^{-1}) ^{a)}	PDI ^{a)}	DS _{Me} ^{b)}	MS _{HP} ^{b)}
K4M	Dow Colorcon	235 000	3	1.15 – 1.57	0.18 – 0.32
K15M		340 000	2.5	1.15 – 1.57	0.18 – 0.32
G4	Shin Etsu	85 000	1.7	1.79 – 2.03	0.18 – 0.34
90SH		780 000	3	1.12 – 1.57	0.10 – 0.32

a) this work; b) calculated from manufacturer specifications.

Depolymerisation of hydroxypropyl methyl cellulose

III.1.4.1. Influence of the methylation degree

The enzyme-substrate complex is hindered by the presence of substituents, and the depolymerisation ability should decrease with an increase in the degree of substitution. As above outlined, EGs need at least 5 unsubstituted AGUs to ensure the formation of enzyme-substrate complex^{14, 24}. However, Adden et al.²⁵ have demonstrated that EGs can tolerate one methyl substitution on O-6 position but not a disubstitution on O-2,3 positions. It can be concluded that the number of cleavages is dependent on the substitution heterogeneity along the chain but also on the substitution position in AGU.

The yield in each fraction P and S obtained after depolymerisation of G4 using enzyme concentrations increasing from 15 to 180 $\mu\text{L}\cdot\text{g}^{-1}$ is reported in Figure III.14. Whatever the enzyme concentration G4 depolymerisation gave P in much larger mass fraction (ca 65-80 %), than S unlike the previous K4M one. The higher resistance to enzyme hydrolysis of G4 samples is related to their higher degree on methyl substitution, compared to other HPMC samples.

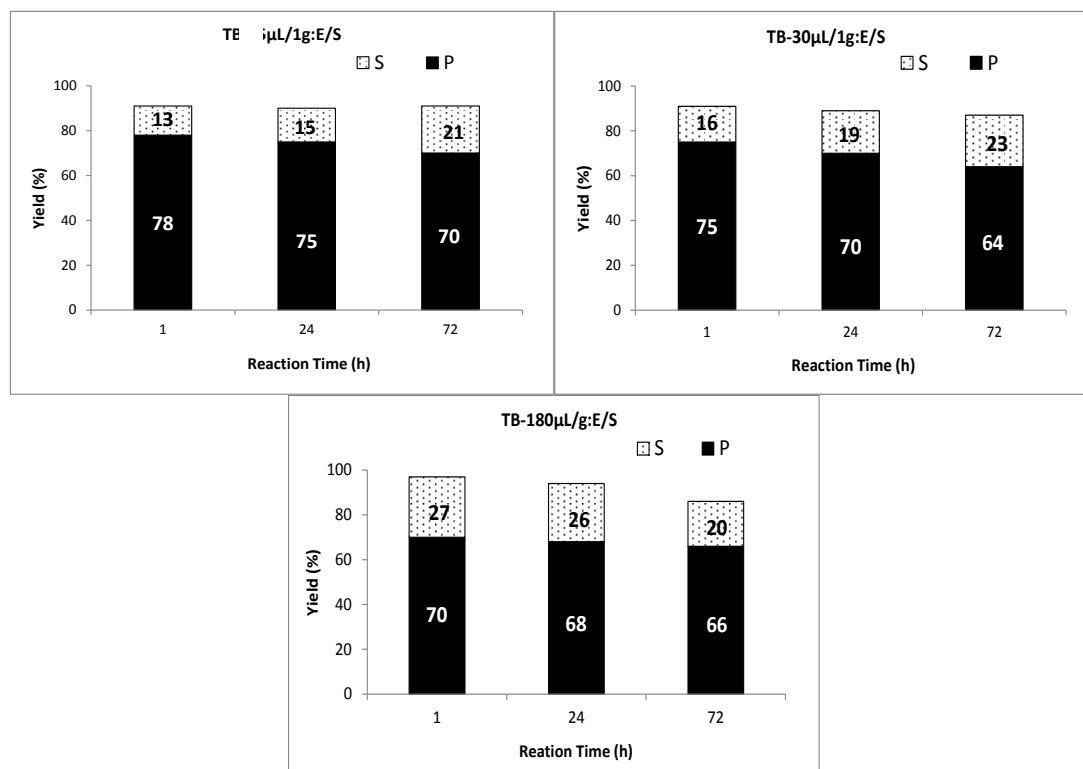


Figure III. 14. Yield of the two isolated short chained fractions as a function of enzyme concentration and reaction time obtained in G4 depolymerisation.

Depolymerisation of hydroxypropyl methyl cellulose

As presented in Figure III.15, fraction P exhibited a decline of M_w during the first day of reaction that leveled off at a value of ca 35 000 g.mol⁻¹ whatever the used enzyme concentration. By contrast, the M_w of fraction S did not evolve greatly over time with a mean value of 11 250 ± 900 g.mol⁻¹.

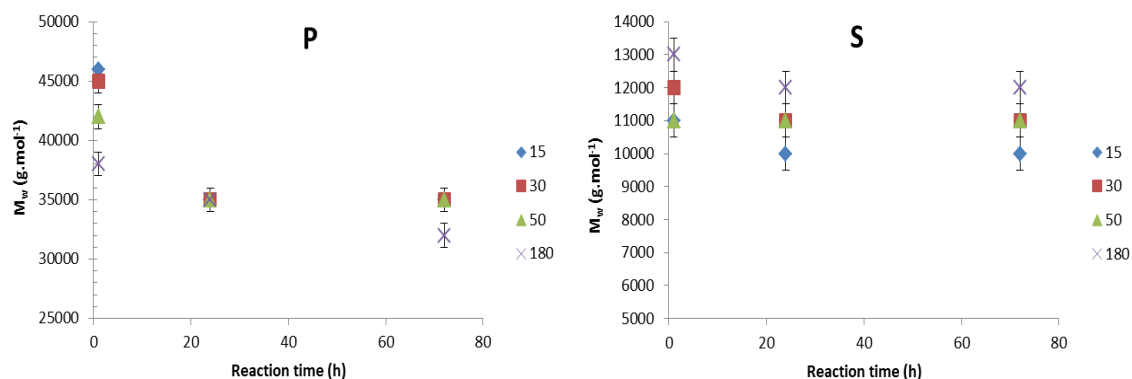


Figure III. 15. M_w variation of P and S fractions as a function of time and enzyme concentration (15 to 180 $\mu\text{L.g}^{-1}$) in G4 depolymerisation.

As done previously for K4M, the average number of chain cleavage (z) of P and S fragments per chain can be estimated from equations III.1 to 4 in the case of G4 depolymerisation. The values calculated for different experimental conditions are summarized in Table III.5.

Table III. 5. The average number of chain cleavage (z) and the mean number of P (x) and S (y) fragments per chain (rounded values for sake of clarity) calculated from equations III.1 to III.4.

Polymer	z	x	y
G4-XX-50-1 ^{a)}	1.5	1.5	1.0
G4-XX-50-24 ^{b)}	2.0	1.5	1.0
G4-XX-180-1 ^{c)}	2.0	1.5	1.5
G4-XX-180-24 ^{d)}	2.0	1.5	1.5

- a) M_n^P and $M_n^S = 32\ 300$ and $7\ 900$ g.mol⁻¹; yield (P) and yield (S) = 78 and 19 %.
 b) M_n^P and $M_n^S = 23\ 300$ and $7\ 900$ g.mol⁻¹; yield (P) and yield (S) = 76 and 21 %.
 c) M_n^P and $M_n^S = 29\ 200$ and $9\ 300$ g.mol⁻¹; yield (P) and yield (S) = 70 and 27 %.
 d) M_n^P and $M_n^S = 26\ 900$ and $7\ 900$ g.mol⁻¹; yield (P) and yield (S) = 76 and 21 %.

The average number of G4 chain cleavage is much lower than that of K4M. Moreover, the proportion of P to S fragments is also higher. These results were expected given the fact that the chain length is shorter ($M_n^{G4} = 50\ 000$ g.mol⁻¹ and $M_n^{K4M} = 78\ 000$ g.mol⁻¹) and the yield of P is three or four times larger than that of S.

Depolymerisation of hydroxypropyl methyl cellulose

In conclusion, our findings are in agreement with the general assumption that an increase of substitution degree entails a resistance to enzyme hydrolysis. In spite of the high degree of substitution, it was demonstrated that about two domains per G4 chain exist where EG can adsorb indicating certain heterogeneity in AGU substitution. These domains can be unsubstituted or O-6 substituted. On the other hand, it was also shown that almost no gradual depolymerisation took place for long time of reaction suggesting that the formation of EX complex is highly hindered by the substitution in G4.

III.1.4.2. Influence of the chain length

In this section, the enzymatic depolymerisation of HPMCs with a similar degree of substitution and various M_w was studied and the obtained fragments compared. Table III.6 shows the data when the reaction was carried out with a $180 \mu\text{L.g}^{-1}$ enzyme concentration.

Table III. 6. Influence of the chain length on the enzymatic depolymerisation.

Fraction P				Fraction S				Total polymer yield (%)
Reference	M_w g.mol ⁻¹	<i>PDI</i>	Yield (%)	Reference	M_w g.mol ⁻¹	<i>PDI</i>	Yield (%)	
K4M-P-180-24	21000	1.2	39	K4M-S-180-24	8000	1.6	51	90
K15M-P-180-24	21000	1.4	53	K15M-S-180-24	7000	1.6	45	98
90SH-P-180-24	23000	1.4	55	90SH-S-180-24	7800	1.5	43	98
K4M-P-180-72	18000	1.4	32	K4M-S-180-72	6500	1.5	54	86
K15M-P-180-72	19000	1.3	54	K15M-S-180-72	7000	1.4	41	95
90SH-P-180-72	18000	1.4	54	90SH-S-180-72	7200	1.7	38	92

As seen, K15M and 90SH hydrolysis generated fragments with same M_w than those produced by K4M samples. It can be concluded that the length of starting polymers does not affect the M_w of obtained short polymers. A deeper insight shows that for a longer time of reaction (72 h), the respective yields between P and S fractions remains more or less constant in the case of HPMCs with longer chains K15M and 90SH, whereas the ratio S(%) / P(%) increases for K4M. This observation implies that the reaction of incremental depolymerisation by EX enzyme was slowed down in the former case compared to K4M. The concentration of short chained polymers is proportional to the chain length of the starting polymer. In these conditions, the ratio EX/substrate decreased when HPMCs with larger M_w

Depolymerisation of hydroxypropyl methyl cellulose

were used as starting material. This assumption is also supported by the fact that the total polymer yield remains almost quantitative suggesting that only a low amount of low average molar mass compounds was formed.

CONCLUSION

Enzymatic catalysis using endoglucanases from *Trichoderma reesei* was proven to lead to partial hydrolysis of HPMCs into two main fragments that can be isolated by selective precipitation. EG action was fast resulting in polymers having respective M_w of about 30 000 and 10 000 $\text{g}\cdot\text{mol}^{-1}$. It is assumed that heterogeneity in chain substitution enables the formation of EG/substrate complex followed by chain cleavage. This means that two chain segments are too highly substituted and not available for EG to ensure the catalysis to take place.

It was also demonstrated that the chain length can be controlled by further incremental depolymerisation by the small amount of EX present in the initial enzyme cocktail. Thus, the M_w of shorter polymers (S fraction) was reduced from 10 000 to about 7 000 $\text{g}\cdot\text{mol}^{-1}$ by extending the time of reaction to 72 h (180 $\mu\text{L}\cdot\text{g}^{-1}$ K4M). It should be noted that this range of HPMC M_w has never been described nor characterized before this work.

As outlined in the previous chapters, our objective was to prepare HPMC with M_w below 10 000 $\text{g}\cdot\text{mol}^{-1}$ to be used as building blocks in block copolymer preparation. This is why we are interested in obtaining S fraction with the highest possible yield. It was found that enzymatic cleavage of HPMC can afford the S fraction in a maximum 50 – 60 % yield.

Acids are known to cleave randomly cellulosic chains in spite of the substitution. In the next section, HPMC hydrolysis using acidic catalysis is tested to examine whether these conditions could give better yields of short HPMC chains.

III.2. Acidic HPMC depolymerisation

Many studies have been done on acid catalysis of cellulose hydrolysis (see Chapter I). HCl is among the mineral acids the most frequently used. It has been demonstrated that high concentrations (6-12 M) lead to complete hydrolysis of cellulose.

Depolymerisation of hydroxypropyl methyl cellulose

It is assumed that milder conditions should allow to obtain short polymers. Therefore, lower HCl concentrations were investigated to achieve partial HPMC hydrolysis. Depolymerisation of K4M and G4 was undertaken by using two acid concentrations (0.6 and 2 M HCl) at 85 °C during 1 h. After the reaction, P and S fractions were recovered following the same procedure as the enzymatic treatment. Following the same nomenclature as that defined for enzymatic depolymerisation, samples were named WW-XX-AC0.6-1 and WW-XX-AC2-1, respectively. Table III.7 summarizes the data regarding these experiments.

Table III. 7. Characteristics of P and S fractions obtained by acid depolymerisation

Fraction P				Fraction S				Total polymer yield (%)
Reference	M_w g.mol ⁻¹	<i>PDI</i>	Yield (%)	Reference	M_w g.mol ⁻¹	<i>PDI</i>	Yield (%)	
K4M-P-AC0.6-1	22000	1.4	46	K4M-S-AC0.6-1	10000	1.3	42	88
G4-P-AC0.6-1	31000	1.3	57	G4-S-AC0.6-1	9000	1.3	25	82
K4M-P-AC2-1	—	—	—	K4M-S-AC2-1	11000	2.1	91	91
G4-P-AC2-1	26000	1.4	91	G4-S-AC2-1	—	—	—	91

In an unexpected way, the acid hydrolysis in 0.6 M HCl yielded two fractions very similar to those obtained by the enzymatic route from K4M and G4, as well. Thus, P fraction showed respective M_w of 22 000 and 31 000 g.mol⁻¹, whereas S fraction M_w was about 10 000 g.mol⁻¹ in both cases. This result suggests that chaining of highly substituted AGUs may also be more resistant to acid treatment as they are for enzymatic cleavage, at least with modest acid concentration and at short time of reaction. Moreover, this assumption is confirmed by the high total polymer yield demonstrating that only a small fraction of low M_w compounds was produced.

By increasing the HCl concentration to 2 M, the reaction gave now only one fraction whatever the starting HPMC, which is an expected result. In the case of G4, a P fraction was isolated in 91 % yield with a M_w slightly lower than that of P fraction in the previous experiment. Our findings suggest that different hydrolysis mechanisms occur in “dilute” and “concentrated” acid concentrations. HPMC was not soluble at 85 °C, and the reaction was performed heterogeneously. In “concentrated” acid solutions, the chain cleavage might be

Depolymerisation of hydroxypropyl methyl cellulose

limited because of strong chain collapsing in polymer globules. Exclusively, the more accessible sites reacted. By contrast, the polymer coil is probably more solvated in “diluted” solution implying better availability of domains easily cleavable (less substituted). The same explanation can be applied to K4M. However, in the latter case the polymer globules may swell more than those of G4 owing to the moderate degree of substitution permitting the hydrolysis to proceed further giving shorter chains ($M_w = 11\,000\text{ g}\cdot\text{mol}^{-1}$) with an excellent yield. Unfortunately, the obtained sample could not be fractionated into P and S fraction as it was entirely soluble at 85 °C. K4M-S-AC2-1 was solely purified by UF removing the low molecular weight compounds. It is why the PDI value is much higher than for the other samples. Although this sample was obtained in an excellent yield, further fractionation and/or chain cleavage are required to be used as building block in block copolymers since the PDI and M_w values are too high.

In conclusion, acid hydrolysis is an alternative to enzymatic depolymerisation. However, it seems to be less versatile than the latter. Actually, it is not obvious that the chain length could be easily adjusted as a function of the acid concentration and the reaction time. Moreover, it is not environmentally friendly from the fact that the acid neutralization generates a large quantity of salts to be discharged.

III.3. Summary of HPMC depolymerisation

Table III.8 summarizes all the polymers prepared in this study either by enzymatic or acidic hydrolysis. As a result, a library of short HPMC was obtained that can be divided into two classes: the “P” family having M_w between 17 000 to 46 000 $\text{g}\cdot\text{mol}^{-1}$ and the “S” family with M_w varying between 6000 to 14000 $\text{g}\cdot\text{mol}^{-1}$. The PDI was generally much lower than the starting HPMC owing to the purification step.

Most of the experiments were performed solely once in order to determine the effect of the various parameters studied. However, the polymers marked with an asterisk were obtained from at least duplicate experiments. Excellent reproducibility was observed in M_w , PDI and yields, thus proving the reliability of our results.

The samples in bold characters were selected as representative of the various conditions used in the present study including reaction time, enzyme/HPMC ratio, M_w of the resulting

Depolymerisation of hydroxypropyl methyl cellulose

short chains (P and S fractions), and nature of the starting HPMC to be characterized in the next chapter. Analogs prepared by acidic hydrolysis in 0.6 M HCl were chosen for comparison.

Table III. 8. Library of short chained HPMC produced by enzymatic and chemical hydrolysis.

HYDROLYSIS PROCESS								
Fraction (P)	M_w (g.mol ⁻¹)	PDI	Yield %	Fraction (S)	M_w (g.mol ⁻¹)	PDI	Yield %	Total polymer yield (%)
K4M-P-15-24	38000	1.3	53	K4M-S-15-24	13000	1.3	45	98
K4M-P-15-72	27000	1.3	52	K4M-S-15-72	9000	1.4	47	99
K4M-P-30-1*	31 000	1.3	54	K4M-S-30-1*	11 000	1.6	44	98
K4M-P-30-24	31 000	1.3	50	K4M-S-30-24	9 000	1.5	40	90
K4M-P-30-72	25 000	1.2	33	K4M-S-30-72	8 000	1.6	55	88
K4M-P-30-96	22 000	1.3	32	K4M-S-30-96	7 500	1.5	53	85
K4M-P-50-1	29 000	1.4	48	K4M-S-50-1	10 000	1.6	50	98
K4M-P-50-24	27 000	1.2	47	K4M-S-50-24	9 000	1.6	49	96
K4M-P-50-72*	20 000	1.3	35	K4M-S-50-72*	8 000	1.5	55	90
K4M-P-180-1	25 000	1.4	45	K4M-S-180-1	10 000	1.6	50	95
K4M-P-180-24	21 000	1.2	39	K4M-S-180-24	8 000	1.6	51	90
K4M-P-180-72*	18000	1.4	32	K4M-S-180-72*	7 000	1.5	54	86
K4M-P-180-96	17000	1.3	29	K4M-S-180-96	6 500	1.5	38	67
K4M-P-AC0.6-1*	22 000	1.4	46	K4M-S-AC0.6-1*	10 000	1.3	42	88
K4M-P-AC2-1	-	-	-	K4M-S-AC2-1	11 000	2.1	91	91
G4-P-15-1	46 000	1.4	78	G4-S-15-1	11000	1.4	13	91
G4-P-15-24	35 000	1.4	75	G4-S-15-24	10000	1.6	15	90
G4-P-15-72	35 000	1.3	70	G4-S-15-72	11000	1.6	21	91
G4-P-30-1	45 000	1.4	75	G4-S-30-1	12 000	1.4	16	91
G4-P-30-24	35 000	1.3	70	G4-S-30-24	11 000	1.4	19	89
G4-P-30-72	35 000	1.3	64	G4-S-30-72	11 000	1.4	23	87
G4-P-50-1	42 000	1.3	78	G4-S-50-1	11 000	1.4	19	97
G4-P-50-24*	35 000	1.5	76	G4-S-50-24*	11 000	1.4	21	97
G4-P-50-72	35 000	1.3	60	G4-S-50-72	11 000	1.6	27	87
G4-P-180-1	38 000	1.3	70	G4-S-180-1	13 000	1.4	27	97
G4-P-180-24	35 000	1.3	68	G4-S-180-24	12 000	1.6	26	94
G4-P-180-72*	32 000	1.3	66	G4-S-180-72*	12 000	1.5	20	86
G4-P-AC0.6-1*	31000	1.3	57	G4-S-AC0.6-1*	9000	1.3	25	82
G4-P-AC2-1	26000	1.4	91	G4-S-AC2-1	-	-	-	91
K15M-P-180-24	21 000	1.4	53	K15M-S-180-24	7 000	1.6	45	98
K15M-P-180-72	19 000	1.3	54	K15M-S-180-72	7 000	1.4	41	95
90SH-P-180-24	23 000	1.4	55	90SH-S-180-24	7 800	1.5	43	98
90SH-P-180-72	18 000	1.4	54	90SH-S-180-72	7 200	1.7	38	92

* these experiments were at least duplicate

Depolymerisation of hydroxypropyl methyl cellulose

CONCLUSION

Both enzymatic and acidic catalysis can be used to partially degrade HPMC and generate polymers with short chains. It was found that the targeted range of M_w (5 000 – 10 000 g.mol⁻¹) we are interested in, was easily reached through enzymatic reaction in fair yield (50 – 60 %). Moreover, the chain length could be precisely monitored by varying the reaction time and the ratio enzyme/substrate.

It is assumed that structures and properties should vary depending on the conditions of depolymerisation. Selected HPMC samples of the library (Table III.8) will then be fully characterized and data presented in the next chapter to precise the interplay between preparation – structure – properties.

REFERENCES

1. Wahlstrom, R. M.; Suumakki, A., Enzymatic hydrolysis of lignocellulosic polysaccharides in the presence of ionic liquids. *Green Chem* 2015, 17 (2), 694-714.
2. Chalamaiah, M.; Kumar, B. D.; Hemalatha, R., *et al.*, Fish protein hydrolysates: Proximate composition, amino acid composition, antioxidant activities and applications: A review. *Food Chem* 2012, 135 (4), 3020-3038.
3. Azadi, P.; Inderwildi, O. R.; Farnood, R., *et al.*, Liquid fuels, hydrogen and chemicals from lignin: A critical review. *Renew Sust Energ Rev* 2013, 21, 506-523.
4. Van Vlierberghe, S.; Dubruel, P.; Schacht, E., Biopolymer-Based Hydrogels As Scaffolds for Tissue Engineering Applications: A Review. *Biomacromolecules* 2011, 12 (5), 1387-1408.
5. Chang, C. Y.; Zhang, L. N., Cellulose-based hydrogels: Present status and application prospects. *Carbohydr Polym* 2011, 84 (1), 40-53.
6. Roy, D.; Semsarilar, M.; Guthrie, J. T., *et al.*, Cellulose modification by polymer grafting: a review. *Chem Soc Rev* 2009, 38 (7), 2046-2064.
7. Patel, T. R.; Morris, G. A.; Ebringerova, A., *et al.*, Global conformation analysis of irradiated xyloglucans. *Carbohydr Polym* 2008, 74 (4), 845-851.
8. Goodwin, D. J.; Picout, D. R.; Ross-Murphy, S. B., *et al.*, Ultrasonic degradation for molecular weight reduction of pharmaceutical cellulose ethers. *Carbohydr Polym* 2011, 83 (2), 843-851.
9. Poinot, T.; Benyahia, K.; Govin, A., *et al.*, Use of ultrasonic degradation to study the molecular weight influence of polymeric admixtures for mortars. *Constr Build Mater* 2013, 47, 1046-1052.
10. Yan, J. K.; Pei, J. J.; Ma, H. L., *et al.*, Effects of ultrasound on molecular properties, structure, chain conformation and degradation kinetics of carboxylic curdlan. *Carbohydr Polym* 2015, 121, 64-70.
11. Rinaldi, R.; Schuth, F., Acid Hydrolysis of Cellulose as the Entry Point into Biorefinery Schemes. *ChemSusChem* 2009, 2 (12), 1096-1107.
12. Akpinar, O.; Erdogan, K.; Bakir, U., *et al.*, Comparison of acid and enzymatic hydrolysis of tobacco stalk xylan for preparation of xylooligosaccharides. *LWT - Food Science and Technology* 2010, - 43 (- 1), - 125.
13. Richardson, S.; Gorton, L., Characterisation of the substituent distribution in starch and cellulose derivatives. *Anal Chim Acta* 2003, 497 (1-2), 27-65.
14. Momcilovic, D.; Schagerlof, H.; Rome, D., *et al.*, Derivatization using dimethylamine for tandem mass spectrometric structure analysis of enzymatically and acidically depolymerized methyl cellulose. *Anal Chem* 2005, 77 (9), 2948-2959.
15. Fitzpatrick, F.; Schagerlof, H.; Andersson, T., *et al.*, NMR, cloud-point measurements and enzymatic depolymerisation: Complementary tools to investigate substituent patterns in modified celluloses. *Biomacromolecules* 2006, 7 (10), 2909-2917.
16. Adden, R.; Melander, C.; Brinkmalm, G., *et al.*, The Applicability of Enzymes in Cellulose Ether Analysis. *Macromol Symp* 2009, 280, 36-44.
17. Sepassi, S.; Goodwin, D. J.; Drake, A. F., *et al.*, Effect of polymer molecular weight on the production of drug nanoparticles. *J Pharm Sci-US* 2007, 96 (10), 2655-2666.

Depolymerisation of hydroxypropyl methyl cellulose

18. Zhang, Y. H. P.; Lynd, L. R., Toward an aggregated understanding of enzymatic hydrolysis of cellulose: Noncomplexed cellulase systems. *Biotechnol Bioeng* 2004, *88* (7), 797-824.
19. Pala, H.; Mota, M.; Gama, F. M., Enzymatic depolymerisation of cellulose. *Carbohydr Polym* 2007, *68* (1), 101-108.
20. Melander, C.; Adden, R.; Brinkmalm, G., *et al.*, New approaches to the analysis of enzymatically hydrolyzed methyl cellulose. Part 2. Comparison of various enzyme preparations. *Biomacromolecules* 2006, *7* (5), 1410-1421.
21. Turon, X.; Rojas, O. J.; Deinhammer, R. S., Enzymatic kinetics of cellulose hydrolysis: A QCM-D study. *Langmuir* 2008, *24* (8), 3880-3887.
22. Saloheimo, M.; Paloheimo, M.; Hakola, S., *et al.*, Swollenin, a *Trichoderma reesei* protein with sequence similarity to the plant expansins, exhibits disruption activity on cellulosic materials. *Eur J Biochem* 2002, *269* (17), 4202-4211.
23. Schagerlof, H.; Johansson, M.; Richardson, S., *et al.*, Substituent distribution and clouding behavior of hydroxypropyl methyl cellulose analyzed using enzymatic degradation. *Biomacromolecules* 2006, *7* (12), 3474-81.
24. Karlsson, J.; Momcilovic, D.; Wittgren, B., *et al.*, Enzymatic degradation of carboxymethyl cellulose hydrolyzed by the endoglucanases Cel5A, Cel7B, and Cel45A from *Humicola insolens* and Cel7B, Cel12A and Cel45Acore from *Trichoderma reesei*. *Biopolymers* 2002, *63* (1), 32-40.
25. Adden, R.; Melander, C.; Brinkmalm, G., *et al.*, New approaches to the analysis of enzymatically hydrolyzed methyl cellulose. Part 1. Investigation of the influence of structural parameters on the extent of degradation. *Biomacromolecules* 2006, *7* (5), 1399-1409.

**CHAPTER IV: PHYSICO-CHEMICAL
CHARACTERIZATION OF SHORT
CHAINED HPMCs**

INTRODUCTION

Hydroxypropyl methylcellulose (HPMC) is a cellulose ether with outstanding properties including water solubility, water retention, emulsifying and dispersing agent, thickening and reversible thermal gelation that make it very useful for numerous industrial applications (see chapter I). HPMC properties are governed by several factors such as chain length, the content of methyl (MeO %) and hydroxypropyl (HPO %) groups, as well as the distribution of substituents along the chain. For instance, the water solubility is enhanced by an increase of HPO content resulting in a reduction of the corresponding HPMC surface activity¹. On the other hand, the higher the MeO content, the higher the surface activity and the lower the critical temperature of gelation. It appears that the final property of HPMC is a subtle balance these different parameters.

In this sense, physicochemical characterization of short chained HPMCs generated by acid and/or enzymatic depolymerisation is essential to demonstrate their potentiality in future applications. Thus, the chemical composition and macromolecular structure were determined by ^1H NMR and size exclusion chromatography, respectively. End group titration of reducing extremity was used to show their end functionality enabling the further preparation of block copolymers. HPMC exhibits phase separation ability and gelation property upon heating. The clouding point temperature (T_c) and the lower critical solution temperature (LCST) of the obtained polymers were determined by UV transmittance. As indicated at the end of the previous chapter, a certain number of samples were chosen as representative of the various experimental conditions used in the depolymerisation process. Table IV.1 presents the selected batches with the reference permitting to retrieve the conditions in which they were prepared. The last column “comments” displays the effect of reaction parameters that will be discussed.

Table IV. 1. Reference of the nine batches corresponding to the selected short chained HPMCs produced by enzymatic and acidic hydrolysis and reaction parameters analyzed.

Batch	1	2			Comments
Reference	K4M-P-30-1 K4M-S-30-1	K4M-P-50-1 K4M-S-50-1			Effect of Enz/HPMC ratio at small reaction time
Batch	3	4	5	6	
Reference	K4M-P-15-72 K4M-S-15-72	K4M-P-30-72 K4M-S-30-72	K4M-P-50-72 K4M-S-50-72	K4M-P-180-72 K4M-S-180-72	Effect of the Enz/HPMC ratio at high reaction time
Batch	1	4	2	5	
Reference	K4M-P-30-1 K4M-S-30-1	K4M-P-30-72 K4M-S-30-72	K4M-P-50-1 K4M-S-50-1	K4M-P-50-72 K4M-S-50-72	Effect of the reaction time
Batch	6	7			
Reference	K4M-P-180-72 K4M-S-180-72	G4-P-180-72 G4-S-180-72			Effect of the methyl substitution
Batch	8	9			
Reference	K4M-P-AC0.6-1 K4M-S-AC0.6-1	G4-P-AC0.6-1 G4-S-AC0.6-1			Effect of the catalyst nature: to be compared to other samples

RESULTS AND DISCUSSION

IV.1. Macromolecular features

IV.1.1. Starting HPMCs

Size exclusion chromatography coupled to multi-angle light scattering and refractive index detectors (SEC-MALS-RI) was used to determine the M_w and molar mass distribution of the prepared HPMCs. Elution was carried out in 10mM of NaCl with 0.02 % NaN_3 (pH about 8). The dn/dc for HPMC in aqueous solution was taken to be 0.137 mL/g and was assumed to be constant for all analyzed samples (short chains included). Figure IV.1 illustrates the chromatographic RI profiles observed for the starting HPMC K4M and G4, as well as the molar mass (M) calculated for each volume increment. As can be seen, each compound seems to be composed of two populations as the peaks present a shoulder on the side of high elution volumes. On the other hand, calculation by the software of M for the second population exhibited a deviation with regard to the linear evolution of $\log M$ vs elution volume (size-exclusion mechanism). This phenomenon might be accounted for by elution

delay due to partial adsorption. Regardless of the reason for this behavior, it was decided to take into account the calculation done by the software assuming the theoretical variation of M as a function of the elution volume.

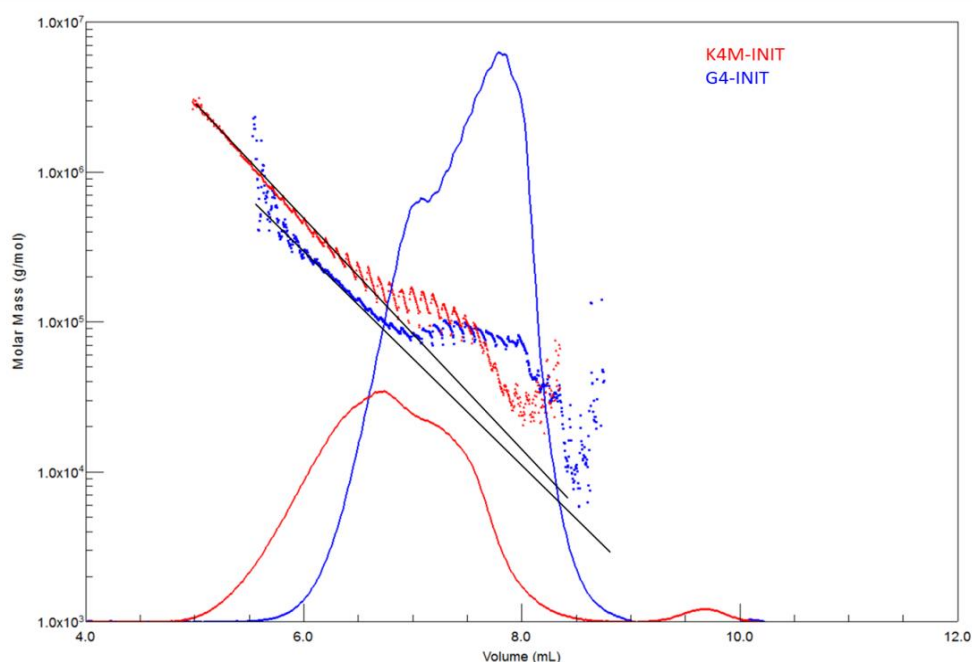


Figure IV. 1. Concentration profiles of K4M and G4 samples observed by SEC-MALS-RI and molar mass calculated from coupled light scattering.

SEC-MALS-RI experiments allow a simultaneous determination of M and the radius of gyration (R_g) for each slice of elution volume. The mean R_g was determined to be 53 and 25 nm for K4M and G4, respectively.

The variation of R_g vs M is generally presented according to:

$$\log R_g = \log K + x \log M \quad \text{Eq. IV.1}$$

The slope x gives information about the conformation of polymers in solution. For example, an x value of 0.33 is representative of a sphere, 0.5-0.6 of a random coil and 1 of a rod². Figure IV.2 displays the log-log plot for both starting HPMC samples. The regression fit shows excellent agreement with the experimental data. The obtained slopes are of 0.49 and 0.40 for K4M and G4, respectively. These values indicate that both polymers have random coil conformation in eluent (0.01 M NaCl + 0.02 % NaN₃). However, the more methylated

structure of G4 compared to K4M makes it more hydrophobic and less solvated by water molecules resulting in a more compact conformation. It is however important to note that the difference diminishes for the short chains with a similar R_g of about 10 nm for M of 10 000 $\text{g}\cdot\text{mol}^{-1}$.

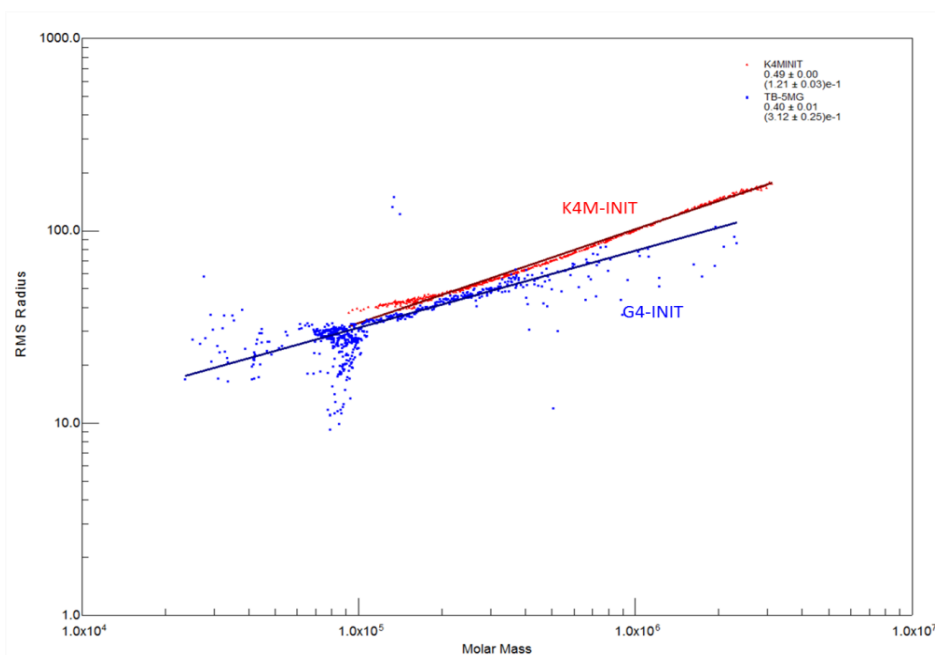


Figure IV. 2. Log-log plot of the radius of gyration vs molar mass for K4M and G4 samples and linear regression fitting.

Table IV. 2. Weight average molar mass (M_w), polydispersity index (PDI), radius of gyration (R_g) and x value of K4M and G4 HPMCs as determined by SEC-MALS-RI.

Sample	M_w ($\text{g}\cdot\text{mol}^{-1}$)	PDI	R_g (nm)	$d\log M/d\log R_g$
K4M	235 000	3.0	53	0.49
G4	85 000	1.7	25	0.40

IV.1.2. Short chained HPMCs

Figure IV.3 shows the chromatographic RI profiles observed for the P and S fractions resulting from the depolymerisation of K4M by using an Enz/HPMC ratio of $180 \mu\text{L}\cdot\text{g}^{-1}$ and a reaction time of 72 h while Figure IV.4 compares the corresponding polymers coming from G4. In both cases, the experimental data showing the relationship between M and the elution volume are also plotted. By contrast, with the starting HPMCs, a quite good

agreement was observed with the linear regression calculated by the software. It is well known that the shorter the polymeric chain, the higher the solubility. The observed behavior was then attributed to the lower M_w of the prepared short chained HPMCs that permits a much better solvation by water molecules strongly inhibiting hydrophobic interactions with the chromatographic stationary phase. Another observation that can be made is the fact that the shorter polymers (K4M-S-180-72 and G4-S-180-72) were eluted at lower volumes than the corresponding P polymers of same molar mass. This means that the latter has a more compact conformation (lower hydrodynamic volume) in solution and will be discussed latter within the chemical composition section.

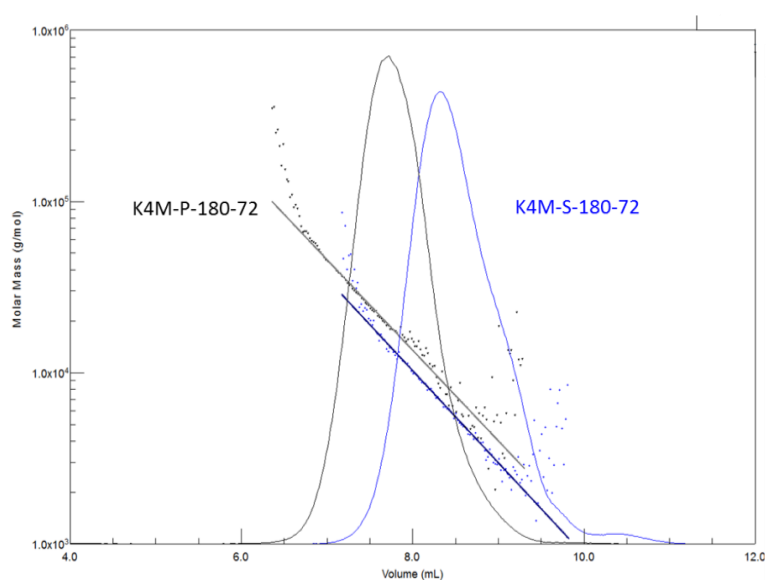


Figure IV. 3. Concentration profiles of P and S fractions yielded with Enz/K4M ratio of $180 \mu\text{L.g}^{-1}$ after 72 h of reaction observed by SEC-MALS-RI and molar mass calculated from coupled light scattering.

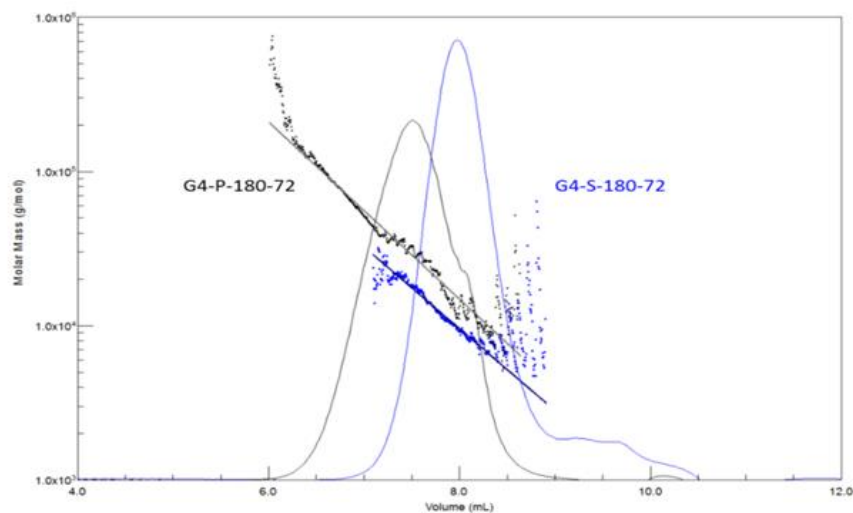


Figure IV. 4. Concentration profiles of P and S fractions yielded with Enz/G4 ratio of $180 \mu\text{L.g}^{-1}$ after 72 h of reaction observed by SEC-MALS-RI and molar mass calculated from coupled light scattering.

The molar mass distributions of the starting and hydrolyzed HPMC fragments were calculated from the previously obtained data. As an example, Figure IV.5 presents the cumulative molar mass diagrams obtained for K4M, K4M-P-180-72 and K4M-S-180-72.

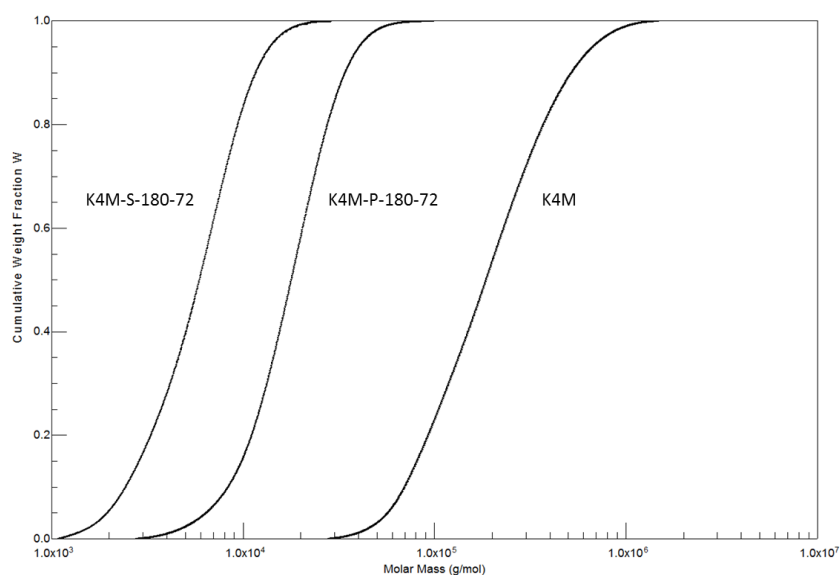


Figure IV. 5. Cumulative molar mass distribution of K4M, K4M-P-180-72, K4M-S-180-72.

This diagram well reflects the chain cleavage of starting HPMC resulting in the production of shorter chains and reduction of PDI. This observation indicates that the used cocktail of enzymes is quite efficient to degrade HPMC into short HPMCs having controlled chain length.

Figures IV-6 and IV-7 display the log-log plot of R_g as a function of M for P and S fraction from K4M and G4, respectively. The log-log fitting shows good correlation with the experimental data for P fractions. Actually, it was true for most of the prepared P samples. Although determined with a margin of error of 20-30 %, the found R_g value and the slope x of its variation with M give an idea of their conformation in solution. By contrast, scattering of experimental data was observed for the S fractions making it difficult to conclude on R_g and x . However, values can be estimated in some cases as shown in Figures IV-6 and IV-7. The conclusions about these data should be drawn with prudence due to the lack of accuracy.

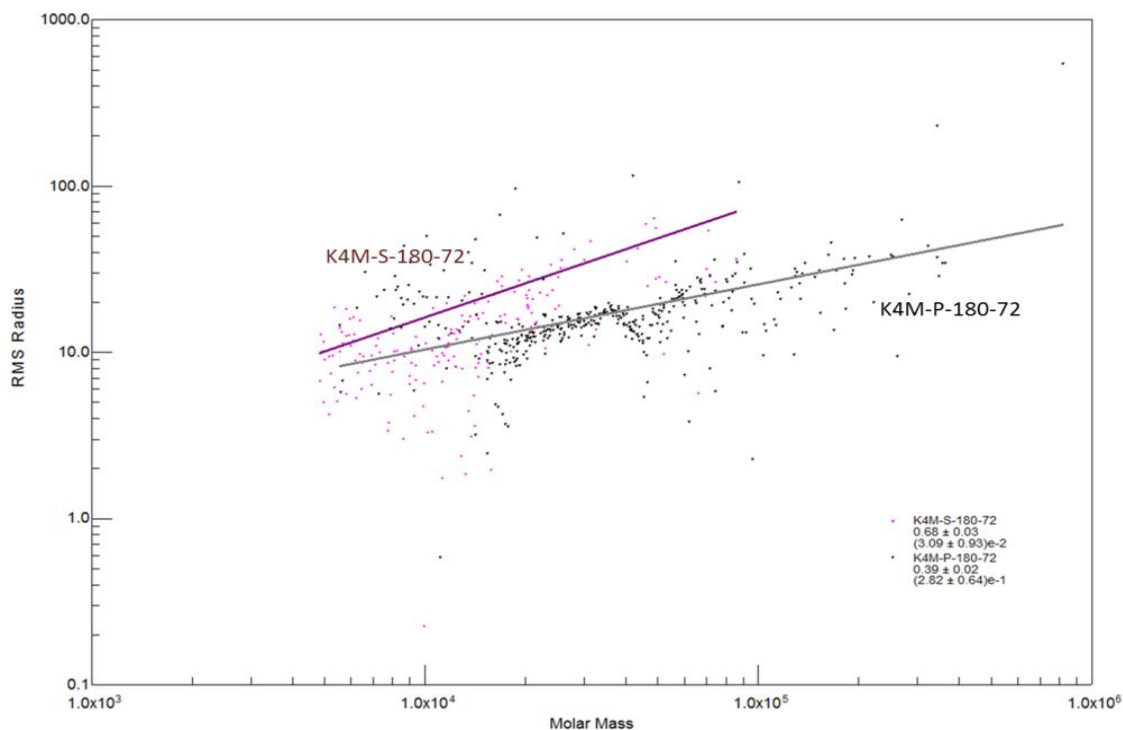


Figure IV. 6. Log-log plot of the radius of gyration vs molar mass for K4M-P-180-72 and K4M-S-180-72 samples and linear regression fitting.

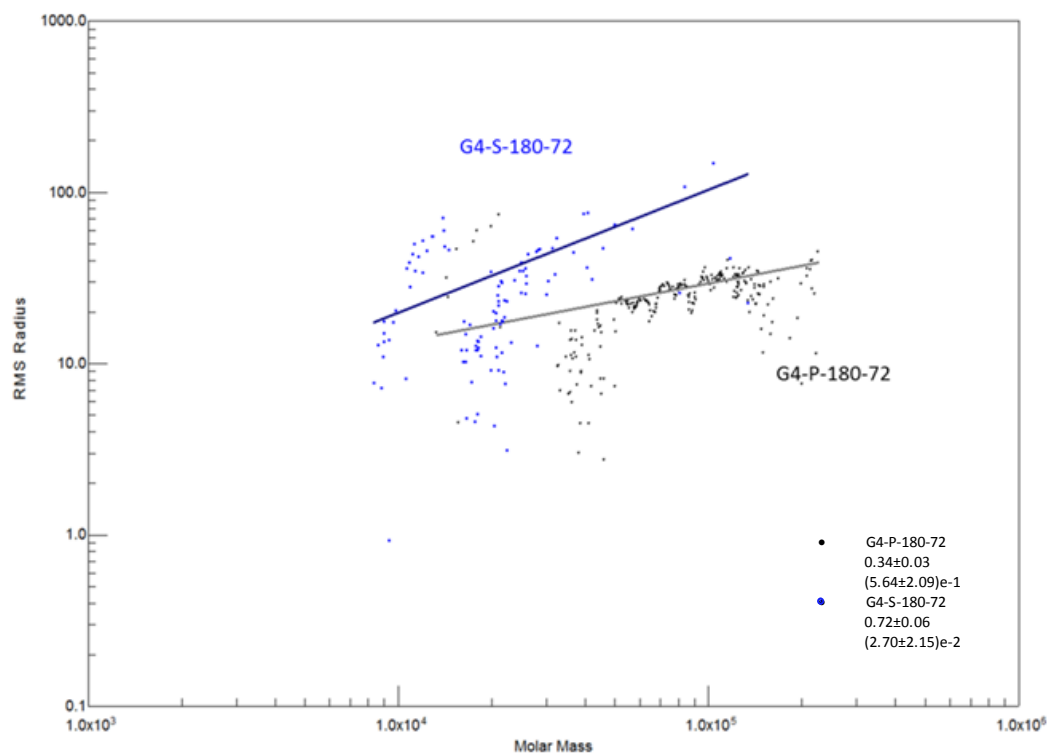


Figure IV. 7. Log-log plot of the radius of gyration vs molar mass for G4-P-180-72 and G4-S-180-72 samples and linear regression fitting.

The macromolecular parameters determined by SEC-MALS-RI are gathered in Table IV.3 for the nine selected batches. The obtained M_w values agree well with those reported previously on enzymatic hydrolysis of cellulose ethers. For instance, Shagerlöf et al.³ studied the enzymatic hydrolysis of methyl cellulose MC ($M_w = 199\,000\text{ g}\cdot\text{mol}^{-1}$, degree of methyl substitution = 1.8) by five different endoglucanases to elucidate the relationship between active site structure and sensitivity for substituents on derivatized cellulose. HPMC fragments of M_w between 11 600 and 44 600 were formed after 72h of reaction depending on the used enzymes. The only fractionation performed in this study was a UF process using membranes of 10 kDa MWCO. The authors were interested in analyzing the low molecular weight compounds in the permeate to determine how the substitution can interfere on the enzyme activity. Fitzpatrick et al.⁴ studied the substitution pattern in modified cellulose. They analyzed the hydrolyzed fragments of methyl cellulose. From the SEC profile, it can be clearly seen a shoulder corresponding to a minority fraction of small polymers with an estimated M_w of 6 000 to 8 000 again depending on the enzyme employed to carry out hydrolysis.

Physico-chemical characterization of short chained HPMCs

The M_w and PDI values have been already presented in Chapter III and will not be further discussed.

The R_g values of P fractions were determined to be between 10 to 20 nm, which are expected values from those measured for the starting HPMCs. On the other hand, the values estimated for the S fraction were below or equal to 10 nm that is the detection limit for the used set-up.

As outlined before, the slope $d(\log M)/d(\log R_g)$ is an important parameter to understand the solution behavior of polymers. The values obtained for the P fractions are generally lower than that of the starting HPMC and the S fraction. The conformation in solution depends on the hydrophobic methyl and the hydrophilic hydroxypropyl substitution. This point will be discussed in more detail in the next section.

Table IV. 3. Macromolecular features of the nine batches corresponding to the selected short chained HPMCs produced by enzymatic and acidic hydrolysis.

Batch	P Fraction					S Fraction				
	Reference	Mw (g.mol ⁻¹)	PDI	R_g (nm)	$\frac{d \log M}{d \log R_g}$	Reference	M_w (g.mol ⁻¹)	PDI	R_g (nm)	$\frac{d \log M}{d \log R_g}$
1	K4M-P-30-1	31 000	1.3	15	0.49	K4M-S-30-1	11 000	1.6	< 10	(a)
2	K4M-P-50-1	29 000	1.4	17	0.38	K4M-S-50-1	10 000	1.6	≤ 10	(a)
3	K4M-P-15-72	27 000	1.3	14	0.38	K4M-S-15-72	9 000	1.4	< 10	(a)
4	K4M-P-30-72	25 000	1.2	14	0.51	K4M-S-30-72	8 000	1.5	< 10	(a)
5	K4M-P-50-72	20 000	1.3	13	0.39	K4M-S-50-72	8 000	1.5	< 10	(a)
6	K4M-P-180-72	18 000	1.4	12	0.39	K4M-S-180-72	7 000	1.5	<10	0.68
7	K4M-P-AC0.6-1	22 000	1.4	13	0.53	K4M-S-AC0.6-1	10 000	1.3	10	0.57
8	G4-P-180-72	32 000	1.3	16	0.34	G4-S-180-72	12 000	1.5	≤10	0.72
9	G4-P-AC0.6-1	31 000	1.3	14	0.58	G4-S-AC0.6-1	13 000	1.3	11	0.50

(a) cannot be determined because of scattered data

IV.2. Chemical composition of the different polymer fractions

As mentioned in Chapter I, the degree of substitution DS refers to the average number of substituted hydroxyl groups per AGU and ranges from 0 (un-substituted AGU) to 3 (fully substituted AGU) while the molar substitution MS is the average number of substituents per AGU⁵⁻⁶. Hydroxypropylation is carried out by using propylene oxide that can react with the three hydroxyl groups of AGU as well as on the hydroxyl of the hydroxypropyl group once substituted on AGU (propagating substitution). In that case, the extent of substitution is characterized by MS and can be theoretically higher than 3. By contrast, methyl groups cannot propagate so that DS and MS have the same value. Both these parameters are average numbers. Indeed, the distribution of substituents along the chain is uneven as the starting cellulose is highly crystalline and generally insoluble in the reaction medium. However, the determination of the substitution pattern is out of the scope of this work. Actually, it is a difficult task that is not fully elucidated in the case of HPMC.

The degree of substitution of methyl (DS_{Me}) and hydroxypropyl groups (MS_{HP}) was determined by 1H NMR. Simplification of spectra was obtained by acetylation of samples that makes it easier quantification of DS_{Me} and MS_{HP} (Figure IV.8). The calculation was done as explained in Chapter II.

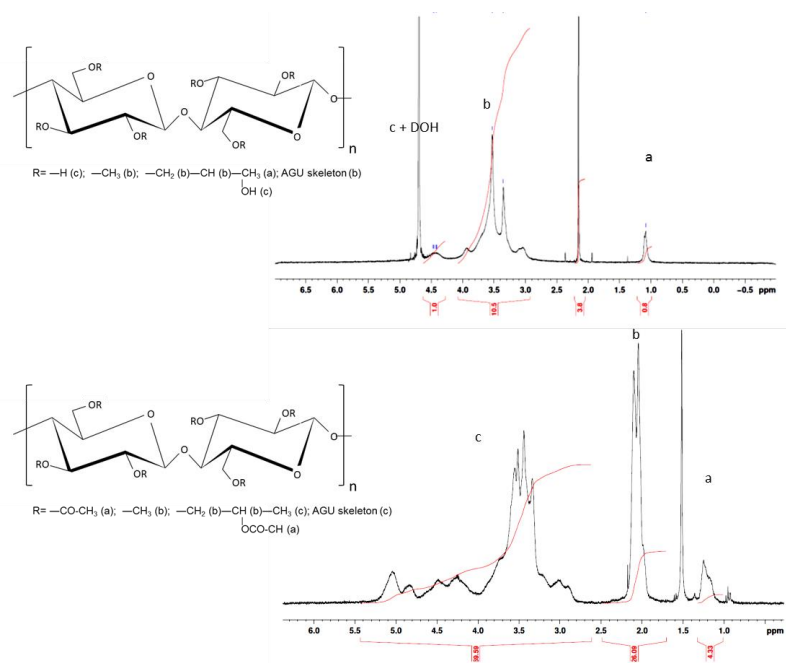


Figure IV. 8. ^1H NMR spectra of (top) native K4M in D_2O and (bottom) of acetylated K4M in CDCl_3 .

Table IV.4 summarizes the DS_{Me} and MS_{HP} values determined from the NMR spectra for the nine selected polymers. Substitution on AGUs is often characterized by the amount of substituent (methoxy and hydroxypropyloxy) groups in weight percent⁷. These parameters are reported in the two last columns of the table as MeO % and HPO %. The two starting HPMCs K4M and G4 were also listed for comparison. Three main conclusions can be drawn from the DS_{Me} data reported in this table:

- 1- The DS_{Me} values of P fraction obtained by enzymatic depolymerisation are always higher than that of the starting HPMC. It can be seen that DS_{Me} reaches a more or less constant value of about 1.5 in the P fractions from K4M whatever the experimental conditions.
- 2- The DS_{Me} values of S fraction obtained by enzymatic depolymerisation are always lower than those of the corresponding P fractions. In this case, a mean value (K4M hydrolysates) close to that of the starting polymer is obtained.
- 3- The DS_{Me} of fractions isolated after acidic hydrolysis is the same as the starting material indicating that a random depolymerisation takes place, contrary to the case of the enzymatic catalysis.

Physico-chemical characterization of short chained HPMCs

It can also be observed that G4-P-180-72 shows a high MeO content similar to that of G4. This result confirmed our data reported in Chapter III on the enzymatic cleavage: the higher the degree of substitution on the polymer chain, the lower the enzyme activity.

Table IV. 4. Data on the chemical composition of the starting HPMCs and of the nine selected batches.

Reference	M_w (g.mol ⁻¹)	MS _{HP}	DS _{Me}	MeO%	HPO%
KMINIT	230000	0.24	1.30	20.8	9.3
K4M-P-30-1	31000	0.28	1.52	23.7	10.5
K4M-P-50-1	29000	0.25	1.43	22.6	9.6
K4M-P-15-72	27000	0.35	1.50	22.9	12.9
K4M-P-30-72	25000	0.32	1.47	22.6	12.0
K4M-P-50-72	20000	0.29	1.51	23.4	10.7
K4M-P-180-72	18000	0.28	1.53	23.7	10.4
K4M-S-30-1	11000	0.29	1.31	20.6	11.1
K4M-S-50-1	10000	0.28	1.17	18.7	10.8
K4M-S-15-72	9000	0.27	1.31	20.7	10.5
K4M-S-30-72	8000	0.30	1.34	21.0	11.3
K4M-S-50-72	8000	0.25	1.30	20.7	9.8
K4M-S-180-72	7000	0.26	1.43	22.5	9.9
K4M-P-AC0.6-1	22000	0.26	1.30	20.6	10.1
K4M-S-AC0.6-1	10000	0.24	1.25	20.0	9.2
G4	85000	0.31	1.66	25.3	11.5
G4-P-180-72	32000	0.30	1.73	26.3	11.2
G4-S-180-72	12000	0.39	1.39	21.1	14.4
G4-P-AC0.6-1	31000	0.30	1.65	25.3	11.0
G4-S-AC0.6-1	13000	0.28	1.68	25.8	10.4

The MS_{HP} values present also a slight fluctuation depending on the samples that can be due to the experimental error of the determination method. It seems to exist a trend in which

MS_{HP} has a higher value from S polymers. However, it is not always true and no direct correlation can be found with M_w of samples.

All these results allow us to conclude that the K4M and G4 structures are not homogeneously substituted. Enzymatic S fractions have about 10 % less of MeO groups than P fragments. On the other hand, the HPO content seems to be more or less constant. The highly methylated block located along the HPMC chain appears to be the limiting parameter where the enzymatic catalyst lost its activity.

DS_{Me} imparts hydrophobic behavior of the HPMC polymer chain whereas MS_{HP} relates on to the balance on hydrophilic part⁸⁻⁹. It was indicated in the previous section that P polymers have a more compact conformation in solution than S ones. It was assumed that this phenomenon might be due to a higher methylation of the P samples. The plot of $d(\log M)/d(\log R_g)$ vs DS_{Me} for all the P samples in Figure IV.9 confirms this assumption as a direct correlation between $d(\log M)/d(\log R_g)$ and DS_{Me} values can be seen. The scattering of the data points is likely due to the inaccuracy of the slope determination and to the diversity of experimental conditions (catalyst, starting material).

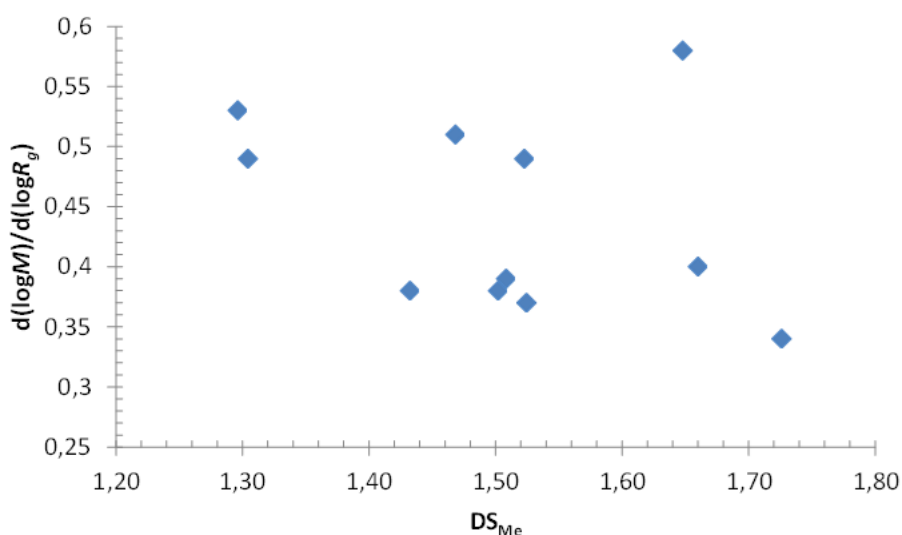


Figure IV. 9. $d(\log M)/d(\log R_g)$ as a function of the DS_{Me} for the starting HPMC (K4M and G4) and the P fractions of the nine selected batches.

IV.3. Reducing end reactivity

Cellulose and their derivatives include at one of their extremities an aldehyde group related to the open form of terminal cellobiose. The purpose of the reducing end analysis was to estimate the end reactivity of the prepared short chained HPMCs. This analysis relies on the oxidation-reduction reaction between the aldehyde group and Cu^{2+} ions. Thus, the UV-Vis absorption intensity of starting and hydrolyzed polymers revealed the availability of hemiketal carbon to reduce Cu^{2+} .

Figure IV.10 shows the amount of reducing end per gram of started and hydrolyzed polymers. As expected, the titration of reducing end is inversely related to the chain length. A given amount of short polymers contains more chain extremities than longer ones. However, attempt to correlate the data from reducing ends to M_n was unsuccessful.

On the other hand, the HPMC fragments produced by enzymatic process exhibited higher availability of reducing ends than those produced by acid hydrolysis. To explain this difference, it should be reminded that acid hydrolysis cleaves randomly the HPMC chain. Therefore, it was assumed that the chain end of acid fragments might be substituted enough to hamper the AGU opening since 2 or more substituents on AGU in end chains is supposed to disturb the mutarotation of aglycone-containing hemiketal function.

By contrast, enzymes are able to hydrolyse glycosidic bond only with an unsubstituted AGU or substituted at the position C-6¹⁰⁻¹¹. Moreover, substituents on position C-2 hinders the enzyme activity. Hydrolysis with enzymes is very helpful in establishing anomeric configuration because they are catalysts with higher specificity for glycosidic linkage than inorganic acids. Mikkelsen et al.¹², mentioned that the advantage of enzymatic hydrolysis over acid hydrolysis is the specificity of the enzyme in function of the substrate, although the process is slower. The authors concluded that oligosaccharides with the desired degree of polymerization might be obtained avoiding monosaccharide or furfural formation.

Consequently, we conclude that enzymatic depolymerisation is a more appropriate technique than acidic hydrolysis to prepare short chained HPMCs in view of using them as building blocks in block copolymers since the end reactivity should be higher.

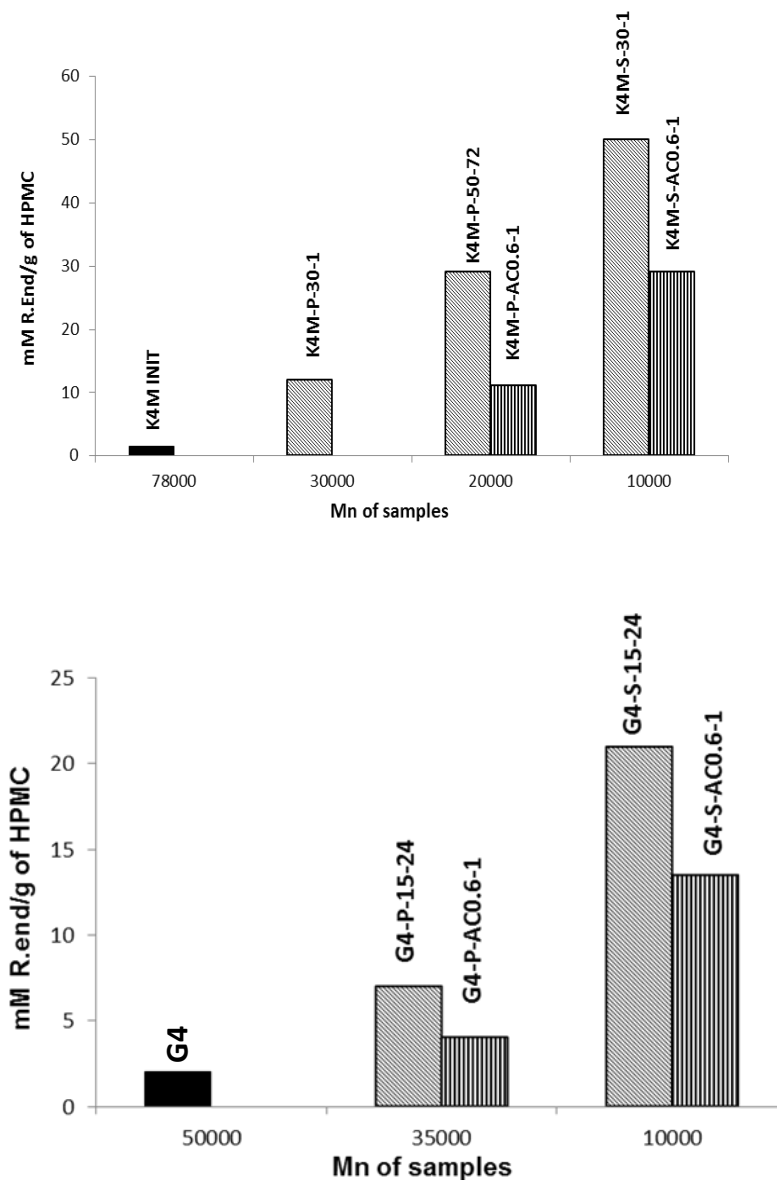


Figure IV. 10. Reducing end titration of HPMCs obtained by enzymatic and acid reaction compared to that of their parent compounds.

IV.4. Thermally induced phase separation - Cloud point

A general property of cellulose ether solutions is their inverse solubility behavior as the polymer solubility decreases beyond a critical temperature. Thus, clear solution of HPMC is obtained at room temperature while the solution loses its transparency at high temperature. The cloud point (C_p) is defined as the temperature at which a phase separation from solution takes place^{3,13}. Actually, the phase separation is coupled to a gelation of the system

leading to the formation of thermoresponsive hydrogel. The mechanism is supposed to be based on weakening of hydrogen bonds at the same time as the strengthening of hydrophobic interactions with increasing temperature. This combined effect implies that a transparent solution is obtained below the C_p whereas in contrast, above the C_p , the polymer becomes increasingly hydrophobic and insoluble leading to gel formation. The phenomenon of thermally induced phase separation is governed by the balance of hydrophilic and hydrophobic moieties on the polymer chain¹⁴. In the case of HPMC, it is related to the distribution of hydrophilic (HPO) and hydrophobic (MeO) groups on the polymer chain³ as well as to its M_w ⁹.

Previous studies proposed several ways to determine the C_p value of HPMC solutions. Ibett and coworkers in 1992¹⁵ have defined C_p as the temperature at which visual clarity is lost. The turbidity measurements consist in scanning the UV-vis transmittance of polymer solution at a given concentration (usually 2 %). Sarkar et al.¹⁶ have mentioned that C_p value can be determined for a loss of 50 % of transmittance. Viriden et al.⁹ have considered two values: low C_p at 96 % transmittance and high C_p at 50 % transmittance. Finally, Fairclough et al.¹⁷ have determined C_p as the intercept between the linear region of the decreasing curve and the 100 % transmittance.

In this work, it was adopted two ways of determining C_p (Figure IV.11). C_{p_0} corresponding to the onset C_p , is defined by extrapolating the linear region of curves to 100 % transmittance and $C_{p_{50}}$ at 50 % transmittance corresponding to the inflexion point of the curve. Indeed, the prepared HPMCs can be divided into two groups: the first series exhibits the usual curve going from 100 % transmittance for clear solution to 0 % after complete phase separation (more or less steep slope), and a second series for which the curve never reached 0 % transmittance (Figure IV.11). Consequently, only C_{p_0} values can be determined in the latter case.

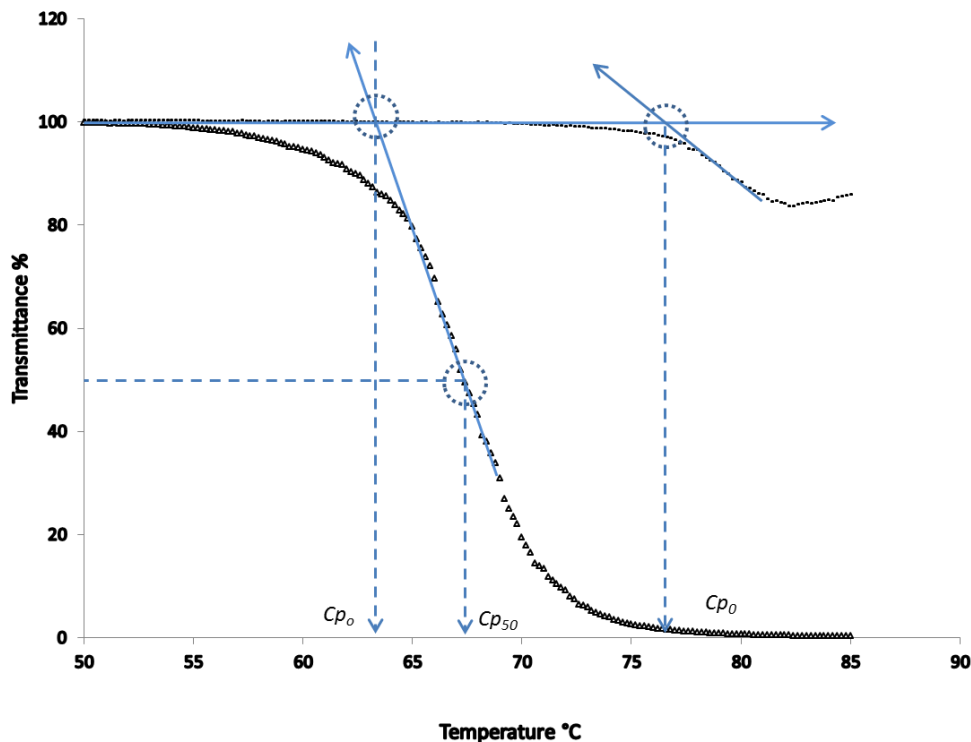


Figure IV. 11. Two ways of determining C_p from the turbidity experiments.

IV.4.1. Influence of M_w

A series of samples was chosen as a function of their M_w and method of preparation (starting HPMC, enzymatic or acidic catalysis). The first and the second groups have M_w values in the range of 30 000 and 20 000 $\text{g}\cdot\text{mol}^{-1}$ isolated as P fraction. The third group belonging to the S fraction gathers polymers having M_w values below 10 000 $\text{g}\cdot\text{mol}^{-1}$.

Table IV.5 summarizes data about the M_w and chemical composition of the samples studied as determined in the previous sections. The two last columns display the obtained values of C_{p_0} and $C_{p_{50}}$ when available. The two first lines of the table give the same data for K4M and G4.

Owing to its high DS_{Me} , G4 presents C_p values about 10°C lower than that of K4M. K4M polymers isolated from P fractions exhibited C_p values lower than the parent HPMC whereas those from S fractions were generally higher. It has to be noted that $C_{p_{50}}$ cannot be determined for most of the S fraction polymers because of incomplete curves (Figure IV.12). Moreover, C_{p_0} could not be detected for the shorter polymer K4M-S-180-72 ($M_w = 7\,000$

$\text{g}\cdot\text{mol}^{-1}$). In the case of G4 polymers, the variation seems to follow the same trend but with a lesser magnitude.

Table IV. 5. Cloud point temperatures (Cp_0 and Cp_{50}) as a function of the structural features of the selected polymers.

Samples	M_w ($\text{g}\cdot\text{mol}^{-1}$)	MS_{HP}	DS_{Me}	Cp_0 ($^{\circ}\text{C}$)	Cp_{50} ($^{\circ}\text{C}$)
K4M	230 000	0.24	1.30	69	72
G4	85 000	0.31	1.66	59	60
K4M-P-30-1	31 000	0.28	1.52	63	67
K4M-P-30-72	29 000	0.25	1.43	63	68
G4-P-180-72	32 000	0.30	1.73	58	59
G4-P-AC0.6-1	31 000	0.30	1.65	59	60
K4M-P-50-72	20 000	0.29	1.51	62	65
K4M-P-AC0.6-1	22 000	0.26	1.30	62	72
K4M-S-30-1	10 000	0.29	1.31	79	—
K4M-S-30-72	8 000	0.30	1.34	78	—
K4M-S-50-72	8 000	0.25	1.30	79	—
K4M-S-180-72	7 000	0.26	1.43	—	—
K4M-S-AC0.6-1	10 000	0.24	1.25	69	78
G4-S-180-72	12 000	0.39	1.39	62	65
G4-S-AC0.6-1	13 000	0.28	1.68	61	62

The starting commercial HPMCs show turbidity curves with a steep decrease of transmittance. As seen in Figure IV.12, the gap between the clear solution and 0 % transmittance occurs in between 3 - 5 $^{\circ}\text{C}$.

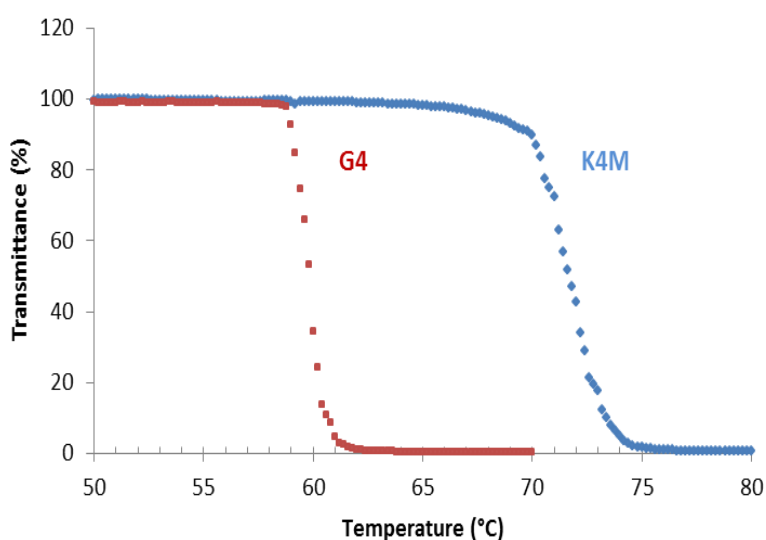


Figure IV. 12. Transmittance variation curves as a function of T for G4 and K4M.

By comparison, the gap is in the range of 15-20°C for P polymers produced by enzymatic and acidic catalysis in spite of its lower PDI values (Figure IV.13 and IV.14). It was assumed that these observations are due to their lower M_w compared to the starting HPMCs. Actually, the polymer solubility increases with decreasing M_w . Thus, the presence of a fraction of low M_w chains provokes a lagging phase separation. No gap could be determined for S polymers as the turbidity curves were incomplete except for K4M-S-AC0.6-1 with a gap estimated to more than 20°C (Figure IV.14).

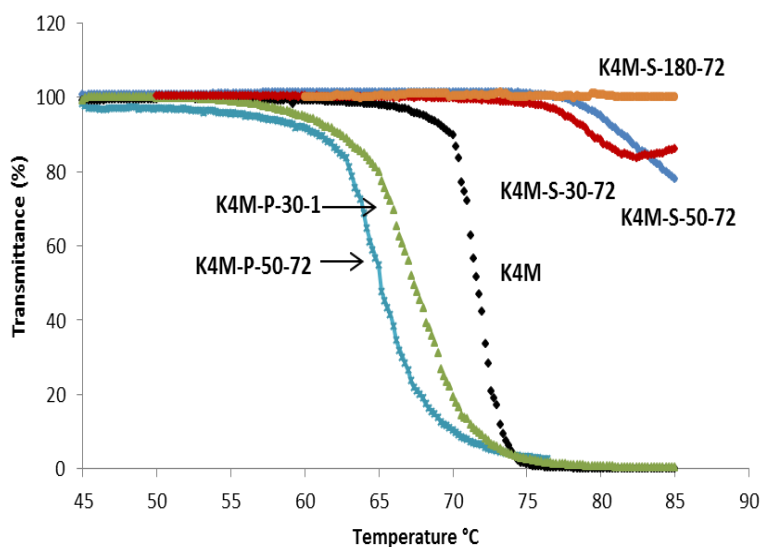


Figure IV. 13. Transmittance curves for K4M and its short chain derivatives prepared by enzymatic depolymerisation.

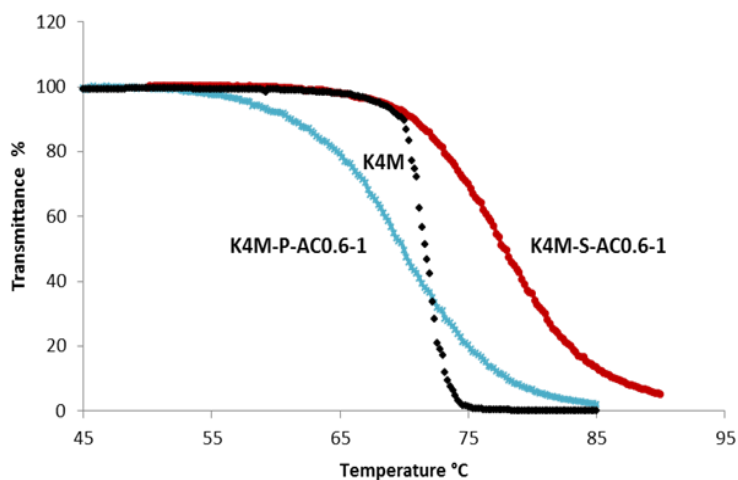


Figure IV. 14. Transmittance curves for K4M and its short chain derivatives prepared by acidic depolymerisation.

IV.4.2. Influence of the chemical composition

As stressed above, Cp_0 and Cp_{50} values should be highly related to the hydrophobic group content on the polymer chain. Figures IV.15, VI.16 present the plotting of Cp_0 and Cp_{50} values as a function of DS_{Me} of the different samples. As expected, a strong correlation can be established between the data of Cp_0 and Cp_{50} obtained for the different polymers including the starting ones. A linear regression fits well with the experimental data except those from the S fractions prepared by enzymatic catalysis in Figure IV.14.

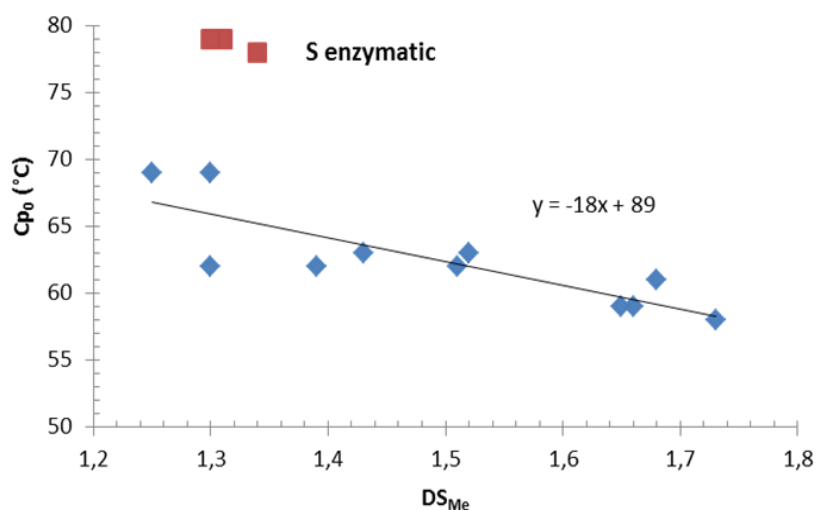


Figure IV. 15. Cloud point temperatures (Cp_0) as a function of the degree of methyl substitution DS_{Me} .

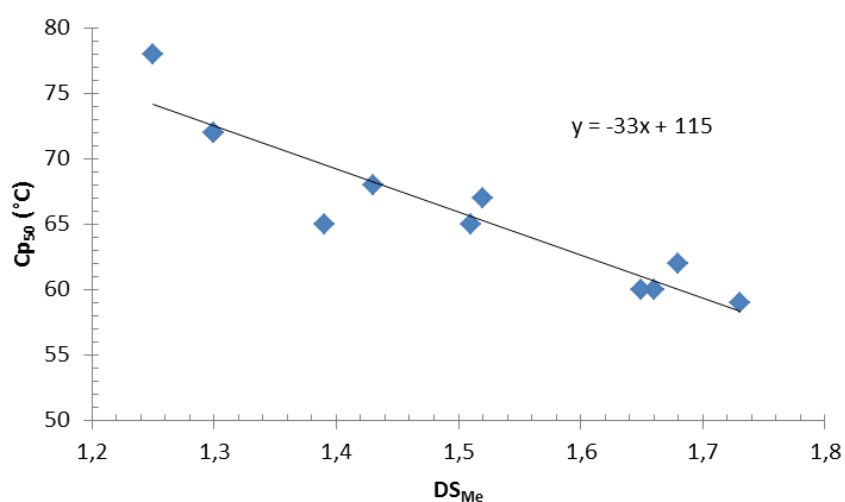


Figure IV. 16. Cloud point temperatures (Cp_{50}) as a function of the degree of methyl substitution DS_{Me} .

These results demonstrate that C_p values primarily depend on the degree of methyl substitution. They agree well with the previous studies of Shagerlöf et al.³ and Viriden et al.⁹, who have found lower C_p values for HPMCs highly substituted by hydrophobic (Me) groups. In contrast, our findings did not show any straightforward correlation between M_w and C_p values at least for M_w higher than 10 000 g.mol⁻¹. However, the influence of M_w cannot be excluded for the shorter chains as illustrated in Figure IV.15. At same DS_{Me} , HPMCs with M_w lower than 10 000 g.mol⁻¹ have C_{p_0} values 10°C higher.

IV.4.3. Influence of the depolymerisation procedure

Another interesting observation concerns the comparison between short chained HPMC prepared from enzymatic and acidic catalysis. HPMC fragment produced by acid hydrolysis exhibited C_p values close to that of their parent polymers (Figure IV.14) compared to that obtained by an enzymatic process (Figure IV.13).

So far, most studies of physicochemical characterization on HPMC samples were performed on commercial ones, which are prepared by acid process. Since enzymatic depolymerisation is highly selective, fragments with original structure and properties based on the substitution degree can be produced.

To exemplify the strong difference between the compounds produced by the both routes, Figure IV.17 shows a comparison of turbidity curve profiles between short chained fragments with the same M_w obtained by enzymatic and acid reaction. Thus, K4M-S-30-1 (10 000 g.mol⁻¹, $DS_{Me} = 1.31$) obtained by enzymatic reaction exhibits an incomplete turbidity curve from which a C_{p_0} value can be determined at 79°C but not a $C_{p_{50}}$ one (Table IV.5). By contrast, both parameters ($C_{p_0} = 69^\circ\text{C}$ and $C_{p_{50}} = 78^\circ\text{C}$, Table IV.5) can be measured from the turbidity curve of K4M-S-AC0.6-1 having the same M_w and a similar DS_{Me} value (1.25) prepared by acid hydrolysis.

In conclusion of this section, it was demonstrated that the phase separation behavior of short chained HPMC can be controlled by adjusting the operating parameters of the depolymerisation. Depending on the procedure and the nature of catalyst, the polymer structure can be tailored to obtain the desired properties.

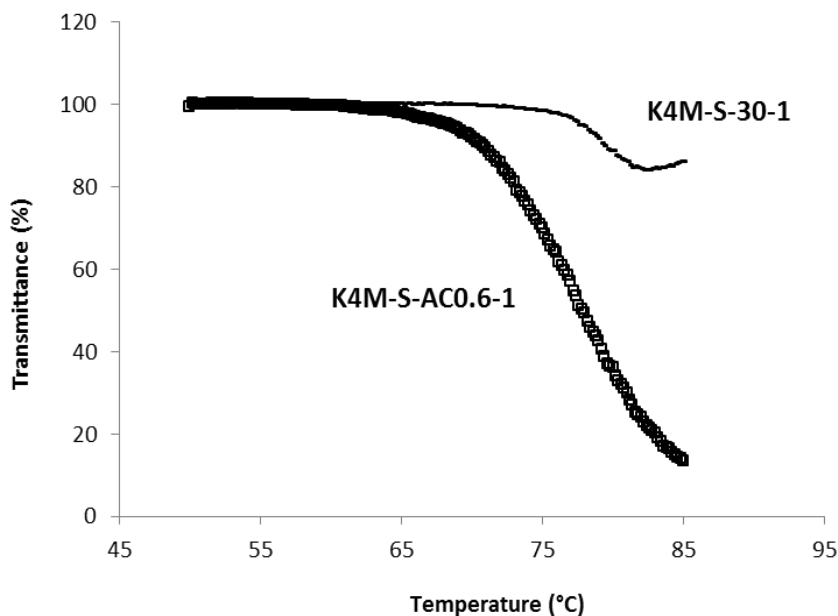


Figure IV. 17. Transmittance curves of short chained HPMC with a M_w of about 10 000 g.mol^{-1} prepared by enzymatic and acid depolymerisation of K4M.

CONCLUSION

Short chained HPMCs produced by enzymatic and acid treatment were characterized and compared to their parent polymers. The macromolecular features showed that short polymers ranging from about 30 000 to 7 000 g.mol^{-1} can be prepared with various solution behavior from compact to expanded. These different properties can be related to the degree of substitution of the obtained polymers. Moreover, the thermally induced phase separation behavior was demonstrated to be primarily connected to the value of DS_{Me} . On the other hand, M_w seems to influence this property only for values lower than 10 000 g.mol^{-1} . For instance, the smaller HPMC prepared by enzymatic hydrolysis did not show any phase separation.

Finally, it was also shown that the enzymatic depolymerisation enables to yield short chained HPMCs with a larger content of reducing end. This end reactivity can be used to functionalize and to prepare block copolymers. Preliminary investigations on the synthesis of amphiphilic block copolymers using short chained HPMCs will be described in the next chapter.

REFERENCES

1. Akash, M. S.; Iqbal, F.; Raza, M., *et al.*, Characterization of Ethylcellulose and Hydroxypropyl Methylcellulose Microspheres for Controlled Release of Flurbiprofen. *J Pharm Drug Deliv Res* 2013, 2 (1), 3-10.
2. De Gennes, P. G., *Scaling Concepts in Polymer Physics*. Cornell University Press: Ithaca, NY, 1979, p. 324.
3. Schagerlof, H.; Johansson, M.; Richardson, S., *et al.*, Substituent distribution and clouding behavior of hydroxypropyl methyl cellulose analyzed using enzymatic degradation. *Biomacromolecules* 2006, 7 (12), 3474-81.
4. Fitzpatrick, F.; Schagerlof, H.; Andersson, T., *et al.*, NMR, cloud-point measurements and enzymatic depolymerisation: Complementary tools to investigate substituent patterns in modified celluloses. *Biomacromolecules* 2006, 7 (10), 2909-2917.
5. Ho, F. F. L.; Ward, G. A.; Kohler, R. R., Determination of Molar Substitution and Degree of Substitution of Hydroxypropyl Cellulose by Nuclear Magnetic-Resonance Spectrometry. *Anal Chem* 1972, 44 (1), 178-&.
6. Cellulose Ethers: Technical Overview and Product Guide. In *Cellulose Ethers: Technical Overview and Product Guide*, Dow Chemical Company, Form No. 832-00226-0512 BBI: U.S.A, 2012.
7. Methocel Cellulose Ethers, Technical Handbook. The Dow Chemical company, Form No. 192-01062-0902 AMS: Midland, 2002.
8. Richardson, S.; Gorton, L., Characterisation of the substituent distribution in starch and cellulose derivatives. *Anal Chim Acta* 2003, 497 (1-2), 27-65.
9. Viriden, A.; Wittgren, B.; Andersson, T., *et al.*, Influence of substitution pattern on solution behavior of hydroxypropyl methylcellulose. *Biomacromolecules* 2009a, 10 (3), 522-9.
10. Momcilovic, D.; Schagerlof, H.; Rome, D., *et al.*, Derivatization using dimethylamine for tandem mass spectrometric structure analysis of enzymatically and acidically depolymerized methyl cellulose. *Anal Chem* 2005, 77 (9), 2948-2959.
11. Enebro, J.; Momcilovic, D.; Siika-aho, M., *et al.*, Investigation of endoglucanase selectivity on carboxymethyl cellulose by mass spectrometric techniques. *Cellulose* 2009, 16 (2), 271-280.
12. Mikkelsen, A.; Maaheimo, H.; Hakala, T. K., Hydrolysis of konjac glucomannan by *Trichoderma reesei* mannanase and endoglucanases Cel7B and Cel5A for the production of glucomannooligosaccharides. *Carbohydr Res* 2013, 372, 60-68.
13. Jain, S.; Sandhu, P. S.; Malvi, R., *et al.*, Cellulose Derivatives as Thermo-responsive Polymer: An Overview. *J Appl Pharm Sci* 2013, 3 (12), 139.
14. Taylor, L. D.; Cerankowski, L. D., Preparation of Films Exhibiting a Balanced Temperature-Dependence to Permeation by Aqueous-Solutions - Study of Lower Consolute Behavior. *J Polym Sci Pol Chem* 1975, 13 (11), 2551-2570.
15. Ibbett, R. N.; Philp, K.; Price, D. M., ¹³C n.m.r. Studies of the thermal behaviour of aqueous solutions of cellulose ethers. *Polymer* 1992, 33 (19), 4087-4094.
16. Sarkar, N.; Walker, L. C., Hydration Dehydration Properties of Methylcellulose and Hydroxypropylmethylcellulose. *Carbohydr Polym* 1995, 27 (3), 177-185.

17. Fairclough, J. P. A.; Yu, H.; Kelly, O., *et al.*, Interplay between Gelation and Phase Separation in Aqueous Solutions of Methylcellulose and Hydroxypropylmethylcellulose. *Langmuir* 2012, 28 (28), 10551-10557.

CHAPTER V: NEW POLYSACCHARIDE FRAGMENTS TO AMPHIPHILIC BLOCK COPOLYMER SYNTHESIS

INTRODUCTION

Polysaccharides have emerged as important functional building blocks to synthesize new amphiphilic block copolymers which are able to self-assemble into nanostructures and/or to form thin films. These properties are widely exploited for applications on biomedical sciences¹⁻³, nanoreactors⁴ and lithography for the semi-conductor industries⁵⁻⁷.

Upon coupling hydrophobic moties onto a hydrophilic polysaccharide, an amphiphilic copolymer is created. In aqueous solution amphiphilic copolymers tend to self-assemble into nanomicelles in which the hydrophobic blocks form the core, and the hydrophilic part forms the corona or outer shell⁸. The hydrophilic shell serves as a stabilizing interface between the hydrophobic core and the external aqueous environment^{2, 9}. Therefore, self-assembly process results from hydrophobic interactions, mainly in order to minimize interfacial free energy.

Diverse morphologies of nano-objects have been obtained by self-assembly of block copolymers in solution. The morphology is governed by three parameters which contribute to the free energy of the system: the degree of stretching of the core-forming blocks, the interfacial tension between the micelle core and the solvent outside the core, and the repulsive interactions among the corona-forming chains¹⁰. More than 20 morphologies of self-assembled block copolymers have been identified, including micelles, lamellae, polymersomes, etc. Some of them are thermodynamically and others are kinetically controlled¹⁰⁻¹¹. These various nanostructures can be obtained by adjusting the length of the hydrophobic and hydrophilic blocks of copolymers⁹, the copolymer concentration, water content, nature of the solvent, and the presence of additives like salts¹².

In this chapter we present the synthesis of novel block copolymers based on polysaccharides. Small fragments of HPMC generated by enzymatic procedure were end-functionalized and attached to end-functional hydrophobic blocks. The resulting amphiphilic block copolymers were characterized by FTIR and DOSY NMR analysis. Their self-assembly properties in water were determined by critical aggregate concentration (CAC), DLS and TEM. Thermo-responsive properties were revealed by measuring their clouding point temperature.

RESULTS AND DISCUSSION

Two types of linear diblock copolymers were synthesized following two different procedures.

- 1) end-to-end coupling reaction that consisted in reacting the native terminal aldehyde end group of the polysaccharide chain with an α -amino functional polymer chain, through a reductive amination process in the presence of sodium cyanoborohydride¹³. Thus, Jeffamine® M-2005 (monoamine $\text{H}_2\text{N-PO}_{29}\text{-EO}_6$) and T-5000 ($(\text{H}_2\text{N})_3\text{-PO}_{85}$; see the formula in Figure V-9) were coupled with short-chained polysaccharide (HPMC K4M-S-50-72 with $M_w = 8000 \text{ g.mol}^{-1}$) obtained via enzymatic hydrolysis, yielding HPMC-*b*- $\text{PO}_{29}\text{-EO}_6$ and tri-branched star block copolymers $(\text{HPMC})_3\text{-}b\text{-PO}_{86}$ by reductive amination.
- 2) The second procedure of synthesizing linear AB block copolymer consisted in introducing a new functional group as thiol at the reducing end of HPMC via reductive amination reaction. Then thiol HPMC is coupled to allyl end-functionalized poly(L-lactide) (PLLA) via UV catalyzed click chemistry, yielding HPMC-*b*-PLLA block copolymers.

V.1. HPMC-*b*- $\text{PO}_{29}\text{-EO}_6$

V.1.1. Synthesis

Reductive amination reaction between HPMC (aldehyde terminated) homopolymer and amino terminated Jeffamine® M-2005 ($\text{H}_2\text{N-PO}_{29}\text{-EO}_6$) was performed in DMSO using sodium cyanoborohydride as reductive agent (Figure V.1). $\text{H}_2\text{N-PO}_{29}\text{-EO}_6$ was used in excess so as to ensure the complete reaction of HPMC. Unreacted $\text{H}_2\text{N-PO}_{29}\text{-EO}_6$ was eliminated by precipitation in water during dialysis purification. Soluble block copolymer HPMC-*b*- $\text{PO}_{29}\text{-EO}_6$ was recovered and lyophilized with a yield of 87 %. The obtained block copolymer was characterized by using SEC/MALS/RI, FTIR, and ^1H NMR spectroscopy.

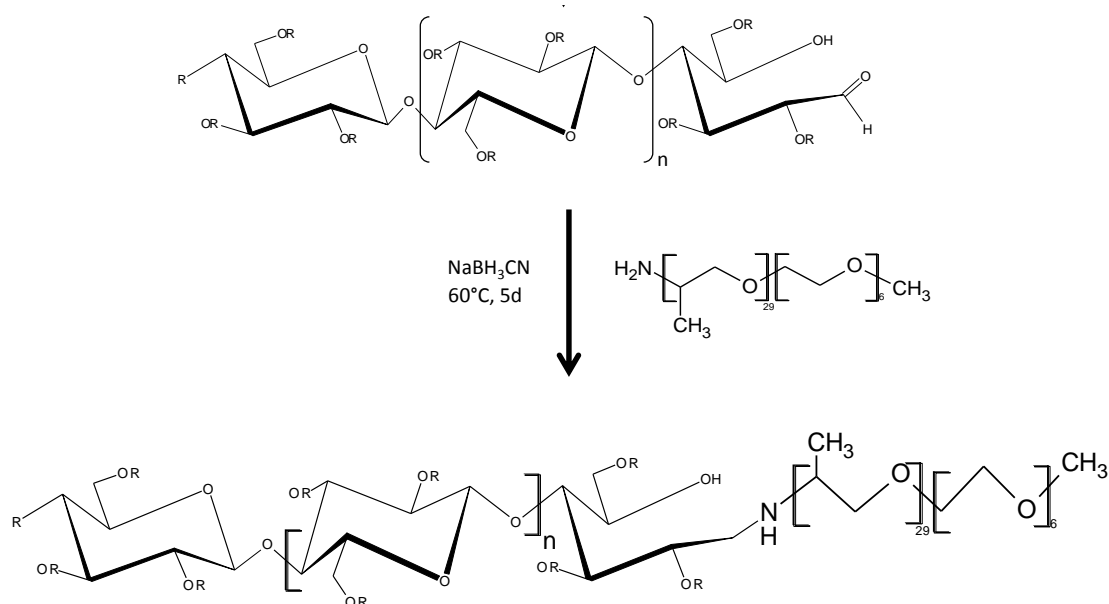


Figure V. 1. Synthesis scheme of HPMC-*b*-PO₂₉-EO₆.

V.1.2. Average molar mass of the block copolymer

HPMC-*b*-PO₂₉-EO₆ was first characterized by SEC/MALS/RI in an aqueous medium. 5 mg of the block copolymer was dissolved in 1 mL of eluent (10 mM NaCl with 0.02 % NaN₃). The solution was placed in cool basin for 15 min before injection to avoid nano-objects interference on the average molar mass determination. Figure V.2 shows the curves of starting HPMC ($M_w = 8000 \text{ g}\cdot\text{mol}^{-1}$, PDI = 1.5) and block copolymer ($M_w = 10\,000 \text{ g}\cdot\text{mol}^{-1}$, PDI = 1.3). The increase of average molar mass indicates that the block H₂N-PO₂₉-PEO₆ ($M_w = 2000 \text{ g}\cdot\text{mol}^{-1}$) was successfully attached to HPMC chains. The diminution of the PDI value from 1.5 to 1.3 can be assigned to the loss of low molecular weight species during the purification process by dialysis.

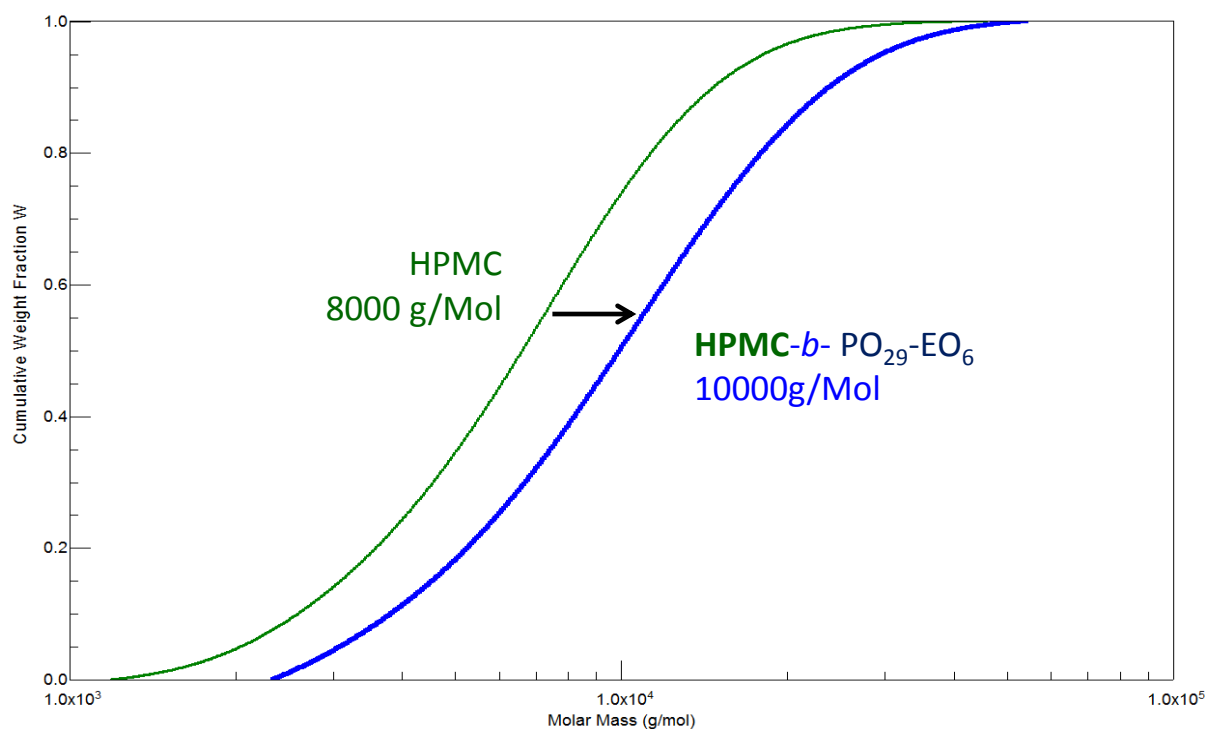


Figure V. 2. Cumulative molar mass distribution of the starting short chained HPMC and the resulting block copolymer HPMC-*b*-PO₂₉-EO₆.

V.1.3. FTIR analysis

Figure V.3 shows the FTIR spectra of HPMC-*b*-PO₂₉-EO₆ compared to that of the reagents H₂N-PO₂₉-EO₆ and HPMC polymers. The intensity changes of the signals at 2900 cm⁻¹ and 1100 cm⁻¹ region suggest the successful coupling between H₂N-PO₂₉-EO₆ and HPMC.

These results well agree with previous studies performed by the research group of Lecerf and Picton¹⁴, where polysaccharides (pullulans) were successfully coupled to Jeffamine®M-2005.

V.1.4. DOSY NMR analysis

Figure V.4 reveal the diffusion ordered NMR spectroscopy (DOSY-NMR) analysis for HPMC-*b*-PO₂₉-EO₆ block copolymer and the ¹H spectrum projected on the top. The ¹H NMR spectrum exhibits signals corresponding to the HPMC block (δ=5-3.2 ppm) and the PO₂₉-EO₆ block (δ=1 ppm), that is also shown in Figure V.5. DOSY analysis and ¹H NMR signals of HPMC and PO₂₉EO₆ present the same diffusion coefficient (Figure V.4), as indicative of successful coupling reaction.

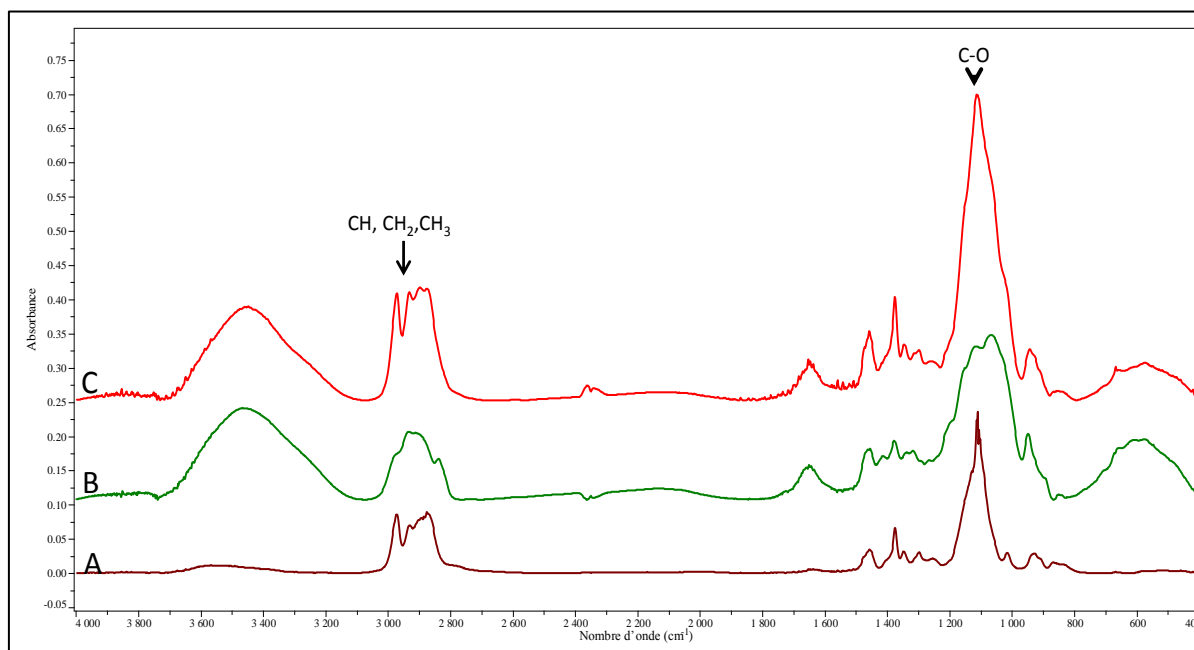


Figure V. 3. FTIR spectra of (A) $\text{H}_2\text{N-PO}_{29}\text{-EO}_6$, (B) HPMC ($M_w = 8000 \text{ g mol}^{-1}$), (C) HPMC-*b*- $\text{PO}_{29}\text{-EO}_6$.

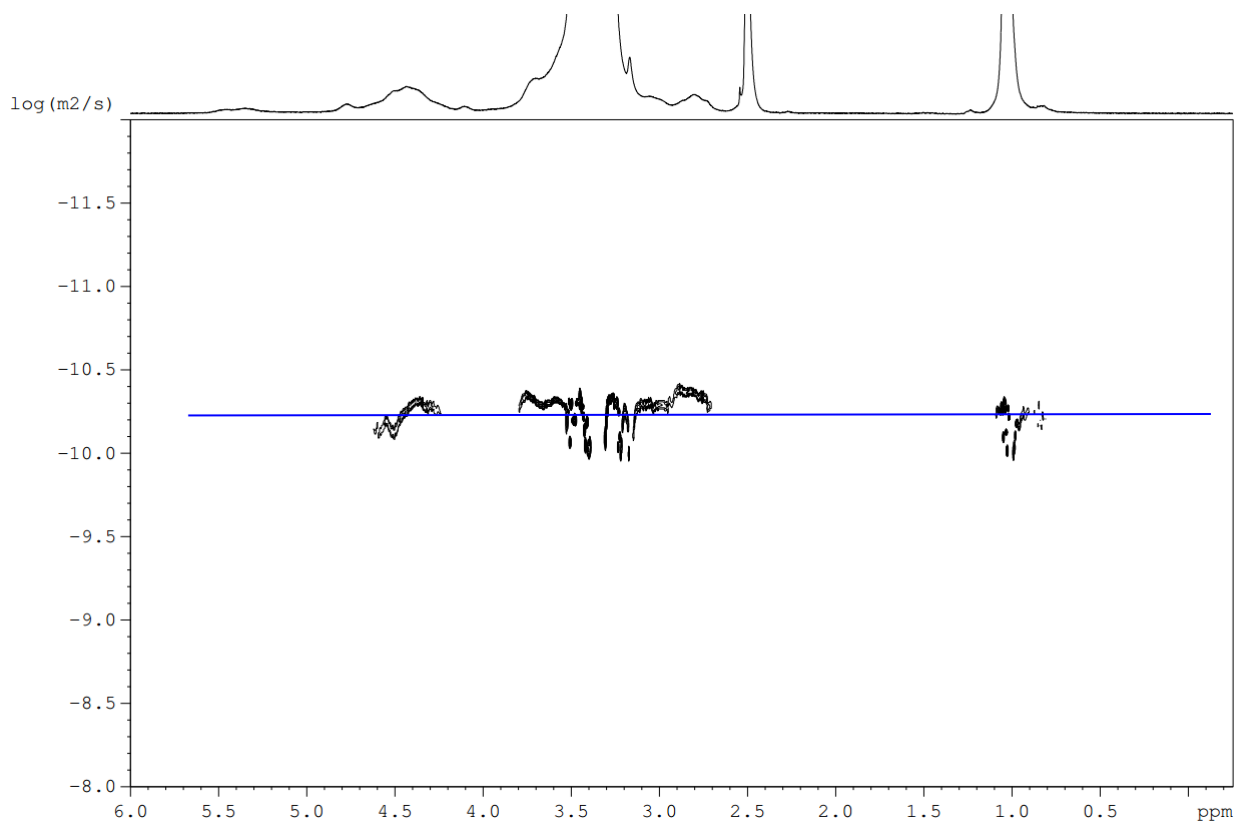


Figure V. 4. DOSY NMR spectra obtained at 298 K in $\text{DMSO-}d_6$ solution of the copolymer HPMC-*b*- $\text{PO}_{29}\text{-EO}_6$.

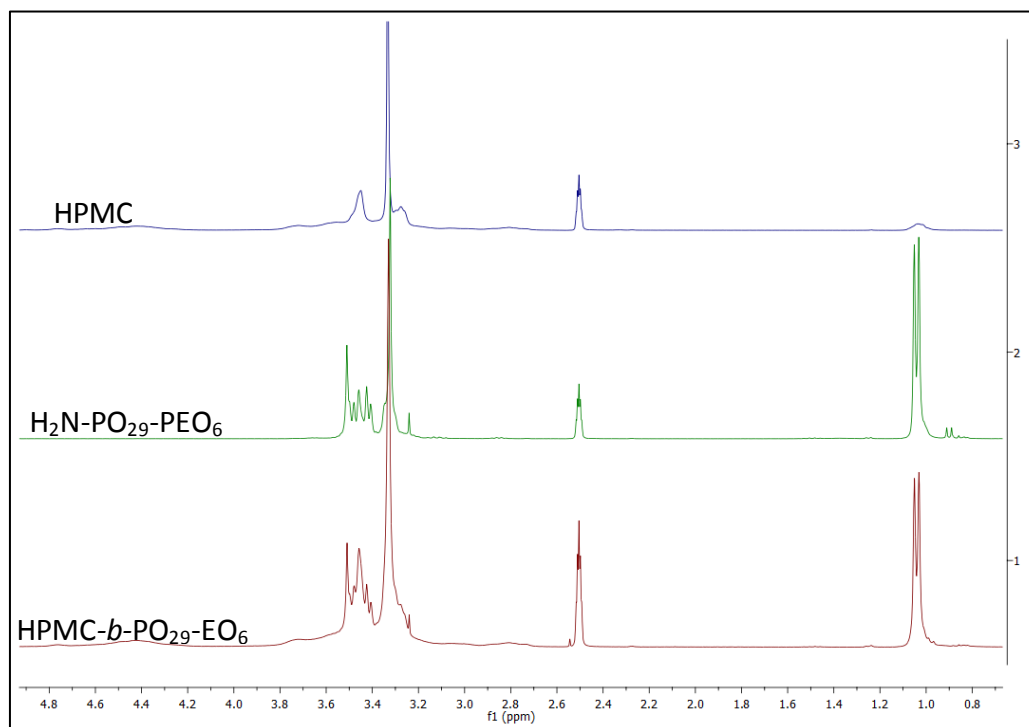


Figure V. 5. ^1H NMR spectra of HPMC, $\text{H}_2\text{N-PO}_{29}\text{-PEO}_6$ copolymer $\text{HPMC-}b\text{-PO}_{29}\text{-EO}_6$ in $\text{DMSO-}d_6$.

V.1.5. Self-assembly of $\text{HPMC-}b\text{-PO}_{29}\text{-EO}_6$ in H_2O

Theoretically, the self-assembly of $\text{HPMC-}b\text{-PO}_{29}\text{-EO}_6$ copolymer in deionized water could lead to two different nanostructures (Figure V.6):

- Micelles with double core (hydrophilic and hydrophobic) and hydrophilic shell,
- polymersomes with double hydrophilic shell.

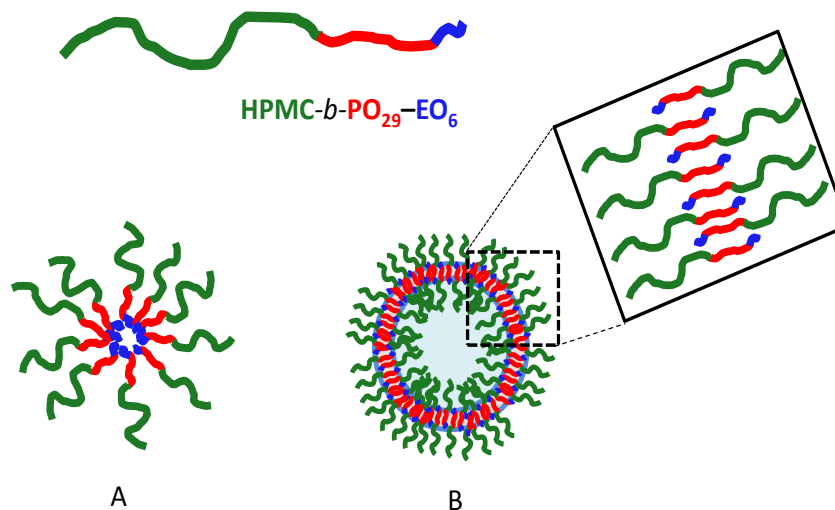


Figure V. 6. Possible morphologies of self-assembled $\text{HPMC-}b\text{-PO}_{29}\text{-EO}_6$.

It is noteworthy that the block copolymer is composed of blocks having a marked hydrophilic character (HPMC and EO₆). The hydrophilic part is 83 wt % and hydrophobic portion is 17 wt % of the total blocks. Moreover, the hydrophobic segment (PO₂₉) is located in between the two hydrophilic blocks so that it was considered HPMC-*b*-PO₂₉-EO₆ chains as a triblock A-B-A. This structure is assumed to strongly affect the stability of nanostructured objects.

Self-assembly property of amphiphilic block copolymers was evaluated using dynamic light scattering (DLS) and transmission electron microscopy (TEM). Thus, the copolymer was dissolved in deionized water at a concentration of 0.3 g L⁻¹. The solution was filtered through 0.45 μm PTFE microfilter and incubated at room temperature overnight. DLS was used to determine the size distribution and hydrodynamic radius (R_H) of aggregates. Figure V.5 shows the DLS results obtained for HPMC-*b*-PO₂₉-EO₆ copolymer. Two families of nano-objects are observed: the first with R_H around 80 nm and the second with the high intensity % of R_H at 250 nm. Therefore, it is highly probably that the size of the nano-objects reaches 250 nm, accompanied by a smaller population with a size around 80 nm (Figure V.7). The blue line corresponds to the correlation coefficient as a function of time. The large size population with R_H around 5000 nm should be assigned to aggregation of micelles.

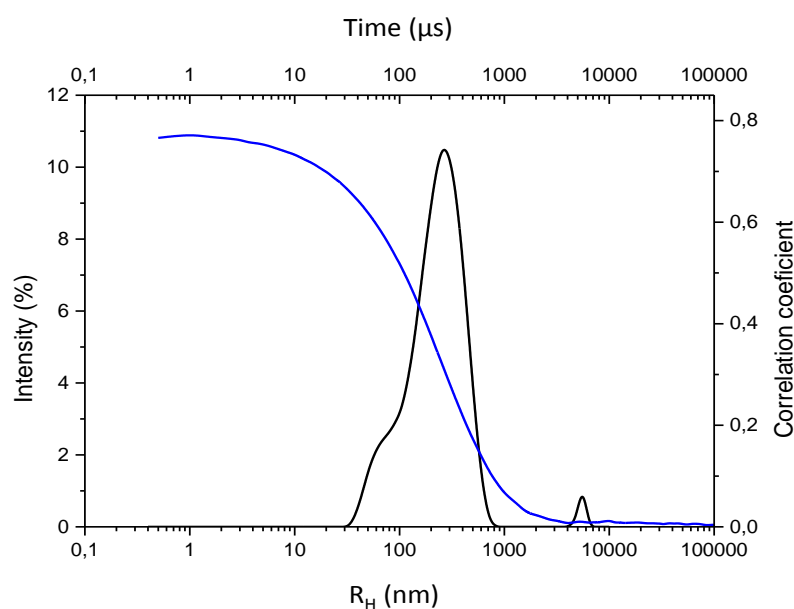


Figure V. 7. Size distribution (black) and autocorrelation function (blue) measured by DLS for HPMC-*b*-PO₂₉-EO₆ copolymer at a concentration of 0.3 g L⁻¹.

Figure V.8 shows the TEM image of the self-assembled nanoparticles of the HPMC-*b*-PO₂₉-EO₆ copolymer. The shape of the nano-objects appears irregular, and the average size measured from TEM image is lower than that obtained by DLS analysis. The difference between the results obtained from TEM and DLS analysis could be contributed to the experimental conditions. Indeed, DLS determines the hydrodynamic diameter of micelles in aqueous solution, whereas TEM shows the dehydrated solid state of micelles. From the TEM image, it could be assumed that nano-objects exhibit micelle-like structure.

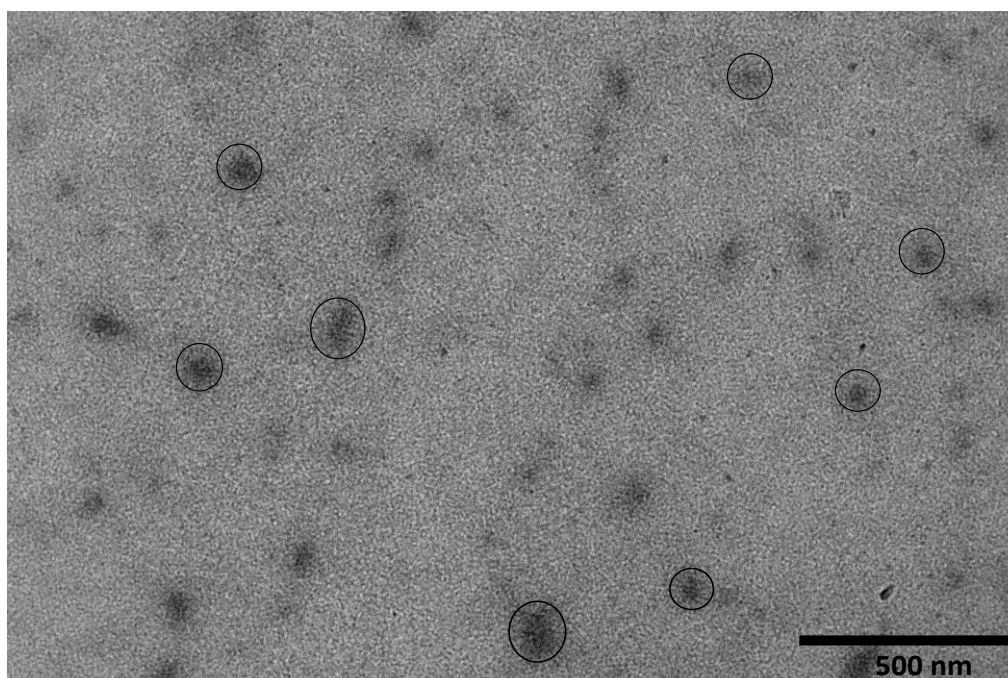


Figure V. 8. TEM image of the self-assembled nanoparticles of HPMC-*b*-PO₂₉-EO₆ copolymer.

The critical aggregate concentration (CAC) was determined by DLS experiments following the methodology proposed by Muller *et al.*¹⁵. Copolymer solutions with concentrations ranging from 1.0×10^{-4} to 1.0 g L^{-1} were prepared in deionized water. The solutions were incubated overnight and the measurements were realized at 35°C. The evolution of the intensity versus copolymer concentration was plotted with linear regression. At the low concentrations, the scattered intensity was very weak because nano-objects were not formed (electrostatic repulsion). In contrast at higher concentrations, the intensity strongly increased with the presence of particles. Experimental CAC was graphically read at the intersection of the two linear regression lines (Figure V.9). Thus, we deduced that the CAC of HPMC-*b*-PO₂₉-EO₆

copolymer is 0.28 g.L^{-1} . Belbekhouche et al.¹⁶ reported similar results for this kind of copolymers (Pullulan-*b*-PO₂₉-EO₆) with CAC values of 0.18 g.L^{-1} at pH = 12 and 0.54 g.L^{-1} at pH = 2. In deionized water, neutral block copolymer aggregation is governed by the hydrophilic-hydrophobic balance. According to the literature, the CAC or CMC value increases when the content of hydrophilic fraction increases^{15, 17-19}. De Mendeiros *et al.*¹⁹ reported a CMC of 0.1 g.L^{-1} for nanoparticles formed by oligosaccharides.

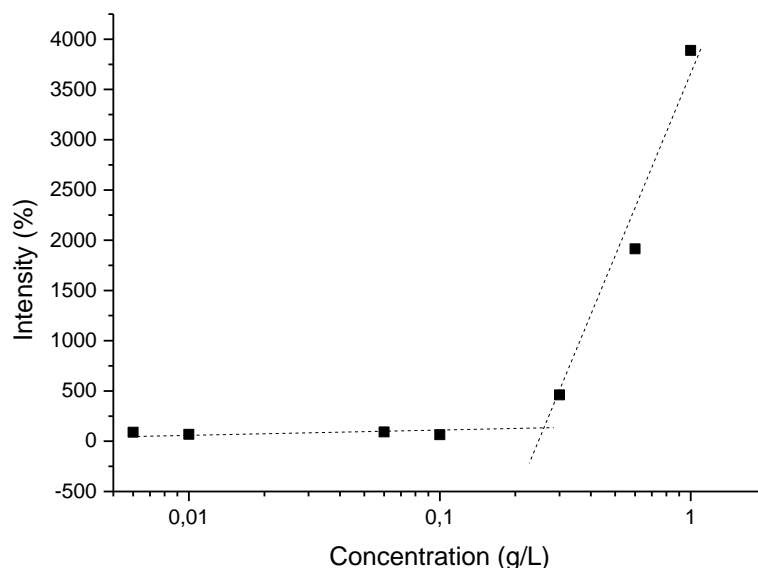


Figure V. 9. Plot of scattered intensity (%) as a function of HPMC-*b*-PO₂₉-EO₆ copolymer concentration.

V.1.6. Thermoresponsive behavior of HPMC-*b*-PO₂₉-EO₆

The thermo-responsive behavior of HPMC-*b*-PO₂₉-EO₆ copolymer was determined by measuring the clouding point of solutions at 10 g L^{-1} in deionized water. Figure V.10 shows the typical phase transition for the copolymer and the starting HPMC. The clouding point temperature Cp_0 is $15 \text{ }^\circ\text{C}$ for the amphiphilic block copolymer, and $79 \text{ }^\circ\text{C}$ for HPMC. Dulong *et al.*²⁰ reported that the Cp_0 value for H₂N-PO₂₉-EO₆ is $18 \text{ }^\circ\text{C}$ in Milli-Q water (pH 11).

The clouding point of the copolymer is much lower than that of the short chained HPMC. This effect could relate at the presence of hydrophobic moieties (PO₂₉). The novel block copolymer HPMC-*b*-PO₂₉-EO₆ evidenced a phase transition completely different from HPMC. This finding could be explained by the methyl substitution along the HPMC chain which

might interact with the hydrophobic PO block increasing the hydrophobic domain, and interfering with the stability of nanostructures.

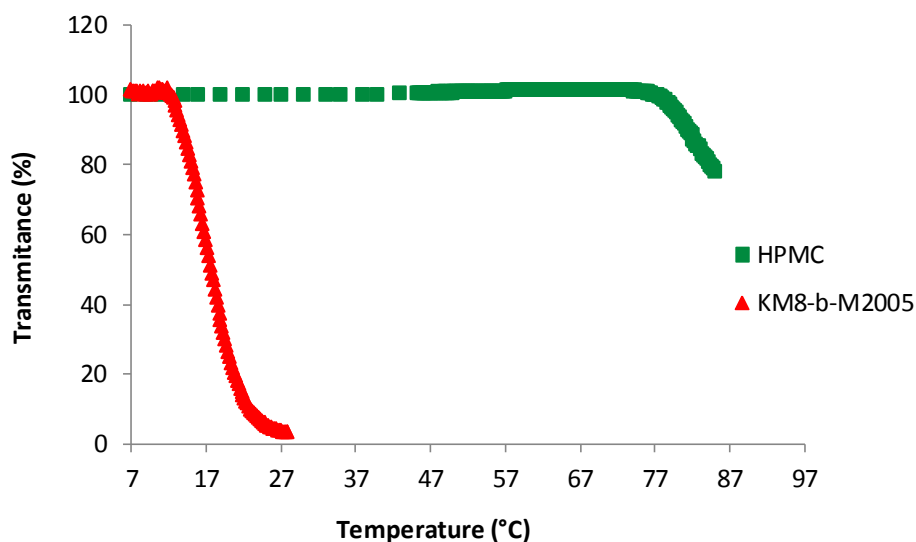


Figure V. 10. Plots of transmittance changes as a function of temperature for aqueous solutions (10 g L^{-1}) for HPMC and HPMC-*b*-PO₂₉-EO₆. Solutions prepared in deionized water.

V.2. Miktoarm block copolymer (HPMC)₃-*b*-PO₈₅

V.2.1. Synthesis

The block copolymer was synthesized using 1 g of HPMC $M_w = 8000 \text{ g.mol}^{-1}$ (0,125mM) and 0,065 g of tri-arm Jeffamine® T-5000 (PO₈₅) $M_w=5000 \text{ g.mol}^{-1}$ (0.0125mM) (Figure V.11). And 8 mg of NaCNBH₃ (0,125mM) was used as the catalyst. The yield of the reaction reaches 92 %.

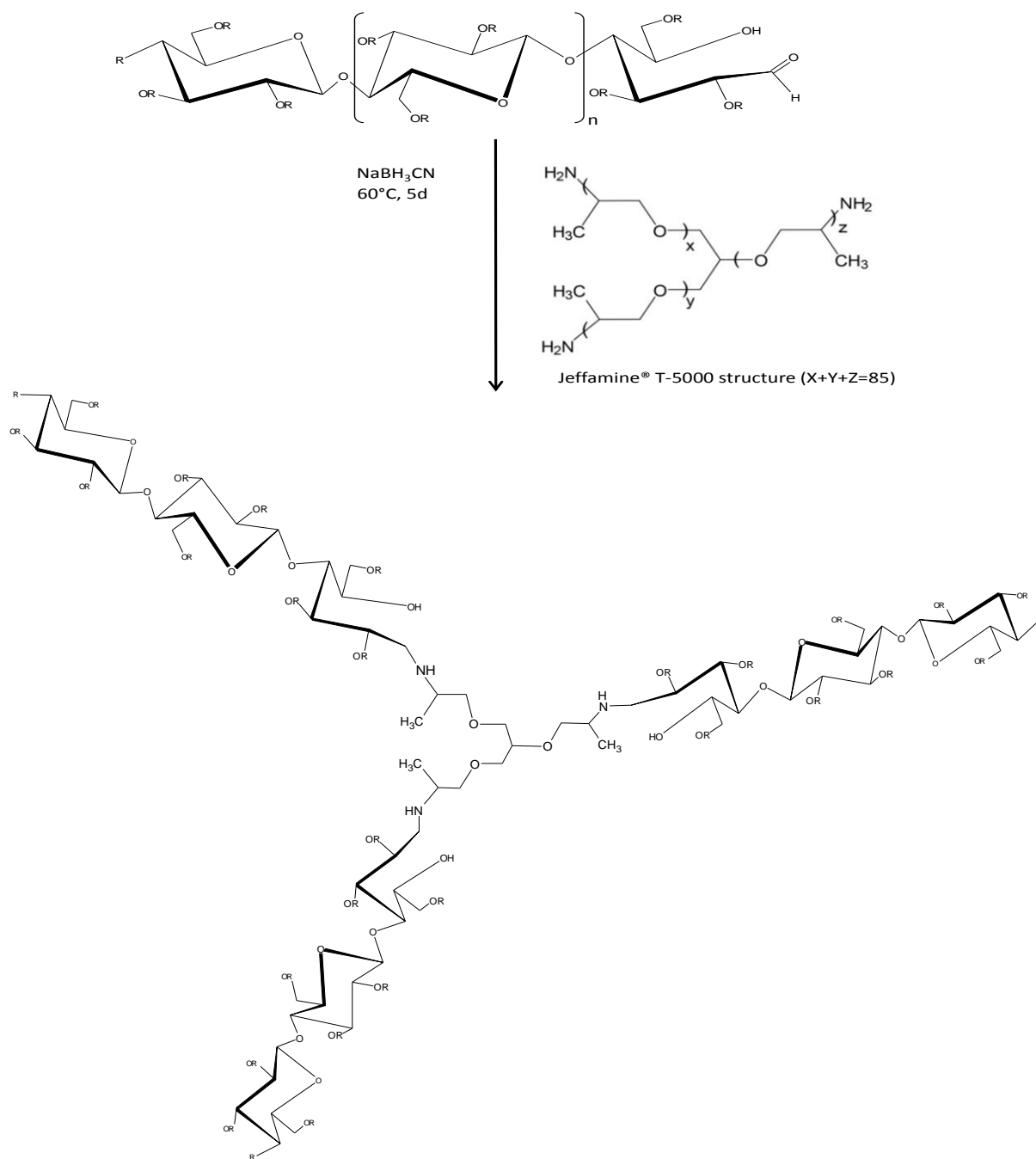


Figure V. 11. Synthesis scheme of $(\text{HPMC})_3\text{-}b\text{-PO}_{85}$.

V.2.2. Average molar mass of $(\text{HPMC})_3\text{-}b\text{-PO}_{85}$ block copolymer

To verify the coupling reaction, the M_w of the copolymer was determined under the same conditions as those copolymers in section V.1. The M_w of $(\text{HPMC})_3\text{-}b\text{-PO}_{85}$ was $25\,000\text{ g}\cdot\text{mol}^{-1}$ while the expected M_w should be about $29\,000\text{ g}\cdot\text{mol}^{-1}$ (Figure V.12). Therefore, it is highly

probable that the coupling reaction was incomplete, and only two amino groups of T-5000 reacted. This finding could be explained by two hypotheses: first, 10 eq of NaCNBH_3 is not sufficient to reduce all iminium groups; second, the third amine is hardly accessible to the reaction due to steric hindrance.

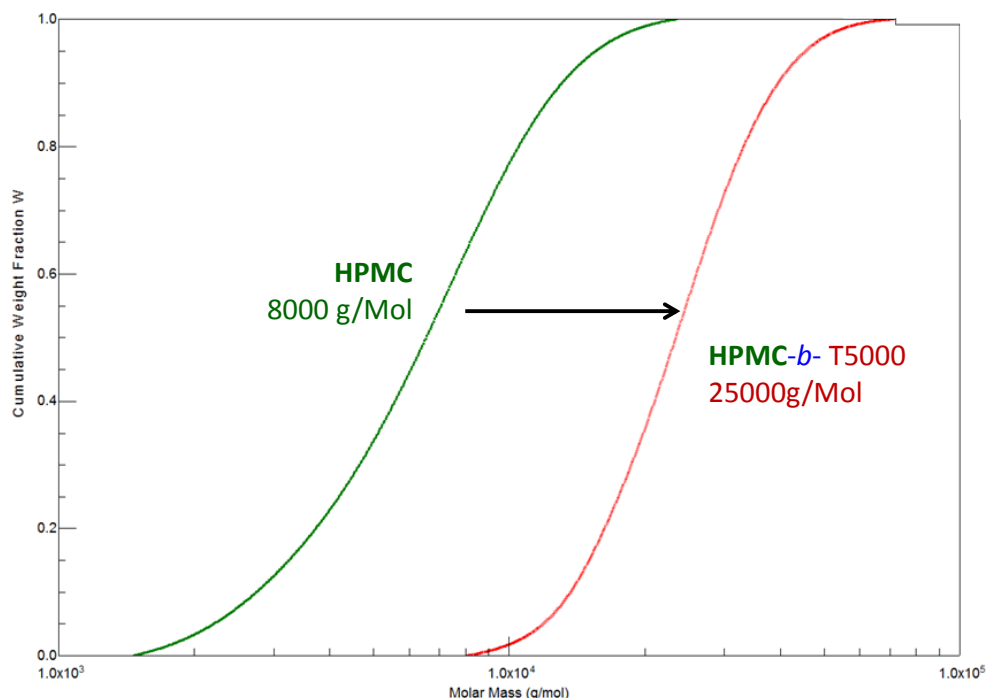


Figure V. 12. Average of molar mass distribution of HPMC and HPMC-*b*-PO₈₆.

V.2.3. FTIR of (HPMC)₃-*b*-PO₈₅ block copolymer

Figure V.13 shows the FTIR spectra of (HPMC)₃-*b*-PO₈₅ copolymer. The stretching vibration of CH, CH₂ and CH₃ are around 2900 cm^{-1} and C-O of ether groups around 1100 cm^{-1} corresponding to PO₈₅. Concerning the HPMC vibration the peak around 1000 cm^{-1} is assigned to C-O groups characterizing polysaccharides and the bands in the region of 3500 cm^{-1} are due to hydroxyl groups. The copolymer presents the OH and C-O vibration at 3500 and 1100 cm^{-1} , respectively. The vibration peaks at 2900 cm^{-1} and 1100 cm^{-1} suggest the efficiency of the coupling reaction as already demonstrate for the previous described block copolymer.

V.2.4. DOSY NMR of (HPMC)₃-*b*-PO₈₅ block copolymer

Figure V.14 also shown the DOSY analysis and ¹H NMR signal of (HPMC)₃-*b*-PO₈₅ blockcopolymers. In the same way of precedent copolymer, HPMC and PO85 reveal the same diffusion coefficient, as a result of the successful synthesis reaction. However, a residues of HPMC ($\delta=3.5-3$ ppm) are also observed in response at the incomplete coupling reaction.

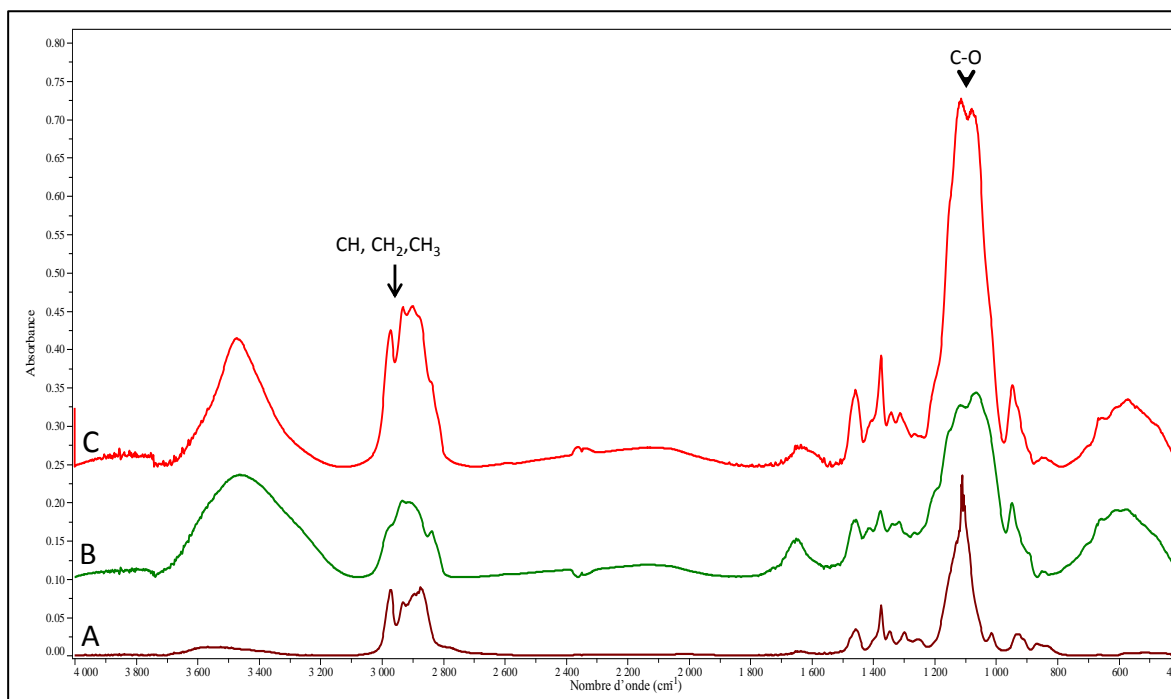


Figure V. 13. FTIR spectra of (A) PO₈₅, (B) HPMC ($M_w = 8000 \text{ g.mol}^{-1}$), (C) (HPMC)₃-*b*-PO₈₅.

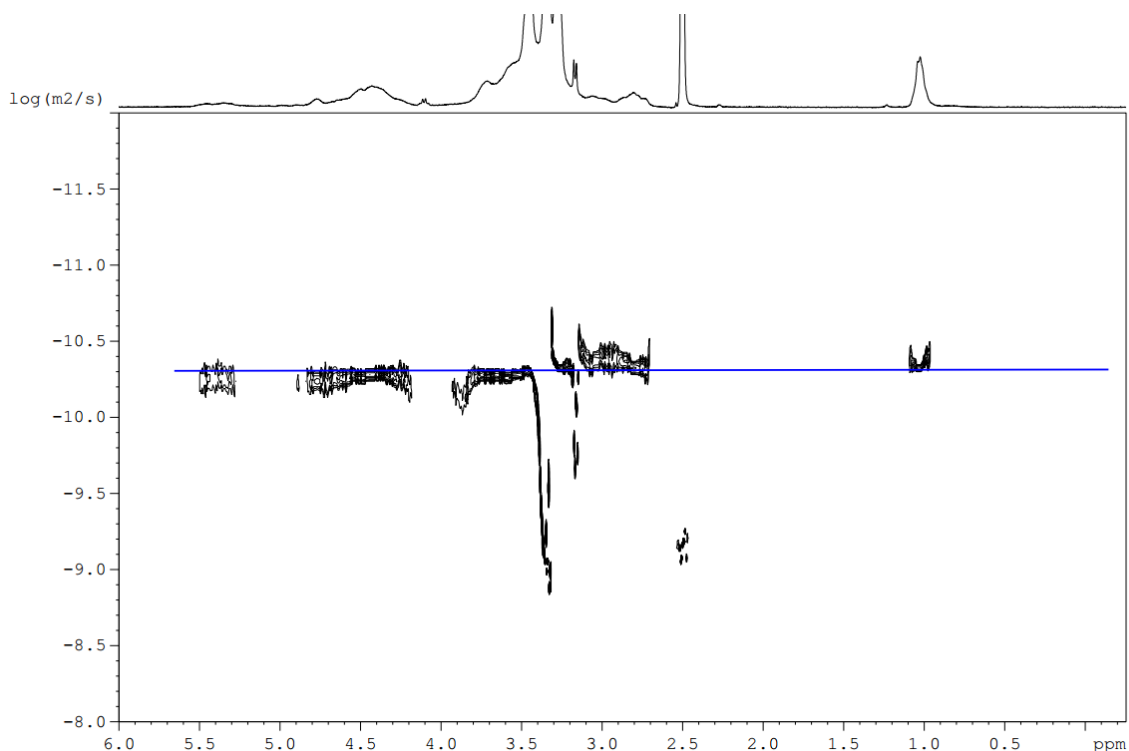


Figure V. 14. DOSY NMR spectrum obtained at 298 K in DMSO- d_6 solution of the copolymer (HPMC) $_3$ - b -PO $_{85}$.

V.2.5. Self-assembly of (HPMC) $_3$ - b -PO $_{85}$ in H $_2$ O

Considering the M_w of (HPMC) $_3$ - b -PO $_{85}$, it was believed that the obtained copolymer was a mixture of triblock copolymer ABA mixed with a three-branched star block-copolymer. The possible self-assembly organization of ABA block copolymer is presented in Figure V.15.

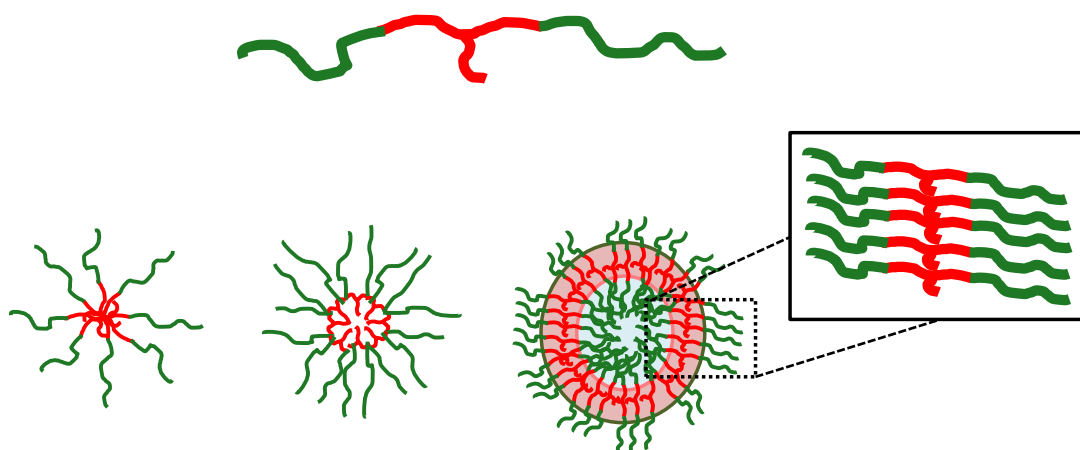


Figure V. 15. Possible self-assembly organizations of ABA-type block copolymer.

New polysaccharide fragments to amphiphilic bloc copolymer synthesis

The self-assembly organization was characterized by TEM. Nanoparticles with a size of approximately 100-150 nm are detected (Figure V.16). It can be noted that $(\text{HPMC})_3\text{-}b\text{-PO}_{86}$ self-assembly is better defined than $\text{HPMC-}b\text{-PO}_{29}\text{-EO}_6$. This finding could be related to the higher percentage of hydrophobic segments (27 wt %) on the total chain of the copolymer. Well defined hydrophobic core allows stabilizing and increasing the micelles formation.

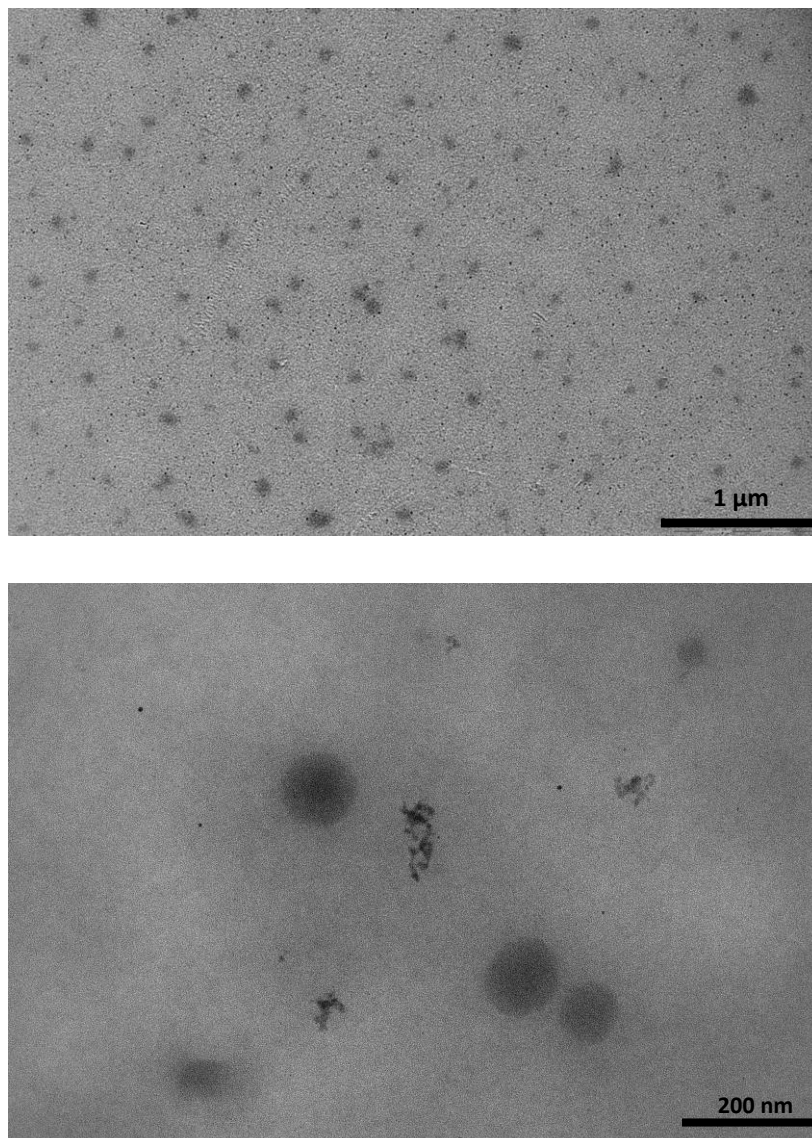


Figure V. 16. TEM images of self-assembled nano-objets of $(\text{HPMC})_3\text{-}b\text{-PO}_{85}$ copolymer.

V.3. HPMC-b-PLLA by using the thiol-ene click reaction

Amphiphilic di-block copolymer was synthesized by using the thiol-ene click reaction. HPMC-*b*-PLLA, was prepared in three steps according to the following reaction sequence: 1) HPMC-thiolation obtained by reductive amination between HPMC and cysteamine, 2) Allyl terminated PLLA obtained by ROP of L-lactide using Sn(Oct)₂ as catalyst and allyl alcohol as initiator, and 3) HPMC-*b*-PLLA synthesized by thiol-ene click reaction.

V.3.1. HPMC-thiolation

Thiolation of HPMC was carried out by coupling reducing aldehyde of HPMC with the amine group of cysteamine (aminothiol compound) in the presence of NaCNBH₃ as a reductive agent (Figure V.17). The ratio of reaction is HPMC:cysteamine:NaCNBH₃ ≈ 1:10:10, after purification process the yield of this reaction was 90 %.

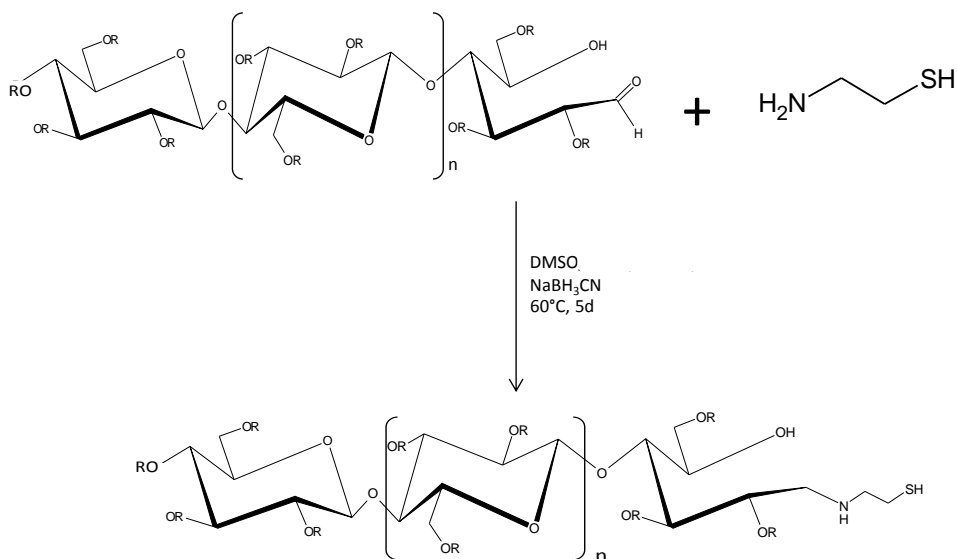


Figure V. 17. Synthesis scheme of thiolation of HPMC.

In this reaction four possible products were expected: 1) unreacted HPMC, 2) HPMC-SH, 3) HPMC-S-S-(CH₂)₂-NH₂, 4) HPMC-S-S-HPMC. The product of the reaction obtained after purification was characterized by Ellman's reaction for thiol titration and by GPC for M_w determination. Ellman's test revealed that the content of thiol group in the final polymer was around 6 % which is very low. SEC of the product confirmed the presence of HPMC-S-S-HPMC because the M_w value obtained is the double as high as that expected (Figure V.18).

Hence, the center disulfide bond (HPMC-S-S-HPMC) was reduced with an excess of dithiothreitol (DTT) over argon at room temperature overnight. Then, the polymer was purified and dried for analysis. Ellman's test showed a value of 88 % of thiol group in the final polymer with M_w close to the expected value. These findings are consistent with those reported in earlier studies by Hoypierres et al.²¹.

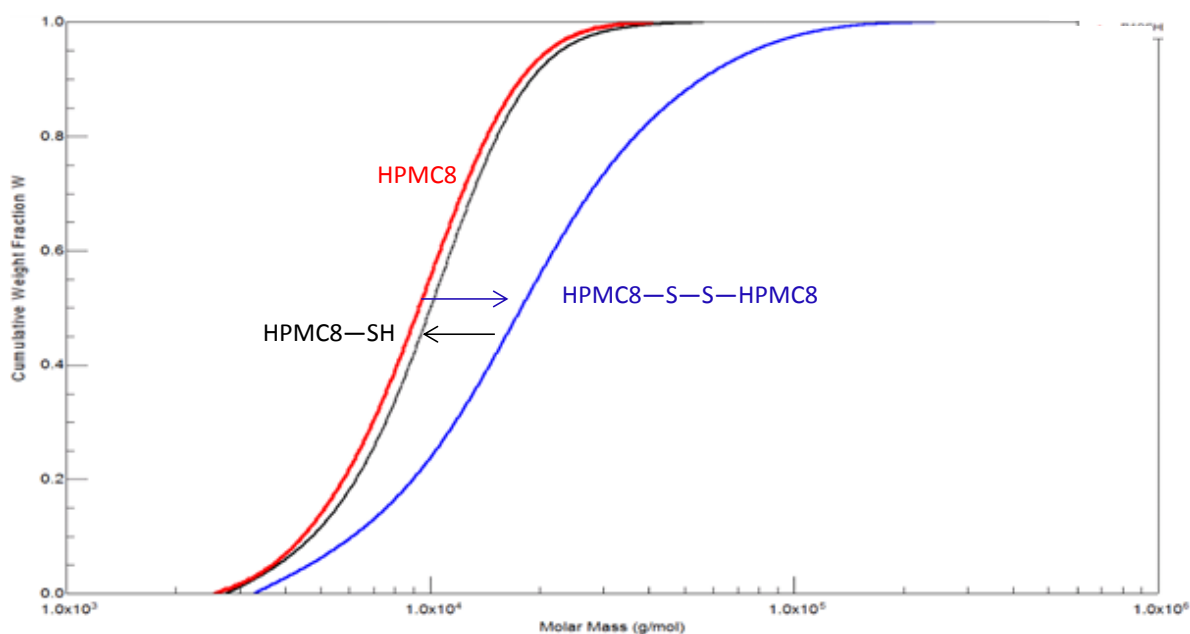


Figure V. 18. Cumulative weight fraction as a function of molar mass: red line corresponds to the initial HPMC, blue line to the disulfide bonded diHPMC and black line to the HPMC-SH after reduction with DTT.

V.3.2. PLLA synthesis

Allyl terminated PLLA was obtained by ROP of L-lactide using $\text{Sn}(\text{Oct})_2$ as catalyst and allyl alcohol as initiator, with a ratio lactide: $\text{Sn}(\text{Oct})_2$:allyl alcohol corresponding to 25:1:25 equivalents (Figure V.19).

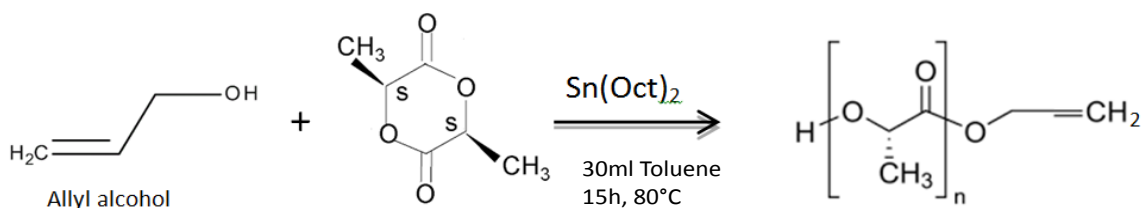


Figure V. 19. Synthesis scheme of $\text{PLA}=\text{CH}_2$.

Figure V.20 shows the ^1H NMR spectrum of $\text{PLA}=\text{CH}_2$. The signals at 5.1 and 1.6 ppm are assigned to the methine and methyl protons of PLA, respectively. Moreover, some signals of lower intensity are detected. The signal at 4.4 ppm is assigned the methine proton of HO-terminal unit. The signals at 5.9, 5.3, 5.2 and 4.6 ppm are assigned to the end functional double bond, thus confirming the successful synthesis of $\text{PLA}=\text{CH}_2$. The molecular weight of $\text{PLA}=\text{CH}_2$ determined by ^1H NMR was $M_{n\text{NMR}} = 3000 \text{ g mol}^{-1}$ (Figure V.19).

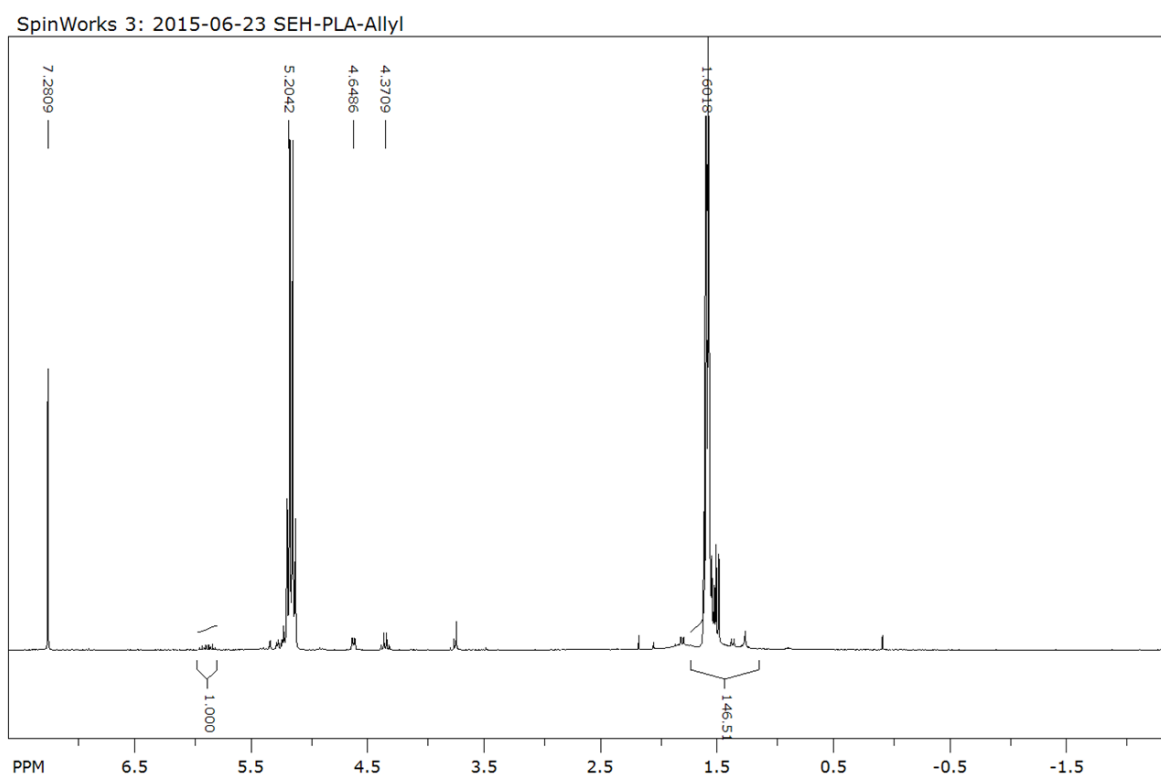


Figure V. 20. ^1H NMR spectrum of $\text{PLA}=\text{CH}_2$.

V.3.3. HPMC-*b*-PLA allyl by coupling using the thiol-ene click reaction

HPMC-*b*-PLA diblock copolymer was synthesized by thio-lene click reaction under UV. HPMC-SH ($M_w = 8077 \text{ g}\cdot\text{mol}^{-1}$, 1 g, 0.13 mmol), $\text{PLA}=\text{CH}_2$ ($M_n = 3000 \text{ g}\cdot\text{mol}^{-1}$, 0.125 g, 0.041 mmol), and photo-initiator DMPA ($M_w = 256 \text{ g}\cdot\text{mol}^{-1}$, 18 mg, 0.070 mmol) were dissolved in DMSO (10 mL) (Figure V.21). After 10 h reaction under UV light, the resulting HPMC-*b*-PLA copolymer was precipitated in excess of acetonitrile, filtered and dried in a vacuum oven overnight at 35 °C. The yield of this reaction was 87 %. The copolymer was characterized by DOSY-NMR and FTIR.

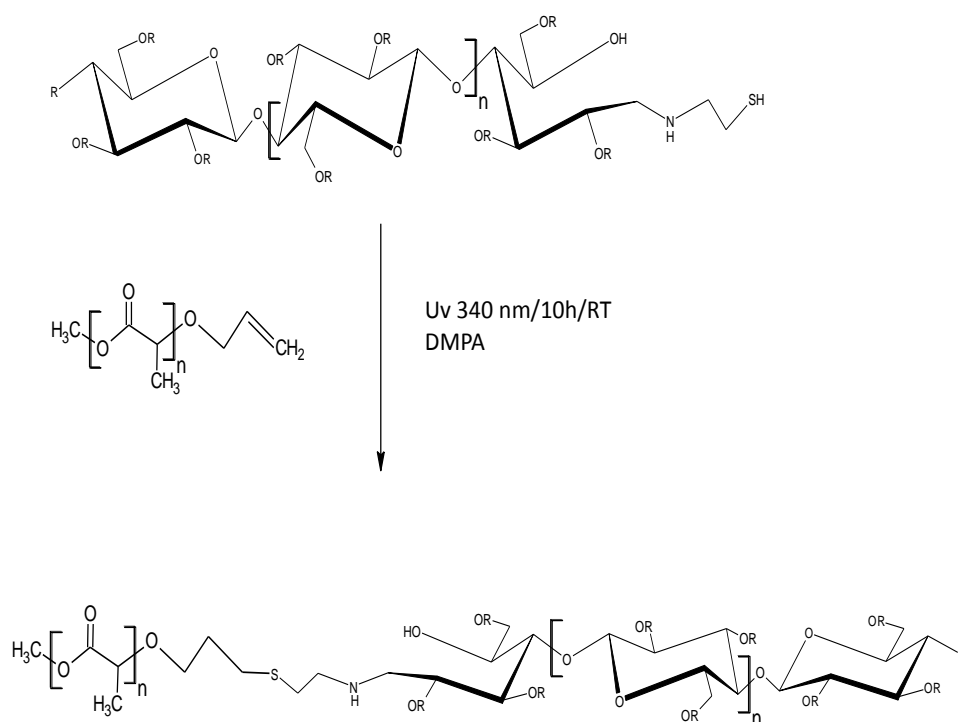


Figure V. 21. Synthesis scheme of PLA=CH₂-*b*-HPMC.

V.3.4. FTIR of PLA allyl-*b*-HPMC

Figure V.22 shows the FTIR spectra of PLLA-*b*-HPMC copolymer, PLA allyl, and HPMC. The spectrum of PLA-*b*-HPMC copolymer presents all the signals of the two components, *i.e.* PLA and HPMC. In particular, the characteristic carbonyl vibration band of PLA chains at 1763 cm^{-1} is detected in the spectrum of the copolymer, suggesting a successful coupling reaction.

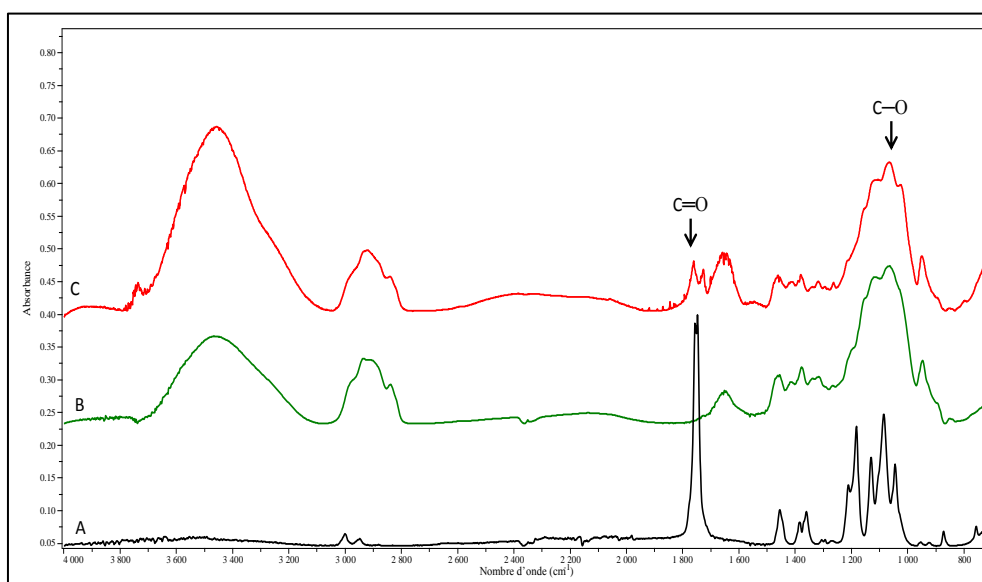


Figure V. 22. FTIR spectra of (A) PLA allyl, (B) HPMC, (C) HPMC-*b*-PLA.

V.3.5. DOSY NMR analysis for PLLA-*b*-HPMC

The diblock copolymer PLLA-*b*-HPMC was also characterized by DOSY NMR to evidence the efficiency of the copolymerization. As shows on the top of DOSY map, ^1H NMR spectrum exhibit signals corresponding to the PLA block ($\delta= 5.2$ and 1.5 ppm) and HPMC block ($\delta= 4.5$ and the region 3.8 - 2.8 ppm) (Figure V.23). ^1H NMR signals of PLA and HPMC present the same diffusion coefficient, as a result of the copolymerization between PLA and HPMC.

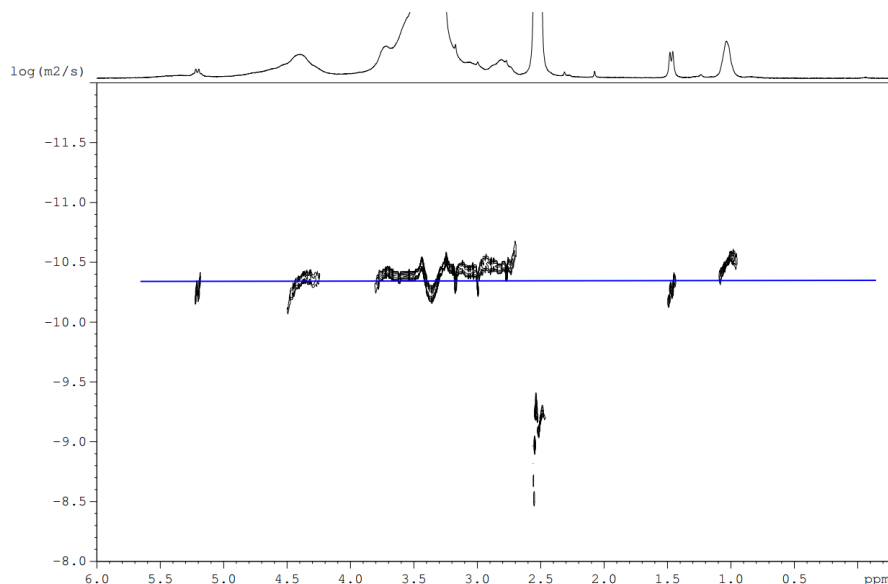


Figure V. 23. DOSY NMR spectrum obtained at 298 K in DMSO- d_6 solution of the copolymer PLLA-*b*-HPMC.

V.3.6. Self-assembly of PLA-*b*-HPMC in H₂O

To our knowledge, this is the first amphiphilic block copolymer (PLA-*b*-HPMC) coupled between PLA and HPMC. Therefore, self-assembly was studied based on the previous work on PLA derived block copolymers²²⁻²³. The copolymer is constituted approximately of 63 wt % of hydrophilic and 37wt % of hydrophobic segments. Figure V.24 reveals their possible self-organizing nanostructures, which can be cylindrical and lamellar micelles.

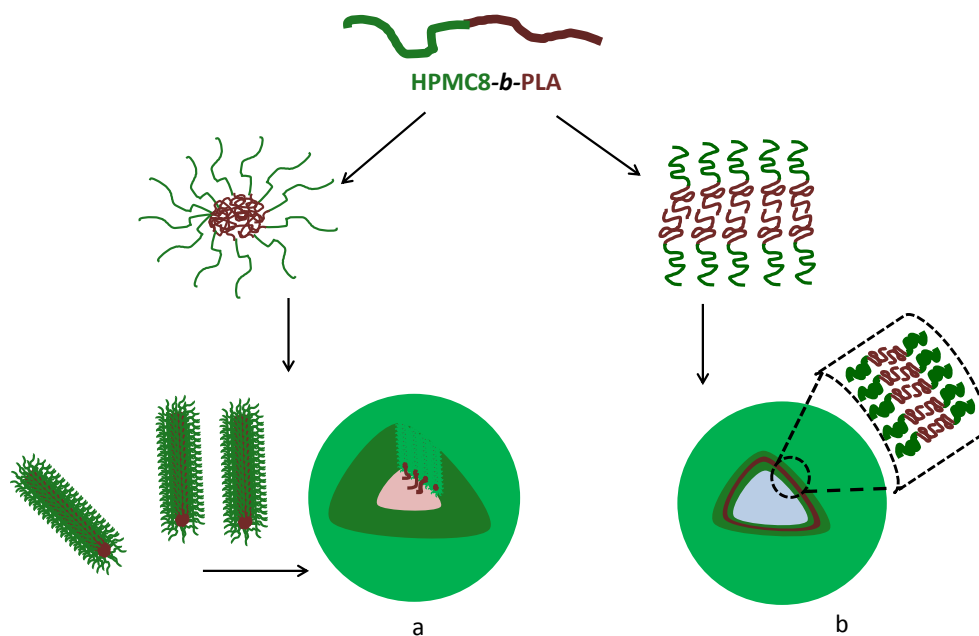


Figure V. 24. Possible self-organization of PLA-*b*-HPMC.

V.3.7. Morphology of PLA-*b*-HPMC

The morphology of self-assembled PLA-*b*-HPMC copolymer was revealed by TEM analysis. Figure V.25 shows clearly the presence of different morphologies: 1) spherical micelle, 2) elongated or rod-like micelle, 3) aggregate of 2 rod-like micelles, and 4) bird-like aggregate of 3 or more rod-like micelles.

The self-assembly of amphiphilic block copolymers has been widely investigated, in particular PLA/PEG copolymers of AB, ABA, and BAB types. These copolymers are able to self-assemble in aqueous medium, yielding various aggregates such as spherical micelles, rod-like micelles, worm-like micelles, nanotubes, polymersomes, etc²³⁻²⁴. This is in agreement with our results showing that PLA-*b*-HPMC copolymer is susceptible to self-assemble to form similar spherical micelles and rod-like micelles.

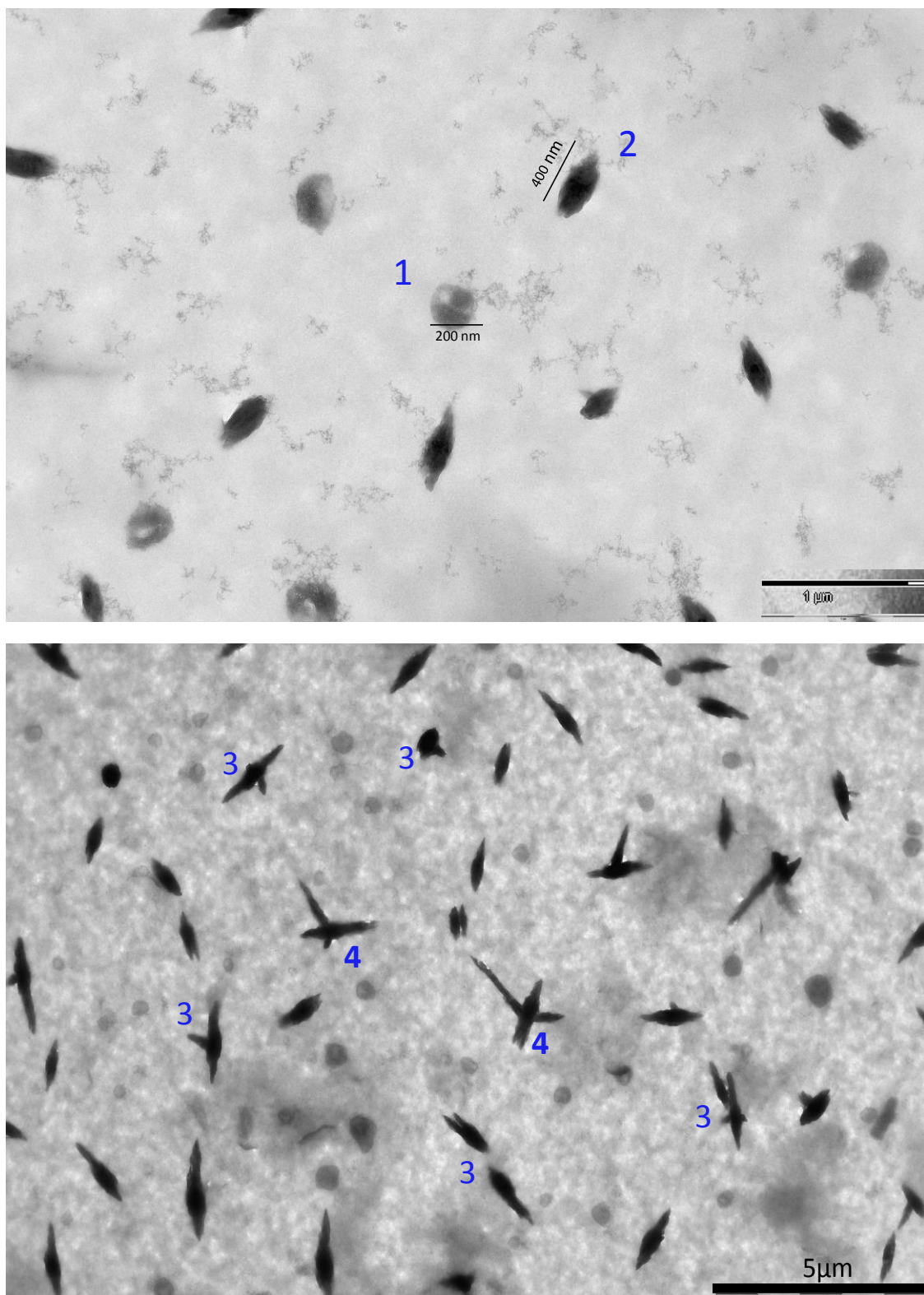


Figure V. 25. TEM images of self-organized architectures of PLA-*b*-HPMC.

CONCLUSION

The formation of diblock copolymers by end to end coupling of preformed macromolecular building blocks is an interesting method provided that chain length of the block is not too large. Both blocks should have a common solvent and no side reactions should occur between functional groups of the blocks. Perhaps because of its easy completion, the coupling technique has been often applied to covalently link polysaccharide chains to synthetic polymer blocks through different reactive end-groups.

Short-chained polysaccharide with a molecular weight around $8000 \text{ g}\cdot\text{mol}^{-1}$ was successfully used to synthesize amphiphilic block copolymers such as HPMC-Jeffamine by reductive amination and HPMC-PLA by UV assisted thiol-ene click reaction. It was demonstrated in this preliminary study that the block copolymers prepared are able to self-assemble to form various aggregates such as spherical micelles and rod-like micelles.

REFERENCE

1. Yang, H. K.; Zhang, L. M., New amphiphilic glycopolyptide conjugate capable of self-assembly in water into reduction-sensitive micelles for triggered drug release. *Mat Sci Eng C-Mater* **2014**, *41*, 36-41.
2. Mizrahy, S.; Peer, D., Polysaccharides as building blocks for nanotherapeutics. *Chem Soc Rev* **2012**, *41* (7), 2623-2640.
3. Myrick, J. M.; Vendra, V. K.; Krishnan, S., Self-assembled polysaccharide nanostructures for controlled-release applications. *Nanotechnol Rev* **2014**, *3* (4), 319-346.
4. Renggli, K.; Baumann, P.; Langowska, K., *et al.*, Selective and Responsive Nanoreactors. *Adv Funct Mater* **2011**, *21* (7), 1241-1259.
5. Hawker, C. J.; Russell, T. P., Block copolymer lithography: Merging "bottom-up" with "top-down" processes. MRS BULLETIN: 2005; Vol. 30, pp 952-966.
6. Stoykovich, M. P.; Nealey, P. F., Block copolymers and conventional lithography. *Mater Today* **2006**, *9* (9), 20-29.
7. Jeong, S.-J.; Kim, J. Y.; Kim, B. H., *et al.*, Directed self-assembly of block copolymers for next generation nanolithography. *Mater Today* **2013**, *16* (12), 468-476.
8. Mikhail, A. S.; Allen, C., Block copolymer micelles for delivery of cancer therapy: Transport at the whole body, tissue and cellular levels. *J Control Release* **2009**, *138* (3), 214-223.
9. Allen, C.; Maysinger, D.; Eisenberg, A., Nano-engineering block copolymer aggregates for drug delivery. *Colloid Surface B* **1999**, *16* (1-4), 3-27.
10. Mai, Y. Y.; Eisenberg, A., Self-assembly of block copolymers. *Chem Soc Rev* **2012**, *41* (18), 5969-5985.
11. Blanz, A.; Armes, S. P.; Ryan, A. J., Self-Assembled Block Copolymer Aggregates: From Micelles to Vesicles and their Biological Applications. *Macromol Rapid Commun* **2009**, *30* (4-5), 267-277.
12. Portinha, D.; Bouteiller, L.; Pensec, S., *et al.*, Influence of preparation conditions on the self-assembly by stereocomplexation of polylactide containing diblock copolymers. *Macromolecules* **2004**, *37* (9), 3401-3406.
13. Borch, R. F.; Bernstein, M.; Durst, H. D., Cyanohydrinborate Anion as a Selective Reducing Agent. *J Am Chem Soc* **1971**, *93* (12), 2897-&.
14. Belbekhouche, S.; Ali, G.; Dulong, V., *et al.*, Synthesis and characterization of thermosensitive and pH-sensitive block copolymers based on polyetheramine and pullulan with different length. *Carbohydr Polym* **2011**, *86* (1), 304-312.
15. Muller, J.; Marchandeu, F.; Prelot, B., *et al.*, Self-organization in water of well-defined amphiphilic poly(vinylacetate)-b-poly(vinyl alcohol) diblock copolymers. *Polym Chem-Uk* **2015**, *6* (16), 3063-3073.
16. Belbekhouche, S.; Desbrieres, J.; Hamaide, T., *et al.*, Association states of multisensitive smart polysaccharide-block-polyetheramine copolymers. *Carbohydr Polym* **2013**, *95* (1), 41-49.
17. Cambon, A.; Alatorre-Meda, M.; Juarez, J., *et al.*, Micellisation of triblock copolymers of ethylene oxide and 1,2-butylene oxide: Effect of B-block length. *J Colloid Interf Sci* **2011**, *361* (1), 154-158.

18. Larue, I.; Adam, M.; Zhulina, E. B., *et al.*, Effect of the soluble block size on spherical diblock copolymer micelles. *Macromolecules* **2008**, *41* (17), 6555-6563.
19. de Medeiros Modolon, S.; Otsuka, I.; Fort, S., *et al.*, Sweet Block Copolymer Nanoparticles: Preparation and Self-Assembly of Fully Oligosaccharide-Based Amphiphile. *Biomacromolecules* **2012**, - *13* (- 4), - 1135.
20. Dulong, V.; Mocanu, G.; Picton, L., *et al.*, Amphiphilic and thermosensitive copolymers based on pullulan and Jeffamine (R): Synthesis, characterization and physicochemical properties. *Carbohydr Polym* **2012**, *87* (2), 1522-1531.
21. Hoypierres, J.; Dulong, V.; Rihouey, C., *et al.*, Two Methods for One-Point Anchoring of a Linear Polysaccharide on a Gold Surface. *Langmuir* **2015**, *31* (1), 254-261.
22. Sun, L.; Pitto-Barry, A.; Kirby, N., *et al.*, Structural reorganization of cylindrical nanoparticles triggered by polylactide stereocomplexation. *Nat Commun* **2014**, *5*, 1-9.
23. Wu, X. H.; El Ghzaoui, A.; Li, S. M., Anisotropic Self-Assembling Micelles Prepared by the Direct Dissolution of PLA/PEG Block Copolymers with a High PEG Fraction. *Langmuir* **2011**, *27* (13), 8000-8008.
24. Wu, X.; Li, S. M.; Coumes, F., *et al.*, Modeling and self-assembly behavior of PEG-PLA-PEG triblock copolymers in aqueous solution. *Nanoscale* **2013**, *5* (19), 9010-9017.

CHAPTER VI: CONCLUSION AND PERSPECTIVES

Conclusion and Perspectives

During this work, a library of short-chained Hydroxypropyl Methylcellulose (HPMC) was successfully produced by enzymatic hydrolysis. The reactivity and thermosensitive properties were studied to evaluate the potential properties of the obtained polymers to be used as a building block in amphiphilic block copolymer preparation. The self-assembly and phase transition were studied to evaluate their prospective properties as nanocarriers. The following conclusions drawn from this work are:

Enzymatic catalysis using endoglucanases (EG) from *Trichoderma reesei* was proven to lead partial hydrolysis of HPMCs into two main fragments that can be isolated by selective precipitation. Enzymatic actions of EG was fast and yielded polymers having respectively M_w of about 30 000 and 10 000 $\text{g}\cdot\text{mol}^{-1}$. The heterogeneity of HPMC substitution enables the formation of EG/substrate complex following by chain cleavages. This means that the two resulting chain segments are too highly substituted and not available for EG to ensure further hydrolysis to take place.

It was also demonstrated that the chain length can be controlled by further incremental depolymerisation owing to the small amount of exocellulases (EX) present in the enzyme cocktail. Thus, M_w of the shorter polymers (S fraction) was reduced from 10 000 to about 7 000 $\text{g}\cdot\text{mol}^{-1}$ by extending the time of reaction to 72 h (180 $\mu\text{L}\cdot\text{g}^{-1}$ K4M). It should be noted that this range of HPMC M_w has never been described or characterized before this work.

Both enzymatic and acidic catalysis can be used to partially degrade HPMC and generate polymers with short chains. It was found that the targeted range of M_w (5 000 – 10 000 $\text{g}\cdot\text{mol}^{-1}$) we are interested in, was easily reached through enzymatic reaction in fair yield (50 – 60 %). Moreover, the chain length could be precisely monitored by the reaction time and the ratio enzyme/substrate.

Small fragments of HPMC generated by enzymatic and acid treatment were characterized and compared with those of starting polymer characteristics. The chemical composition of short fragments varied as a function of the degradation procedure. Fragments isolated by precipitation (P fraction) during the enzymatic process showed higher values in molar substitution in hydroxypropyl group (MS_{HP}) and degree of substitution in methyl group (DS_{Me}) than starting HPMC samples. In the case of fragments produced by acid degradation,

Conclusion and Perspectives

the value of MS_{HP} and DS_{Me} did not vary compared to the starting polymers owing to the random cleavage characteristic of this catalysis.

Enzymatic S fractions have 12 % less of MeO group than P fragments. HPO substituents did not vary significantly for all produced fragments. These results suggest that the highly methylated domains unevenly located along the K4M and G4 chains are the limiting parameter in enzyme catalyzed hydrolysis.

The macromolecular features showed that short polymers ranging from about 30 000 to 7 000 $g.mol^{-1}$ can be prepared with various solution behavior from compact to expanded conformation. These different properties can be related to the degree of substitution of the obtained polymers. Moreover, the thermally induced phase separation behavior was demonstrated to be primarily connected to the extent of DS_{Me} . On the other hand, M_w seems to influence this property only for values lower than 10 000 $g.mol^{-1}$. For instance, the smaller HPMC with low DS_{Me} prepared by enzymatic hydrolysis did not showed any phase separation.

The phase separation behavior of short chained HPMC can be controlled by adjusting the operating parameters of the depolymerisation. Depending on the procedure and the nature of catalyst, the polymer structure can be tailored to obtain the desired properties.

The enzymatic depolymerisation enables to yield short chained HPMCs with a larger content of reducing end than the acidic catalysis. This end reactivity was used to functionalize the HPMC chains and to prepare block copolymers.

Three amphiphilic and thermo-responsive block copolymers were successfully synthesized by two routes: end-to-end coupling reaction and thiol-ene click reaction. Thus, short chained HPMC blocks were coupled with Jeffamine® M-2005 ($H_2N-PO_{29}-EO_6$) and T-5000 ((tri amino) PO_{85}) and with allyl terminated PLLA. The self-assembling properties of these block copolymers showed to form aggregates such as spherical micelles and rod-like micelles.

The formation of diblock copolymers by end-to-end coupling of preformed macromolecular building blocks is an interesting method that provided the molecular weight of the block when it is not too large. Both blocks should have a common solvent and no side reactions occurring between functional groups of the blocks. Perhaps because of its easy completion,

Conclusion and Perspectives

the coupling technique has been often applied to covalently link polysaccharide chains to synthetic polymer blocks through different reactive end-groups.

These novel products fulfil the new demand of research platforms around of biopolymers, materials and nanomaterial's sciences. Nanomaterial applications are requested mainly in the biomedicine field but also can be extended to material science. Nanomaterials are now often used to produce smart materials. New fragments of biopolymers are now available for new syntheses of block copolymers.

Perspectives

Among the several viewpoints that can help to complete this work, the following perspectives were identified:

- **Physicochemical characterization of diblock copolymer**

Analysis including surface properties and rheology can allow understand the aggregation behavior of block copolymers.

- **Novel block copolymer formation**

The short chained HPMC could be coupled with synthetic blocks like PS, PMMA, or other natural polymers like proteins in order to form plataforms for building new materials.

- **Biomedical Application**

The novel block copolymers could be also good candidate to produce nanoparticles with stimuli response for drug delivery.

Abstract:

Following the concept of bio-refinery, we propose to produce small fragments of biopolymers that can be used further as building blocks to prepare novel polymeric architectures. In the case of polysaccharides, enzymatic hydrolysis enables to form reducing end groups after each cleavage on the polymer chain. Reaction by reductive amination affords the possibility to introduce polysaccharides fragments in a large variety of materials going from amphiphilic copolymers to more sophisticated devices. Hydroxypropyl methylcellulose (HPMC) was used in this work because of its remarkable properties including biocompatibility, biodegradability, water retention and thermoreversible gelation beneficial for many applications such as drug delivery, film and biomaterial formation. Enzymatic hydrolysis using endo cellulases from *Trichoderma reesei* was investigated to produce a library of HPMC fragments with molecular weight (M_w) from 6000 to 30000 g mol⁻¹. M_w control was carried out by varying the procedure conditions including the nature of starting HPMC, reaction time and enzyme concentration. The obtained polymers were compared to those produced by acidic hydrolysis. According to the preparation conditions, the structure of short chain polymers regarding substitution degrees varied for the same M_w giving rise to different clouding temperature and thermoreversible gelation properties. Amphiphilic block copolymers HPMC-*b*-poly(propylene glycol) and HPMC-*b*-PLA were prepared by reductive amination and by the thiol-ene click reaction, respectively. Self-assembly properties of these novel block copolymer were characterized by dynamic light scattering (DLS), transmission electron microscope (TEM), and clouding point temperature.

Résumé :

Parmi les bio-polymères issus des ressources renouvelables, les polysaccharides fournissent une alternative intéressante aux polymères de synthèse. Dans ce contexte, l'objectif de ce travail de thèse est basé sur la conception des copolymères amphiphiles pour la préparation de nouveaux biomatériaux. Ainsi, l'hydroxypropylméthylcellulose (HPMC) a été choisie en raison de ses propriétés remarquables, dont la biocompatibilité, la biodégradabilité, la rétention d'eau et la gélification thermoréversible. Ces propriétés sont utiles pour de nombreuses applications telles que le relargage de médicament, la préparation des membranes et la formation de biomatériaux. L'hydrolyse enzymatique avec des endo cellulases issues de *Trichoderma reesei* a été étudiée pour produire des fragments d'HPMC ayant une masse molaire (M_w) entre 6000 et 30000 g mol⁻¹. Les paramètres de l'activité enzymatique ont été étudiés en fonction de : la nature de substrat, le temps de réaction et la concentration de l'enzyme. Les polymères obtenus ont été comparés à ceux produits par hydrolyse acide. Il a été constaté que la structure des polymères issus d'un procédé d'hydrolyse, varie en termes de degré de substitution pour un même M_w . Cet effet donne lieu à différentes propriétés de gélification thermoréversible. Des copolymères amphiphiles tels que HPMC-*b*-poly (propylène glycol) et HPMC-*b*-PLA ont été préparés par amination réductrice et par couplage click thiol-ene, respectivement. Les propriétés d'agrégation ont été caractérisées par la diffusion de la lumière (DLS), le microscope électronique en transmission (TEM) et par la séparation de phase obtenue par la mesure du point de trouble.